NOVEL SENSORS FOR DETECTION OF ANTI-ASTHMA DRUGS IN PHARMACEUTICAL FORMULATIONS

By

Kilele. C. Joan

Student No.: 21854352

Submitted in fulfilment of the requirements for the Degree of Master of Applied Science in Chemistry in the Faculty of Applied Sciences at the Durban University of Technology

2022

DECLARATION

I, **Joan Chepkoech Kilele,** hereby declare that this work is my own and that the thesis submitted for the degree of Master of Applied Science in Chemistry at the Durban University of Technology, has not been submitted for any degree or examination to any other university and no portion of this or any other closely related work is under consideration for publication elsewhere in any medium.

Student: Joan Chepkoech Kilele

Signature: **Date**……09/03/2022…….

Supervisor: Prof. Gan G Redhi

Signature: **Date**……16/03/2022…….

Co-supervisor: Dr. Rajasekhar Chokkareddy

Signature: **Date**……16/03/2022…….

DEDICATION

This work is dedicated to my entire family and to the late Daniel Kibet Chesot, may your soul continue resting in eternal peace.

ACKNOWLEDGEMENTS

First, I would like to thank the Almighty God for the gift of life and for seeing me through to the completion of my Master's degree.

I extend my sincere gratitude to my supervisors Prof. Gan G Redhi and Dr. Rajasekhar Chokkareddy for their immeasurable guidance, advice and encouragement throughout my studies. I must also express my appreciation to EA lab technician Mrs. M. Xhakaza for her support and her willingness to assist me anytime I needed help.

Many thanks to my fellow lab mates Dr.Kwanele, Dr. Kabane, Lephalala, Benni, Senzi, Jiyane and to my friends from Chemical Engineering and Institute for Water and Wastewater Technology, for their constant support and words of encouragement throughout the study. I may not mention all of you but you are always in my heart. It has been great to know all of you during my time here at Durban University of Technology.

I acknowledge Durban University of Technology's Research and Postgraduate support team for their assistance especially during the writing retreat workshop. I also thank the National Research Foundation of South Africa for their financial support.

A special thanks to my entire family for their unending love, sacrifice, prayers, understanding and financial support.

Finally, I am grateful to my dear husband, Dr. Eric Kiprotich Kosgey, for his undying love, solid support, understanding, taking up family responsibilities and bearing up the pressure as we both studied, and at the same time fulfilled parenting duties. You are and remain to be the best God sent gift to me. Also, to my loving son Shujaa Kiptoo and daughter Zahara Chelimo for understanding that mummy needed to time to study at their age. Much love to you all.

ABSTRACT

The development of an effective technique for detecting anti-asthma drugs with adverse effects in the human body at high dosages remains a serious challenge. For this purpose, herein, we report a novel electrochemical detection method based on nanocomposite modified glassy carbon electrode (GCE) nano-sensors. Cobalt ferrite ($CoFe_2O_4$), titanium oxide (TiO_2) and zinc oxide (ZnO) nanoparticles (ZnONPs) were synthesized as well as their respective nanocomposites ($CoFe_2O_4$-MWCNTs-Lipase, TiO_2-MWCNTs-IL, ZnONPs-MWCNTs-Cytochrome c and MWCNTs-Ionic liquid-L-lysine) were successfully prepared. Subsequently, their surface morphology, crystal structure, functional groups, thermal stability, surface area as well as pore size distribution of the synthesized nanoparticles and the nanocomposites aspects were analysed. The characterization analyses were undertaken using scanning electron microscopy (SEM), transmission electron microscopy (TEM), X-ray diffraction (XRD), Brunauer-Emmett Teller (BET) adsorption analyses, thermal gravimetric analysis (TGA) and Fourier-transform infrared spectroscopy (FTIR). In addition, electrochemical characterization of the fabricated electrodes were examined using electrochemical impedance spectroscopy (EIS) in order to ensure the material's suitability in electro-catalytic sensing by investigating the electron transfer kinetics of the redox probe at the modified electrode-solution interface.

The fabricated nanocomposite based sensors; ZnONPs-MWCNTs-Cyt c-GCE, $CoFe_2O_4$-MWCNTs-Lipase-GCE, MWCNTs-IL-L-lysine-GCE and TiO_2-MWCNTs-IL-GCE were tested for electrochemical determination of theophylline, salbutamol, prednisolone and terbutaline, respectively, using cyclic voltammetry (CV) and differential pulse voltammetry (DPV). The effect of varying scan rates, pH of the supporting electrolyte and accumulation time on the peak potential position and peak-currents, were studied with each electrode, and the optimum working parameters were selected. The ZnONPs-MWCNTs-Cyt c-GCE, $CoFe_2O_4$-MWCNTs-Lipase-GCE, MWCNTs-IL-L-lysine-GCE and TiO_2-MWCNTs-IL-GCE sensors were found to exhibit excellent electro-catalytic activity towards theophylline, salbutamol, prednisolone and terbutaline. The synergy between these nanocomposite materials increased the electrochemical activity, the electron transfer rate and the electrode surface area, leading to high peak-current response for the determination of each drug.

ZnONPs-MWCNTs-Cyt c-GCE sensor presented acceptable long-term stability, good reproducibility and repeatability. The limit of detection (LOD = 0.0012 µM) obtained was

much lower than most of the given literature studies. Similarly, the $CoFe_2O_4$-MWCNTs-Lipase nanocomposite modified GCE for salbutamol (SAL) exhibited excellent stability, reproducibility and sensitivity with lowest detection limit (0.0240 µM) and limit of quantification (LOQ) of 0.0120 µM, over the concentration range of 0.05- 3.9 µM. In addition, the MWCNTs-IL-L-lysine-GCE exhibited outstanding electro-catalytic activity including excellent reproducibility, with LOD and LOQ of 0.0214 µM and 0.3016 µM, respectively, for prednisolone (PDN) detection. Moreover, at optimized electrochemical experimental conditions, the electrochemical performance of the constructed TiO_2-MWCNTs-IL-GCE sensor for determination of terbutaline (TBS) was also evaluated. Stability, reproducibility as well as the detection limits were determined. A wide linear range of 0.5 µM to 3.0 µM as well as LOD and LOQ of 0.0162 µM and 0.2140 µM, respectively, were obtained and the results were compared with similarly reported electrodes for terbutaline detection. The selectivity of each sensor was also evaluated in presence of common interferences.

There was no significant interference on the electrochemical peak-current response and peak position of each target analyte. The practical applicability of each fabricated sensor was investigated by the DPV method with respect to the detection of the four drugs under study in commercial pharmaceutical samples. In all cases, the sensors showed good percentage recovery performance in real dosage samples. From the experimental results, it is evident that the fabricated nanocomposite based sensors are ultra-sensitive for selective detection of the investigated four drugs in pharmaceutical formulations and other sample matrices.

TABLE OF CONTENTS

1 INTRODUCTION 2
1.1 Background information 2
1.2 Problem statement 7
1.3 Aim 8
1.4 Objectives 8
2 LITERATURE REVIEW 9
2.1 Bronchodilators 9
2.1.1 Salbutamol 9
2.1.2 Terbutaline 12
2.2 Methylxanthines 14
2.3 Corticosteroids 17
2.4 Analytical techniques for quantification of selected anti-asthma drugs 19
2.4.1 Chromatographic techniques 24
2.4.2 Spectroscopy techniques 25
2.4.3 Electrophoresis methods 26
2.4.4 Electrochemical techniques 27
3 THEORETICAL PRINCIPLES OF VOLTAMMETRIC TECHNIQUES AND ELECTROCHEMICAL SENSORS 34
3.1 Instruments used in voltammetry 35
3.1.1 The types of electrodes used in voltammetry 36
3.1.2 Supporting electrolyte 37
3.2 Voltammetry methods 38
3.2.1 Cyclic voltammetry (CV) 38
3.2.2 Differential pulse voltammetry (DPV) 39
3.3 Electrochemical sensors 40

4 MATERIALS AND METHODOLOGY 42
4.1 Materials and reagents 42
4.2 Synthesis of nanoparticles 43
4.2.1 Synthesis of ZnONPs 43
4.2.2 Synthesis of $CoFe_2O_4$NPs 43
4.2.3 Synthesis of TiO_2NPs 43
4.3 INSTRUMENTATION 44
4.3.1 Characterization analysis 44
4.3.2 Electrochemical measurements 44
4.3.3 Voltammetry determinations 45
4.4 Preparation of supporting electrolytes and standard solutions 45
4.5 Preparation and fabrication of nanocomposites-based sensors for detection of anti-asthma drug. 46
4.5.1 ZnO NPs-MWCNTs-Cyt c-GCE sensor for detection of TPN. 46
4.5.2 MWCNTs-$CoFe_2O_4$NPs-Lipase-GCE for detection of SAL 46
4.5.3 MWCNTs-IL-L-lysine-GCE for detection of PDN 47
4.5.4 TiO_2-MWCNTs-IL-GCE for detection of TBS 47
4.6 Sample preparations 47
5 RESULTS AND DISCUSSION 49
5.1 Detection of theophylline (TPN) 50
5.1.1 Surface morphology, crystal structure and functional groups 50
5.1.2 Surface area and porosity 53
5.1.3 Electrochemical impedance spectroscopy (EIS) 55
5.1.4 Electro-oxidation of TPN 56
5.1.5 Electrochemical performance of ZnONPs-MWCNTs-Cyt c-GCE for TPN 58
5.1.6 Method validation analyses via DPV 59
5.1.7 Practical application of the fabricated sensor in real samples 62

5.2 Determination of salbutamol 64
5.2.1 Functional groups, thermal stability analysis, crystal structure and surface morphology 65
5.2.2 CV and EIS characterization of the GCE and MWCNTs-$CoFe_2O_4$-Lipase modified GCE 68
5.2.3 Electro-oxidation of SAL at GCE and composite modified GCE 69
5.2.4 Selection, optimization and study of the effect of pH 71
5.2.5 Effect of deposition time 73
5.2.6 Influence of the scan rate 74
5.2.7 Sensitivity of MWCNTs-$CoFe_2O_4$-Lipase-GCE sensor 75
5.2.8 Selectivity, stability and reproducibility of MWCNTs-$CoFe_2O_4$-Lipase-GCE . 77
5.2.9 Analysis of SAL in real drug sample using MWCNTs-$CoFe_2O_4$-Lipase-GCE 79
5.3 Electrochemical sensing of prednisolone (PDN) 80
5.3.1 Functional group identification and thermal stability 80
5.3.2 Surface morphology 81
5.3.3 EIS characterization of the MWCNTs-IL-L-lysine-GCE 82
5.3.4 The electro-catalytic reduction of PDN 84
5.3.5 Effect of pH 85
5.3.6 Influence of accumulation time 86
5.3.7 Impact of varying scan rate on both modified and unmodified GCE at constant concentration of PDN. 86
5.3.8 DPV analysis of PDN using MWCNTs-IL-L-lysine-GCE sensor 88
5.3.9 Effect of interferences and stability of MWCNTs-IL-L-lysine-GCE 90
5.3.10 Detection of PDN in pharmaceutical dosage sample 91
5.4 Electrochemical detection of terbutaline 93
5.4.1 Thermal properties, functional groups and morphological properties of the nanocomposite 93
5.4.2 Electrochemical characterization of the modified GCE surface 96

5.4.3 Electro-catalytic oxidation of terbutaline on TiO_2-MWCNTs-IL-GCE 97
5.4.4 Optimization of working parameters 98
5.4.5 Quantitative determination of terbutaline using DPV 103
5.4.6 Method validation studies using the developed sensor.....105
5.4.7 Determination of TBS in real drug sample using TiO_2-MWCNTs-IL-GCE...105
6 SUMMARY AND CONCLUSION 107
REFERENCES 109
APPENDIX.....128

LIST OF TABLES

Table 2.1: Detection limits for the convectional analytical methods for detection of TPN, SAL, TBS and PDN 21

Table 4.1: Chemicals and reagents used.....42

Table 5.1: The LOD of ZnONPs-MWCNTs-Cyt c-GCE sensor compared with other reported sensors for electrochemical sensing of TPN.....61
Table 5.2: Determination of TPN in drug formulation sample 63
Table 5.3: Linear equations and the regression values of the different modified electrodes ..75
Table 5.4: Comparison of the MWCNTs-$CoFe_2O_4$-Lipase-GCE sensor with other SAL sensors 77
Table 5.5: Determination of SAL in Venteze syrup sample. 79
Table 5.6: Comparison of MWCNTs-IL-L-lysine-GCE with previous electrodes reported for PDN detection.....90
Table 5.7: Determination of PDN in pharmaceutical Aspelone syrup sample.....92
Table 5.8: The regression equations and correlation coefficient of the respective plots of I/µA vs. V/s 103
Table 5.9: Comparison of the LOD of TiO_2-MWCNTs-IL-GCE with previous reported electrodes for TBS detection.....105
Table 5.10: Determination of TBS in real pharmaceutical sample 106

LIST OF FIGURES

Figure 2.1: Chemical structure of salbutamol.....10
Figure 2.2: Electrochemical oxidation mechanism of salbutamol.....10
Figure 2.3: Chemical structure of terbutaline.....12
Figure 2.4: Electrochemical oxidation mechanism of terbutaline.....13
Figure 2.5: Chemical structure of theophylline.....15
Figure 2.6: Electro-catalytic oxidation mechanism of TPN.....16
Figure 2.7: Chemical structure of prednisolone.....18
Figure 2.8: Electrochemical reduction mechanism of prednisolone.....18
Figure 2.9: Analytical approaches reportedly used for detection of the four anti-asthma drugs 20
Figure 2.10: Chemical structure of L-lysine.....33

Figure 3.1: A pictorial representation of voltammetry instrumentation.....35
Figure 3.2: Unmodified glassy carbon electrode representation.....37
Figure 3.3: Schematic illustration of the principle of a chemical sensor.....40
Figure 3.4: Diagrammatic representation of a biosensor.....41

Figure 5.1: Schematic illustration of the fabricated ZnONPs/MWCNTs/Cyt c/GCE biosensor for TPN detection.....50
Figure 5.2: TEM images of ZnONPs (a), MWCNTs (b) and ZnONPs-MWCNTs composite (c). XRD pattern of ZnONPs (d).....51
Figure 5.3: FTIR spectra of ZnONPs and ZnONPs-MWCNTs-Cyt c nanocomposite.....52
Figure 5.4: TGA curves of MWCNTs, ZnONPs and ZnONPs/MWCNTs nanocomposite...53
Figure 5.5: Nitrogen adsorption/desorption isotherm and pore size distribution curve of ZnONPs/MWCNTs (inset).....54
Figure 5.6: Nitrogen adsorption/desorption isotherm and pore size distribution curve of MWCNTs (Inset).....55
Figure 5.7: Nyquist plots of ZnONPs-MWCNTs-GCE, MWCNTs-GCE and ZnONPs - MWCNTs-Cyt c-GCE in 0.1 M KCl solution containing 0.1 mM $[Fe(CN)_6]^{-3/-4}$.....56
Figure 5.8: Cyclic voltammograms of TPN recorded at bare GCE showing the effect of varying deposition time (a), effect of pH of PBS (b) and effect of scan rates (c). Plot of peak-current (I/µA) Vs $[V/s]^{1/2}$(d).....58

Figure 5.9: Cyclic voltammogram of 0.1 M TPN in 0.1 M PBS pH 3.5 at ZnONPs-MWCNTs-Cyt c-GCE sensor obtained at various sweep rates (0.1 V/s-1.0 V/s) 59
Figure 5.10: DP voltammogram of 0.1 M TPN with various concentration range (from 0.4 µM to 15 µM) in 0.1 M PBS (pH 3.5) at the ZnONPs/MWCNTS/Cyt c/GCE (a) (Conditions: pulse amplitude 0.09 V, sweep rate 0.1 V/s, voltage step 0.005951 V, Pulse time 0.05 s, deposition potential -0.1009 V and deposition time 60 s). Plot of peak-current (I/µA) against concentration (µM) of TPN (b) 60
Figure 5.11: DP voltammogram of 0.1 M TPN at the ZnONPs-MWCNTs-Cyt c-GCE upon addition of different interfering compounds 62
Figure 5.12: Schematic representation of the electrochemical detection of SAL using MWCNTs-$CoFe_2O_4$-Lipase modified GC electrode surface 64
Figure 5.13: FTIR Spectra of $CoFe_2O_4$NPs, MWCNTs-$CoFe_2O_4$ and MWCNTs-$CoFe_2O_4$-Lipase samples 65
Figure 5.14: (a) TGA curves of commercial MWCNTs, MWCNTs-$CoFe_2O_4$ and $CoFe_2O_4$NPs samples. (b) XRD pattern of the synthesized $CoFe_2O_4$NPs.....67
Figure 5.15: SEM micrographs of $CoFe_2O_4$ NPS and $CoFe_2O_4$-MWCNTs and MWCNTs-$CoFe_2O_4$-Lipase nanocomposite 68
Figure 5.16: TEM images of $CoFe_2O_4$NPs and MWCNTs-$CoFe_2O_4$ nanocomposite samples 68
Figure 5.17: CV voltammograms (A) and the Nyquist plots (B) obtained at the GCE MWCNTs-GCE, MWCNTs-$CoFe_2O_4$-GCE and MWCNTs-$CoFe_2O_4$-Lipase-GCE. Figure 5. 17B (Inset) presents the employed equivalent circuit used to fit the impedance results 69
Figure 5.18: Cyclic voltammograms of SAL showing effect of scan rates at GCE (a), MWCNTs-GCE (b), MWCNTs-$CoFe_2O_4$-GCE (c) and MWCNTs-$CoFe_2O_4$-Lipase-GCE (d) 71
Figure 5.19: Cyclic voltammograms of the supporting electrolytes; KPBS, PBS, ABS and BBS 72
Figure 5.20: Effect of the pH of the PBS on the electrochemical response of SAL on the un-modified GCE 73
Figure 5.21: Plot of peak-current vs time; displaying the effect of varying deposition time .74
Figure 5.22: (a) DP voltammogram of SAL @ MWCNTs-$CoFe_2O_4$-Lipase-GCE and (b) is the plot of peak-current (µA) as a function of SAL concentration (µM) 76
Figure 5.23: The effect of interfering substances on the electrochemical responses of SAL at MWCNTs-$CoFe_2O_4$-Lipase-GCE.....78

Figure 5.24: Schematic illustration of the application of the fabricated MWCNTs-IL- L-lysine -GCE sensor for electrochemical detection of PDN 80
Figure 5.25: FTIR spectra of MWCNTs (blue curve) and MWCNTs-IL-L-lysine nanocomposite (red curve) (a). TGA curves of MWCNTs (black curve) and MWCNTs-IL-L-lysine nanocomposite (green curve) (b).....81
Figure 5.26: SEM images of (a) MWCNTs, (b) MWCNTs-IL and (c) MWCNTs-IL-L-lysine nanocomposite 82
Figure 5.27: TEM images of MWCNTs (a) and MWCNTs-IL nanocomposite (b).....82
Figure 5.28: Nyquist plots obtained at bare GCE, MWCNTs-GCE, MWCNTs-IL-GCE and MWCNTs-IL-L-lysine-GCE 83
Figure 5.29: Cyclic voltammograms of PDN at GCE (black curve), MWCNTs-GCE (green curve), MWCNTs-IL-GCE (blue curve) and MWCNTs-IL-L-lysine-GCE (red curve) electrodes 85
Figure 5.30: Cyclic voltammograms of 0.1 M PDN obtained in the pH 6.0-pH 9.0 values of 0.2 M PBS (a); plot of $I/\mu A$ vs pH (inset) and plot of $I/\mu A$ vs deposition time (b).....86
Figure 5.31: Cyclic voltammogramms (a-d) of 0.1 M PDN (in 0.2 M PBS, at 50 s) on bare GCE, MWCNTs-GCE, MWCNTs-IL-GCE and MWCNTs-IL-L-lysine-GCE, respectively. The plots of the $I/\mu A$ vs. [V/s] (e) as well as $I/\mu A$ vs. $[V/s]^{1/2}$ (f).....88
Figure 5.32: DPV voltammogram of MWCNTs-IL-L-lysine-GCE in varying concentration of PDN (0.4 µM -1.4 µM) (a). Plot of $I/\mu A$ vs. [µM] (b).....89
Figure 5.33: DPV voltammogram of PDN in the presence of potential interferences 91
Figure 5.34: Schematic illustration of the electrochemical detection of the of TBS at the TiO_2-MWCNTs-IL-GCE surface.....93
Figure 5.35: TGA curves of MWCNTs, TiO_2NPs and TiO_2-MWCNTs-IL nanocomposite samples (a). FTIR spectra of TiO_2NPs (Black curve) and TiO_2-MWCNTs-IL nanocomposites (red curve) samples (b) 94
Figure 5.36: SEM images of (a) TiO_2NPs, (b) TiO_2NPs supported on MWCNTs and (c) IL functionalised TiO_2-MWCNTs nanocomposite.....95
Figure 5.37: TEM images of MWCNTs (a), TiO_2NPs (b), TiO_2-MWCNTs (c) and TiO_2-MWCNTs-IL nanocomposite (d).....96
Figure 5.38: Nyquist plots of EIS obtained at MWCNTs-TiO_2-IL-GCE (a), MWCNTs-GCE (b) and MWCNTs-TiO_2-GCE (c) performed in 0.5 mM $[Fe(CN)_6]^{3-/4-}$ containing 0.1 M KCl

(Conditions; frequency range of 0.1 Hz to 10000 Hz, voltage amplitude of 0.01 V_{RMS} and scan rate of 0.05 V_{RMS}) 97
Figure 5.39: (a) CVs of TBS at bare GCE (black curve), MWCNTs-GCE (red curve), MWCNTs-TiO_2-GCE (blue curve) and MWCNTs-TiO_2-IL-GCE (green curve) electrodes under optimal experimental conditions; (b) Comparison of the anodic peak-currents obtained at each electrode.....98
Figure 5.40: Influence of pH of 0.1M KPBS on the anodic peak-current of TBS at bare GCE (a), plot of anodic peak-currents against pH (b) and plot of peak potentials against pH (c) ...99
Figure 5.41: Effect of accumulation time on the peak-current response of TBS at bare GCE surface (a). Plot of anodic peak-current vs. time (b).....100
Figure 5.42: Cyclic voltammograms of 0.1 M TBS in 0.1 M KBPS (pH 7) at different sweep rates (0.07 V/s-0.15 V/s) (a); Plot of peak-currents vs scan rates (b).....101
Figure 5.43: Cyclic voltammograms of 0.1 M TBS at MWCNTs/GCE, MWCNTs/TiO_2/GCE and TiO_2/MWCNTs/IL/GCE, respectively (a-c), with their respective plots of I/µA vs. V/s(inset) and plot of log (I/µA) vs log (V/s) obtained at the TiO_2-MWCNTs-IL-GCE sensor (d).....102
Figure 5.44: DPV curve of TiO_2-MWCNTs-IL-GCE at different concentrations of TBS (a). Plot of anodic peak-current vs. concentration of TBS (b) 104

SYMBOLS AND ABBREVIATIONS

TPN	Theophylline
SAL	Salbutamol
PDN	Prednisolone
TBS	Terbutaline sulfate
CV	Cyclic voltammetry
CVs	Cyclic voltammograms
DPV	Differential pulse voltammetry
EIS	Electrochemical impedance spectroscopy
GCE	Glassy carbon electrode
CPE	Carbon paste electrode
NPs	Nanoparticles
ZnONPs	Zinc oxide nanoparticles
$CoFe_2O_4$NPs	Cobalt ferrite nanoparticles
Fe_3O_4	Magnetite
TiO_2NPs	Titanium oxide nanoparticles
CNTs	Carbon nanotubes
MWCNTs	Multi-walled carbon nanotubes
SWCNTs	Single-walled carbon nanotubes
IL	Ionic liquid
Cyt-c	Cytochrome c

NiO	Nickel oxide
TEM	Transmission electron microscope
TGA	Thermogravimetric analysis
XRD	X-ray diffraction
FTIR	Fourier transform infrared spectroscopy
BET	Brunauer-Emmett Teller
HPLC	High-performance liquid chromatography
LC	Liquid chromatography
GC	Gas chromatography
HPTLC	High-performance thin-layer chromatography
TLC	Thin layer chromatography
UV	Ultra-violet
MS	Mass spectroscopy
CE	Capillary electrophoresis
DMF	N, N dimethyl formamide
PBS	Phosphate buffer solution
KPBS	Potassium phosphate buffer solution
ABS	Acetate buffer solution
LOQ	Lowest limit of quantification
LOD	Lowest limit of detection
RSD	Relative standard deviation

PUBLICATIONS

1. **Joan Chepkoech Kilele,** Rajasekhar Chokkareddy, Nicholas Rono, Gan G Redhi, 2020 "A novel electrochemical sensor for selective determination of theophylline in pharmaceutical formulations" **Journal of the Taiwan Institute of Chemical Engineers**; Volume 111, Pages 228-238.

Manuscripts in Press

1. **Joan Chepkoech Kilele,** Rajasekhar Chokkareddy, Gan G Redhi **"**Ultra-sensitive Sensor for Salbutamol by Utilising Lipase- $CoFe_2O_4$-MWCNTs Nanocomposite Modified Glassy Carbon Electrode." Submitted to **Materials Chemistry and Physics**

CONFERENCES

1. **Joan Chepkoech Kilele,** Rajasekhar Chokkareddy, Gan G Redhi **"**Ultra-sensitive Sensor for Salbutamol by Utilising Lipase- $CoFe_2O_4$-MWCNTs Nanocomposite Modified Glassy Carbon Electrode." **5th Interdisciplinary Research and Innovation Conference 2020,** held by Durban University of Technology, Durban, South Africa, 15-17 September 2020.

THESIS OUTLINE

CHAPTER 1: Introduction, aims and objectives.

CHAPTER 2: Deals with detailed literature review on asthma, prevalence, anti-asthma drugs, previous work on detection of these drugs and nanomaterials used for fabrication of the sensors

CHAPTER 3: Theoretical principle of voltammetry techniques as well as the electrochemical sensors

CHAPTER 4: Outlines the methodology employed in this study including materials and reagents, instrumentation, synthesis, characterization, preparation of each standard solutions, buffer solutions, nanocomposites and fabrication of working electrodes, electrochemical measurements and real samples analysis.

CHAPTER 5: Results and general discussion on characterization, optimization of experimental parameters, electrochemical behaviour of each drugs on the developed sensors, application on real sample analysis and method validation studies.

CHAPTER 6: Summary and conclusion.

REFERENCES

APPENDIX

CHAPTER 1

1 INTRODUCTION

1.1 Background information

Asthma is a chronic respiratory-related disease affecting individuals of all ages often throughout their entire lives (Bateman et al., 2008). This disorder is characterized by bronchial inflammation and airway hypersensitivity that leads to frequent occurrences of airway obstruction. The main features of this disease are cough, shortness of breath and wheezing (Valizadeh et al., 2021). Nowadays, it is commonly reported among children globally and is projected to affect approximately 339 million people worldwide (Morales, 2018). In addition, it is predicted to increase by the year 2025 owing to the rising effects of urbanization (Bissell et al., 2019, Adeloye et al., 2013, Dharmage et al., 2019). Recently published report show that South Africa's asthma commonness rate ranks 25th in the world and 5th in terms of asthma fatality (Masekela et al., 2018, Lion-Cachet et al., 2021). The alarming prevalence and severity (both in the developing and developed countries) is a major concern as it causes long term health problems to the asthmatic patients and a heavy economic burden (de Roos et al., 2018). Various factors triggering asthma attacks include allergens, air pollution, strong odours, cigarette smoke, seasonal changes, drugs such as beta-blockers and nonsteroidal anti-inflammatory drugs (Baldacci et al., 2019). Previous studies in South Africa reported that some diseases such as obesity appear to be risk factors for the development of asthma (Masekela et al., 2018).

Early diagnosis and medication of asthma significantly reduces the related morbidity and fatality rates. Use of anti-asthma drugs is still the most efficient preference for management of both mild and chronic asthma conditions. Currently, the key asthma therapy is classified into two categories (Barnes, 2006, Bonini et al., 2020);

a) Relievers such as methylxanthines and β_2-adrenoceptor agonists
b) Controllers such as corticosteroids and antileukotrienes

The β_2-adrenoceptor agonists used as bronchodilators are the most effective treatment available to prevent and to dilate bronchi and hence relieve the symptoms. These drugs include salbutamol, terbutaline and formoterol (Sears et al., 2005), and are also prescribed for treatment

of other airway ailments including chronic obstructive pulmonary diseases (Al Majidi et al., 2019). They are available in different dosage forms such as tablets, syrups, inhalers and injections. Unfortunately, most of them are illegally used to promote growth and as fattening agents at high doses in livestock and poultry (Zhou et al., 2017a, He et al., 2020). The limitations of β_2-agonists are the side effects that might take place within the therapeutic range or adverse effects due to overdose. They include nausea, headache, tremors, tachycardia, and peripheral vasodilation and sometimes may be fatal (Bonini et al., 2020, Li et al., 2020). Methylxanthines such as theophylline have both anti-inflammatory and bronchodilation properties at low doses thus are used in treatment of severe asthma (Sankar et al., 2008, Cazzola et al., 2020). Theophylline is prevalently used worldwide because it is relatively cheap and available; however, excessive intake causes heartburn, coma and cardiac arrest (Makino et al., 2004, Gan et al., 2018). Corticosteroids such as prednisolone are used as the first line treatment of asthmatic patients in combination of bronchodilators to treat the underlying inflammation (Sears et al., 2005). In addition, athletes also extensively abuse them. Long-term intake of these corticosteroids causes adverse side effects including weight gain, hypertension, cataract, peptic ulceration and diabetes mellitus (Primpray et al., 2019).

Robust, precise and accurate analytical approaches for quantitative analysis of these medications in pharmaceutical forms (tablets, suspension as well as capsules), bio fluids (such as blood, urine and serum) as well as in other samples is essential to investigate the cases of side effects and drug interactions. Generally, this is because of the wide range usage of the selected drugs and lower range of approved concentration in plasma (Chen et al., 2016, Baytak et al., 2016, Feng et al., 2018). Besides, quantitative investigation of these medications in their commercial preparations is essential for fruitful quality control. Theophylline is naturally present in foods such as cocoa, consequently, it is necessary to develop an accurate, straightforward and fast method to quantify theophylline in food products (Bartella et al., 2019). Salbutamol and terbutaline are also used as doping drugs and are among the forbidden list of drugs by World Anti-Doping Agency (WADA) and International Olympic Committee (IOC) (Goyal et al., 2009a, Lee et al., 2018, Zvereva et al., 2018a). In addition, the alarming increase in abuse of salbutamol to boost growth in livestock/poultry is becoming a major concern worldwide (Zvereva et al., 2018b, Ni et al., 2014). Residues of these drugs and their metabolites raise a major concern as it poses potential health hazards to humans through the consumption of animal products. On this basis, it is necessary to develop simple analytical

method that offer economical instrumentation for real-time qualitative and quantitative determination of these anti-asthma drugs.

Literature review reveals that a number of methods including chromatographic, spectroscopic and electroanalytical techniques have been described for the assay of the above mentioned anti-asthma drugs in biological, drug dosages as well as other sample matrices such as food products (Díez et al., 2018, Huck et al., 2005a, Kalyani et al., 2018). These techniques are used for both qualitative and qualitative analysis with satisfactory selectivity, sensitivity and reproducibility. However, most of these analytical techniques such as separation-based methods suffer from a number of limitations such as:

i. require relatively expensive instrumentation
ii. highly trained personnel to run the instruments
iii. tedious and time consuming sample preparation steps, which involves the use of solvents that may contaminate the environment making them inappropriate for regular analysis (Sousa et al., 2019, Aydin et al., 2019)

Thus, it is critical to devise other methods for determination of these anti-asthma medications by using readily obtainable and relatively low cost cheap materials that are safe to the environment. Electrochemical approaches for the detection of these anti-asthma medications and other electro-active substances are increasing. Electroanalytical methods are distinguished by their superior sensitivity, minimal or no sample preparation methods and extremely low LODs compared to commonly used chromatographic procedures. Additionally, electroanalytical instruments are relatively low cost and portable hence may be used selectively for everyday analysis of drugs in their drug dosages and body fluids (de Lima et al., 2020, Shaikshavali et al., 2020a).

Regrettably, the traditional unmodified working electrodes like glassy carbon electrode are not suitable for detection of the chosen anti-asthma drugs due to insignificant electrochemical response (Li et al., 2017a). To overwhelm these inconveniencies, it is vital to use appropriate single nanomaterials for instance metal oxides, polymers and carbon nanotubes or a combination of these nanomaterials to modify the bare electrode surface to enhance electrochemical performance (Jadon et al., 2016). A nanocomposite is a combination of two or more different nanomaterials, owning sizes in nanometres range (Pal, 2020). Combination of the different properties of these multi-functional nanomaterials leads to fabrication of novel

nanocomposite with augmented both physical and chemical properties (improved conductivity, enhanced effective surface area, high selectivity and stability) (Singh et al., 2013, Khoshroo et al., 2019, Dakshayini et al., 2019b). These nanocomposite materials have attracted attention in the fabrication of cheap and safe sensors/biosensors for electrochemical sensing applications. Nanocomposites based sensors exhibit superior sensitivity with very low LODs even at trace concentration levels (Rezvani et al., 2019). The remarkable electrochemical performance as compared to the solid electrodes or to those electrodes modified with one nanomaterial is because of the synergistic effects (Pal, 2020, Dakshayini et al., 2019b).

Among the carbon nanotubes, multi-walled carbon nanotubes (MWCNTs) are extensively utilized to modify the electrode surface in electrochemical sensor fabrication due to their excellent electro-catalytic performance (Shalauddin et al., 2019). The combination of MWCNTs with metal oxides and other novel nanomaterials is useful for constructing hybrid nanocomposites with captivating novel properties (Mallakpour et al., 2016). As is well known, metal oxides nanoparticles such as ZnONPs (Shaikshavali et al., 2020a), TiO_2NPs (Munir et al., 2019) and $CoFe_2O_4$NPs (Shaterian et al., 2020), have been synthesized and used for the design of electro-catalytic sensors. The electrodes modified with metal oxide nanocomposites show enhanced electro-catalytic effect in comparison with unmodified electrodes owing to the exceptional properties of the metal oxide nanoparticles.

The sensitivity and overall performance of enzymatic/protein biosensors has improved tremendously owing to incorporation of nanomaterials such as carbon nanotubes and metal oxides in their fabrication (Lopes et al., 2017). Enzymes are used as bio recognition agents because they provide outstanding selectivity for their targeted substrate and have high catalytic activity (Liu et al., 2019b, Erkmen et al., 2020, Kurbanoglu et al., 2020).

Ionic liquids (ILs) based composites have also received extensive attention in electrochemical detection considering their remarkable properties including low cost, and outstanding conductivity and thermal stability (Bijad et al., 2013, Shabani-Nooshabadi et al., 2016). Shabani-Nooshabadi et al. (2016) modified carbon paste electrode with NiO/graphene oxide/IL nanocomposite for detection of sulfamethoxazole. The proposed sensor showed good electro-catalytic activity with lower LOD of 0.04 μM (Shabani-Nooshabadi et al., 2016). A new approach for determination of dihydro-nicotinamide adenine dinucleotide (NADH) using IL-MWCNTs-magnetite nanocomposite was developed. The MWCNTs and IL provided a

platform for Fe_3O_4 nanoparticles with high conductivity. The LOD and LOQ of the proposed sensor was 34.6 nM and 0.115 µM respectively (Atta et al., 2017).

In this study, therefore, a novel approach to modify the GCE with ZnO-MWCNTs-Cytochrome c, MWCNTs-$CoFe_2O_4$-Lipase, MWCNTs-IL-L-lysine and TiO_2-MWCNTs-IL nanocomposites for detection of theophylline, salbutamol, prednisolone and terbutaline, respectively, in pharmaceutical formulations is presented. The proposed sensors combine the characteristic features of its individual components towards electro reduction/oxidation reaction of the drugs under study. None of the reviewed articles reported on the detection of the proposed drugs in drug dosages using the fabricated sensors via DPV and CV.

The working electrode, GCE, is extensively used because its surface can be easily renewed and modified to increase the electro-active surface area and the active adsorptive sites (Gholivand et al., 2019a). Selectivity and sensitivity of the measurements greatly depends on the surface area of the GCE (Miraki et al., 2019). Modification increases the surface area of GCE, which accelerates the electrochemical redox reactions due to rapid electron transfer rate. As a result, high peak-currents are recorded at the same time over potentials of redox reactions may change in relation to electro catalysis process. Voltammetry techniques have been employed for detection of these anti-asthma drugs and numerous other electro-active compounds (Afzali et al., 2019). These techniques are vastly selective and sensitive towards detection of electro-active species with lower LODs over a wide linear range. In addition, they are portable, uses small sample volumes (5-10 µL) as well as relatively low cost instrumentation (Naveen et al., 2017, Kalambate et al., 2016).

CV is one of the most effective methods for studying the electrochemical behavior of electro-active substances in the voltammetry method. This is because it can quickly locate the redox potential of an electro-active analyte. DPV is a fast method with excellent analytical sensitivity, thus it can be used for simultaneous detection of electro-active substances with close redox potentials. Recorded peak-current is proportional to the analyte's concentration; hence, this makes it possible to estimate its concentration.

In this work, synthesis (of ZnONPs, $CoFe_2O_4$NPs and TiO_2NPs) and the application of novel nanocomposite-based modified GCE sensors for quantification of four proposed drugs is described. CV was employed to investigate the electrochemical behavior of each selected drug, while DPV was used for quantitative analysis. The electro-catalytic ability of the developed sensors was investigated on real pharmaceutical dosage samples.

1.2 Problem statement

Worldwide, the prescriptions for asthma drugs are on the rise (Khakban et al., 2019, Allen et al., 2019). However, anti-asthma drugs have side effects and can lead to fatal death at higher doses. Quite often, these drugs are abused as growth promoters in poultry/livestock as well as by athletes to enhance their performance (Lomae et al., 2019, Chang et al., 2018).Consequently, it is vital to design uncomplicated, portable, rapid and highly sensitive means of detecting these anti-asthma drugs in pharmaceutical formulations and other sample matrices. Electrochemical sensors represent alternative methods to conventional analytical techniques based on separation, for instance high performance liquid chromatography, which requires long and tedious extraction, pre-concentration and clean up steps. In addition, they are expensive, require highly trained personnel to operate, and require the use of harmful reagents known to generate huge amount of non-environmental friendly chemicals. Hence, the whole process is expensive and unaffordable at most resource-limited research facilities. The proposed electrochemical sensors will offer an affordable cost of analysis of the selected asthma drugs in any sample matrix. This will, in turn, improve financial viability, outlook and control in many of the health facilities and pharmaceutical industries.

The nano-composite based electrochemical sensors offer further advantages such as inexpensive field sensors that can sensitively, selectively and routinely detect a series of target compounds present in various sample matrices such as food without (or with reduced) sample pre-treatment. Furthermore, development of highly sensitive and selective method will provide more precise and accurate results for quality and doping control. Health and overall wellbeing of asthmatic patients and non-patients may be improved.

1.3 Aim

To fabricate electrochemical sensor/biosensors based on nanocomposites for the quantification of theophylline, prednisolone, terbutaline and salbutamol in their pharmaceutical formulations using novel nano-materials with good electro-catalytic activity and conductivity.

1.4 Objectives

- To synthesize and characterise titanium oxide (TiO_2), zinc oxide (ZnO) and cobalt ferrite ($CoFe_2O_4$) nanoparticles and their respective nanocomposites.
- To fabricate glassy carbon electrode with potent electrode modifiers acting as electro-catalysis agents towards the drugs under investigation.
- To study the electrochemical behaviour of each drug at the fabricated working electrodes under optimized working conditions via cyclic voltammetry technique.
- To determine the sensitivity, selectivity, stability, reproducibility and repeatability of the developed sensors using the differential pulse voltammetry method.

CHAPTER 2

2 LITERATURE REVIEW

This chapter attempts to discuss the four anti-asthma drugs, namely; prednisolone, theophylline, terbutaline and salbutamol under study, analytical methods developed for quantitative and qualitative study of the previously mentioned medications enlightening their benefits along with limitations. In addition, the nanomaterials used for fabrication of the four electrochemical sensors are discussed.

The key asthma medications are; **bronchodilators** (beta-agonists) primarily used to reverse bronchoconstriction in order to relieve the symptoms and **corticosteroids** used to treat the underlying airway inflammation. Since asthma is a chronic persistent disease, the affected individual uses these medicines on a long-term basis. Beta agonists include salbutamol, terbutaline, theophylline among others; they are used in combination of corticosteroids such as prednisolone and with other drugs including ephedrine injection in treatment of asthma.

2.1 Bronchodilators

These compounds are categorised as phenylethanolamines. They have various substituent groups on the aromatic group as well as terminal amino group. Generally, they are used to reverse the airway contraction associated with exacerbation of asthma and other pulmonary related infections. They are classified into three categories based on different substituents;

i. Phenolic group such as salbutamol
ii. Resorcinol group such as terbutaline
iii. Aniline containing group, which include clenbuterol

2.1.1 Salbutamol

Salbutamol (SAL) also known as albuterol [2-(tert-butylamino)-1-(4-hydroxy-3-hydroxy methylphenyl) ethanol], is a short acting β_2-adrenergic receptor agonist. It has phenolic hydroxyls and ethanol amine substituents groups on the aromatic ring (Figure 2. 1) (Chen et al., 2016). The existence of a chiral center in SAL structure results in S- and R-enantiomers which allows it to be administered (orally, parenteral or inhaled) as an equal racemic mixture (R-) and (S-) (Jacobson et al., 2003). (R-) has bronchodilator effects whereas (S-) is reported to have no bronchodilation properties. It works by dilating the bronchi and as a result relaxes

the bronchial muscles hence improves breathing in asthma patients. It is widely prescribed for the cure of acute airway ailments such as asthma (including acute and severe, exercise induced and childhood) and chronic obstructive pulmonary diseases (Moore et al., 2019, Bateman et al., 2008). SAL is often the first line therapy in most patients as it offers a rapid bronchodilation effects (Cordell et al., 2018). Furthermore, it is illegally used in livestock as feed additive to promote growth hence it is a threat to food safety and the environment (He et al., 2020, Zhang et al., 2016). Excessive dosage and intake of SAL for a long period is reported to cause regular and troublesome side effects such as tremor, hypertension, palpitations, tachycardia, peripheral vasodilatation and nausea (Li et al., 2020, Guo et al., 2017).

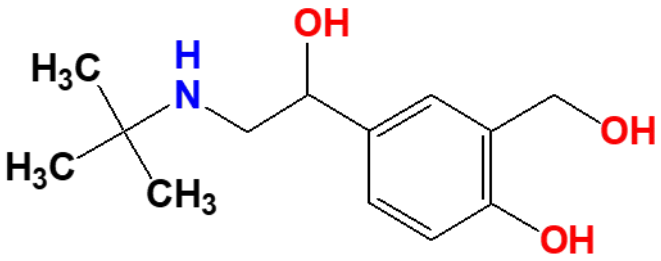

Figure 2.1: **Chemical structure of salbutamol**

Electrochemical reaction of SAL is by oxidation of the OH group on its aromatic ring to form dimers that can be adsorbed on the surface of the electrode (Figure 2. 2). By electrochemical analysis, the main anodic peak recorded is due to one-electron/proton oxidation of the OH group on the aromatic ring (Li et al., 2017a).

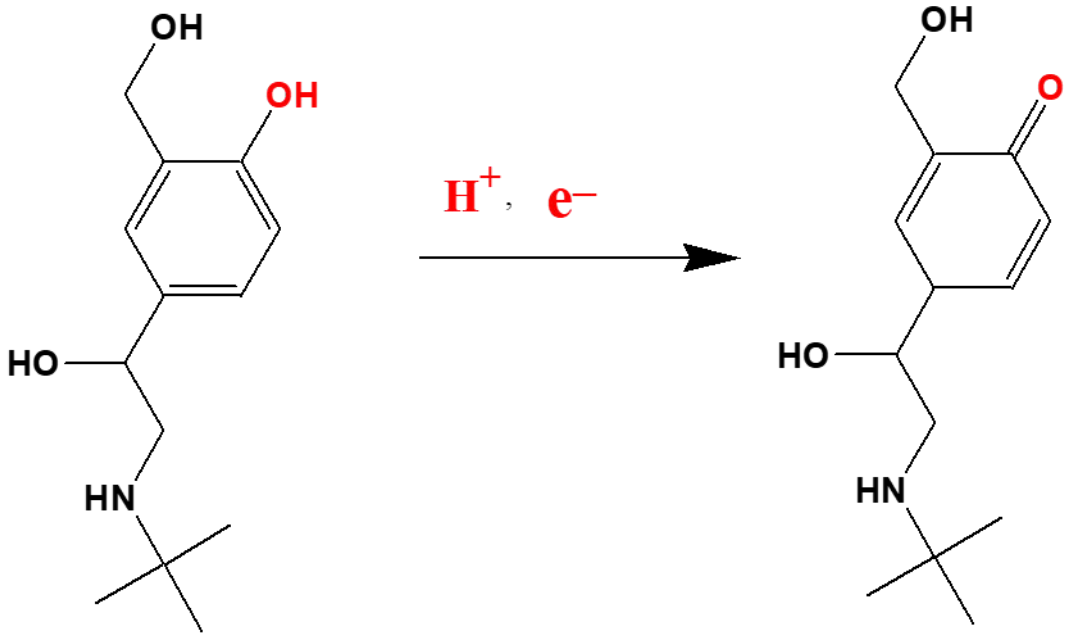

Figure 2.2: **Electrochemical oxidation mechanism of salbutamol**

Quantitative determination of SAL drug is essential for routine analysis, clinical pharmacology studies as well as for doping detection and food quality control analysis. A comprehensive literature survey reveals that the reported analytical methods for quantitative analysis of SAL alone or in combination with other drugs in food products, pharmaceutical formulations and other samples are:

i. chromatography based methods (Yan et al., 2012, Wu et al., 2011b)
ii. spectroscopy methods (Kalyani et al., 2018, Cheng et al., 2018, Zhai et al., 2017)
iii. immunoassays (Fang et al., 2019, Xu et al., 2015, Liu et al., 2018)
iv. capillary electrophoresis (Wang et al., 2010)
v. electroanalytical techniques (Lin et al., 2016, Lomae et al., 2019, Guo et al., 2017, Chen et al., 2016)

These techniques have been used to detect SAL with sufficient precision, sensitivity and selectivity. However, most of these techniques have a number of deficiencies such as requirement of sophisticated and costly equipment. In addition, they usually require long and tedious sample preparation steps and in the process may generate harmful chemical wastes (Lin et al., 2016). Therefore, it is vital to fabricate a safe, rapid, selective, sensitive and relatively cost effective means of detecting SAL in drug forms and other sample matrices at trace concentrations. The electroanalytical techniques are extremely selective and ultra-sensitive. In addition, these methods are rapid, simple to operate and are cost-effective as compared to chromatography based and spectroscopy methods.

Currently, varieties of unique nanomaterials are used in modification of the working electrodes to enhance electrochemical sensing performance of the fabricated sensors. For instance, nano-catalysts with a combination of spinel ferrites, carbon nanotubes and bio-recognition elements were recently exploited in the fabrication of biosensors due to the benefits of the synergistic effect arising from the nanocomposite materials (Sobczak-Kupiec et al., 2016, Ensafi et al., 2019, Dong et al., 2017). $CoFe_2O_4$NPs, in particular, has been reported to be an effective electro catalyst for sensing various analytes owing to its excellent electro-catalytic activity, good biocompatibility, low cost and the easy synthesis methods (Shanmugam et al., 2020).

In the last decade, carbon nanotubes such as MWCNTs have become attractive nanomaterials in electro analysis because of their outstanding semi-conductor, mechanical and chemical properties. It has extensively been used to improve the catalytic behaviour of metal oxides and

other electrode modifiers for electrochemical determination of pharmaceuticals. Due to the combination of the exceptional properties of functionalized MWCNTs and the excellent electro-catalytic activity of $CoFe_2O_4$NPs, stabilizing $CoFe_2O_4$NPs on MWCNTs can significantly accelerate the electrochemical oxidation of SAL (Taei et al., 2016). MIP/Ag-N-RGO/GCE sensor was fabricated by Li et al. (2017a) for quantification of SAL in urine and pork samples. The invented MIP/Ag-N-RGO/GCE displayed excellent sensitivity with good percentage recovery rates in the range of 98.9 % - 105.3 %. He et al. (2020) recently devised a colorimetric immunoassay for quantification of SAL. The developed method showed extraordinary sensitivity with LOD of 26.14 pg/mL.

2.1.2 Terbutaline

Terbutaline sulfate (TBS) [2-tert-butylamino-1-(3, 5-dihydroxyphenyl) ethanol hemisulfate], a selective β_2-adrenoceptor agonist, is used as a bronchodilator to treat asthma, bronchitis as well as an anti-contraction agent during preterm birth (Gopal et al., 2018a, Zhou et al., 2017a). Its available dosages can be administered through injection, oral consumption or by inhalation (Sayed et al., 2013). An overdose and prolong use of TBS can lead to bothersome side effects such as tremor, tachycardia, cephalalgia, intestinal problems and sometimes it can be deadly (Liu et al., 2014). Furthermore, TBS is reportedly abused as feed additive to stimulate growth in cattle as well as by athletes to improve their performance (Costa et al., 2018, Kalambate et al., 2017).

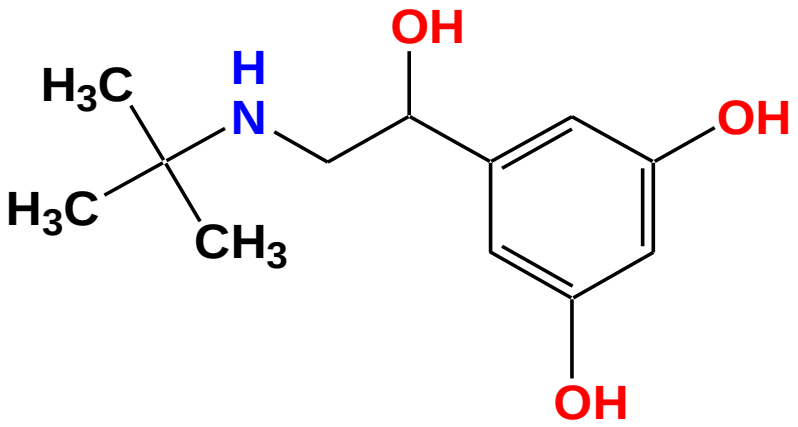

Figure 2.3: **Chemical structure of terbutaline**

Analytical determination of TBS in food, drug dosages and body fluid samples has been done using various methods. These techniques include; chemiluminescence (Han et al., 2012b), chromatography (Herring et al., 2000, Lomae et al., 2019, Zhou et al., 2017b), capillary electrophoresis (Li et al., 2009b), spectrophotometry and electrochemical methods (Kalambate

et al., 2017, Baytak et al., 2016, Li et al., 2012). Although the above-mentioned methods are effective, the instruments involved are costly, require highly skilled personnel to run them and time-consuming sample preparation procedures. Therefore, the whole process is tedious, and expensive to employ for detection of TBS. Electrochemical sensing methods using working electrodes modified with potent nanocomposite based modifiers are expedient since they are rapid, relatively cost effective, have superior sensitivity and easy to operate.

TBS structure (Figure 2. 3) contains hydroxyl groups on the aromatic ring as electro-active centres hence it can be analysed via electrochemical techniques. TBS can undergo electrochemical oxidation of OH group present on its aromatic ring whereby equal protons and electrons takes part in the oxidation reaction (Li et al., 2012, Gopal et al., 2018a) (Figure 2. 4).

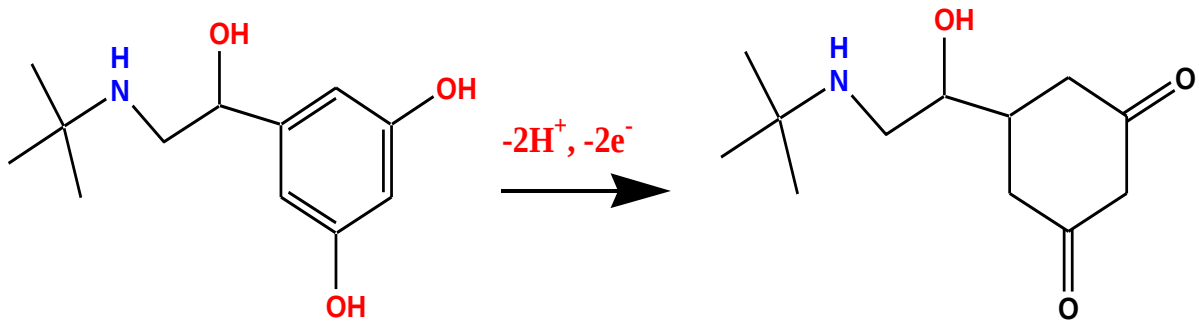

Figure 2.4: **Electrochemical oxidation mechanism of terbutaline**

To date, few voltammetry reports using nanocomposite-modified GCE for detection of TBS in single dosage or in combination of other pharmaceuticals have been reported. GCE modified with carbon nanotubes and europium oxide NPs was recently developed for detection of TBS. The fabricated sensor exhibited excellent sensitivity which was estimated to be 0.2557 μA/μM (Teker et al., 2019). In addition, MWCNTs/graphene-GCE sensor was designed for electrochemical sensing of TBS in its drug dosage sample (Gopal et al., 2018a). The estimated LOD and LOQ was 6.527×10^{-7} M and 2.175×10^{-6} M, individually (Gopal et al., 2018a). The unmodified GCE recorded a small oxidation peak, which is attributed to slow transfer of electrons. Therefore, it is necessary to utilize other electro catalysts with unique and multi-functional properties, to promote rapid transfer of electrons thus achieve excellent sensitivity, lower LOD and LOQ values.

Literature review scrutiny reveals that there is no report describing the use of GCE modified with TiO_2-MWCNTs-IL nanocomposite for determination of TBS in pharmaceutical

formulations. TiO_2 is a photocatalytic semiconductor. Because of its good biocompatibility, large band gap and easy functionalization, it is extensively used in the fabrication of sensors/biosensors for various applications (Perillo et al., 2012). Ru/TiO_2/MWCNTs nanocomposite-modified CPE was used to detect cetirizine in urine and drug samples (Shetti et al., 2019c). A lower LOD of approximately 3.10 nM was achieved (Shetti et al., 2019c). MWCNTs have outstanding properties such as exceptional electrical conductivity due to their large substantial surface area, which enhances electro-catalytic activity hence have been used effectively as electrochemical sensing nanomaterials (Cheng et al., 2020, Munir et al., 2019).

Another approach to improve the sensitivity of the TiO_2-CNTs nanocomposite-based sensors is by incorporating highly conductive ILs (Mohamed et al., 2019). According to previous research, the TiO_2-MWCNTs nanocomposite coupled with ILs could speed up transfer of electrons therefore increasing detection sensitivity. The superb electrochemical sensing performance of the proposed TiO_2-MWCNTs-IL nanocomposite is through synergistic effect.

2.2 Methylxanthines

These are groups of compounds that belong to the alkaloid class; mainly the purine as they have nitrogen atoms in their structure. They are named based on the existence of various number and location of the methyl groups in the purine structure. Theophylline (1, 3-dimethylxanthine), caffeine (1,3,7-trimethylxanthine) and theobromine (3, 7-dimethylxanthines) are some of them.

Theophylline (TPN) is a type of methylxanthine found naturally in tea, coffee as well as cocoa beans (Bartella et al., 2019). TPN molecule contains three active sites (two methyl and an amino group) and is reportedly electro-active due to existence of amino-group in its structure (Figure 2. 5) (Sun et al., 2006). It is substantially used as a bronchodilator to remedy illnesses like emphysema and asthma (Cazzola et al., 2012, Wang et al., 2018a). The accepted curative concentration of TPN is in the range of 5-20 µg/mL. Concentrations higher than 20 µg/mL are reported to be poisonous and might cause detrimental complications including cardiac arrest, seizures and vomiting (Mahemuti et al., 2018, Calzetta et al., 2018, Ganjali et al., 2018). Consequently, it is of utmost importance to determine the concentration of TPN in drug doses using a fast, relatively inexpensive and precise technique.

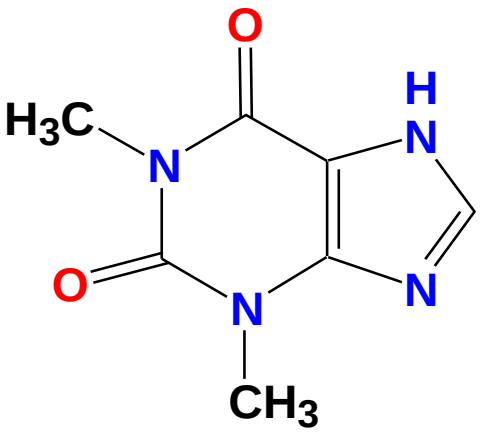

Figure 2.5: **Chemical structure of theophylline**

Various methods have been utilized for detection of TPN including electroanalytical methods, capillary electrophoresis, spectrometry and chromatographic approaches (Badea et al., 2017, Bartella et al., 2019, Oellig et al., 2018, Li et al., 2009a, Ma et al., 2009, Zhuang et al., 2017, Park et al., 2014, Kesavan et al., 2019, Chen et al., 2018). Although spectrometric and chromatographic methods have presented reliable results for quantitative analyses of TPN, they suffer from a few inadequacies like expensive and sophisticated equipment, long sample preparation procedures and the use of large amounts of harmful solvents (Chen et al., 2020). In addition, they are not suitable for regular testing due to their low sensitivity and selectivity and (Gan et al., 2017). Alternatively, the electrochemical approach provides a practical and fast means due to its high sensitivity, portability, relatively inexpensive equipment, and small sample size requirements (Shashikumara et al., 2020). In addition, the sample preparation procedures are fast, simple and sometimes are not required (Peng et al., 2017b).

Several electrochemical sensors/biosensors have been developed for sensing of electro-active analytes such as drugs based on different nanocomposite modifiers owing to their distinctive and multifunctional properties (Goud et al., 2019a, Kumar et al., 2019a). For example, Ca-ZnO/GCE (Kulkarni et al., 2020), ruthenium-TiO_2/reduced graphene oxide/CPE (Bukkitgar et al., 2020) and nano clay/CPE (Shetti et al., 2020) were reportedly used for determination of antihistamine, ambroxol and nimesulide medications, individually , in drug dosage forms and urine samples. In addition, Mg-ZnO/CPE and Ru-TiO_2/MWCNTs/CPE sensors have been reportedly used for quantification of flufenamic acid and mefanic acid, respectively, (Bukkitgar et al., 2019, Shetti et al., 2019d). The proposed electrochemical sensors provided exceptional sensitivity with much lower LOD compared to the other electrodes, as well as promising potential utilization in quantification of these drugs in real sample solutions.

Chokkareddy et al. (2020b) constructed an IL-based sensor for determination of pyrazinamide in pharmaceutical samples. The estimated LOD and LOQ of the sensor was 0.0102 µM and 0.3658 µM, respectively.

Metal oxide/MWCNTs composites have been expansively explored as electrochemical sensing platforms of electro-active compounds owing to their improved electro-catalytic activity (Shaikshavali et al., 2020b). Furthermore, the metal oxide/MWCNTs nanocomposites offers a biocompatible platform for immobilization of bio-recognition elements such as enzymes and proteins, in fabrication of biosensors (Ghanbari et al., 2019, Chokkareddy et al., 2017, Chokkareddy et al., 2018). Due to the synergistic effects between nanocomposite materials, these nanocomposites have proven critical in improving the electrochemical performance in sensing of pharmaceuticals (Dakshayini et al., 2019a).

Previous electrochemical work reveals that TPN is oxidized on the surface of working electrode to form 1, 3-dimethyluric acid (Figure 2. 6). The irreversible reaction mechanism of TPN involves two-electrons/protons (Bukkitgar et al., 2018, Quintanilla et al., 2016).

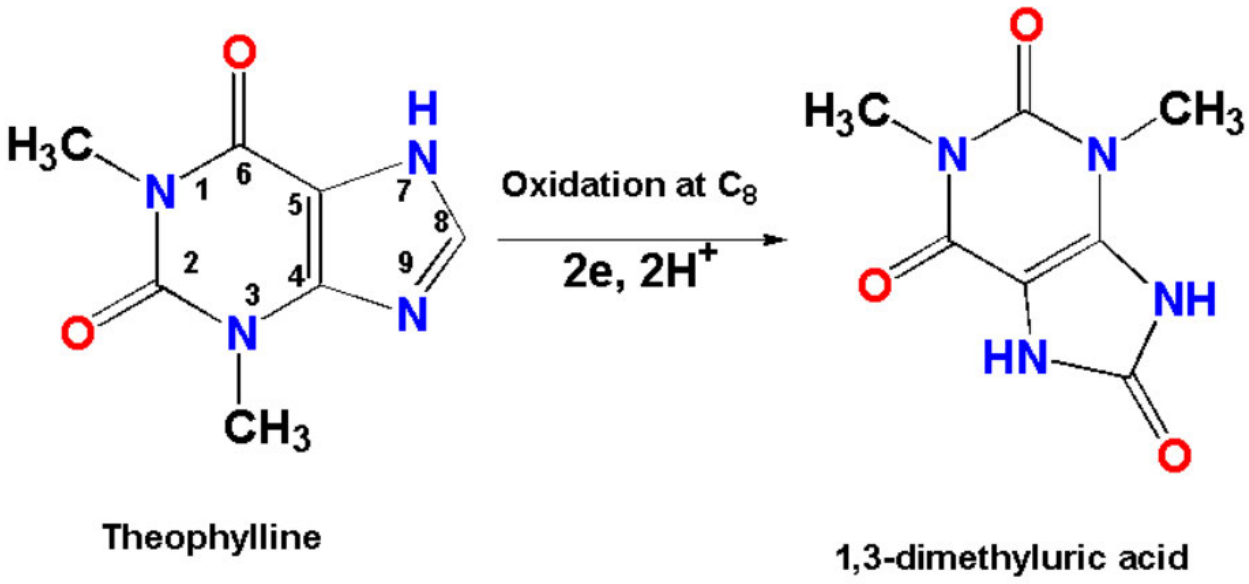

Figure 2.6: **Electro-catalytic oxidation mechanism of TPN**

Electrochemical response of TPN at the unmodified GCE is very poor due to sluggish transfer of electrons (Bandi et al., 2019, Janaj et al., 2019). Accordingly, it is necessary to modify the GCE surface with novel composites such as metal oxide/carbon-nanotube/enzyme nanocomposites, which are reported to have superb electro-catalytic activity. None of the reviewed articles has reported the electrochemical behaviour of TPN at the

ZnONPs/MWCNTs/Cyt c/GCE sensor. Therefore, the novelty of this work was to fabricate a ZnONPs/MWCNTs/Cytochrome c nanocomposite modified GCE for electrochemical detection of TPN via CV and DPV.

Zinc oxide (ZnO), a semi-conductor having a high excitation bond energy of 60 meV and a large band gap of 3.37 eV, has been used lengthily in the construction of novel modified electrodes for electrochemical sensing. The ZnONPs is a promising nanomaterial as an electro-catalyst due its low toxicity, superb stability, excellent conductivity, availability and it is relatively easy to synthesize (Shetti et al., 2019a, Bukkitgar et al., 2019). In the recent past, MWCNTs are suggested to be one of the most suitable carbon nanotubes for modification of solid electrodes due to their exceptional properties including its large surface area and its outstanding conductivity (Soylak et al., 2017, Soylak et al., 2013). The MWCNTs modified electrodes present enhanced electrochemical performance than the un-modified solid electrodes (Keerthika Devi et al., 2020).

Herein, MWCNTs was employed as platform for incorporation of ZnONPs as previously described in several studies (Mwafy et al., 2019, Mukdasai et al., 2016, Chokkareddy et al., 2019a). Cyt c was immobilized on the ZnONPs/MWCNTs modified GCE surface to fabricate a highly selective biosensor for TPN detection.

2.3 Corticosteroids

Corticosteroids were discovered in 1950s, and their anti-inflammatory properties have since been exploited to treat chronic asthma as effective controllers (Barnes, 2006). Examples of corticosteroids are dexamethasone and prednisolone. However, long-term usage and overdose of these medications may result to significant adverse side effects such as high blood pressure, diabetes, cataract and fluid retention to the asthmatic patient.

Prednisolone (PDN) (11b,17a,21-trihydroxy-pregna-1,4-diene-3,20-dione), is an artificial corticosteroid commonly prescribed for clinical treatment of a number of inflammatory conditions such as bronchial asthma and allergic reactions due to its anti-inflammatory and immunosuppressive properties (Mansur et al., 2020). The use of prednisolone can cause decreasing organ rejection before, during and after organ transplant (Arabi et al., 2016). An overdose intake of PDN may lead to hypertension, increase in weight, deterioration of diabetes as well as hindrance of growth in children (Goyal et al., 2009b). In addition, athletes are misusing PDN in sports and World Anti-Doping Agency (WADA) forbids its usage (Beotra et al., 2009, Touber et al., 2007).

PDN molecule reportedly has two electro-active sites in its structure that can undergo reduction and oxidation at negative and positive potentials, respectively (Figure 2. 7) (Rezaei et al., 2011). The reductive site of PDN molecule is more active and the suggested mechanism for electrochemical reduction of PDN is shown in Figure 2. 8. The electro-catalytic reduction process lead to the transfer of two protons and two electrons (Smajdor et al., 2016)

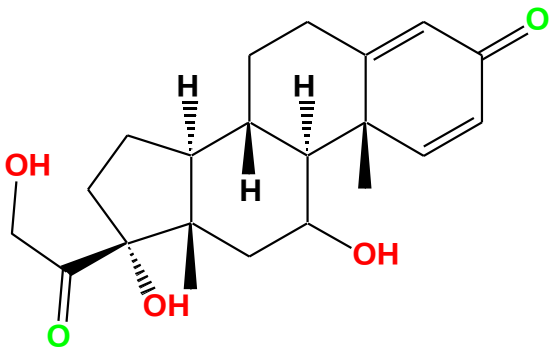

Figure 2.7: **Chemical structure of prednisolone**

The conventional analytical techniques widely used for detection of PDN in different sample matrices include chromatography-based techniques (Klinsunthorn et al., 2011, Limmatvapirat et al., 2012, AbuRuz et al., 2003, Fidani et al., 2013, Liu et al., 2016, Chitlange et al., 2011), UV spectrophotometry (Chitlange et al., 2011) and voltammetry (Goyal et al., 2009a, Yilmaz et al., 2007). The downsides of most of these conventional methods include the costly instrumentations and the time consuming sample preparation procedures (Primpray et al., 2019). An alternate and more practicable solution to these drawbacks is the application of electrochemical techniques. The popularity of these methods lies in the numerous advantages it offers, such as fast and simple to use equipment, increased selectivity as well as excellent sensitivity.

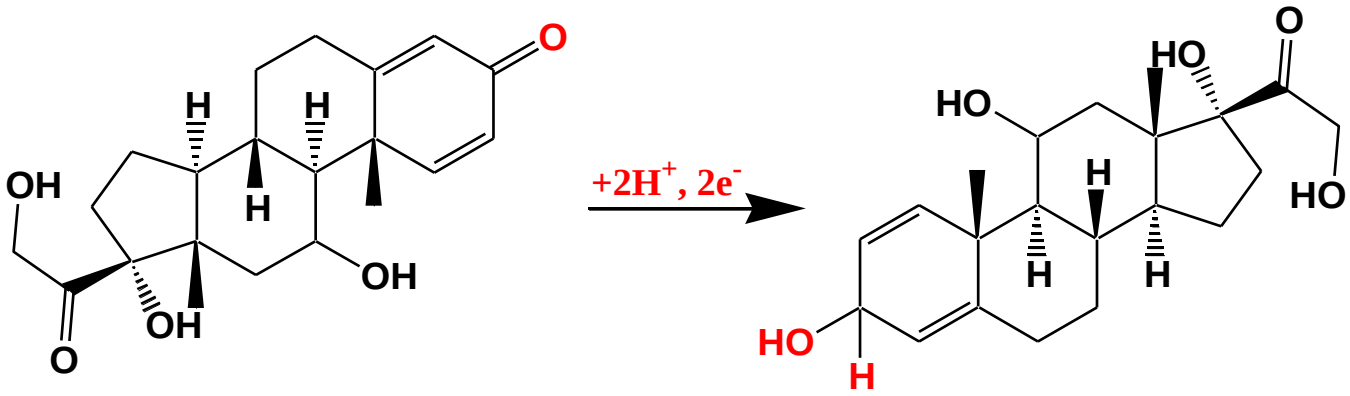

Figure 2.8: **Electrochemical reduction mechanism of prednisolone**

Nanocomposite based nanomaterials are being explored to incorporate in fabrication of modified electrode sensors for detection of PDN and other drugs because they offer a synergistic effect with improved electro-catalytic activity and conductivity. These sensors are reported to have high sensitivity along with reduced limits of detection. Modified convectional electrodes have shown good potential for prednisolone detection. Fullerene/C_{60} was used to modify gold electrode for detection of PDN. The LOD of the fabricated fullerene/C_{60}/Au sensor was calculated to be about 26 nM (Goyal et al., 2009b).

MWCNTs are one of the remarkable and most used CNTs in modification of electrodes because they possess exceptional properties suitable for electrochemical analysis. However, they are difficult to be dispersed in an aqueous solution and in numerous organic solvents because they tend to agglomerate (Shalauddin et al., 2019). To avoid this, various approaches have been employed such as chemical treatment with acids, ultra-sonification, functionalization with ILs, surfactants, polymers, or other nanomaterials (Mohamed et al., 2015).

Carbon nanotubes could interact with ILs through "cation–π" interaction to obtain a well-dispersed suspension (Fukushima et al., 2003, Khezrian et al., 2013). MWCNTs and IL nanocomposite has been used to fabricate a number of sensors/biosensors mainly for electrochemical sensing application (Chen et al., 2014, Khezrian et al., 2013). ILs are used in electrochemical sensing as a solvent and electrode modifier to accelerate rapid transfer of electrons owing to its outstanding conductivity, great potential window and its thermal stability (Wang et al., 2012). The surface of MWCNTs-IL composite can also be improved by modifying it with electro-active and highly conductive polymers such as L-lysine and chitosan to improve their electrochemical performance (Gholivand et al., 2019b). L-lysine, an essential amino acid, is electro-active and highly conductive polymer that have been used in electrochemical sensing to improve the performance of the fabricated sensors (Laurinavičius et al., 2019). It is thus evident that a significant synergistic amplification of electrochemical performance can be realized through combination of MWCNTs, ILs and L-lysine nanomaterials for the fabrication of MWCNTs-ILs-L-lysine /GCE sensor for detection of PDN in pharmaceutical formulations.

2.4 Analytical techniques for quantification of selected anti-asthma drugs

Several conventional methods have been developed and evaluated for detection of anti-asthma drugs in different sample matrices (table 2.1). In summary, chromatographic-based techniques

comprising; High Performance Liquid Chromatography (HPLC), Gas Chromatography (GC), Liquid Chromatography (LC), GC/mass spectrometry, Liquid Chromatography/Tandem Mass Spectrometry, immunological and electrochemical sensor-based techniques. These conventional techniques can be categorised broadly into electroanalytical, chromatographic, capillary electrophoresis and spectroscopic methods (Figure 2. 9). Different LODs for different analytes have been reported in literature (table 2.1). Although this could be study specific, its analysis has revealed that the LODs of some of these conventional methods are too high for TPN, SAL, TBS and PDN. The situation is less favourable in some media including wastewater, where these drugs are found in ultra-low concentrations thus requiring the development of ultrasensitive and selective methods for detection.

Generally, the conventional methods used for detection of the drugs under study and other pharmaceuticals in various sample matrices suffer from a number of limitations as mentioned earlier. This has led to the new generation of electrochemical sensing techniques and a step ahead using nanomaterials enabled sensors and biosensors to enhance sensitivity, rapidity and on-site detection of determination of electro-active compounds in various sample matrices.

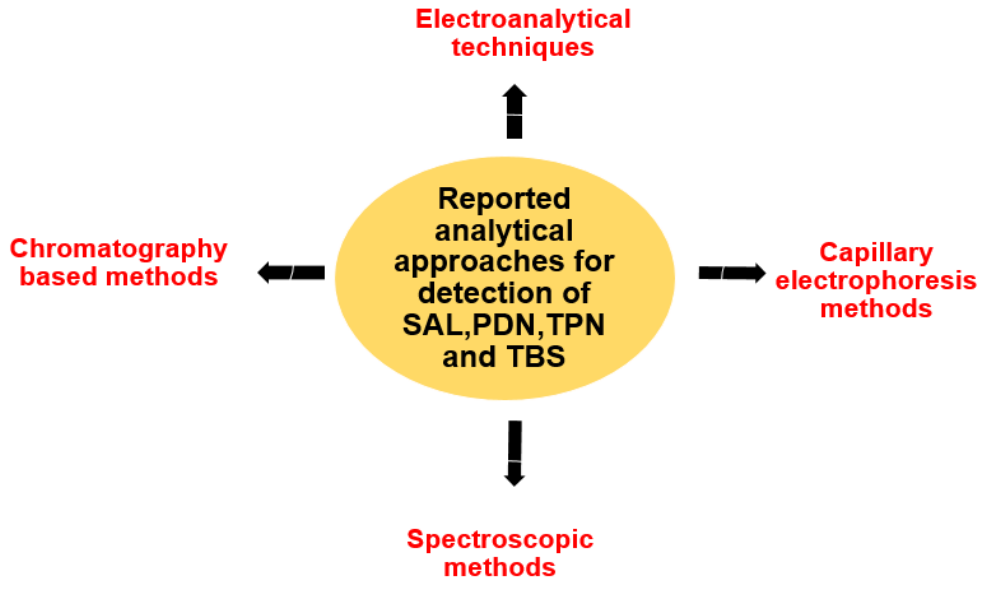

Figure 2.9: **Analytical approaches reportedly used for detection of the four anti-asthma drugs**

Table 2.1: **Detection limits for the convectional analytical methods for detection of TPN, SAL, TBS and PDN**

	DRUG	ANALYTICAL TECHNIQUE	LOD	LOQ	REFERENCE
1	**Theophylline**	Liquid chromatography (GC) coupled to diode array UV detection	8 ng/ml	24 ng/mL	(Aresta et al., 2005)
		High performance liquid chromatography (HPLC)-UV detection	0.1 µg /mL	-	(Schreiber-Deturmeny et al., 1996)
		Near infrared spectroscopy (NIRS)	0.05 g/100 g percent	-	(Huck et al., 2005b)
		Electrospray ionisation ion mobility spectrometry (ESI-IMS)	0.3 µg/ mL	-	(Jafari et al., 2011)
		Micellar electro-kinetic chromatography	0.01 µmol/mL	-	(Huang et al., 2003)
		HPLC with amperometric detection	1 ng		(Meyer et al., 1996)
		Liquid chromatography/mass spectrometry	-	0.5 ng	(Kanazawa et al., 2000)
		Fluorescence detection	1.8 µM		(Park et al., 2014)
		High performance liquid chromatography	0.067 µg/mL	0.2 µg/mL	(Fernandes et al., 2017)
2	**Salbutamol**	Surface-enhanced Raman spectroscopy	0.1 ng/mL	0.2 ng/ mL	(Cheng et al., 2018)
		Liquid chromatography/tandem mass spectrometry	-	50 pg/mL	(Wu et al., 2011b)
		Reversed phase -High performance liquid chromatography	0.0297 µg/mL	0.090 µg/mL	(Solanki et al., 2016)
		Capillary electrophoresis	0.17 g/mL	0.59 gm/L	(Wang et al., 2010)
		Enzyme immunoassay	0.021 µg/L	-	(Liu et al., 2018)
		Solid phase extraction/High performance liquid chromatography coupled to ultraviolet detection	0.20 ng/g	0.68 ng/g	(Yan et al., 2012)
		UV spectrophotometry method	0.003 µg/mL	0.01 µg/mL	(Kalyani et al., 2018)

		Time-resolved fluoroimmunoassay	-	0.66 ng/L	(Fang et al., 2019)
3	**Terbutaline**	High performance liquid chromatography coupled to fluorescence detection	0.3 ng/mL	-	(Kim et al., 2001)
		Chemiluminescence method	0.01µg/mL	-	(Han et al., 2012a)
		High performance liquid chromatography	4.4 nmol/l	1 ng/mL	(Herring et al., 2000)
		Capillary electrophoresis with chemiluminescence detection	3.0×10^{-8} M	-	(Li et al., 2009b)
		Reverse-phase high performance liquid chromatography-ultra-violent detection	1.0 µg/mL	3.3 µg/mL	(Itagimatha et al., 2019)
		Liquid chromatography–tandem mass spectrometry	0.4 ng /mL	1 ng/mL	(Luo et al., 2010)
		Micro-dialysis sampling combined with flow-injection chemiluminescence analysis	3×10^{-8} mol/ L	-	(Wang et al., 2003)
		Ultra high performance liquid chromatography coupled to electrochemical detection	0.04 µg /mL		(Lomae et al., 2019)
4	**Prednisolone**	Solid phase extraction / Ultra-High Pressure Liquid Chromatography / quadrupole time of flight mass spectrometry	623 ng/L		(Wood et al., 2017)
		Matrix solid phase dispersion (MSPD)-liquid chromatography - ultraviolet detection method	0.50 µg /kg	3 µg/kg	(Dési et al., 2008)
		Liquid chromatography coupled to fluorescence detection			
		Liquid chromatography coupled to tandem mass spectrometry	10 pg/mL	50 pg/mL	(Fidani et al., 2013)
		Ultra high performance liquid chromatography coupled to tandem mass spectrometry (UPLC–MS/MS)	-	1 ng/mL	(Liu et al., 2016)

Ultra high performance Liquid chromatography/mass spectrometry/mass spectrometry (UHPLC-MS/MS)	7.30 ng /mL	22.77 ng/ mL	(Elzayat et al., 2019)
Liquid chromatography/electrospray ionisation coupled to tandem mass spectrometry	0.41 ng/mL	0.51 ng/mL	(Chiesa et al., 2016)
Solid phase extraction (SPE) together with HPLC detection	7.0 ng/mL	11.6 ng/mL	(AbuRuz et al., 2003)

2.4.1 Chromatographic techniques

Chromatographic methods have been used to quantitatively analyze diverse analytes including drugs in several sample matrices (Siddiqui et al., 2017). Analytical separation is grounded on the dispersion of analytes between stationary phase and mobile phase. Organic solvents such as acetonitrile and methanol are used in mobile phase (Itagimatha et al., 2019). Each column has its own pH range of analysis thus pH control is very important prior to any experimental analysis to prevent degradation of the stationery phase.

Prior to analysis, the analyte of interest has to be extracted into an individual entity from its surrounding complex matrix. This can be done through sample extraction procedures;

i. solid phase extraction
ii. solid phase micro extraction and
iii. liquid/liquid extraction (Qu et al., 2011, Meyer et al., 1996).

The extraction and clean-up steps are relatively slow, solvent intensive and add extra costs (Baytak et al., 2016). Chromatographic techniques include HPLC (for non-volatile analytes) and high performance thin layer chromatography (HPTLC-for determination of volatile solvents), LC, GC (for volatile analytes) and thin layer chromatography (TLC). A remarkable advancement has been made in coupling these separation techniques to various highly sensitive detectors such as:

i. mass spectrometry (Caban et al., 2011, Lomae et al., 2019, Zhou et al., 2017b, Domínguez-Romero et al., 2013)
ii. ultraviolet (Itagimatha et al., 2019, Aresta et al., 2005)
iii. fluorescence to achieve lower detection limits(as presented in table 1) for quantification and identification of drugs (Siddiqui et al., 2017)

However, there are a number of problems limiting the use of mass spectrometry as a means of detection. Firstly, it is the complex instrument system, which requires trained personnel to run it. Secondly, the equipment is costly and is very expensive to maintain (Lomae et al., 2019). HPLC is the most usual approach for quantification of most target compounds due to its excellent precision. However, the equipment and columns used in this method are expensive and involves use of a large amount of solvents (Herring et al., 2000). In addition, they suffer from low sensitivity therefore they are unsuitable for the routine analysis (Herring et al., 2000, Teker et al., 2019).

2.4.2 Spectroscopy techniques

Spectroscopy refers to the study of the splitting of electromagnetic radiation to its constituent wavelengths by matter. The transmission properties of a sample as a function of wavelength are measured. Spectroscopy methods are used to determine the structural composition of the analytes by identifying specific functional groups present in a compound. The amount of the target compounds in the sample matrix can also be determined. Spectroscopy methods such as ultraviolet (UV) spectroscopy, fluorescence spectroscopy, Raman spectroscopy, near infrared (NIR) spectroscopy, infrared (IR) spectroscopy and mass spectrometry have been used frequently for qualitative and quantitative analysis of many compounds of interest.

The UV/Vis technique quantifies the percentage of radiation transmitted through the sample. The sample is prepared by dissolving in a suitable solvent and then its absorption is observed at specific wavelengths of interest (from 190 to 800 nm wavelength). Compared to other methods, this technique is rapid and is easy to use to analyze drugs and other substances. However, other interfering substances that absorb at the same wavelength may be in the sample matrix hence influencing the accuracy of the obtained results in the quantification of analytes. In addition, sample preparation usually involves varying the concentration of the sample, thus requiring the preparation of a large number of sample solutions.

IR spectroscopic methods are extensively used for structural analysis of various organic compounds in various liquid, solid as well as gaseous samples. IR method is based on the absorption of light by a chemical compound, which promotes a shift in vibrational energy levels. As a result, different functional groups present in the compound absorb the IR radiation at different frequencies. NIR spectroscopy (12800–4000 cm^{-1}) is used to identify particular functional groups existing in the analyte, while mid-infrared radiation (4000–400 cm^{-1}) is used in quantitative analysis (Reich, 2005). TPN was quantified in liquid coffee using the NIR spectroscopy method. The proposed method was rapid, however, the sensitivity was low as compared to that of HPLC-MS (Huck et al., 2005b). Recently, ATR/FTIR (Attenuated total reflectance Fourier transform infrared spectroscopy) was used for the quantification of bambuterol and TBS. Relatively low LODs were achieved due to the remarkable sensitivity of the method (Algethami et al., 2020). In Raman spectroscopy, a monochromatic light interacts with the compound of interest and as a result scattered light is produced which contains information associated to the vibrational modes of the chemical species constituting the sample. They are advantageous compared to the other methods since they are non-destructive, requires

small or no solvents, less or no sample preparation procedures thus are time saving and eco-friendly (Xu et al., 2013).

Fluorescence spectroscopy is also a very attractive technique because it is rapid, highly sensitive and simple to operate as compared to other methods such as chromatographic methods. Literature survey revealed that this method has been exploited for quantification of various drugs in different sample matrices. For instance, this method has been used effectively for the analysis of quetiapine fumarate in its formulations, as well as in human plasma (Mostafa et al., 2018). The proposed assay exhibited satisfactory sensitivity with LOD and LOQ of 0.05 and 0.17 μg/mL, respectively (Mostafa et al., 2018). In addition, some of the drugs under study have also been quantified using this method as shown in table 2.1. Although this method is reliable, its use is limited to fluorescent molecules. Moreover, the sample preparation steps are laborious and time consuming.

2.4.3 Electrophoresis methods

Capillary electrophoresis (CE) is one of the separation-based analytical methods. CE analysis encompasses the separation of charged analytes via a narrow fused silica capillary under the influence of an electric field. The target analytes are separated based on their difference in electrophoretic mobility. This technique is more efficient compared to other separation based methods such as chromatography owing to its exceptional features such as quick analysis, great separation efficiency and requires only a small sample volume (Saar-Reismaa et al., 2019, Kubáň et al., 2019). Recently, sensitivity and selectivity of CE have been improved by;

a. using different means of detection including chemiluminescence, ultraviolet spectroscopy and mass spectrometry
b. coupling to other separation methods such as chromatography
c. using various capillary electrophoresis modes which allow the analysis of different compounds of interest (Gogolashvili et al., 2018).

Analysis is generally more rapid and effective compared to chromatographic methods (Trapiella-Alfonso et al., 2016, Montaseri et al., 2018). However, both CE and chromatography-based techniques require sample preparation steps such as solid-phase extraction that are time-consuming (Karami et al., 2019). This is because direct injection of samples to their respective columns lead to column blockage resulting in a decrease in the separation efficiency (Karami et al., 2019).

2.4.4 Electrochemical techniques

Electroanalytical methods are the most efficient methods for drug detection in a number of sample matrices such as body fluids and pharmaceutical formulations (Hatamluyi et al., 2019). The key advantage of these approaches is that the excipients cause minimum interference, and usually, the sample procedures are simple. This can be a sustainable and cost-effective alternative method to the common analytical techniques such as chromatographic methods, which involve tedious and time-consuming sample preparation steps.

The performance of voltammetry techniques greatly depends on the surface of the working electrode. The electrochemical response is poor or insensible at low concentrations at unmodified conventional working electrodes (Asadian et al., 2019). To overcome this problem, the surface of the working electrodes has been modified using various nanomaterials to increase the surface area. The hybrid composite materials used to fabricate electrochemical sensors are reported to effectively lower detection limit and quantification limit.

The introduction of wide range of new functional nanomaterials creates an opportunity for construction of ultrasensitive and selective electrochemical sensors and biosensors that are generally user friendly, portable, relatively cheap, easy to fabricate and with lower detection limits (nano-molar). Recently, the fabrication of nanocomposite-based electrodes have been focused on primarily owing to the benefit of synergistic effect. The combination of different nanomaterials including metal oxides NPs and CNTs with ILs, enzymes or polymers has provided multifunctional hybrid composites that can significantly enhance electrochemical sensing performance as they exhibit excellent catalytic activity. Nanocomposite-modified electrodes can effectively facilitate rapid transfer of electrons, leading to generation of impressive peak-current responses compared to single layer modified or unmodified working electrode surfaces.

In this research work, ZnONPs-MWCNTs-Cyt c, MWCNTs-$CoFe_2O_4$-Lipase, TiO_2-MWCNTs-IL and MWCNTs-IL-L-lysine nanocomposites were used in fabrication of GCE modified sensors for quantification of the four selected anti-asthma drugs in pharmaceutical formulations. The following nanocomposites were selected for fabrication of electrochemical sensors:

- **Multi-walled carbon nanotubes (MWCNTs) based nanocomposites**
- **Metal oxides ($CoFe_2O_4$, ZnO and TiO_2) nanocomposites**

- **IL based nanocomposites**
- **Enzymes (cytochrome C, lipase and L-lysine) based sensors**

Sensors based on carbon nanotubes have generated great interest since their discovery in 1991 (Hou et al., 2018). Single-walled carbon nanotubes (SWCNTs) have one single graphite layer, while multi-walled carbon nanotubes (MWCNTs) have multiple graphite layers of sp^2 hybridized carbon atoms which enable their extensive application in the modification of the surfaces of the working electrodes (Shalauddin et al., 2019). MWCNTs-based sensors generally facilitate rapid transfer of electrons, exhibit higher sensitivities and relatively lower detection limits compared to un-modified solid electrodes. This is attributed to their capability of increasing the roughness and electro-active surface area of an electrode, providing an enhanced electro-catalytic activity towards a wide variety of electro-active analytes. In addition, they have a wide potential window as well as high mechanical and chemical stability (Liu et al., 2019a).

MWCNTs are likely to agglomerate owing to high Van der Waal's forces of interaction among the carbon particles (Clark et al., 2011). This has been a major barrier as the forces of interactions hinder solubility or dispersion of CNTs in solvents such as DMF (N, N dimethyl formamide) and ethanol. Different surface functionalization processes such as chemical and physical (e.g. surfactant adsorption) treatment have been successfully developed to enhance dispersion of these nanomaterials (Alharthi et al., 2019). Chemical functionalization introduces polar groups such as COOH. Physical functionalization is preferred because it reduces the Van der Waal's forces and does not interfere with the structure of the CNTs (Madhan Kumar et al., 2015). Moreover, they are easily available, cost effective and present low toxicity compared to covalent methods that involve acid treatment. Furthermore, MWCNTs can be functionalized by using metal/metal oxides NPs. Working electrodes modified with MWCNTs- metal/metal oxide nanocomposites reveal improved electro-catalytic activity as compared to MWCNTs modified electrodes and bare electrodes (Cheng et al., 2020).

To date, a number of metal oxide nanoparticles including magnetic metal oxides and nonmagnetic metal oxides have been used in detection of drugs as electrode modifiers because of their excellent electro-catalytic properties (Rahi et al., 2016). Various conventional methods comprising chemical, physical and biological procedures have been used to synthesize these metal-based NPs with well-controlled size and shape. Alternative biosynthetic green approaches that use green solvents, natural microorganisms, polysaccharides and plant extracts

for reduction and stabilization of metal ions are presently preferred (Yáñez-Sedeño et al., 2019).

Metal ferrites (also spinel ferrites denoted as MFe_2O_4, where M =Ni^{+2}, Co^{+2} , Zn^{+2}, Mn^{+2} and Cu^{+2}) have been utilized as effective electro catalyst for electrochemical sensing of various analytes such as drugs and pesticides (Sobczak-Kupiec et al., 2016, Ensafi et al., 2019, Dong et al., 2017) owing to their:

i. excellent catalytic activity
ii. high specific surface area
iii. bio-compatibility
iv. relatively low cost and easy synthesis methods

Cobalt ferrite ($CoFe_2O_4$) is a metal ferrite having an inverse spinel structure; where Co^{2+} and Fe^{3+} ions occupy the octahedral and tetrahedral sites, respectively (Thu et al., 2019). A few electrochemical sensors based on $CoFe_2O_4$ nanocomposites have been reported. For instance, Kumar et al. (2019b) recently quantified paracetamol and dopamine using $CoFe_2O_4$/graphite electrode sensor with lower LOD of 250 nM and 350 nM, respectively. Shaterian et al. (2020) fabricated a highly sensitive $CoFe_2O_4$/graphene/ carbon paste electrode for quantification of atenolol. The combination of $CoFe_2O_4$NPs with other nanomaterials such as CNTs and biological compound such as enzymes give rise to hybrid nanocomposites with superior properties for electrochemical sensing of electro-active analytes (Vajedi et al., 2020).

Their magnetic properties depend on the method of preparation as well as the morphology and the size of the NPs (Daffé et al., 2018) . Various methods that have been used for their synthesis include electrospinning, co-precipitation, hydrothermal-solvothermol and sol-gel auto combustion (Revathi et al., 2020). In these methods, control of size and size distribution is not easy. Therefore, to overcome this problem, co-precipitation (wet chemical) method is preferred (Ojha et al., 2019, Revathi et al., 2020).

Co-precipitation synthesis is a simple method that involves dissolution of compound salt precursors using a suitable aqueous media followed by precipitation via pH adjustment. The advantage of co-precipitation method over the others is that control of production of particles, their sizes and distribution is relatively easy. Surface coating materials such as oleic acid and sodium dodecyl sulfate are used to modify the surfaces of magnetic nanoparticles in order to prevent agglomeration (Vadivel et al., 2016). Therefore, $CoFe_2O_4$NPs were synthesized via co-precipitation method and oleic acid was used to coat the surface of the magnetic NPs.

ZnO has good electrical conductivity, high chemical and thermal stability, is biocompatible and relatively cheap (Hassanein et al., 2017, Shaikshavali et al., 2020a, George et al., 2018). It is widely used for fabrication of relatively cheap and stable electrochemical sensors for detection of various drugs and electro-active compounds owing to its outstanding electro-catalytic properties (Sebastian et al., 2019, Alavi-Tabari et al., 2018).

ZnO nanoparticles have been synthesized through various methods including co-precipitation, thermal decomposition as well as by green synthesis approaches (Yusof et al., 2019, Adam et al., 2018, Golmohammadi et al., 2020). However, some of these approaches require tedious multiple steps, complex equipment, high temperature and toxic solvents. Alternatively, wet chemical method is reported to be a cost effective and a straight-forward method for rapid synthesis of ZnONPs (Hassanein et al., 2017). Hybridization of ZnONPs with carbon nanomaterials such as MWCNTs and enzymes display exceptional performance like excellent electro-catalytic ability, large specific surface area and good conductivity leading to improved electrochemical sensing performance (Shetti et al., 2019b).

Titanium oxide (TiO_2) is a commonly used semiconductor photo-catalyst. It occurs in three crystallographic forms, viz.; rutile, anatase and brookite; (Kaplan et al., 2015, Alkaim et al., 2013, Kanan et al., 2020). It is widely used in various applications because it is abundant and is environmentally friendly. To date, it has been applied as electrode modifier material for fabrication of photocatalytic sensors and biosensors owing to its outstanding electro-catalytic activity, biocompatibility, and it is relatively cheap. Furthermore, TiO_2NPs in combination of other nanomaterials has exhibited improved electrochemical performance of the sensors as compared to only TiO_2NPs modified electrodes (Ravishankar et al., 2016).

TiO_2-graphene/GCE sensor was fabricated for detection of adenine and guanine by Fan et al. (2011). The as-prepared TiO_2-graphene nanocomposite exhibited remarkable electro-catalytic activity with relatively high sensitivity since the as prepared nanocomposite significantly facilitates the electron transfer kinetics (Fan et al., 2011). Ru-TiO_2/MWCNTs/CPE sensor was fabricated by Shetti et al. (2019d) for electrochemical detection of mefenamic and flufenamic acid drugs. Lower LOD values of 0.68 nM and 0.45 nM for flufenamic acid and mefenamic acid, respectively, were obtained by Shetti et al. (2019d).

Excellent thermal and electrical conductivity of TiO_2/CNTs-based nanocomposite materials have been reported (Bazli et al., 2019, Askari et al., 2017). Their ease of surface functionalization with ionic liquids has led to the formation of hybrid nanocomposites for electrochemical sensing of pharmaceuticals and other target electro-active species. Indeed,

TiO_2/1-butyl-3-methylimidazolium Chloride [BMIM]Cl /poly(3, 4-ethylene-dioxythiophene) (PEDOT)/CPE was constructed for quantification of diclofenac sodium (Farghali et al., 2018). Its estimated LOD was 1.17×10^{-8} M (Farghali et al., 2018).

ILs are organic salts or mixtures of salts, which have melting points close or less than room temperature, and they consist of positive and negative ions (Faridbod et al., 2011). They are extensively used in electrochemical sensing as supporting electrolyte, electrode modifier with other nanocomposite materials or as a binder on the electrode (Saleem et al., 2019). This is attributed to their exceptional properties such as super conductivity, low volatility, high viscosity, high chemical stability, low cost as well as its good biocompatibility (Wang et al., 2016, Faridbod et al., 2011).

IL-modified solid electrodes are associated with high conductivity, rapid charge transfer and high peak-current height compared to common bare conventional electrodes (Chokkareddy et al., 2020a). CNTs such as MWCNTs and IL nanocomposites based sensors; combine the benefits of both nanomaterials, which subsequently improve the electrochemical performance in detection of drugs and other electro-active analytes (Sanati et al., 2017, Mert et al., 2018, Atta et al., 2017). Furthermore, metal/metal oxide-IL and Metal/metal oxide-CNTs-IL nanocomposite-based sensors/biosensors have been utilized in electrochemical quantification of drugs and other electro-active substances in different sample matrices (Boobphahom et al., 2019, Miraki et al., 2019).

Enzymes are proteins that have been used widely in electrochemical sensing because they are acknowledged to be environmentally friendly compared to conventional chemical catalysts (Zdarta et al., 2018, Kurbanoglu et al., 2020). They are used in construction of biosensor as the bio-recognition element owing to their outstanding selectivity for their targeted electro-active analyte as well as great catalytic activity (Liu et al., 2020). Immobilization of these enzymes onto cost effective nanomaterials with exceptional properties including large surface areas, outstanding chemical as well as thermal stability has allowed the development of satisfactorily selective as well as sensitive biosensors (Putzbach et al., 2013). The nanomaterials-based electrodes offer a favourable biocompatible electro-active platform for immobilization of enzymes. Immobilization of enzymes on nanomaterials such a carbon nanotubes, ILs and metal oxides can be achieved by covalent bonding, physical adsorption, cross-linking and entrapment (Putzbach et al., 2013). Lipase and Cyt c enzymes were explored in the fabrication of MWCNTs-$CoFe_2O_4$-Lipase-GCE and ZnO-MWCNTs-Cyt c-GCE

biosensors, respectively. In addition, L-lysine (a protein) was used in construction of MWCNTs-IL-L-lysine-GCE sensor.

Cyt c belonging to the class of haemoproteins (has the heme prosthetic group covalently bonded to protein), has been widely used to design electrochemical biosensors for determination of a number of target analytes owing to its high thermal stability and is relatively cheap (Manickam et al., 2017). It is active over a wide range of pH (2-11). Electrochemical detection of drugs and other molecules is poor on an enzyme modified electrode surface because of slow transfer of electrons. Thus, this enzyme has been immobilized on carbon nanotubes platforms, as well as metal, metal oxide, and some inorganic materials such as polymeric materials and their nanocomposites to enhance electron transfer and achieve high selectivity, while still maintaining the electrochemistry and good stability nature of the enzyme.

Lipase (triacylglycerol hydrolases, E.C. 3.1.1.3) a biocatalyst, is mainly used to catalyse hydrolysis of oil reactions as well as esterification (Wang et al., 2019). Lipase-immobilized sensors have been successfully used in determination of a number of electro-active compounds since they are relatively cheap and readily available (Ma et al., 2018). Lipase enzyme-immobilized magnetic NPs could potentially lead to exclusive properties including superb stability, high sensitivity and rapid electrochemical response towards the electro-active compound of interest (Zdarta et al., 2018) .

L-lysine (Figure 2.10) is a vital amino acid, which has two amino groups (Laurinavičius et al., 2019). It is among the conductive polymers that have been used in the fabrication of functional modified working electrodes owing to their extraordinary specific selectivity (Li et al., 2017b, Zhang et al., 2017). In general, electro-polymers such L-lysine increase the stability of the modified electrodes by adhering strongly on their surface. In addition, it provides more active sites for redox reactions involving the analyte of interest (Jayaprakash et al., 2018). L-lysine modified electrodes are characterized by their stability and excellent electro-catalytic activity (Laurinavičius et al., 2019).

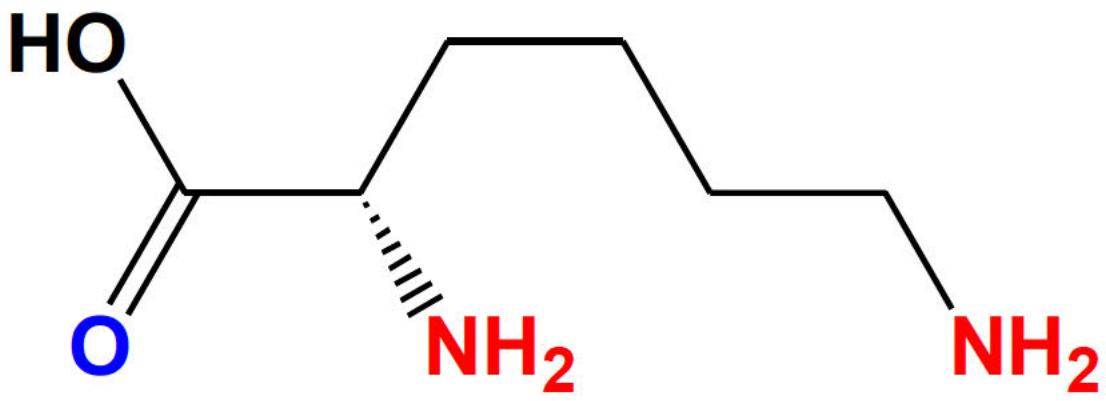

Figure 2.10: **Chemical structure of L-lysine**

CHAPTER 3

3 THEORETICAL PRINCIPLES OF VOLTAMMETRIC TECHNIQUES AND ELECTROCHEMICAL SENSORS

Electroanalytical procedures are simple and useful methods that offer cost-effective instrumentation, small reagent consumption, suitability for real-time determination, rapid analysis along with greater sensitivity over a wide linear concentration range (Rahi et al., 2016). Voltammetry, developed in 1922 by Czech scientist Jaroslav Heyrovsky, is one type of electrochemical technique. Other types include chronocoulometry, potentiometry and impedance measurement methods. Voltammetry has been effectively used in detection of quite a lot of drugs in various drug formulations as well as in biological fluids because most active ingredients of the drug-formulations can readily undergo oxidation or reduction (Jadon et al., 2016).

Voltammetry mode is based on the principle of applying a varying potential (relative to a reference electrode) to a working electrode that is in contact with electro-active compound in the electrochemical cell solution. The corresponding current (I) that flows because of transfer of electrons due to redox reactions taking place at the working electrode (WE) is measured as a function of the applied potential (E) (Naveen et al., 2017). The measured potential and current are related to the qualitative and quantitative properties of the analyte, respectively.

In electrochemical experiments, the solution containing a buffer in addition to the sample solution of the active drug constituent is placed in an electrochemical cell. Three electrodes, namely; counter electrode (CE), WE, and reference electrode (RE) are immersed into the cell. A varying potential is applied to the WE and the resultant current produced by the redox reactions is recorded over a certain period. The applied potential causes the electro-active drug compound present in the solution to be oxidized or reduced at the electrode's surface leading to transfer of electrons (Varghese et al., 2017). Current flows through the two electrodes only (working and auxiliary). Cathodic current is the current recorded due to the reduction of the electro-active compound on the surface of a WE, whereas the current measured due to oxidation is known as anodic current. The redox reactions which in most cases correspond to the conversion of one form of the analyte into another and which involves electrons transfer are studied herein.

The main advantage of voltammetry methods is that the excipients cause minimal or no interference on the electrochemical peak-current response recorded and, generally, the sample preparation procedures are straightforward. Preparation of the real sample usually involves dissolving the active ingredient from the drug dosage form in appropriate solvent such as a buffer (Ozkan et al., 2016). An aliquot of this sample solution is analysed using standard addition procedure via voltammetry technique.

3.1 Instruments used in voltammetry

A potentiostat, data processing unit and an electrochemical cell constitute the basic components of instrumentation used (Figure 3. 1). The cell contains the supporting electrolyte solution, sample solution and mainly the three electrodes immersed into the solution (Fiel et al., 2019, Lu et al., 2018). These electrodes are joined to an electrochemical workstation embedded with an in built power source. The three-electrode system is run by a potentiostat. It is used to apply potential and to monitor the current at the electrode-electrolyte interface of the working electrode. The electrochemical workstation is connected to a computer installed with required software package that monitors the experiment, record the data and analyses the obtained results (Bansod et al., 2017).

Figure 3.1: **A pictorial representation of voltammetry instrumentation**

3.1.1 The types of electrodes used in voltammetry

Current is passed between the WE and the auxiliary electrode (AE) or counter electrode (CE). The obtained potential is measured with respect to the RE (Kurbanoglu et al., 2019).

i. **Reference electrode (RE);** is employed to control the potential of the WE and it has a known and fixed electrode potential. The commonly used reference electrodes are standard hydrogen electrode (SHE) which is used when the ionic conductor is an aqueous solution and standard calomel or Ag/AgCl electrode (Hu et al., 2016, Napporn et al., 2018).

ii. **Counter electrode (CE);** such as the platinum wire completes the circuit hence allowing flow of charge though it does not take part in the electrochemical reaction (it is inert hence has no effect on the behaviour of the WE)(Bansod et al., 2017).

iii. **Working electrode (WE);** are ones on which the reactions of interest occur and are of two types:

   a. **Mercury**; static mercury drop electrode (SMDE), hanging mercury drop electrode (HMDE) and dropping mercury electrode (DME)-used for studying reducible electro-active compounds only. These electrodes are characterized by exceptional sensitivity, speed of analysis, ease of surface renewal and wide potential window in cathodic region (positive region) (Alrashdi et al., 2019) , However, mercury is toxic, very expensive and cannot be used to analyse substances that are oxidised(Yilmaz et al., 2007). Replacement of the mercury drop electrode has been recommended (Gonçalves-Filho et al., 2020). Polarography is a type of voltammetry describing the electrochemical measurement obtained using DME with a constant flow of mercury drop.

   b. The new trend in electrochemical determination of electro-active species at lower concentrations is focused on using inert solid electrodes (made of inert metals and carbon materials), including; glassy carbon, gold (Au), platinum (Pt) and graphite (Kurbanoglu et al., 2019). The solid electrodes can be used for studying substances that can be oxidised as well as reduced. The main advantages of these electrodes are high mechanical stability, chemical resistance and broad potential window (that is both negative and positive). One of main challenges in using these electrodes is that the electrochemical response on its bare active surface is poor or insensitive, hence the need to modify its surface (Karthika et al., 2019).

Glassy carbon electrode (GCE) is one of the most widely used conventional solid electrode in electrochemical measurements (Gholivand et al., 2019a, Jadon et al., 2016). The main reasons for its popularity are; good electro-chemical stability, biocompatibility and its very low thermal expansion coefficient. Prior to electrochemical measurements, the GCE is cleaned thoroughly so to ensure a uniform surface area. Alumina powder is used and alumina slurry is prepared by placing a drop of deionized water in approximately 40 mg of alumina powder to make a paste. The bare GCE (Figure 3. 2) surface is rubbed on a polishing cloth with the paste and is repeatedly washed with deionized water.

Figure 3.2: **Unmodified glassy carbon electrode representation**

Modification of GCE surface and other convectional electrodes using nanomaterials has been achieved by various methods including drop casting, electrodeposition and electro-polymerization (Aydin et al., 2019, Sandhyarani, 2019). Drop casting method is often used because it is cost effective and is the simplest. It involves micro pipetting a specific amount of the prepared nanocomposite paste and dropping it onto the surface of electrode. The paste is then left to dry at approximately 25 °C (Yuan et al., 2019).

3.1.2 Supporting electrolyte

Supporting electrolyte used in electrochemical experiments is an electrolyte comprising the chemical compounds that are not electro-active within potential window selected for the electrochemical examination (Sanghavi et al., 2015). These supporting electrolytes are often

buffers (such as phosphate buffer, borate buffer and acetate buffer), strong acid solution such as HCl or a strong base solution e.g. sodium hydroxide prepared usually within the concentration range of 0.05-1.0 M (Sanghavi et al., 2015). The electrolytes have a greater ionic strength and are highly conductive, thus, they are often used to enhance the conductivity of the solution. In addition, the electrolyte is used to maintain a uniform ionic strength as well as pH (Sanghavi et al., 2015). The type and pH of the supporting electrolyte selected during electrochemical experiments can have a significant effect on the shape of the peak shape, peak-current as well as peak potential of the electro-active compound (Soleymani et al., 2017). Consequently, the main aim when developing voltammetric method is to find and optimize the pH of the selected supporting electrolyte in which the electrochemical response obtained in the existence of an electro-active analyte are best quantifiable.

3.2 Voltammetry methods

The principal voltammetry methods that have been found to be very sensitive for the electrochemical quantification of electro-active organic compounds include (Shumyantseva et al., 2020);

a. Cyclic voltammetry
b. Linear sweep voltammetry
c. Differential pulse voltammetry
d. Square wave voltammetry
e. Stripping voltammetry

Most of these user-friendly voltammetry modes are based on the idea of changing the applied potential constantly and the resultant current is measured as a function of the applied potential. A number of variables such as pH of the buffer, surface area of the WE, deposition time, electrode material used and scan rate affects the height of the measured peak-current. The primary concepts of cyclic voltammetry and differential pulse voltammetry methods employed in this study are briefly discussed in sections 3.2.1 and 3.2.2.

3.2.1 Cyclic voltammetry (CV)

CV has emerged as one of the best electrochemical technique used to study the electro-catalytic behaviour of electro-active analyte of interest at the WE surface. This is mainly because it can rapidly locate the electrochemical redox reaction potentials of an electro-active compound (Ozkan et al., 2016). Therefore, it is often the first experiment to be done in voltammetry

experiments as it helps obtain vital information such as the adsorption processes, kinetics of electron-transfer reactions and mechanism of redox reactions (Özkan et al., 2003). CV is based on monitoring the peak-current while the applied potential is varied in both forward and reverse directions at a constant scan rate. The potential is scanned with a triangular waveform and the current flowing through the WE is measured using a potentiostat as function of applied potential. The scan rate or sweep rate is defined as the rate of change of potential with time.

The peak potentials and peak-currents of the redox peaks are the paramount parameters in CV that describes the information about the analyte of interest. Resulted peak potential in the recorded voltammogram identifies the electro-active species whereas the measured peak-current height is proportional to the analyte's concentration; hence, this makes it possible to estimate its concentration. Reversible, irreversible and quasi-reversible reactions gives rise to unique voltammograms (plots of current vs potential). For a reversible reaction, the relationship between the concentration and the peak-current is defined by the **Randles-Sevcik equation** (Uslu et al., 2011);

$$i_{pa} = 2.69 \times 10^5 A C_0 n^{3/2} {D_R}^{1/2} v^{1/2} \qquad \textbf{3. 1}$$

Where; *i*; is the measured peak-current, *A*; electrode's area, C_0; concentration, *n*; the number of electrons involved, D_R; the diffusion coefficient and *v* is the sweep rate.

3.2.2 Differential pulse voltammetry (DPV)

DPV technique is extensively used for quantitative analysis of electro-active constituent in pharmaceuticals formulations, biological fluids and other samples at lower limits of detection (Thapliyal et al., 2016). It is a fast voltammetry mode with excellent analytical sensitivity thus can be used for simultaneous detection of electro-active compounds with close redox potentials. DPV like square wave voltammetry employs the concept of superimposing a pulse on a staircase waveform. These pulse techniques suppresses the background current and therefore relatively lower detection limits can be achieved. The electrochemical current response (X1) shortly before the pulse is applied and the current (X2) before the end of each pulse are recorded. The difference between these values (X2-X1) is plotted against the staircase potential (Barbosa et al., 2019). A voltammogram [Current (ΔX) vs potential (E) curve] is obtained. The obtained peak-current height is directly proportional to the concentration of the analyte in the sample solution. During DPV measurements; pulse amplitude, pulse width, pulse time and sample period working parameters are optimized to obtain maximum sensitivity.

3.3 Electrochemical sensors

Sensors/biosensors are promising future tools for quick and on-site detection of drugs and other electro-active compounds. They are categorized into amperometric, impedimetric and potentiometric sensors based on the electroanalytical methods used (Naveen et al., 2017). In this study, amperometric/voltammetric sensors were fabricated. The working principle of an amperometric sensor is to measure electrochemical current response relative to a RE generated as a result of applying a potential to the WE. The measured current is directly proportional to the concentration of the electro-active compound of interest in the real sample. A variety of novel nanomaterials has been used in the fabrication of ultra-sensitive and selective electrochemical sensors/biosensors. Currently available sensors are:

i. **Chemical sensors** are electrochemical sensing devices, which are mainly used to detect and quantify electro-active analytes. It works on the principle that the interaction between the analyte and the sensor is transformed into a measurable signal that is proportional to the concentration of the electro-active analyte (Figure 3. 3). The sensor component is coupled to a transducer, which converts the analyte-sensor interaction into a quantifiable analytical signal such as current depending on the type of transducer used (Goud et al., 2019b).

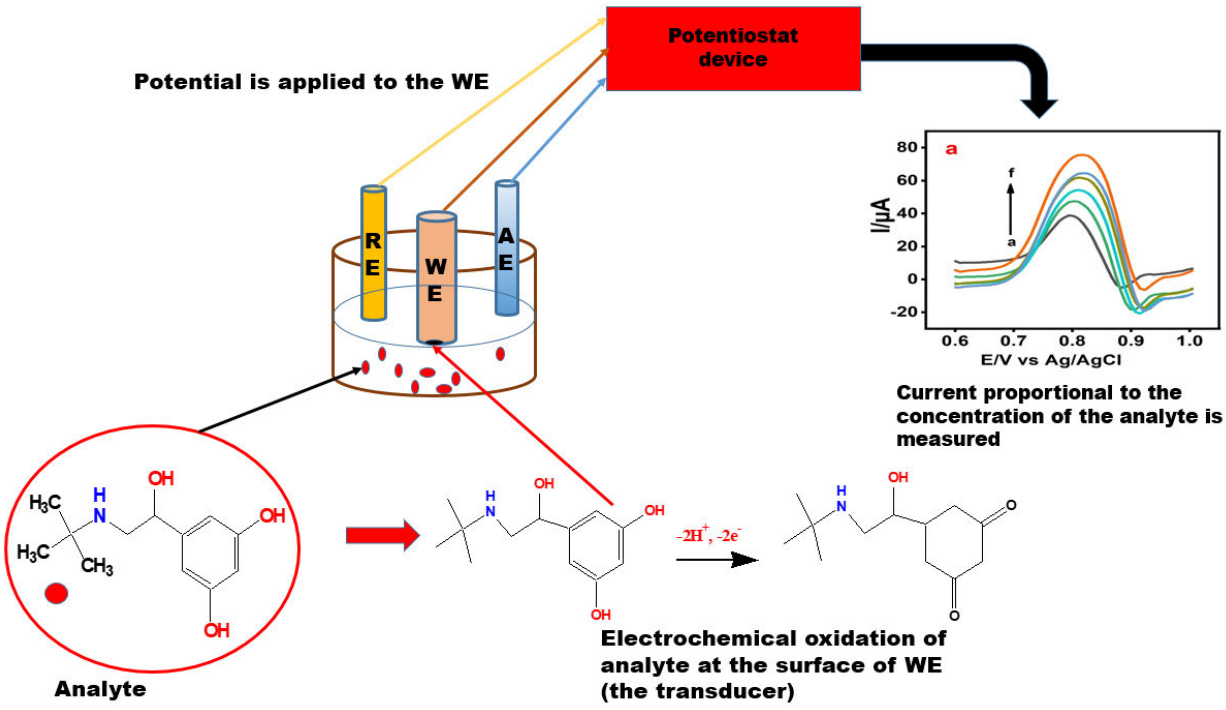

Figure 3.3: **Schematic illustration of the principle of a chemical sensor**

ii. **Electrochemical biosensor** is a chemical sensor that incorporates biological recognition element such as antibodies, enzymes, proteins and DNA as a recognition element. These elements are immobilized in a signal transducer (that is an electrode such as bare or modified GCE) (Aydin et al., 2019). The interaction between the analyte and the bio-recognition component produces a chemical or physical change, which is detected by the transducer (Figure 3.4). The transducer then converts the electrochemical signal generated during the redox reactions that occurs between the analyte of interest and a biocatalyst immobilized on a suitable substrate, into a quantifiable signal proportional to the amount of target analyte. Advantages of electrochemical biosensors include;

   a. high sensitivity and selectivity
   b. rapid responses
   c. Relatively cheap and readily available of the commercial biological elements

There are relatively few studies addressing the development and use of electrochemical biosensors for the determination of anti-asthma drugs under investigation.

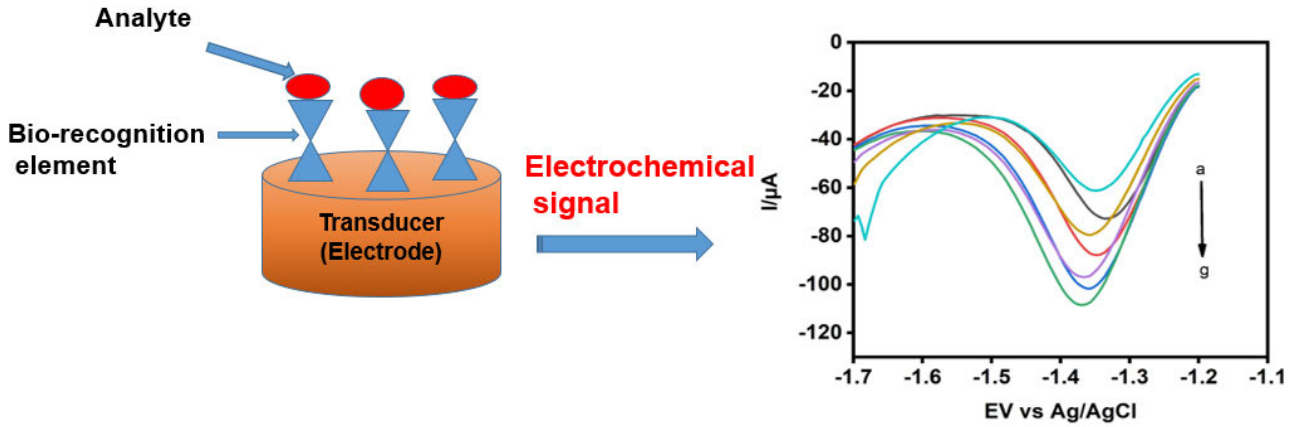

Figure 3.4: **Diagrammatic representation of a biosensor**

CHAPTER 4

4 MATERIALS AND METHODOLOGY

4.1 Materials and reagents

The following chemicals and solvents were bought from Associated Chemical Enterprises (Pty) Ltd (Johannesburg, South Africa):

Table 4.1: **Chemicals and reagents used**

➢ Sodium dihydrogen orthophosphate (NaH_2PO_4)	➢ Methanol (CH_3OH)
➢ Anhydrous disodium hydrogen orthophosphate (Na_2HPO_4)	➢ Sodium hydroxide (NaOH)
➢ Potassium chloride(KCl)	➢ HPLC grade oleic acid
➢ Potassium hexacyanoferrate(III) ($K_3[Fe(CN)_6]$)	➢ Urea (NH_2CONH_2)
➢ Potassium hexacyanoferrate(II) trihydrate ($K_4[Fe(CN)_6].3H_2O$)	➢ Titanium(IV) chloride ($TiCl_4$)
➢ Zinc chloride ($ZnCl_2$)	➢ Ethanol (C_2H_6O)
➢ Potassium hydroxide (KOH)	➢ 99.10% pure Cobalt chloride hexahydrate ($CoCl_2.6H_2O$)
➢ N, N dimethyl formamide (DMF)	➢ 99.10% Ferric chloride hexahydrate ($FeCl_3.6H_2O$)
➢ Sulphuric acid (H_2SO_4)	➢ 1-ethyl-3-methylimidazolium tetrafluoroborate

Theophylline, salbutamol hemi sulfate, terbutaline, prednisolone, glucose, ascorbic acid, sucrose, acetaminophen, chlorogenic acid, nafion® perfluorinated resin solution (5 wt. %), streptomycin and MWCNTs (95% carbon, 5 µm long and 6-9 nm diameter) were purchased

from Sigma-Aldrich (Durban, South Africa). All the other chemicals and solvents used for this research were of analytical grade and they were used directly as received.

4.2 Synthesis of nanoparticles

4.2.1 Synthesis of ZnONPs

ZnONPs were synthesized through wet chemical methods (Rao et al., 2015). First, 0.4 M $ZnCl_2$ was dissolved in 200 mL deionized water under vigorous magnetic stirring. Subsequently, a prepared 100 mL ethanolic solution containing 0.8 M KOH was slowly added into the solution under stirring until a white suspension was formed. The mixture was allowed to stir for 2 hours at room temperature to achieve complete reaction. The suspension obtained was left to settle for about 12 hours. The precipitate was collected by decantation and was washed with deionized water several times. Thereafter, the cleaned product was dried in an oven at 70 °C to remove water as well as to decompose $Zn(OH)_2$ to ZnONPs. The obtained pure ZnONPs was crushed to powder form for further studies.

4.2.2 Synthesis of $CoFe_2O_4$NPs

$CoFe_2O_4$NPs were synthesized via co-precipitation method (Maaz et al., 2007). Equivalent volume of 0.4 M $FeCl_3.6H_2O$ and 0.2 M $CoCl_2.6H_2O$ were prepared in deionized water separately, after which, the two precursor solutions were mixed together by the help of a magnetic stirrer. The pH of the resulting mixture was checked and adjusted to the required value (about pH 12) using 3 M NaOH solution under continuous stirring. Approximately 4 mL of oleic acid was added slowly to the precipitate obtained under vigorous stirring. The resulting precipitate was heated at 90 °C under magnetic stirring for 1 hr, and then it was cooled to room temperature. After centrifugation, the obtained brown product containing $CoFe_2O_4$NPs was cleaned with deionized water and ethanol to remove impurities and excess surfactant. The final product was then dried in an oven at 100 °C for about 12 hours. Lastly, it was crushed to powder form for characterization and further experiments.

4.2.3 Synthesis of TiO_2NPs

TiO_2NPs were synthesized via hydrothermal procedure utilizing urea as the nitrogen source and $TiCl_4$ salt as the precursor (Hu et al., 2010, Du et al., 2011). 50 mL of $TiCl_4$ was added dropwise into 200mL deionized water under magnetic stirring in an ice bath (0 ºC). NH_2CONH_2 aqueous solution was prepared by dissolving roughly 12 g of urea in 250 mL deionized water. The dissolved urea solution was added slowly onto the prepared $TiCl_4$ solution under magnetic stirring. Afterwards, it was heated at 110 ºC on a hot plate for about 1h under

continuous stirring. The obtained solution was cooled down and centrifuged. It was then cleaned with deionized water severally, after which, it was left in the oven to dry at 80 ºC for about 12 hrs. The final product was crushed to powder form and was later calcined at 400 ºC for 1 hr.

4.3 INSTRUMENTATION

4.3.1 Characterization analysis

X-ray diffraction (XRD) patterns of $CoFe_2O_4$NPs and ZnONPs were obtained by a Bruker AXS D8 diffractometer with Cu Kα radiation (λ=1.5418 E) working at 40 kV at a sweep rate of 0.5 min^{-1}. Thermal stability of all the nanocomposite samples was probed using a thermal gravimetric analysis (TGA)-differential scanning calorimetry (DSC) 1SF model 1346 (Columbus, USA) with a STARe software version (Mettler Toledo) instrument. The Brunauer-Emmett Teller (BET) surface areas and the total pore sizes distribution of pure MWCNTs and ZnONPs-MWCNTs composites were determined from N_2 adsorption-desorption isotherms at 77 K with a Micromeritics TriStar II surface area and porosity analyzer (Tristar II 3020, USA). The surface morphology of ZnONPs, $CoFe_2O_4$NPs, TiO_2NPs, MWCNTs, MWCNTs-$CoFe_2O_4$, ZnONPs-MWCNTs, TiO_2-MWCNTs, TiO_2-MWCNTs-IL and MWCNTs-IL nanocomposites were determined using FEI T20 Transmission electron microscopy (Hillsboro, Oregon, United States). In addition, the SEM analysis of $CoFe_2O_4$NPs, MWCNTs-$CoFe_2O_4$, MWCNTs-$CoFe_2O_4$-Lipase, TiO_2, TiO_2-MWCNTs, TiO_2-MWCNTs-IL, MWCNTs, MWCNTs-IL and MWCNTs-IL-L-lysine nanocomposite samples was done using the FEI NovaNano Schottky Field Emission Scanning Electron Microscope (Hillsboro, Oregon, United States) equipment. The functional groups of ZnONPs, MWCNTs, MWCNTs-IL-L-lysine, TiO_2, TiO_2-MWCNTs-IL, $CoFe_2O_4$NPs, MWCNTs-$CoFe_2O_4$, ZnONPs-MWCNTs-Cyt c and MWCNTs-$CoFe_2O_4$-Lipase nanocomposites samples were analysed directly without sample preparation by a Cary 630 (Santa Clara, USA) Fourier transform infra-red (FTIR) Spectrometer in the range of 400-4000 cm^{-1}.

4.3.2 Electrochemical measurements

CV and DPV experiments were carry out via 797 VA computrace system (Metrohm, Herisau, Switzerland) equipment at room temperature (Figure 3.1). The system uses three-electrodes; comprising, WE, RE and AE. The following modified GCE sensors were used as WEs; MWCNTs-GCE, MWCNTs-TiO_2-GCE, TiO_2-MWCNTs-IL-GCE, MWCNTs-IL-GCE, MWCNTs-IL-L-lysine-GCE, MWCNTs-$CoFe_2O_4$-GCE, MWCNTs-$CoFe_2O_4$-Lipase-GCE

and ZnONPs-MWCNTS-Cyt c-GCE. Additionally, platinum wire and standard calomel electrode (Ag/AgCl/KCl) were employed as the AE and RE, respectively. Furthermore, the electrochemical impedance spectroscopy (EIS) characterization analysis of GCE and the MWCNTs-$CoFe_2O_4$-Lipase, MWCNTs-IL-L-lysine and TiO_2-MWCNTs-IL modified GCE electrodes were conducted using Metrohm- Autolab (Holland)-instrument. The EIS instrument is also a three-electrode system connected with the Nova 2.1 software installed to the computer. All the EIS experiments were performed in 0.5 mM $[Fe(CN)_6]^{3-/4-}$ in 0.1 M KCl as a redox probe solution at frequency range of 0.1 Hz -10000 Hz, voltage amplitude of 0.01 V_{RMS} and sweep rate of 0.05 V_{RMS}. Furthermore, the CV measurements of both the un-modified GCE and the modified GCE electrodes were obtained within the potential range of -0.1 V to +0.5 V at a sweep rate of 50 mV/s. A pH 211 microprocessor pH meter was used to adjust pH of the prepared solutions to the desired pH values. Nanocomposite paste for GCE modification was prepared with the aid of the ultra-sonic bath (Labcon UBM2, South Africa). Nitrogen gas (N_2) was used to eliminate dissolved oxygen gas in the electrochemical cell contents.

4.3.3 Voltammetry determinations

CV was used for qualitative analysis while DPV was used for quantitative analysis of each anti-asthma drug in pharmaceutical formulations. Prior to all the voltammetric determinations, the electrochemical cell contents were purged using nitrogen gas (N_2) for about 20 minutes to eliminate dissolved oxygen gas (O_2). Current resulting from the applied potential was recorded. Qualitative analysis was then done from the generated voltammogram. Prior to quantification analysis the paramount working parameters, viz., scan rates, pH of the chosen electrolyte solution and the deposition time were optimized. The dependence of the sweep rate and pH of the buffer solution on the peak-current and peak potential was determined from the generated data. Furthermore, based on calibration plots obtained, LOD as well as LOQ values of each fabricated sensor were calculated. In addition, method validation and interference studies of each developed method were done. Lastly, each anti-asthma drug under study was quantified in their respective pharmaceutical formulations.

4.4 Preparation of supporting electrolytes and standard solutions

Standard solutions (0.1M TPN, 0.1M TBS and 2 mM SAL) were prepared by weighing the calculated masses into separate conical flasks and diluting up to the calibration marks with deionized water. Standard solution of PDN with 0.1M concentration was also prepared the same way using methanol solution instead of deionized water.

Phosphate buffer solution (PBS) with 0.1 M concentration was prepared from NaH_2PO_4 and Na_2HPO_4 salts in deionized water for SAL and TPN experimental analyses. Similarly, 0.1M Potassium phosphate buffer solution (KPBS) and 0.2M PBS solution were also prepared from their respective salts for TBS and PDN determinations, respectively. The pH of the prepared electrolyte solutions was adjusted to the required values by using 1 M H_2SO_4 and 1 M NaOH. The standard and electrolyte solutions were kept in the refrigerator at 4°C.

4.5 Preparation and fabrication of nanocomposites-based sensors for detection of anti-asthma drug.

4.5.1 ZnONPs-MWCNTs-Cyt c-GCE sensor for detection of TPN.

Before modification procedure of GCE, the surface of the bare GCE was cautiously polished by rubbing on a polishing cloth using alumina paste. It then was sonicated in a mixture of ethanol and deionized water, washed repeatedly and then dried at 25°C. ZnONPs-MWCNTs paste was prepared by sonicating 0.2 g of the synthesized ZnONPs and 0.1 g of commercial MWCNTs in 10 mL DMF solution for approximately one hr. After a well dispersed paste was formed, 2- μL Nafion® solution was added to it and the mixture was continued to be stirred for additional 10 minutes. The GCE surface was modified using the ZnONPs-MWCNTs dispersion by dropping a given quantity of the paste onto the surface with the aid of a micropipette. The ZnONPs-MWCNTs modified GCE was then dried in the oven at 40 °C to evaporate the DMF solvent used as previously described by Chokkareddy et al. (2019b). In a similar way, MWCNTs modified GCE was prepared.

ZnONPs-MWCNTs-Cyt c nanocomposite modified GCE was prepared using pre-prepared Cyt c enzyme solution. The Cyt c enzyme solution was prepared in 10 mL volumetric flask using of deionized water and 1 mg of Cyt c enzyme powders. Moreover, the mixture was sonicated to get a homogeneous solution. Cyt c solution was immobilized on the surface of ZnO-MWCNTs-GCE by micro-pipetting about 2 μL of the Cyt c solution on it. The fabricated ZnONPs-MWCNTs-Cyt c/GCE was dried for nearly 20 minutes at 4 °C.

4.5.2 MWCNTs-$CoFe_2O_4$NPs-Lipase-GCE for detection of SAL

Approximately 0.1 g MWCNTs and 0.1 g of $CoFe_2O_4$NPs were dispersed in about 10 mL of DMF solution with the help of ultra-sonicator for about an hour to obtain a black paste of $CoFe_2O_4$NPs-MWCNTs nanocomposite. $CoFe_2O_4$NPs-MWCNTs-GCE was fabricated by micro-pipetting about 8 μL of the nanocomposite paste onto the polished GCE surface after

which it was dried at 40 °C in the oven. MWCNTs/GCE was also prepared in the same way. A solution of lipase enzyme was prepared in 10 mL of 0.1 M PBS. To obtain the magnetic based nanocomposite biosensor (MWCNTs-$CoFe_2O_4$-Lipase-GCE); lipase solution and MWCNTs-$CoFe_2O_4$ suspension was thoroughly mixed with the help of the ultra-sonicator. Approximately 8 µL of the obtained MWCNTs-$CoFe_2O_4$-Lipase nanocomposite was dropped on a cleaned GCE surface and allowed to dry at 4 °C for about half an hour.

4.5.3 MWCNTs-IL-L-lysine-GCE for detection of PDN

A weighed 0.1 g of commercial MWCNTs was sonicated in about 10 mL of DMF solution to obtain a black dispersion for MWCNTs-GCE fabrication. Subsequently, approximately 10 µL of the IL was added to the black suspension and was further sonicated to obtain a homogeneous MWCNTs-IL nanocomposite paste for MWCNTs-IL-GCE fabrication by drop casting method and drying it at 30 °C in the oven. Furthermore, 0.1M L-lysine stock solution was prepared by dissolving the calculated amount of 0.1M L-lysine powder in 0.1M PBS and sonicated for about 5 minutes. The MWCNTs-IL-L-lysine-GCE sensor was fabricated by drop casting approximately 5 µL of the L-lysine solution on the prepared MWCNTs-IL-GCE. MWCNTs-IL-L-lysine-GCE was then dried at 4 °C for almost an hour.

4.5.4 TiO_2-MWCNTs-IL-GCE for detection of TBS

Prior to electrochemical measurements, the surface of the bare GCE was thoroughly cleaned as previously described (section 4.5.2). A homogeneous TiO_2-MWCNTs-IL black suspension was prepared in about 20 mL of DMF by dispersing 0.1 g TiO_2NPs, 0.05 g MWCNTs and 10 µL of IL by the help of a sonicator. 8 µL of the obtained TiO_2-MWCNTs-IL suspension was coated onto the surface of GCE using a micropipette. The TiO_2-MWCNTs-IL-GCE was dried in the oven at 40 ºC. The control electrodes; MWCNTs-GCE and TiO_2-MWCNTs-GCE were also prepared following the same procedure.

4.6 Sample preparations

Adco-Alcophyllin described to contain 26.667 mg/5 mL of TPN, venteze syrup (containing 2 mg of SAL in each 5 mL of the syrup) and aspelone syrup (containing 15 mg of PDN per 5 mL) and bricanyl syrup with a specified content of terbutaline as 1.5 mg/5mL were procured from a local pharmacy. Each drug sample was prepared by simply diluting 1 mL aliquot of each oral sample solution with supporting electrolyte solution in a 10 mL measuring cylinder. There was no any further sample pretreatment step. Known concentrations of TPN, SAL, PDN and TBS standard solutions were spiked into their respective pharmaceutical samples and the

recovery studies were investigated. DPV quantification measurements of TPN, SAL, PDN and TBS were carried out using standard addition method under optimum experimental conditions.

CHAPTER 5

5 RESULTS AND DISCUSSION

The present chapter presents the experimental results. Briefly, the characterization analysis results of the synthesized ZnO nanoparticles and its nanocomposite (ZnO-MWCNTs and ZnO-MWCNTs-Cytochrome c), $CoFe_2O_4$ nanoparticles and its nanocomposites ($CoFe_2O_4$-MWCNTs and $CoFe_2O_4$-MWCNTs-Lipase), TiO_2 nanoparticles and its nanocomposites (TiO_2-MWCNTs and TiO_2-MWCNTs-IL) as well as the characterization results of the prepared MWCNTs-IL-L-lysine nanocomposites are discussed. The electrochemical behavior of TPN, SAL, PDN and TBS at ZnO-MWCNTs-Cytochrome c-GCE, $CoFe_2O_4$-MWCNTs-Lipase-GCE, MWCNTs-IL-L-lysine-GCE and TiO_2-MWCNTs-IL-GCE sensors, individually, is also described in detail. In addition, the optimization procedures of the working parameters (pH, time and scan rates) are discussed in this section in detail. Furthermore, method validation studies and the investigation of the applicability of the fabricated sensors in their real drug dosages are also presented in this chapter.

5.1 Detection of theophylline (TPN)

Herein, a simple ZnONPs/MWCNTs/Cyt c modified GCE was fabricated for electro-catalytic oxidation of TPN. Figure 5. 1 displays the stepwise modification of GCE using;

i. MWCNTs,
ii. MWCNTs-ZnONPs
iii. ZnONPs/MWCNTs/Cyt c

EIS method was used to confirm the successful modification of GCE surface.

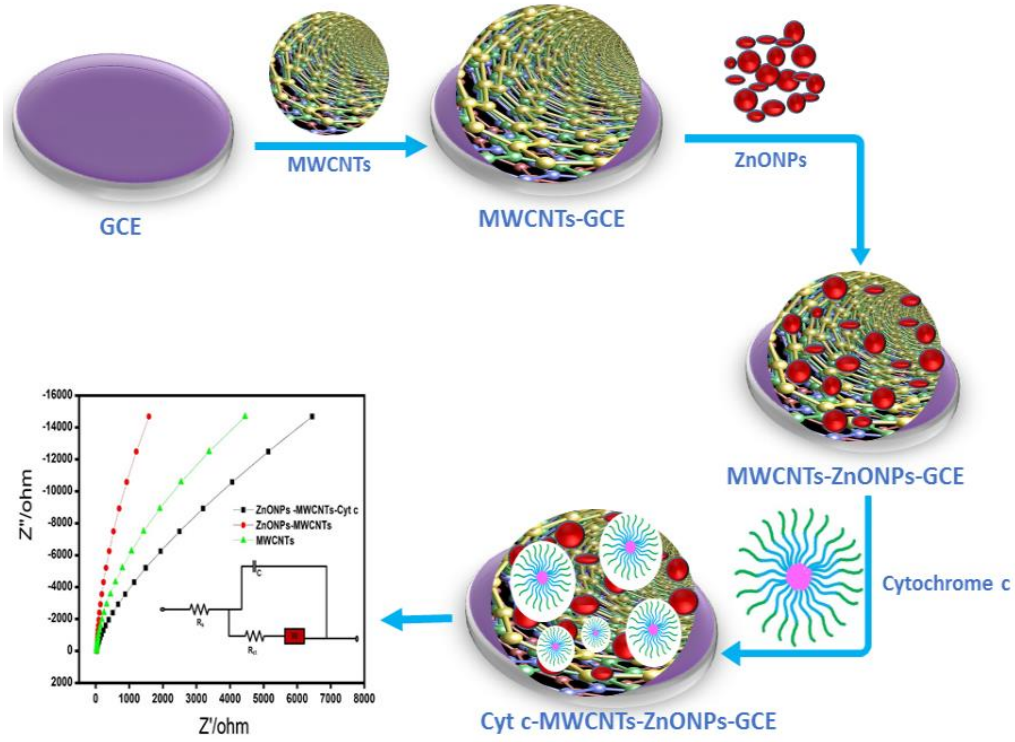

Figure 5.1: **Schematic illustration of the fabricated ZnONPs/MWCNTs/Cyt c/GCE biosensor for TPN detection**

5.1.1 Surface morphology, crystal structure and functional groups

The TEM analysis revealed that ZnONPs exhibited spherical shape (red circles, Figure 5. 2a) with little agglomeration and the average particle size of ZnONPs was estimated to be roughly 18 nm, whereas MWCNTs were tube-shaped (blue arrow, Figure 5. 2b). The attachment of ZnONPs on the tube-like MWCNTs surface (yellow arrow, Figure 5. 2c) confirms the interaction between Zn-O and MWCNTs to form ZnONPs/MWCNTs nanocomposite. Figure 5. 2d reveals the diffraction patterns of the synthesized ZnONPs by XRD. It can be observed

that there are four well-defined peaks at 2θ = 53.27°, 45.53°, 36.95° and 34.23° corresponding to the reflection planes(110), (102), (101) and (100), separately. The four peaks were due to the wurtzite structure of ZnONPs (Yogamalar et al., 2009).

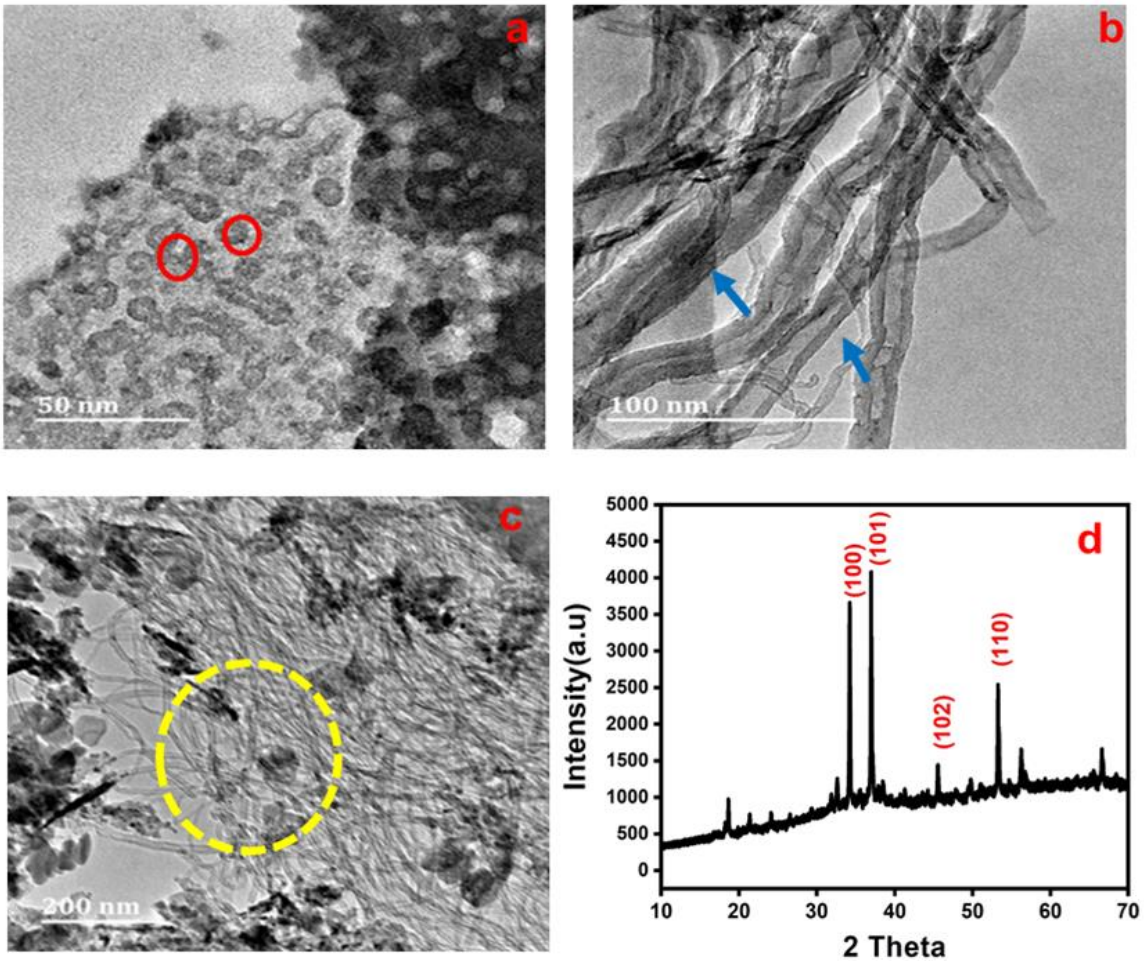

Figure 5.2: **TEM images of ZnONPs (a), MWCNTs (b) and ZnONPs-MWCNTs composite (c). XRD pattern of ZnONPs (d)**

The FTIR spectra of ZnONPs/MWCNTs/Cyt c nanocomposite and ZnONPs are presented in Figure 5. 3. As the spectra revealed in Figure 5. 3, the distinctive peaks at about 3390 cm^{-1} and 3450 cm^{-1} corresponds to the O-H stretching vibrations. The peaks seen at 657 cm^{-1}, 711cm^{-1} and 898 cm^{-1} are ascribed to the Zn–O bond vibrations confirming the successful synthesis of ZnONPs. The new peak at 1646 cm^{-1} observed on the ZnONPs/MWCNTs/Cyt c spectrum correspond to the amide stretching vibration bond of Cyt c. Furthermore, the peaks observed at around 1099 cm^{-1} and 2931 cm^{-1} are due to the bending and stretching of C-H, respectively (Shams et al., 2019). TGA curves of ZnONPs-MWCNTs, MWCNTs and ZnONPs are displayed in Figure 5. 4. The ZnONPs sample showed two decomposition stages whereby the

first mass loss (between 25 °C - 150 °C) was due to the loss of absorbed water on the surface of ZnONPs. The final step at temperature range of 350 °C - 440 °C is attributed to the decomposition of $Zn(OH)_2$ to form ZnONPs, while beyond 440 °C, the ZnONPs curve flattens. ZnONPs/MWCNTs curve also revealed two thermal decomposition stages. The initial step around 25 °C - 130 °C could be attributed to the evaporation of H_2O and the solvent molecules used in preparation of the nanocomposite. The second step observed between 300 °C and 400 °C was due to thermal degradation of MWCNTs (Zou et al., 2017). The TGA curve of pure MWCNTs displays a single decomposition step below 100 °C, owing to evaporation of adsorbed water.

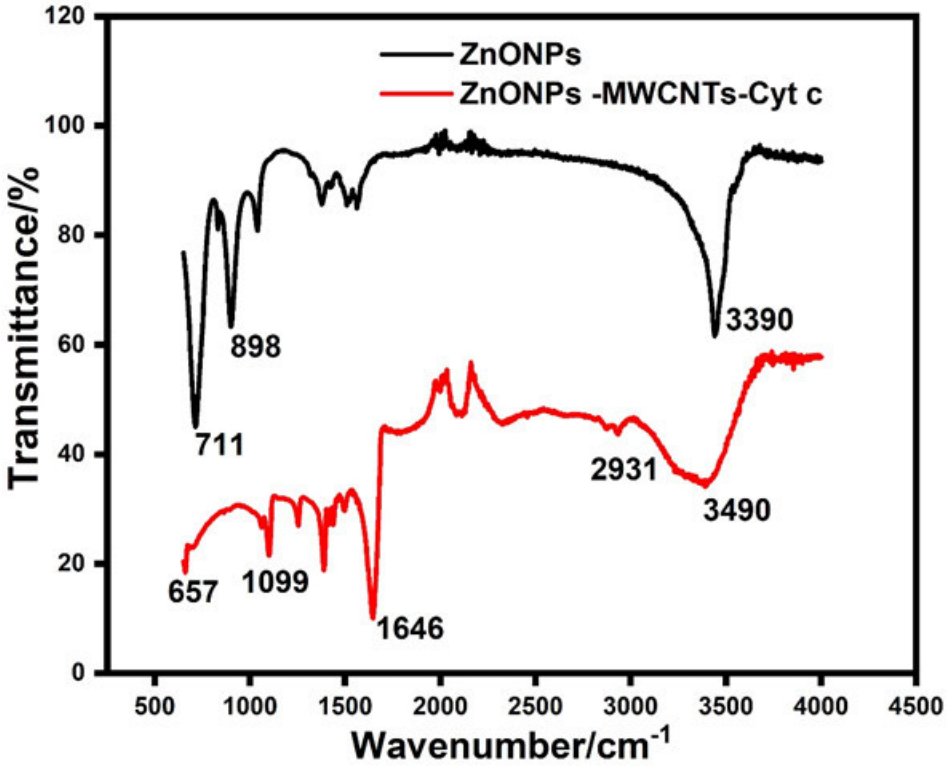

Figure 5.3: **FTIR spectra of ZnONPs and ZnONPs-MWCNTs-Cyt c nanocomposite**

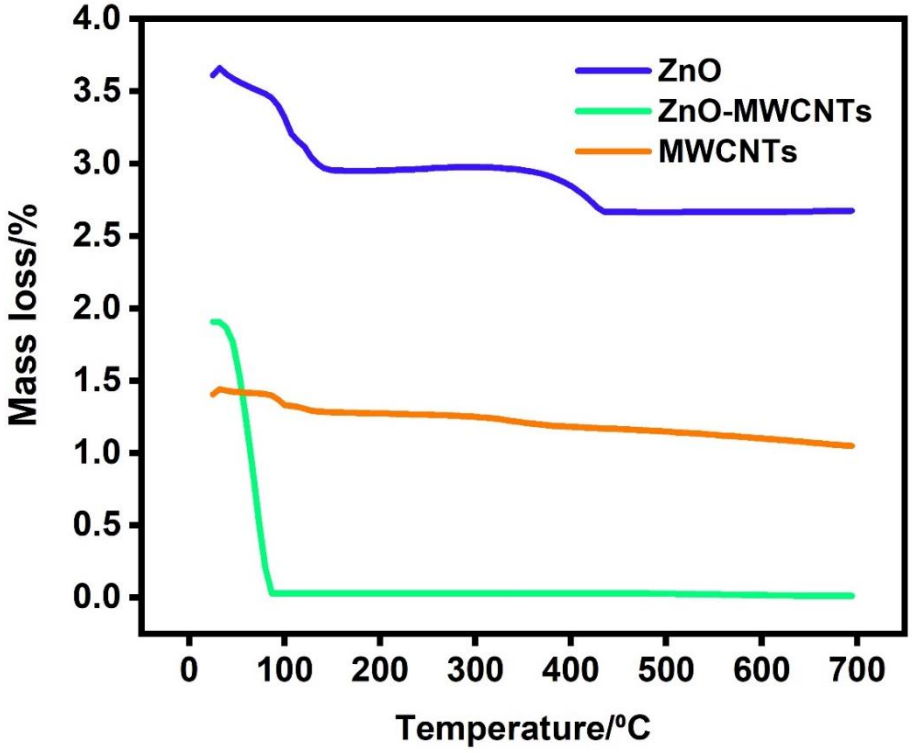

Figure 5.4: **TGA curves of MWCNTs, ZnONPs and ZnONPs/MWCNTs nanocomposite**

5.1.2 Surface area and porosity

Figure 5. 5 and 5. 6 presents the BET results (porosity and surface area properties) of ZnONPs/MWCNTs and MWCNTs samples. As displayed, the isotherms of ZnONPs/MWCNTs and MWCNTs were of type IV with H3 hysteresis loops suggesting that the sample was a powder in crystalline form (Septiani et al., 2018). The estimated surface areas of ZnONPs/MWCNTs and MWCNTs were found to be 119.99m^2/g and 31.38 m^2/g, respectively. Moreover, the total pore volumes 0.32 cm^3/g and 1.36 cm^3/g were for ZnONPs/MWCNTs and MWCNTs, respectively. These results confirm that incorporation of MWCNTs to ZnONPs can increase the active surface area of the resulting ZnONPs/MWCNTs nanocomposite due to the distinctive large surface area of the MWCNTs (119.99m^2/g).

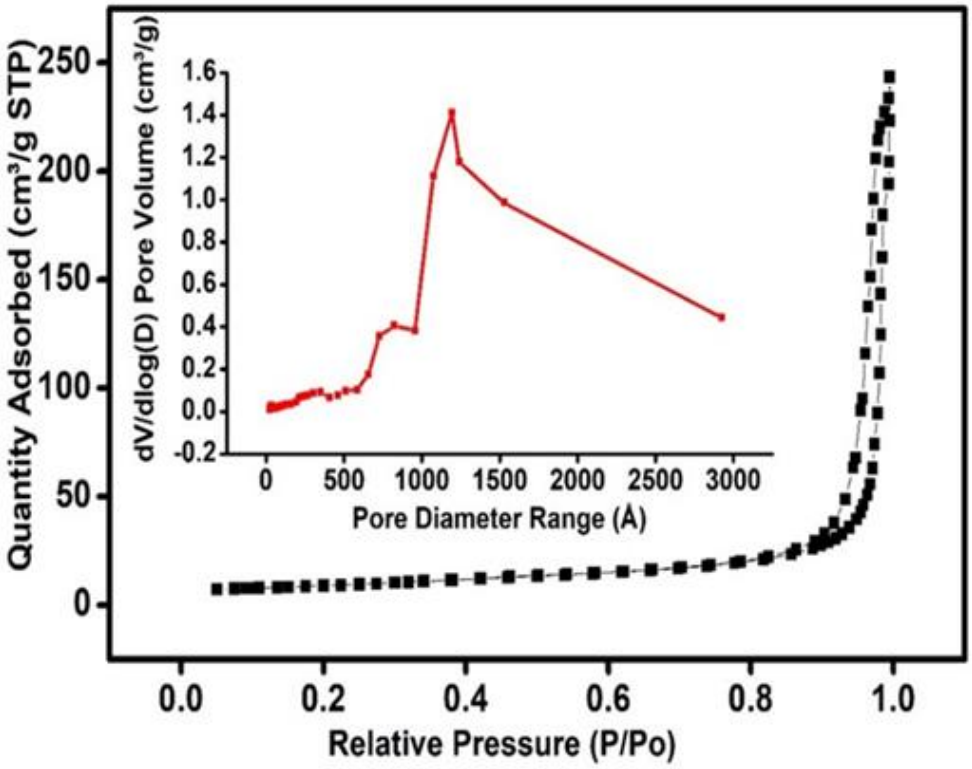

Figure 5.5: **Nitrogen adsorption/desorption isotherm and pore size distribution curve of ZnONPs/MWCNTs (inset)**

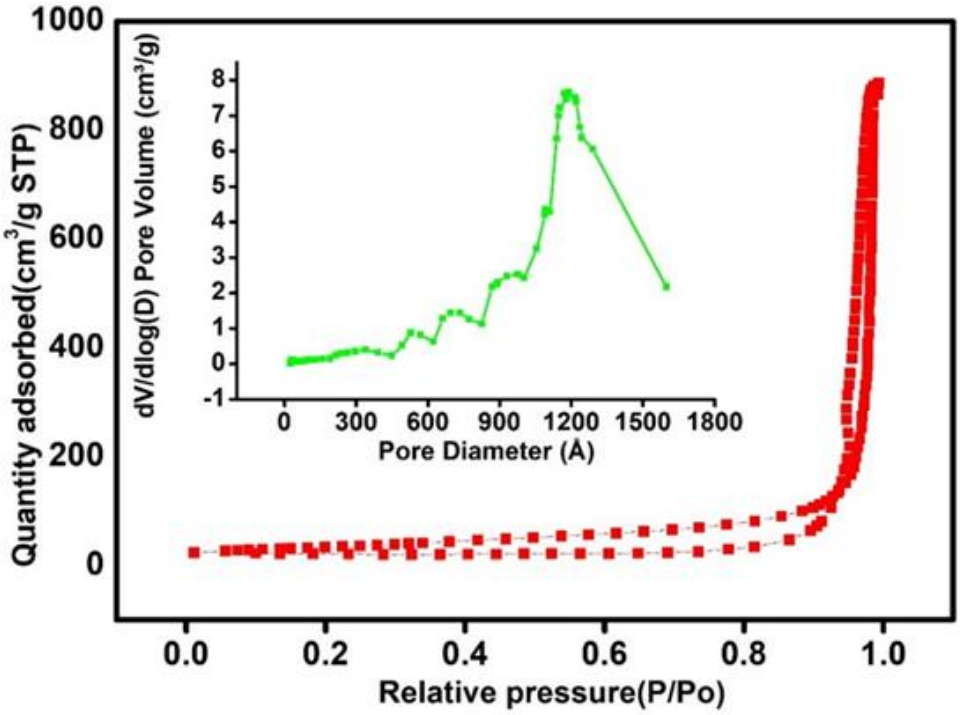

Figure 5.6: **Nitrogen adsorption/desorption isotherm and pore size distribution curve of MWCNTs (Inset)**

5.1.3 Electrochemical impedance spectroscopy (EIS)

The fabricated ZnONPs/MWCNTs/Cyt c/GCE sensor and the control electrodes MWCNTs/GCE and ZnONPs/MWCNTs-GCE were characterized via EIS in 0.1 M KCl containing 0.1 mM $[Fe(CN)_6]^{-3/-4}$. The semi-circular portion of each electrode, which indicates the conductivity of the material, was not observed due to negligible charge transfer resistance (Rct) values. Figure 5. 7 displays only the linear portion of each electrode, confirming the superior conductivity of the novel ZnONPs/MWCNTs/Cyt nanocomposite (Shaikshavali et al., 2020b). MWCNTs/GCE recorded low Rct values due to the presence the highly conductive MWCNTs on the GCE surface. Moreover, the ZnONPs/MWCNTs/Cyt c modified GCE (black curve) exhibited the lowest Rct value suggesting that immobilization of Cyt c on to the ZnONPs/MWCNTs expedites rapid transfer of electrons. The results also confirm that, the synergistic effect of ZnONPs/MWCNTs/Cyt c nanocomposite improves conductivity of GCE. Thus, ZnONPs/MWCNTs/Cyt c nanocomposite is a promising material for electrochemical sensor construction.

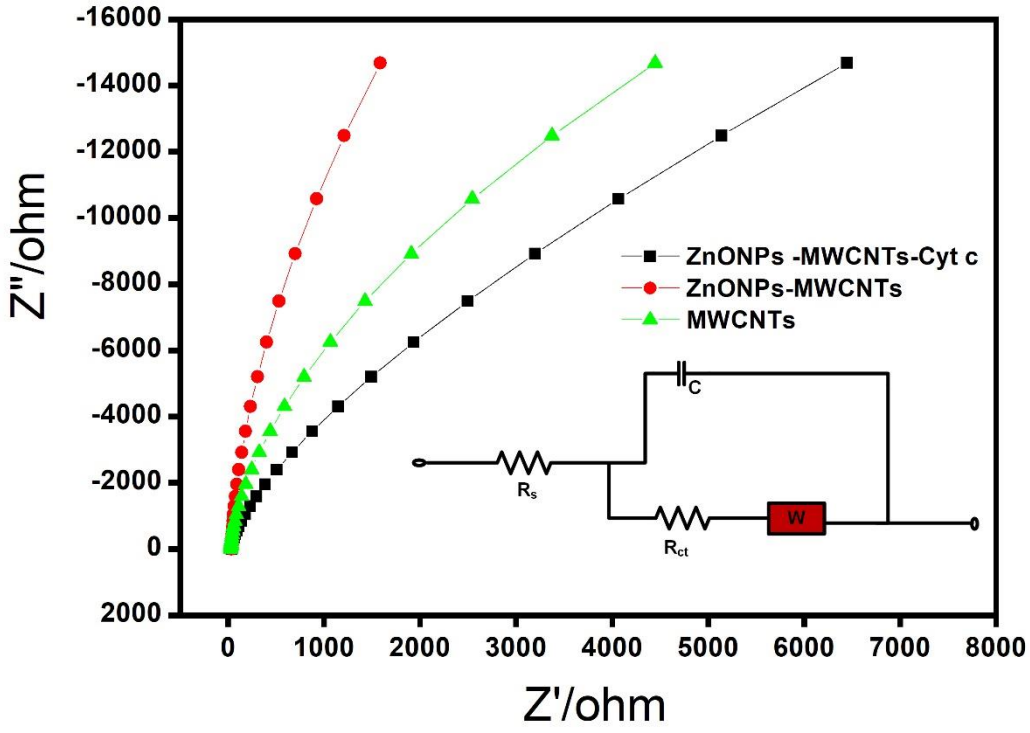

Figure 5.7: **Nyquist plots of ZnONPs-MWCNTs-GCE, MWCNTs-GCE and ZnONPs -MWCNTs-Cyt c-GCE in 0.1 M KCl solution containing 0.1 mM $[Fe(CN)_6]^{-3/-4}$**

5.1.4 Electro-oxidation of TPN

The electro-oxidation of 0.1 M TPN in 0.1 M PBS at the developed ZnONPs-MWCNTs-Cyt c-GCE sensor was studied using CV within the applied potential window of 0.7 V to 1.6 V. The sweep rate, accumulation time and the pH of the 0.1 M PBS were optimized and the optimum values of each parameter were chosen based on the peak-current height of TPN, the anodic peak shape as well as good peak separation. In addition, the influence of each working parameter on the peak potential and on the oxidation current response of TPN was studied.

5.1.4.1 The pH of the supporting electrolyte

The effect of pH of 0.1 M PBS on the electrochemical current response and peak potential of 0.1 M TPN via CV. Figure 5. 8b presents the cyclic voltammograms at GCE recorded at a sweep rate of 0.1 V/s and over the pH range of 1.0-5.0. The CV did not record any peak (Figure 5. 8b, PBS) at the unmodified GCE in absence of TPN stock solution. An irreversible anodic peak was seen upon micro-pipetting 0.1 M standard solution into the 0.1 M PBS for all the pH range as displayed in Figure 5. 8b. Furthermore, the current response decreased as the value of the pH increased towards basic values revealing that protonation of TPN is more favorable at low pH values. However, Based on the stable and sharp peak with maximum anodic current,

pH value of 3.5 was chosen for further analyses of TPN. Furthermore, the peak potential of TPN shifted negatively with increasing pH values. The relationship between peak potential and pH determines the number of protons and electrons transferred during the electrochemical oxidation of TPN. The irreversible oxidation process of TPN reportedly involves the transfer of two protons and two electrons (Malode et al., 2012) (Figure 2. 6).

5.1.4.2 Effect of accumulation time

Figure 5. 8a displays the cyclic voltammogram of 0.1M TPN in 0.1 M PBS (pH 3.5) at the surface of the GCE from 5 s to 60 s. The oxidation peak-current response of 0.1 M TPN solution increased steadily with increasing deposition time from 5 s - 60 s reaching a maximum peak-current height at 60 s. Beyond 60 s, the peak-current response remained almost constant. This can be ascribed to the saturation of adsorbed TPN molecules on the surface of GCE (Kulkarni et al., 2020). Consequently, 60 s was chosen for further TPN analyses.

5.1.4.3 Effect of sweep rate

The CV voltammogram of 0.1 M TPN at the bare GCE at various sweep rates (from 0.1 V/s to 1.0 V/s) under optimal time (60 s) and pH (3.5) is shown in Figure 5. 8c. An anodic peak was recorded at the bare GCE and the measured peak-currents increased with increasing sweep rates from 0.1 V/s to1.0 V/s. A linear relationship between the anodic current (I/µA) and the scan rate (V/s) was obtained as presented in Figure 5. 8c (inset). In addition, the plot of anodic current (I/µA) vs $\sqrt{scan\ rates(\frac{V}{s})}$ (Figure 5. 8d) was found to be linear with regression equation of $\mathrm{I}/\mu\mathrm{A} = 33.408\mathrm{x} - 6.279, R^2 = 0.9937$. Furthermore, the anodic peak potential of TPN shifted positively with increase in scan rates implying that the oxidation reaction is an adsorption-controlled process (Kesavan et al., 2019). The optimum scan rate for further TPN studies was selected as 1.0 V/s.

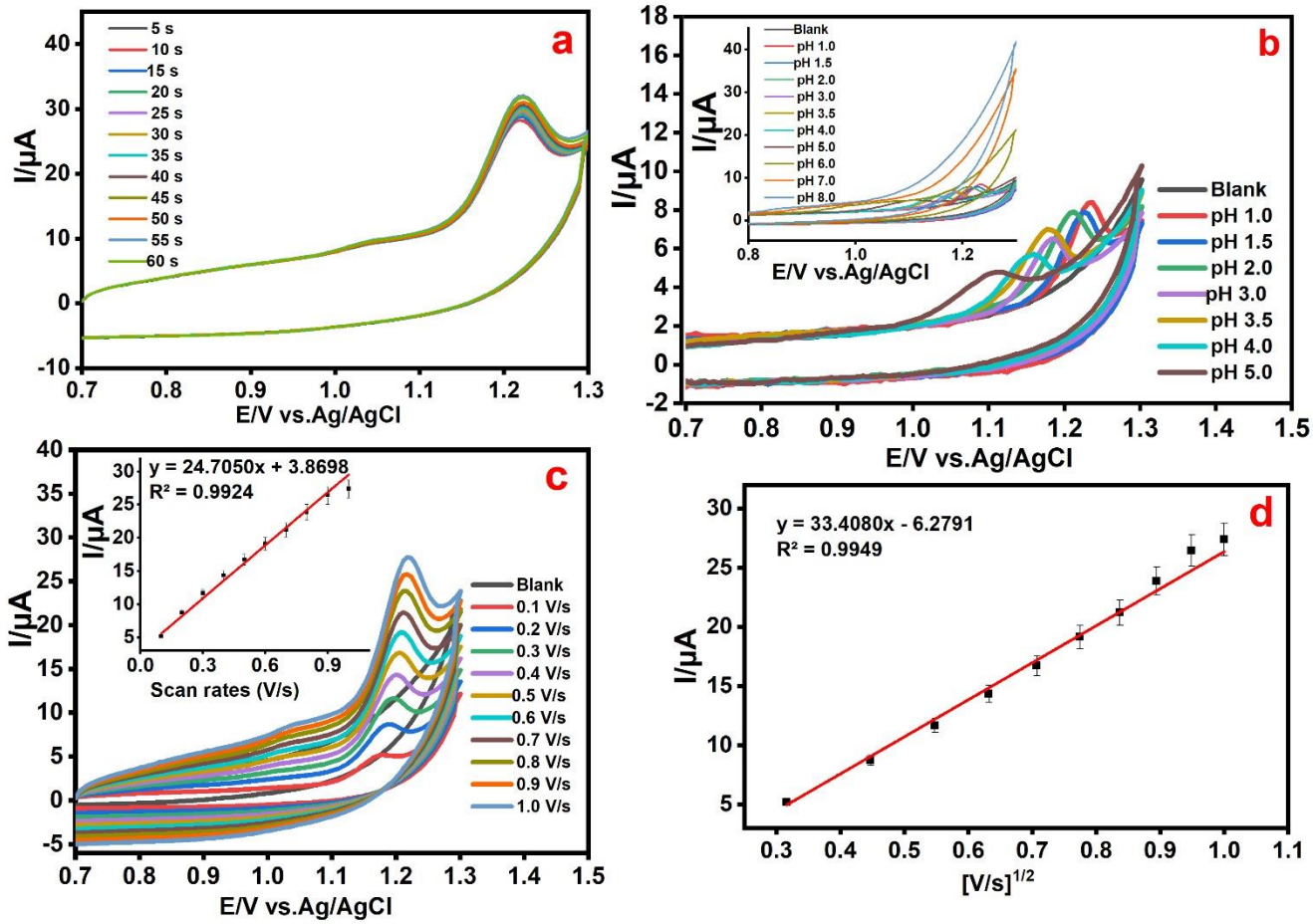

Figure 5.8: **Cyclic voltammograms of TPN recorded at bare GCE showing the effect of varying deposition time (a), effect of pH of PBS (b) and effect of scan rates (c). Plot of peak-current (I/µA) Vs $[V/s]^{1/2}$(d)**

5.1.5 Electrochemical performance of ZnONPs-MWCNTs-Cyt c-GCE for TPN

The electrochemical performance of the fabricated sensor for TPN detection was studied using CV method at various sweep rates in the range of 0.1 V/s -1.0 V/s. Distinct anodic peaks were recorded at the surface of the modified GCE unlike at the bare GCE surface. Modification of GCE with MWCNTs remarkably improved the anodic peak-currents of TPN. This may be ascribed to the highly conductive MWCNTs, which increases the rate at which electrons are transferred. In addition, the ZnONPs/MWCNTs modified GCE exhibited higher peak-current response than MWCNTs/GCE because the ZnONPs/MWCNTs nanocomposite possesses excellent electro-catalytic activity, which further accelerates transfer of electrons. Furthermore, there was a dramatic increase of anodic peak-currents of TPN at the proposed sensor ZnONPs/MWCNTs/Cyt c/GCE (Figure 5. 9). This can be attributed to the synergy between the Cyt c, ZnONPs and MWCNTs, which undoubtedly improves the conductivity of the

nanocomposite (ZnONPs/MWCNTs/Cyt c) hence it magnifies the current response. Besides, ZnONPs/MWCNTs composite acts as the supporting material for the immobilization of Cyt c enzyme. This may possibly accelerate electron transfer, and Cyt c offers sufficient active sites for the adsorption of more TPN molecules. The excellent electrochemical performance confirm the successful fabrication of ZnONPs/MWCNTs/Cyt c/GCE for sensitive determination of TPN. TPN is oxidized at the surface of the fabricated electrode to 1, 3-dimethyluric acid and the possible electro-oxidation mechanism (Figure 2. 6) is based on two-electron/two-proton transfer process (Bukkitgar et al., 2018, Quintanilla et al., 2016).

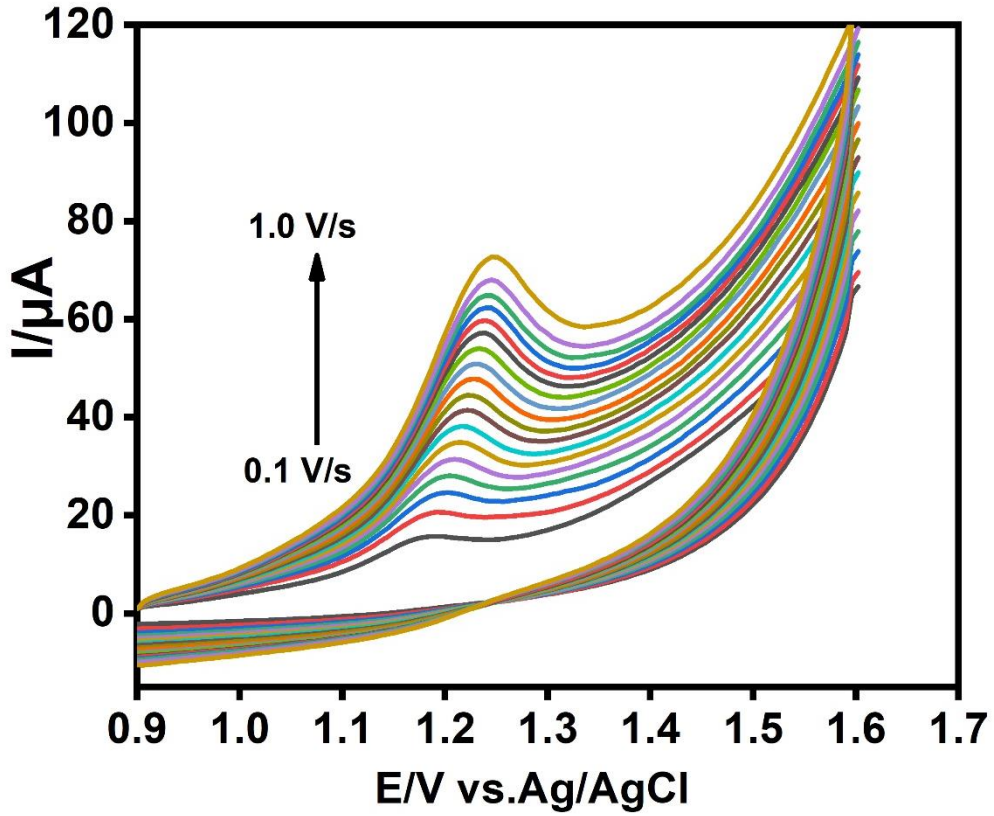

Figure 5.9: **Cyclic voltammogram of 0.1 M TPN in 0.1 M PBS pH 3.5 at ZnONPs-MWCNTs-Cyt c-GCE sensor obtained at various sweep rates (0.1 V/s-1.0 V/s)**

5.1.6 Method validation analyses via DPV

DPV is a more sensitive and rapid mode than CV thus it is often adopted for quantitative determination of electro-active compounds at trace concentration levels (Li et al., 2015). Figure 5. 10a displays the DP voltammogram of various concentrations of 0.1 M TPN in 0.1 M PBS (pH =3.5 at the fabricated ZnONPs/MWCNTs/Cyt c/GCE. Under optimum experimental conditions, a stable and distinct oxidation peak was recorded at about 1.0 V vs Ag/AgCl (Figure 5. 10a). The oxidation peak-current increased with the increase of TPN concentration in the

range of 0.4 µM - 15 µM (Figure 5. 10b). The plot of the TPN anodic peak-current (I/µA) vs its concentration (µM) is presented in Figure 5.10b. The corresponding regression coefficient (R^2) was 0.9903 and the LOD of the ZnONPs/MWCNTs/Cyt c/GCE was estimated from the calibration curve. The calculated LOD was as low as 0.0012 µM, which was much lower than that of the previous fabricated electrodes (Table 5.1) for TPN detection in drug dosages and other samples.

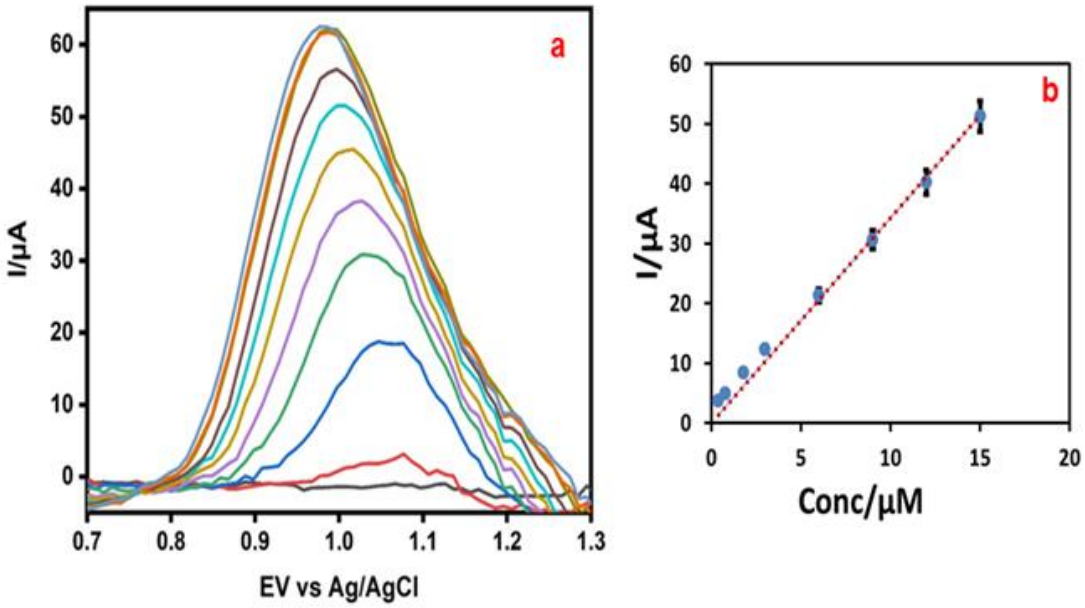

Figure 5.10: **DP voltammogram of 0.1 M TPN with various concentration range (from 0.4 µM to 15 µM) in 0.1 M PBS (pH 3.5) at the ZnONPs/MWCNTS/Cyt c/GCE (a) (Conditions: pulse amplitude 0.09 V, sweep rate 0.1 V/s, voltage step 0.005951 V, Pulse time 0.05 s, deposition potential -0.1009 V and deposition time 60 s). Plot of peak-current (I/µA) against concentration (µM) of TPN (b)**

Table 5.1: **The LOD of ZnONPs/MWCNTs/Cyt c/GCE sensor compared with other reported sensors for electrochemical sensing of TPN**

Electrochemical electrodes	LOD/ µM	References
MWCNTs/Au/Poly-L-lysine/Screen printed electrode	2.0	(Peng et al., 2017a)
MWCNTs-GCE	0.05	(Zhu et al., 2005)
Graphene quantum dots/Screen printed electrode	0.2	(Ganjali et al., 2018)
Poly(L-aspartic acid)/f-MWCNTs-GCE	0.02	(Mekassa et al., 2017)
Poly(CTAB)-GCE	0.11	(Yang et al., 2016)
Molecularly imprinted polyargine/sodium alginate/ MWCNTs/GCE	0.0032	(Salajegheh et al., 2019)
Molecularly imprinted poly (4-amino-5-hydroxy-2,7-naphthalenedisulfonic acid)/GCE	0.32	(Aswini et al., 2016)
Nitrogen-doped carbon nanotubes decorated poly (L-Cysteine)-GCE	0.033	(Wang et al., 2018b)
Zinc oxide nanoparticles-MWCNTs-Cytochrome c-GCE	0.0012	This work

5.1.6.1 Selectivity, reproducibility and stability

The interference of various compounds such as sugars on the electrochemical response of 0.1 M TPN was examined by DPV in order to evaluate the selectivity of the fabricated ZnONPs/MWCNTs/Cyt c/GCE biosensor. Addition of salts, sugars, ascorbic acid, chlorogenic acid, acetaminophen and streptomycin presented insignificant effect at the anodic peak position and peak-currents of TPN. The constructed ZnONPs/MWCNTs/Cyt c/GCE biosensor demonstrated incredible specificity for TPN in presence of interfering substances with only two other anodic peaks at 0.45 V vs. Ag/AgCl and 0.29 V vs. Ag/AgCl for acetaminophen and

chlorogenic acid, respectively (Figure 5. 11). The excellent selectivity achieved is because of the immobilization of Cyt c on the ZnONPs/MWCNTs nanocomposite. Cyt c acts as a bio-recognition agent because it is exceptionally specific and selective (Aghamiri et al., 2018). Moreover, the reproducibility of the developed method was investigated by fabricating six different ZnONPs-MWCNTs-Cyt c-GC electrodes using the same procedure for detection of 0.1 M TPN under similar optimized DPV working parameters. All the prepared electrodes exhibited roughly same peak-current height at the same anodic peak position. Furthermore, the stability of the ZnONPs-MWCNTs-Cyt c-GCE was examined by measuring DPV current response of 0.1 M TPN each day for five days. The ZnONPs-MWCNTs-Cyt c-GCE was stored at 4 °C daily after use. The results showed that there was no great decrease in the oxidation peak-currents response of TPN at the ZnONPs-MWCNTs-Cyt c modified GCE after the five days, indicating the good stability of the proposed sensor.

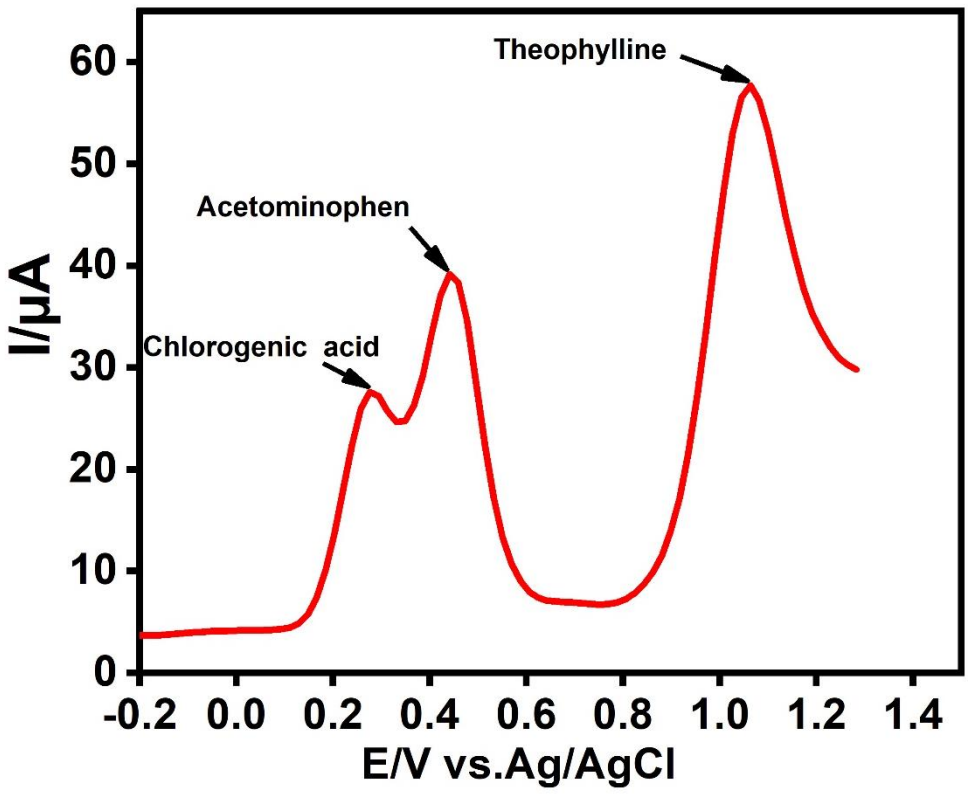

Figure 5.11: **DP voltammogram of 0.1 M TPN at the ZnONPs-MWCNTs-Cyt c-GCE upon addition of different interfering compounds**

5.1.7 Practical application of the fabricated sensor in real samples

The ZnONPs-MWCNTs-Cyt c modified GCE was used to determine TPN in Adco-Alcophyll; an oral sample solution, containing TPN anhydrous (26.667 mg/5 mL). The sample was diluted

by 0.1 M PBS and known concentrations of TPN standard solution was spiked into the real sample and used for DPV analysis via standard addition method. The percentage recovery of the sample solution for each addition was calculated (Table 5.2). Satisfactory percentage recoveries and relative standard deviation (RSD) percentage results were achieved.

Table 5.2: **Determination of TPN in drug formulation sample**

Sample	**Spiked (mg/mL syrup)**	**Found (mg/mL syrup)**	**Recovery (%)**	**RSD (%)**
Adco-Alcophyllin syrup (26.667 mg/5mL)	10.00	10.29	102.90	1.62
	20.00	19.88	99.40	1.38
	30.00	32.05	106.80	1.86
	40.00	41.02	102.50	1.52

5.2 Determination of salbutamol

SAL was determined using a novel MWCNTs-$CoFe_2O_4$-Lipase-GCE sensor. The electro-catalytic activity of the proposed sensor for electro-oxidation of SAL was investigated by using CV and the practical potential of the developed sensor was investigated in SAL oral formulation via DPV as demonstrated in Figure 5. 12.

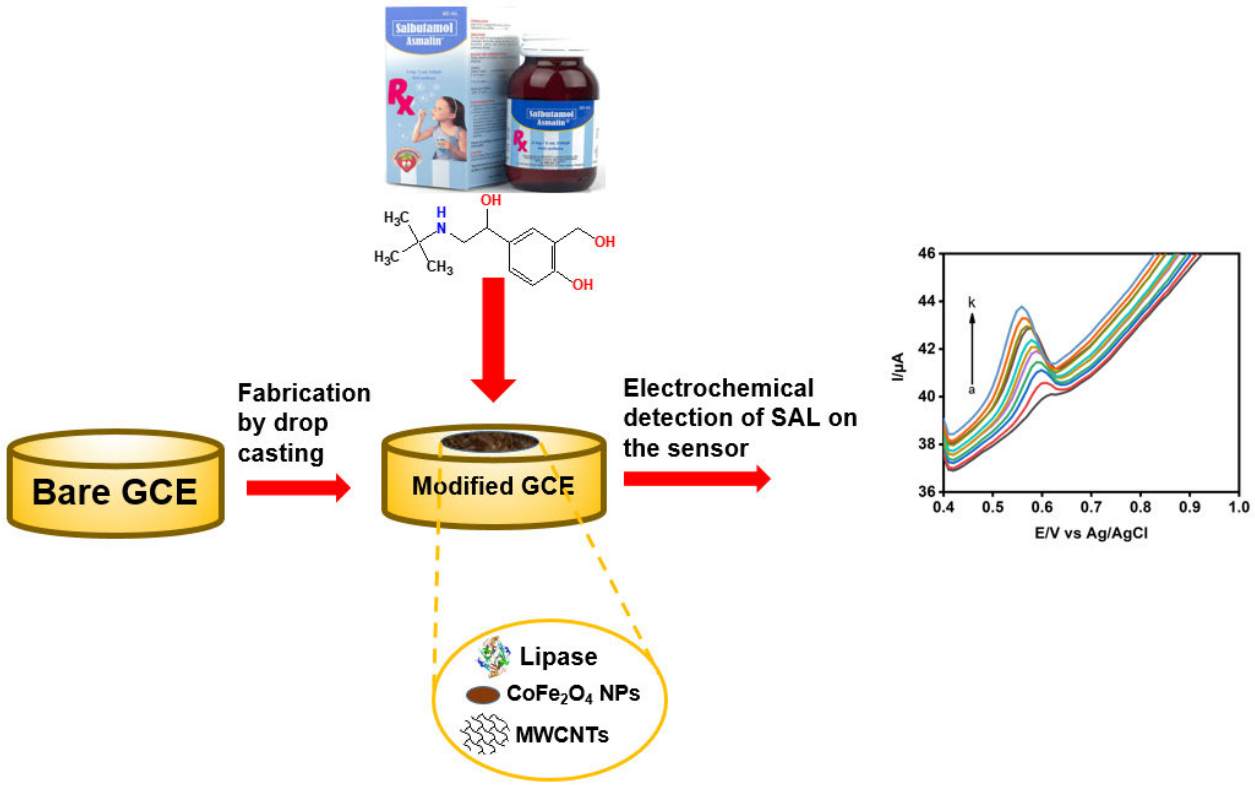

Figure 5.12: **Schematic representation of the electrochemical detection of SAL using MWCNTs-$CoFe_2O_4$-Lipase modified GC electrode surface**

5.2.1 Functional groups, thermal stability analysis, crystal structure and surface morphology

Figure 5. 13 presents the FTIR spectra of $CoFe_2O_4$NPs, MWCNTs-$CoFe_2O_4$ and that of MWCNTs-$CoFe_2O_4$-Lipase nanocomposite. The peaks observed at around 3384 cm^{-1}-3463 cm^{-1} on the spectra are attributed to the stretching vibrations of hydroxyl groups because of the absorbed H_2O (water) on the surface of the NPs and the nanocomposites (Vadivel et al., 2016, Acharya et al., 2020). Furthermore, the absorption peak at 1700 cm^{-1} can be attributed to the bending vibrations of the O-H group. The characteristic peaks located at 598 cm^{-1}, 550 cm^{-1}, 529 cm^{-1} and 684 cm^{-1} are assigned to the Co-O and Fe-O stretching vibrations in their specific sites. This attests the $CoFe_2O_4$NPs spinel phase formation (Karaagac et al., 2019, Mahdi Ghazanfari n, 2015). The MWCNTs-$CoFe_2O_4$-Lipase and MWCNTs-$CoFe_2O_4$ nanocomposites revealed three distinctive peaks at 2859 cm^{-1}, 1541 cm^{-1} and 1345 cm^{-1} assigning to the C=C, C–H, and COO^- groups, respectively. The shift in the peak position of the characteristic bands observed at the nanocomposite samples may be due to the interactions between the functional groups forming the respective nanocomposites.

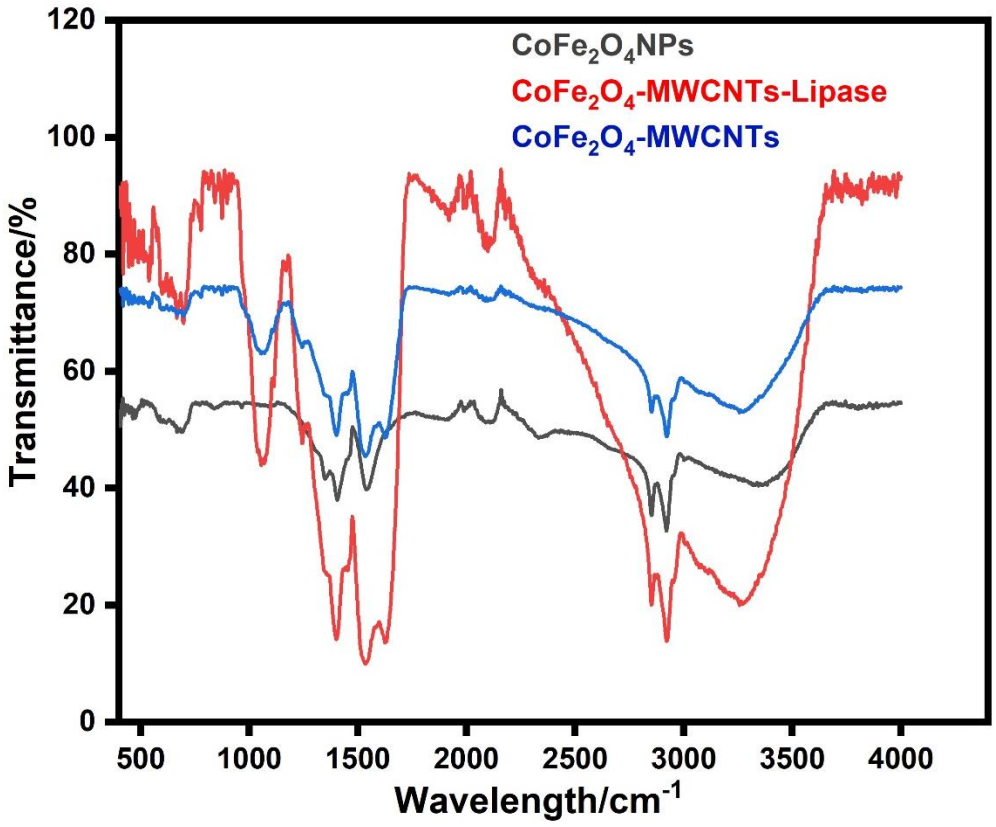

Figure 5.13: **FTIR Spectra of $CoFe_2O_4$NPs, MWCNTs-$CoFe_2O_4$ and MWCNTs-$CoFe_2O_4$-Lipase samples**

Thermal behaviour of the commercial MWCNTs, $CoFe_2O_4$-MWCNTs nanocomposite and $CoFe_2O_4$NPs was studied under nitrogen gas. Figure 5. 14a displays the thermal curves of $CoFe_2O_4$NPs and $CoFe_2O_4$-MWCNTs prepared. The synthesized $CoFe_2O_4$NPs displays three decomposition phases representing the three different mass loss. The first loss occurring at 110°C is due to the loss of solvent molecules on the surface of $CoFe_2O_4$NPs. $CoFe_2O_4$NPs curve shows that second weight loss occurred between 300 °C and 450 °C. This may be due to loss of the surfactant used in synthesis of cobalt ferrite nanoparticles (Ayyappan et al., 2011). It can be further observed that, the final loss corresponding to the structural change of $CoFe_2O_4$NPs occurred around 750 °C - 850 °C. Past 850 °C, the curve of $CoFe_2O_4$NPs is roughly flat, indicating the existence of $CoFe_2O_4$NPs only (Prabhakaran et al., 2016). For commercial MWCNTs curve (not shown), one decomposition phase was observed at around 550 °C- 800 °C. This may be due to the degradation of MWCNTs resulting to loss of the corresponding functional groups (Bibi et al., 2017). For the MWCNTs-$CoFe_2O_4$ composite, the initial weight loss observed at lower temperature (below 200 °C) might be because of the evaporation of ethanol and water molecules. The second decomposition step due to decomposition of MWCNTs was observed between 350 °C and 600 °C (Acharya et al., 2020), whereas the last step at 800-900 °C indicates the existence of $CoFe_2O_4$NPs in the composite (Zhang et al., 2015). Figure 5. 14b displays the XRD patterns of $CoFe_2O_4$NPs. The peaks noted at $2\theta = 75.27°$, 56.44°, 45.40° and 32.00° were assigned to (5 3 3), (5 1 1), (4 0 0) and (2 2 0) planes of the spinel crystal structure of the synthesized $CoFe_2O_4$NPs, respectively (Wu et al., 2011a).

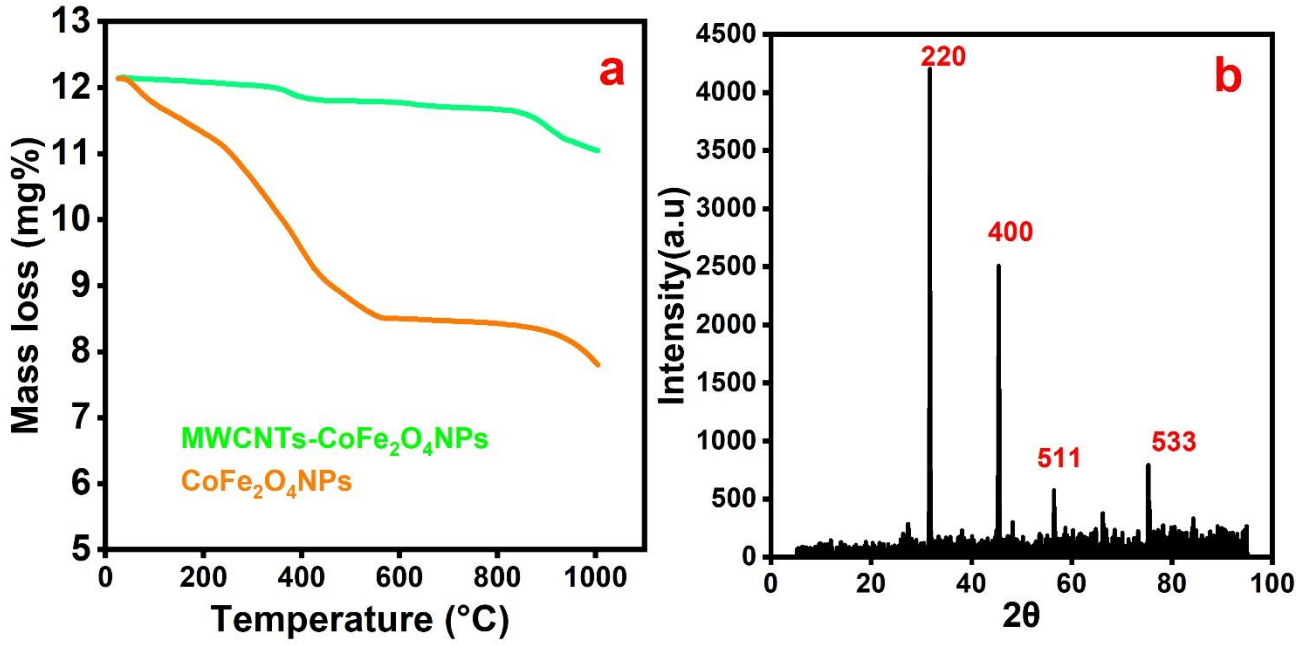

Figure 5.14: **(a) TGA curves of commercial MWCNTs, MWCNTs-$CoFe_2O_4$ and $CoFe_2O_4$NPs samples. (b) XRD pattern of the synthesized $CoFe_2O_4$NPs**

SEM micrographs of the $CoFe_2O_4$NPs, MWCNTs-$CoFe_2O_4$ and MWCNTs-$CoFe_2O_4$-Lipase samples are presented in Figure 5. 15. A good number of the $CoFe_2O_4$NPs seem to cluster as revealed in Figure 5. 15a. Nevertheless, on addition of MWCNTs by the help of ultra-sonification, only few particles seem to aggregate (Figure 5. 15b), suggesting that a higher dispersion is achieved by coating of the spinel ferrite with MWCNTs. A scrutiny of Figure 5. 15c presents an even distribution of $CoFe_2O_4$NPs on the surface of MWCNTs and the lipase enzyme forming the hybrid nanocomposite. In addition, Figure 5. 16 reveals the TEM images of the synthesized $CoFe_2O_4$NPs and that of the prepared MWCNTs-$CoFe_2O_4$ nanocomposite samples. As shown in Figure 5. 16a, most of the synthesized $CoFe_2O_4$NPs are spherical in shape; however, the SEM micrograph also confirms that some of the nanoparticles appear to cluster as exhibited by the TEM image. The mean size of $CoFe_2O_4$NPS was estimated to be 35 nm. From Figure 5. 16b, MWCNTs are tube-shaped and it further shows the attachment of the spherical $CoFe_2O_4$NPS on the MWCNTs surface.

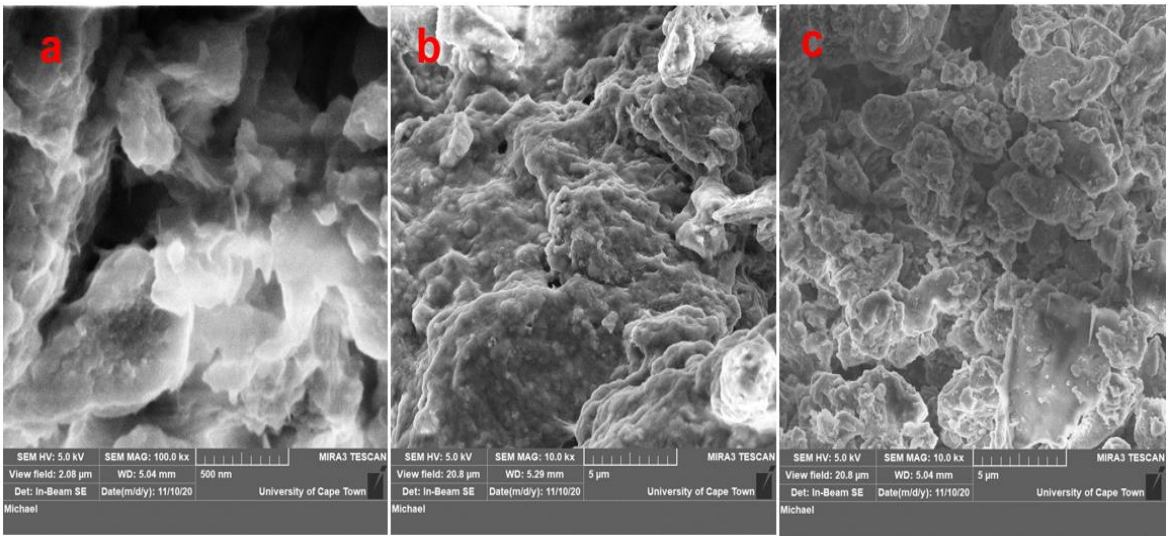

Figure 5.15: **SEM micrographs of $CoFe_2O_4$NPS and $CoFe_2O_4$-MWCNTs and MWCNTs-$CoFe_2O_4$-Lipase nanocomposite**

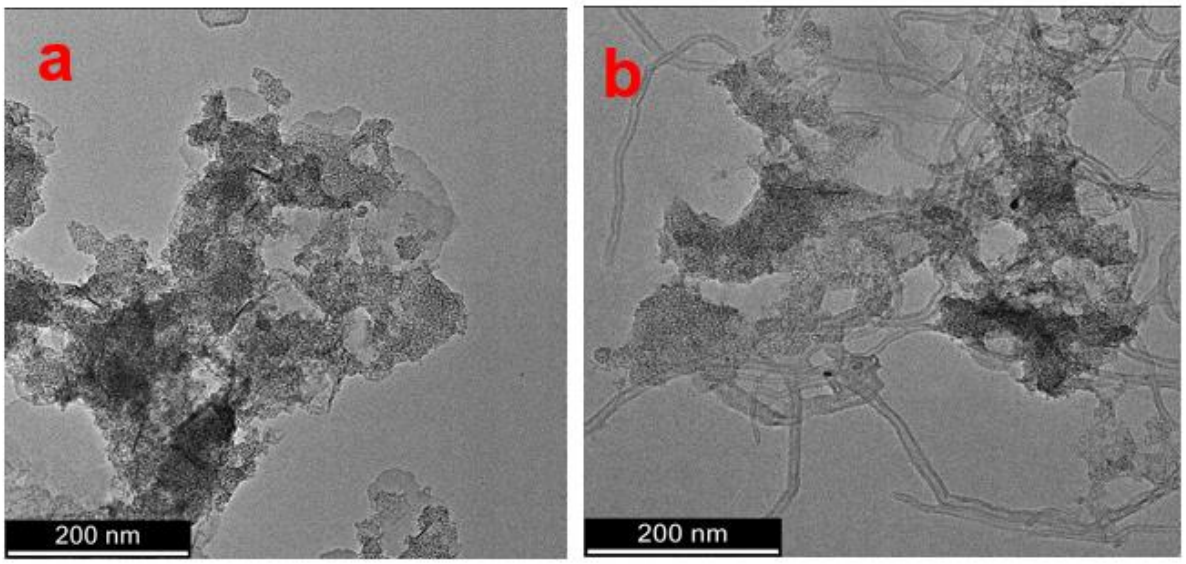

Figure 5.16: **TEM images of $CoFe_2O_4$NPs and MWCNTs-$CoFe_2O_4$ nanocomposite samples**

5.2.2 CV and EIS characterization of the GCE and MWCNTs-$CoFe_2O_4$-Lipase modified GCE

The stepwise modification of GCE using MWCNTs-$CoFe_2O_4$-Lipase hybrid nanocomposite was probed by CV and EIS techniques. The cyclic voltammogram of 0.5 mM $[Fe(CN)_6]^{-3/-4}$ in 0.1 M KCl solution on the MWCNTs-$CoFe_2O_4$-Lipase-GCE, MWCNTs-$CoFe_2O_4$-GCE, MWCNTs-GCE and on the unmodified GCE surfaces are presented in Figure 5. 17A. Compared to the unmodified GCE, the modified electrodes showed an increased peak-current

response, which is attributed to the increase in the GCE active surface area during the modification. This incredible electrochemical response clearly indicates successful modification of GCE surface. Figure 5. 17B shows the Nyquist plots of the same four electrodes. The GCE (black curve) exhibited the largest semi-circle with Rct value of 7160.40 Ω confirming the low transfer of electrons on its surface (Shaikshavali et al., 2019). Upon modification of GCE, the semicircle dramatically decreased. The Rct values of MWCNTs-GCE (blue curve) and MWCNTs-$CoFe_2O_4$-GCE (green curve) Rct reduced to 413.38 Ω and 9179.60 Ω, respectively. The Rct value of the MWCNTs-$CoFe_2O_4$-Lipase nanocomposite modified GCE (red curve) decreased further to 1050.80 Ω. These results are consistent with the CV results and confirms the successful fabrication of the MWCNTs-$CoFe_2O_4$-Lipase-GCE.

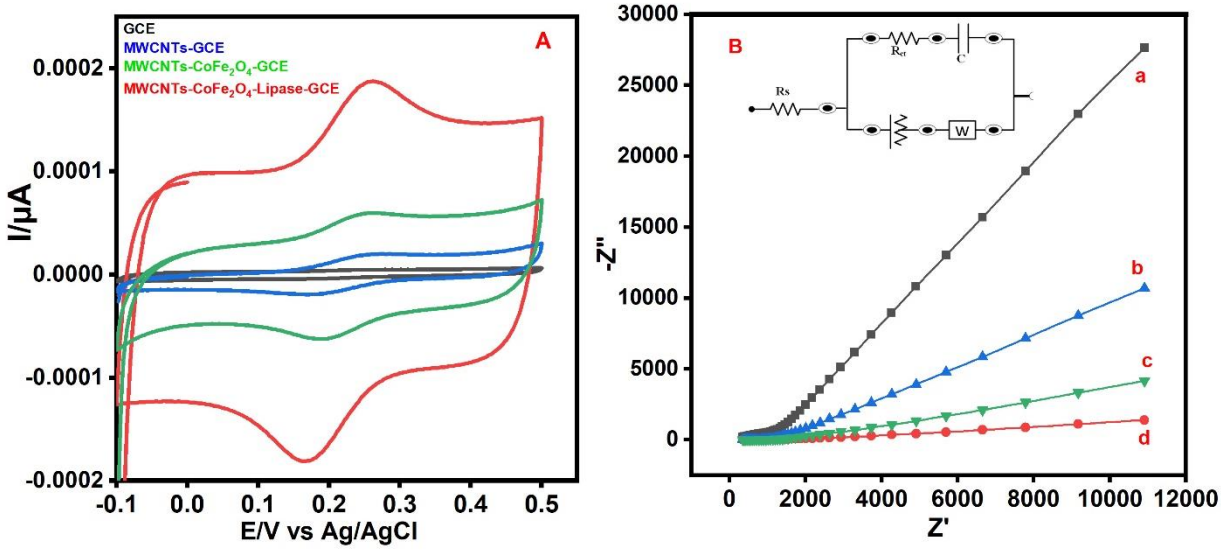

Figure 5.17: **CV voltammograms (A) and the Nyquist plots (B) obtained at the GCE MWCNTs-GCE, MWCNTs-$CoFe_2O_4$-GCE and MWCNTs-$CoFe_2O_4$-Lipase-GCE. Figure 5. 17B (Inset) presents the employed equivalent circuit used to fit the impedance results**

5.2.3 Electro-oxidation of SAL at GCE and composite modified GCE

Figure 5. 18 presents the cyclic voltammograms of bare GCE as well as that of the MWCNTs-$CoFe_2O_4$-Lipase nanocomposite modified GCE. The CV experiments were conducted in 0.1 M PBS at 0.1 V/s scan rate and deposition time of 60 s. On addition of 2 mM SAL stock solution, an irreversible anodic peak was observed within the potential widow of 0.3 V to 1.0 V. However, GCE exhibited a weak broad anodic peak at 0.71 V vs. Ag/AgCl (Figure 5. 18a). The poor electrochemical response at the bare GCE is due to slow electron transfer.

Interestingly, upon modification of the GCE with MWCNTs, MWCNTs-$CoFe_2O_4$ and MWCNTs-$CoFe_2O_4$-Lipase nanocomposite, a well-defined anodic peak with high anodic peak-currents was recorded as shown in Figure 5. 18b, 5. 18c and 5. 18d, respectively. Fast electron transfer as shown by greater peak-current response distinguishes MWCNTs-$CoFe_2O_4$-Lipase-GCE. The amplified current response indicates the superb electro oxidation ability of the nanocomposite modified GCE towards SAL. From previous works, MWCNTs have been reported to possess superior features such as greater conductivity and large surface area, hence are able to speed up transfer of electrons during the electro-oxidation reaction of SAL. In addition, $CoFe_2O_4$NPS have large surface area of active sites with high electro conducting ability. Therefore, the incorporation of the pooled unique properties of the MWCNTs with that of $CoFe_2O_4$NPS as well as enzyme immobilization, enhance selectivity and sensitivity towards electro-catalytic oxidation of SAL on the GCE surface. The amplification of peak-current height confirmed the successful fabrication the proposed sensor for sensitive determination of SAL.

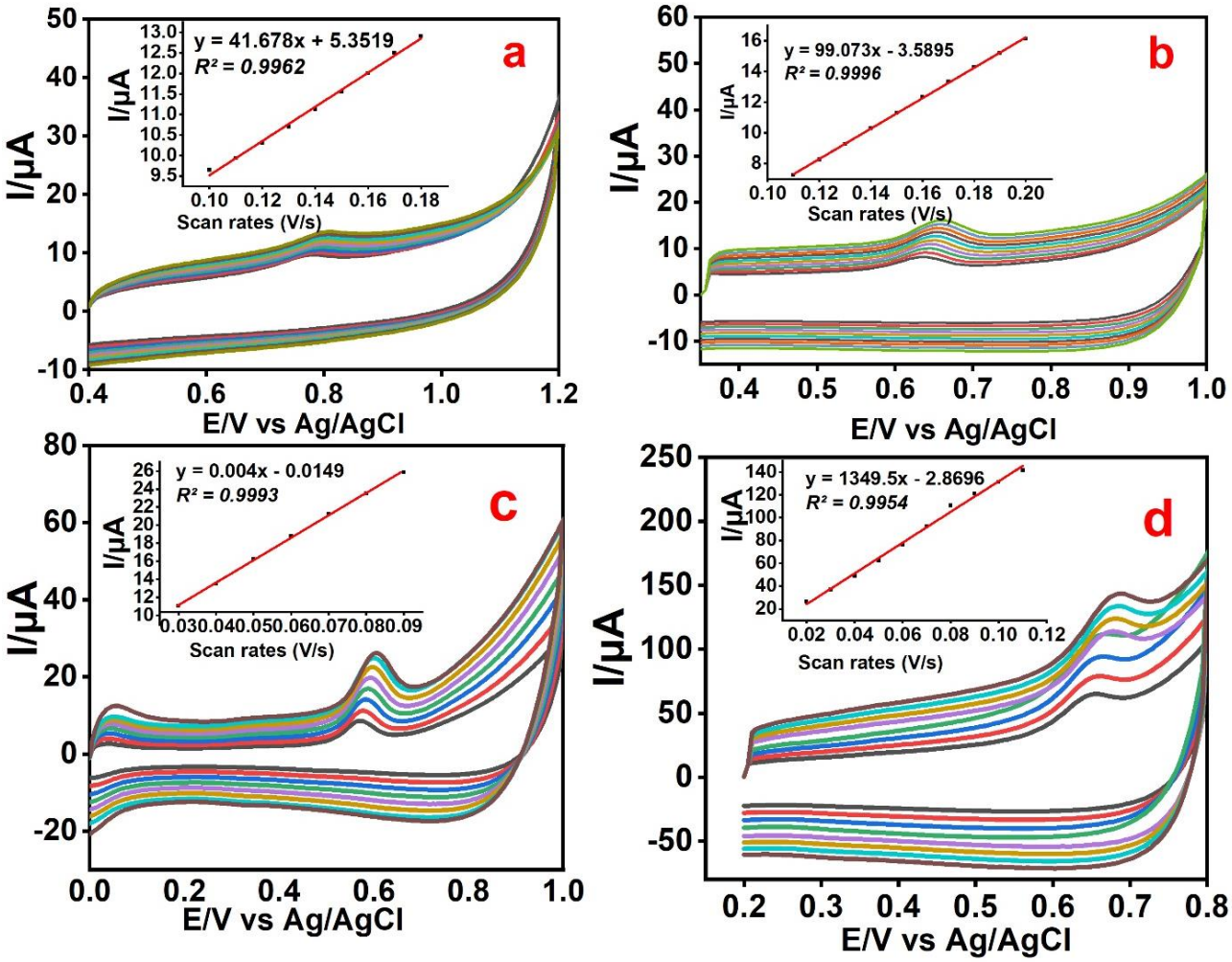

Figure 5.18: **Cyclic voltammograms of SAL showing effect of scan rates at GCE (a), MWCNTs-GCE (b), MWCNTs-$CoFe_2O_4$-GCE (c) and MWCNTs-$CoFe_2O_4$-Lipase-GCE (d)**

5.2.4 Selection, optimization and study of the effect of pH

To obtain the most stable peak with higher peak-current response, 0.1 M KPBS, 0.1 M PBS, 0.1 M acetate buffer solution (ABS) and 0.1 M borate buffer solution (BBS) (each pH 7) were experimented. From the cyclic voltammograms shown in Figure 5. 19, the anodic peak of SAL in 0.1 M PBS exhibited the maximum peak height current response. Therefore, 0.1 M PBS was selected as the electrolytic solution for SAL experiments.

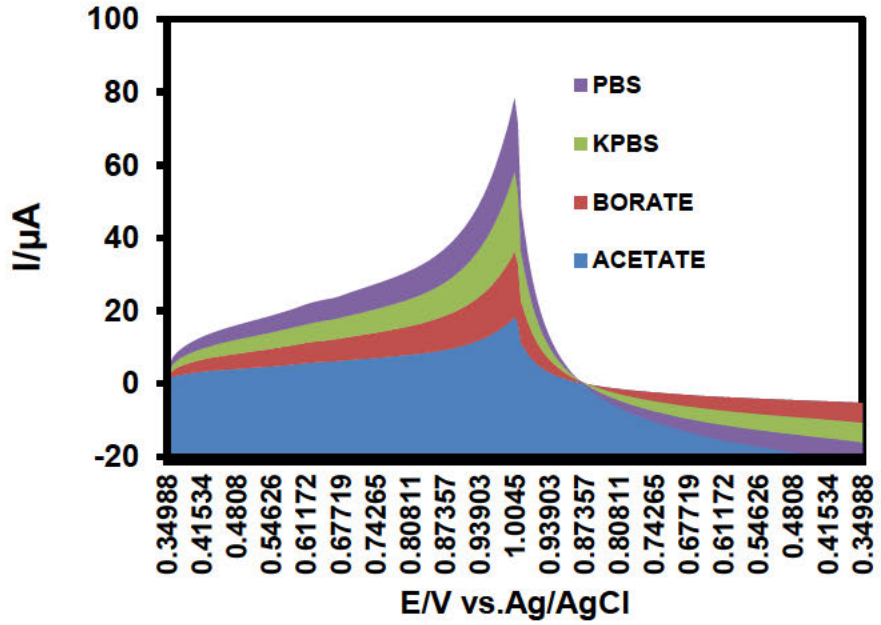

Figure 5.19: **Cyclic voltammograms of the supporting electrolytes; KPBS, PBS, ABS and BBS**

Figure 5. 20 shows the cyclic voltammograms of 2 mM SAL determined with GCE in different pH values (5.0–8.0) using 0.1 M PBS at a sweep rate and deposition time of 0.1 V/s and 20 s, respectively. The anodic peak-current of SAL increased gradually to pH value of 7 (Figure 5. 20a). Beyond the pH value of 7, the peak-currents decreased gradually (Figure 5. 20b). Consequently, to obtain the best sensitivity, pH 7 of PBS was considered as the optimum for the electrochemical determination of SAL. In addition, the influence of pH of the PBS on the electrochemical peak-current and peak potential of 2 mM SAL was also analysed using CV in 10mL 0.1 M PBS. The position of the peak potential of SAL moved towards negative values with increase in pH values, thus suggesting that protons take part in the electrochemical oxidation of SAL.

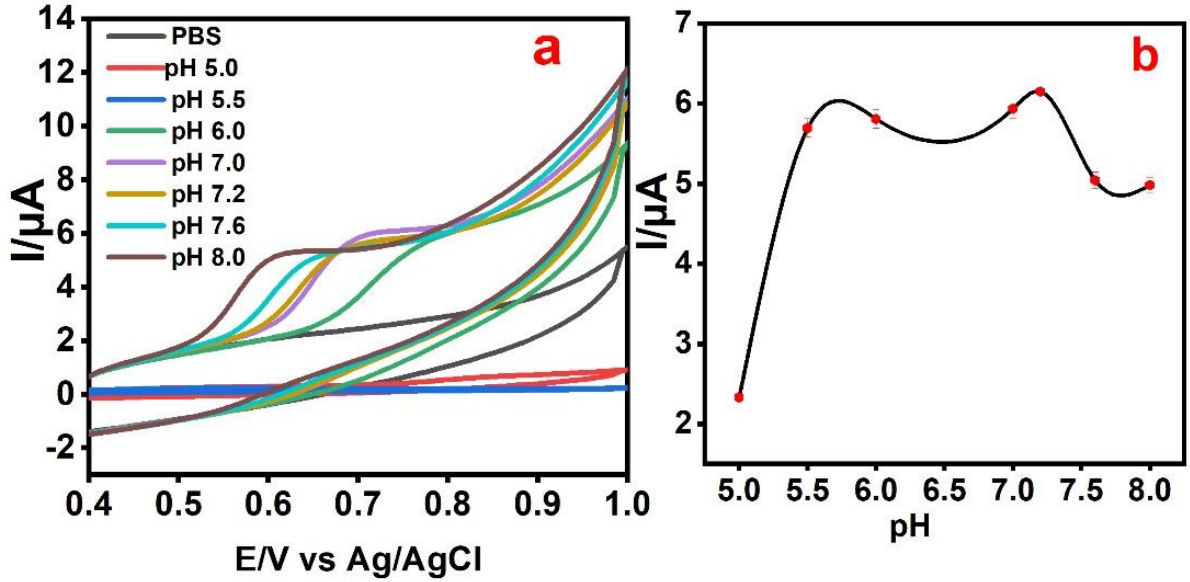

Figure 5.20: **Effect of pH on the position of the peak potential and peak-current of SAL (a). Variation of peak-current with change in pH on the un-modified GCE (b)**

5.2.5 Effect of deposition time

The effect of deposition time (in the range 5 s-60 s) on the anodic current was evaluated using CV at the GCE in 0.1 M PBS (pH 7) and at a sweep rate of 0.1 V/s. From the cyclic voltammogram obtained (not shown), the amount of SAL adsorbed on the unmodified GCE surface increased with increase in deposition time. However, beyond 60 s, the adsorbed amount of the SAL molecules on the electrode surface decreased because of saturation of the electrode surface. Since the maximum peak-current was recorded at 60 s (Figure 5. 21), 60 s was considered as the optimal accumulation time for the determination of SAL.

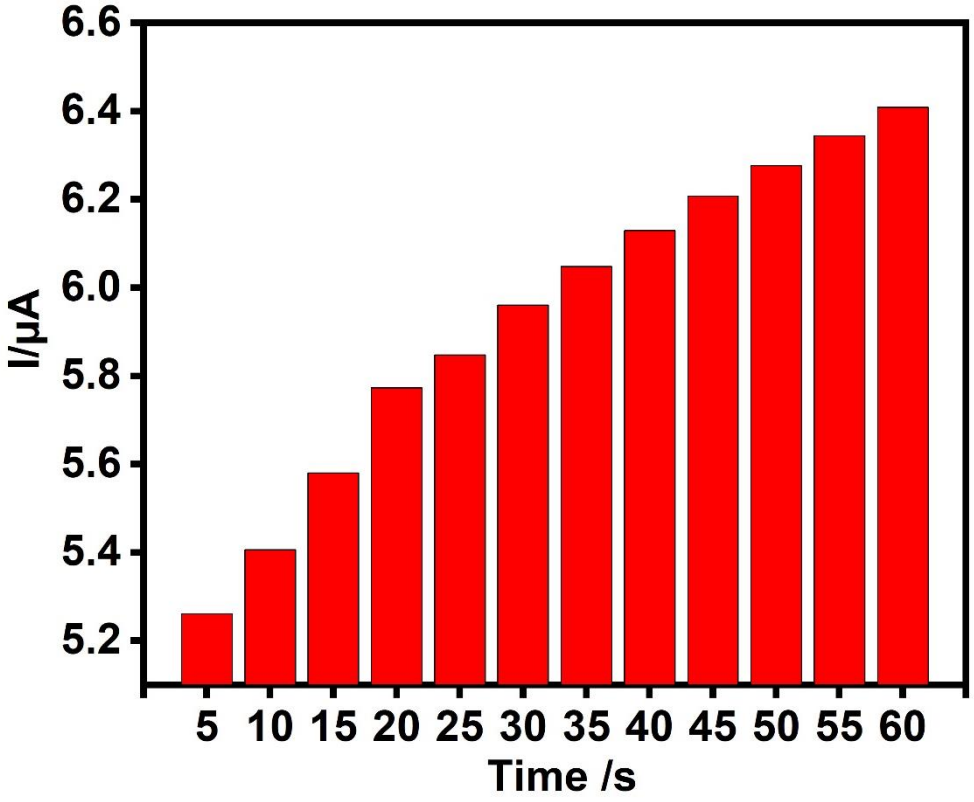

Figure 5.21: **Plot of peak-current vs time; displaying the effect of varying deposition time**

5.2.6 Influence of the scan rate

The effect of scan rate on the peak-currents and peak potentials of SAL at the GCE, MWCNTs-GCE, MWCNTs-$CoFe_2O_4$-GCE and MWCNTs-$CoFe_2O_4$-Lipase-GCE in 10 mL of 0.1 M PBS (pH 7) were investigated at various sweep rates and the corresponding cyclic voltammograms were generated. The peak-current increased linearly with increasing scan rate at each electrode (Figure 5. 18). Furthermore, the peak potential shifted to more positive peak potentials with each increase in the sweep rate, confirming that the oxidation reaction of SAL is not reversible. The linear equations and the regression values of the different modified electrodes are summarized in Table 5.3. The relationship between the peak-currents and sweep rates studied indicate that the electrochemical mechanism of SAL at the fabricated sensor is a diffusion-controlled process (Santos et al., 2018).

Table 5.3: **Linear equations and the regression values of the different modified electrodes**

	Electrodes	Linear equation	R^2
1	GCE	$y = 41.678x + 5.3519$	0.9962
2	MWCNTs-GCE	$y = 99.073x - 3.5895$	0.9996
3	MWCNTs-$CoFe_2O_4$-GCE	$y = 0.004x - 0.0149$	0.9993
4	MWCNTs-$CoFe_2O_4$-Lipase-GCE	$y = 1349.5x - 2.8696$	0.9954

5.2.7 Sensitivity of MWCNTs-$CoFe_2O_4$-Lipase-GCE sensor

MWCNTs-$CoFe_2O_4$-Lipase-GCE was further used for determination of SAL under optimum DPV experimental conditions. The potential was scanned in the range of 0.4 V to 1.0 V vs Ag/AgCl in 0.1 M PBS having different SAL concentrations. The resulting DP voltammogram and its calibration curve are exhibited in Figure 5. 22a and Figure 5. 22b, respectively. The results revealed that there was a linear relationship between the oxidation peak-currents and the concentration of SAL from 0.05 µM to 3.90 µM. The LOD (0.0240 µM) and the LOQ (0.0120 µM) values were calculated from the calibration curve obtained using the expressions $\mathrm{LOQ} = 3 \times \mathrm{Sd/x}$ and $\mathrm{LOQ} = 10 \times \mathrm{Sd/x}$, where (x) is the gradient of the calibration curve and (Sd) is the standard deviation of blank. Furthermore, the results of the proposed MWCNTs-$CoFe_2O_4$-Lipase-GCE sensor are comparable with other previous SAL sensors. MWCNTs-$CoFe_2O_4$-Lipase-GCE presented an excellent sensitivity with lower limit of detection under reasonable range compared with previous electrodes (Table 5.4). This confirms that the MWCNTs-$CoFe_2O_4$-Lipase hybrid nanocomposite provides an appropriate sensing platform for electrochemical detection of SAL. The outstanding performance is due to the remarkable electro-conductivity of the prepared MWCNTs-$CoFe_2O_4$-Lipase composite.

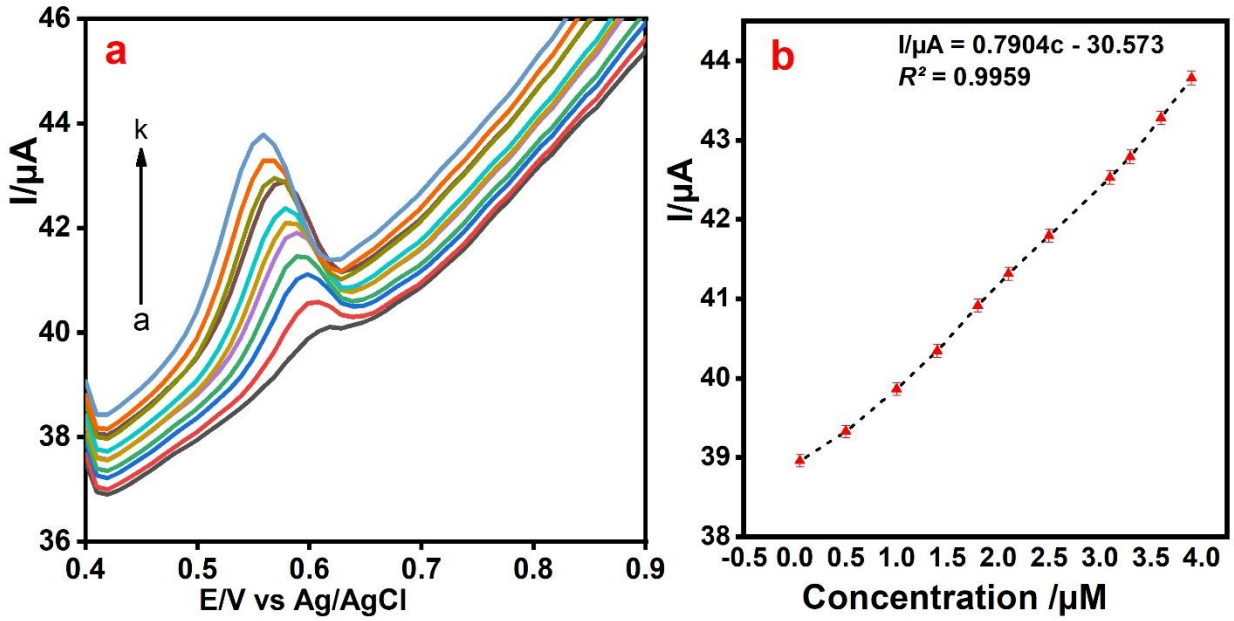

Figure 5.22: **(a) DP voltammogram of SAL @ MWCNTs-$CoFe_2O_4$-Lipase-GCE and (b) is the plot of peak-current (µA) as a function of SAL concentration (µM)**

Table 5.4: **Comparison of the MWCNTs-$CoFe_2O_4$-Lipase-GCE sensor with other SAL sensors**

Electrochemical sensors	Linear range	LOD	References
AgNP-ILFG-NF-GCE	79 nmol/L - 2.9 µmol/L	13 nmol /L	(Santos et al., 2018)
(CPT-BDD) electrode	1.73 x 10^{-5} -3.47 x 10^{-4} M	5.06 x 10^{-6} M	(TALAY PINAR et al., 2018)
Poly taurine-ZrO_2-GCE	5 – 220 µM	0.02 µM	(Rajkumar et al., 2013)
CNTs-NF composites	0.1 – 33 µM	0.1 µM	(Lin et al., 2013)
Poly(4-amino-3-hydroxynaphthalene sulfonic acid-GCE	0.2 to 8 µM	6.8×10^{-8} M	(Amare et al., 2017)
Chitosan-MWCNT-GCE	0.5 – 40 µM	0.08 µM	(Cao et al., 2011)
MWCNTs-$CoFe_2O_4$-Lipase-GCE	0.05 - 3.90 µM	0.0240 µM	This work

5.2.8 Selectivity, stability and reproducibility of MWCNTs-$CoFe_2O_4$-Lipase-GCE

The effect of some possible interfering constituents including sucrose, citric acid, glucose, ascorbic acid, Na^+, SO_4^{2-} and Cl^- on the anodic peak-current of SAL was tested to find out the selectivity of MWCNTs-$CoFe_2O_4$-Lipase-GCE biosensor. From the voltammogram obtained (Figure 5. 23), the intrusive substances did not cause an obvious effect on the anodic peak position and the anodic peak-current of SAL. The selectivity of the developed sensor may be due to the excellent specific recognition ability of lipase enzyme immobilized on MWCNTs-$CoFe_2O_4$ nanocomposite material.

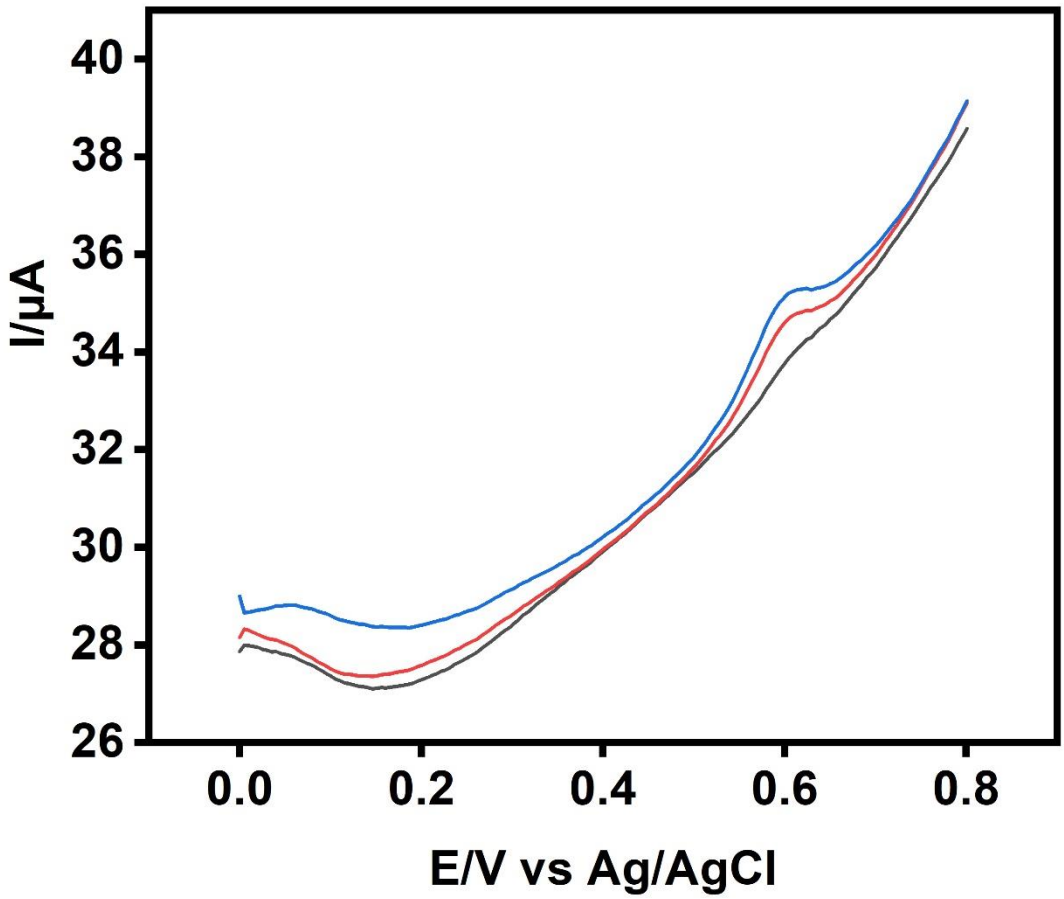

Figure 5.23: **The effect of interfering substances on the electrochemical responses of SAL at MWCNTs-$CoFe_2O_4$-Lipase-GCE**

The fabricated sensor was further examined for its reproducibility. Under the same DPV experimental conditions, four different MWCNTs-$CoFe_2O_4$-Lipase-GCE sensors were fabricated using the same procedure, used to determine the same amount of 2 mM SAL and the current response was recorded. The four MWCNTs-$CoFe_2O_4$-Lipase modified GCEs exhibited almost the same oxidation peak-currents height at unchanged anodic peak position. The calculated RSD of the four sensors was found to be 1.68 %. This implies that MWCNTs-$CoFe_2O_4$-Lipase-GCE had an acceptable reproducibility. The stability of MWCNTs-$CoFe_2O_4$-Lipase-GCE biosensor was further determined by investigating the DPV current response of the same electrode before and after storage in the refrigerator (4 °C) for a week interval. From the DPV results, no major decrease in the electrochemical current response was recorded after two weeks storage, signifying the good stability of the MWCNTs-$CoFe_2O_4$-Lipase-GCE biosensor.

5.2.9 Analysis of SAL in real drug sample using MWCNTs-$CoFe_2O_4$-Lipase-GCE

To examine the practical application of the developed method, Venteze syrup (containing 2 mg of SAL in each 5 mL of the syrup) was analysed using DPV under optimal conditions. Venteze syrup sample was diluted with PBS (pH 7), and then spiked with known concentrations of SAL. The DPV analysis was done via standard addition method. The percentage recoveries were in the range of 96.0 to 100.6 % and the RSD % of each addition was less than 5 % (Table 5.5), proving that this fabricated biosensor can be applied in quantification of SAL in drug formulations.

Table 5.5: **Determination of SAL in Venteze syrup sample**

Sample	**Added (μM)**	**Found (μM)**	**Recovery (%)**	**RSD (%)**
Venteze syrup (containing 2mg/5mL)	0.50	0.48	96.00	1.58
	5.00	5.03	100.60	2.36
	10.00	9.95	99.50	1.96
	15.00	14.98	99.80	2.01

5.3 Electrochemical sensing of prednisolone (PDN)

In this work, MWCNTs-IL-L-lysine nanocomposite was used to modify GCE surface (Figure 5.24) and the developed sensor was used for electrochemical detection of PDN. The combination of highly conductive IL and MWCNTs with L-lysine polymer enables this nano-hybrid to display excellent electrochemical performance towards PDN detection.

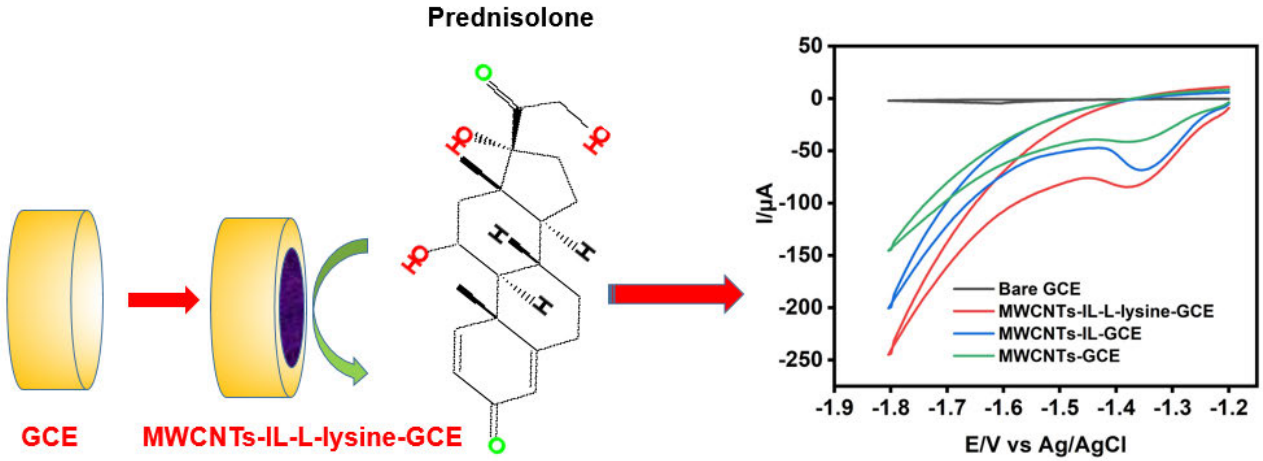

Figure 5.24: **Schematic illustration of the application of the fabricated MWCNTs-IL-L-lysine-GCE sensor for electrochemical detection of PDN**

5.3.1 Functional group identification and thermal stability

Figure 5. 25a show the FTIR spectrum of commercial MWCNTs and the prepared MWCNTs-IL-L-lysine nanocomposite samples. In the FTIR spectrum of MWCNTs (blue curve), the characteristic peaks at around 2913 cm^{-1} and 1173 cm^{-1} are designed to the COOH and C=O functional groups, respectively. The peaks at 1576 cm^{-1}, 1421 $cm^{-1}$and 1165 $cm^{-1}$of the prepared MWCNTs-IL-L-lysine nanocomposite correspond to the imidazolium ring (Matandabuzo et al., 2018). The results thus confirm the functionalization of MWCNTs using IL. Besides that, MWCNTs-IL-L-lysine (red curve) FTIR spectrum also unveiled a characteristic peak at 1691 cm^{-1} probably because of the presence of L-lysine on the composite. Figure 5. 25b shows the TGA curves of MWCNTs and MWCNTs-IL-L-lysine nanocomposite. MWCNTs curve presents only two decomposition step. The initial weight loss between 25ºC - 200 ºC is because of the loss of water adsorbed on the MWCNTs surface (Matandabuzo et al., 2018). The second weight loss that transpired between 450ºC and 680 ºC is as a result of the combustion of MWCNTs (Matandabuzo et al., 2018). At higher temperatures,there was no weight loss recorded (Figure 5. 25b). On the other hand, the MWCNTs-IL-L-lysine composite

exhibited two decomposition stages also. The loss of adsorbed water on the surface of the MWCNTs-IL-L-lysine nanocomposite occurred below 150 ºC. The second decomposition step in the temperature range of 280ºC - 400 ºC is due to thermal degradation of the functionalised IL. Beyond 400 ºC the MWCNTs-IL-L-lysine is thermally stable as represented by the flattened curve.

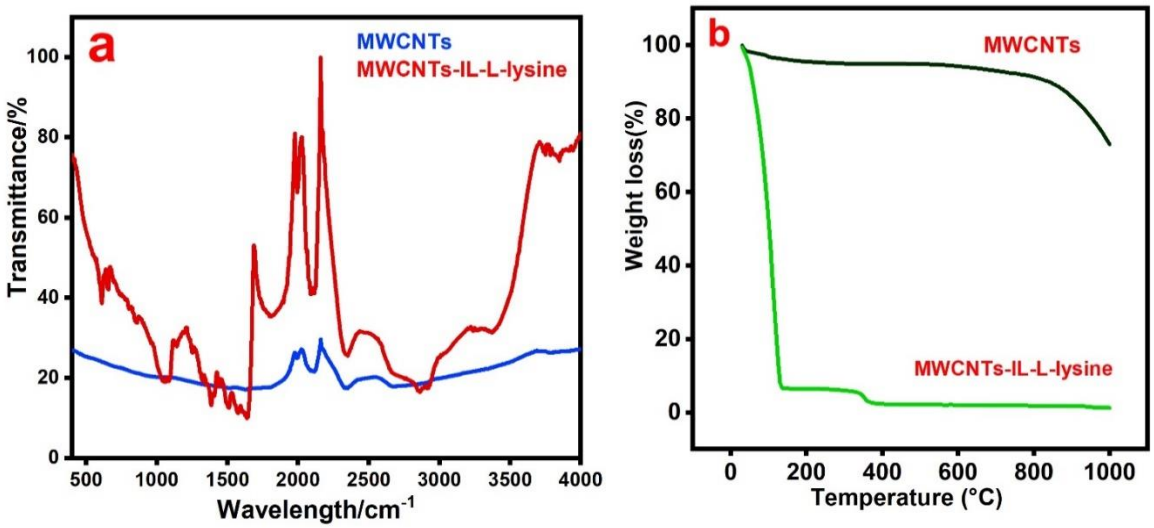

Figure 5.25: **FTIR spectra of MWCNTs (blue curve) and MWCNTs-IL-L-lysine nanocomposite (red curve) (a). TGA curves of MWCNTs (black curve) and MWCNTs-IL-L-lysine nanocomposite (green curve) (b)**

5.3.2 Surface morphology

SEM analysis showed spherical clusters in MWCNTs, a possible indication of agglomeration of the carbon nanotubes (Figure 5. 26a). SEM analysis of MWCNTs-IL revealed the presence of small bundles dispersed within the matrix (Figure 5. 26b). The excellent homogeneous distribution of MWCNTs-IL is due to the porous structure and the large surface area of the functionalized MWCNTs. This promotes greater conductivity and quicker transfer of electrons. On the other hand, a well-dispersed nanocomposite of MWCNTs-IL-L-lysine was observed as displayed in Figure 5. 26c with little agglomeration. Therefore, MWCNTs-IL-L-lysine structure will effectively provide a large surface area with high conductivity offered by MWCNTs, IL and L-lysine collectively. Further analysis through TEM revealed that MWCNTs and MWCNTs-IL have tube-like shapes (Figures 5. 27a and 5. 27b). Furthermore, TEM analysis confirmed that IL enhances the dispersion of MWCNTs and does not interfere with the original tubular structure of MWCNTs (Figure 5. 27b).

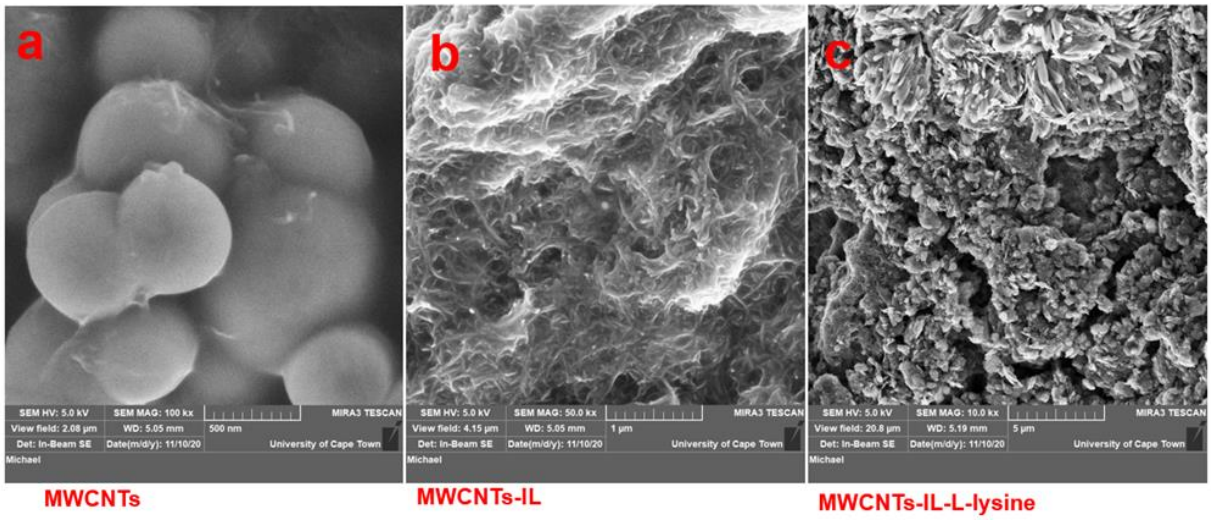

Figure 5.26: **SEM images of (a) MWCNTs, (b) MWCNTs-IL and (c) MWCNTs-IL-L-lysine nanocomposite**

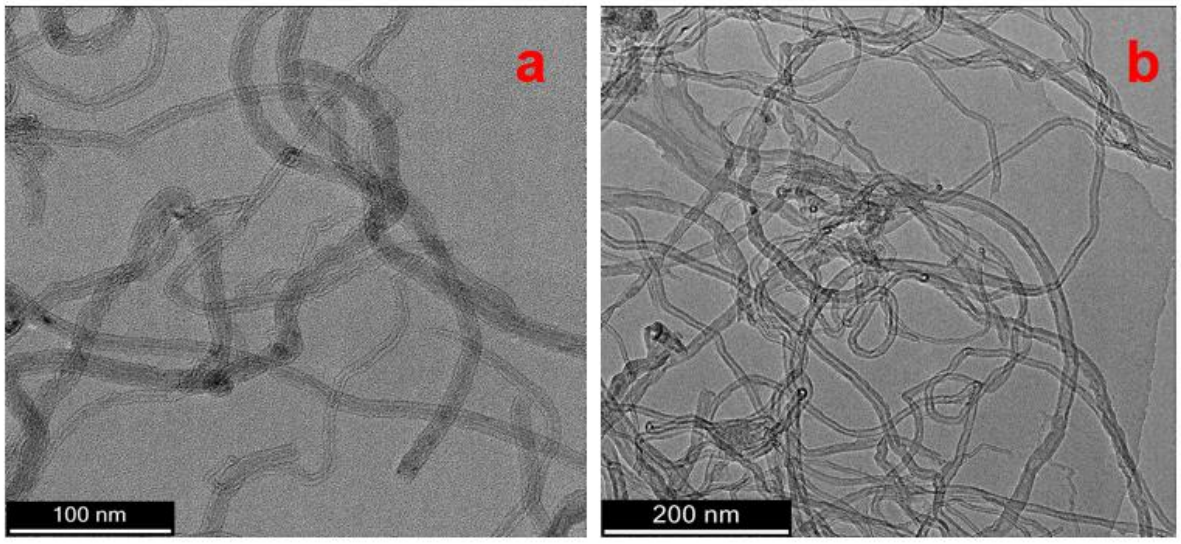

Figure 5.27: **TEM images of MWCNTs (a) and MWCNTs-IL nanocomposite (b)**

5.3.3 EIS characterization of the MWCNTs-IL-L-lysine-GCE

The electron transfer resistance (Rct) properties of the bare GCE and the MWCNTs-IL-L-lysine modified GCE surface were investigated via EIS and the results obtained are presented using the Nyquist plots (Figure 5. 28). The Nyquist plots contained a semi-circle segment and the linear part recorded at lower and higher frequencies, respectively. The diameter of this portion can be used to calculate the Rct at the electrode's surface (Gopal et al., 2018b). The electrode's charge transfer resistance was determined for each modifier by fitting the measured EIS data

using the Randle's equivalent circuit. The Rct value (7160.40 Ω) of the unmodified GCE (exhibited by a small diameter-Figure 5. 28 inset) is significantly higher than for the modified GCE due to the slow transfer of the electrons on the GCE. The lower Rct value for the MWCNTs-GCE (413.38 Ω) is due to the good electrical conductivity nature of the MWCNTs. Interestingly, much lower Rct value (305.00 Ω) was recorded by modifying GCE with MWCNTs-IL nanocomposite. Furthermore, the Rct value (201.70 Ω) for the MWCNTs-IL-L-lysine-GCE sensor was lower than the control electrodes, which demonstrates an excellent electrical conductivity for the nanocomposite MWCNTs-IL-L-lysine. The developed nanocomposite thus proves to be highly conductive and offers a large active surface for fast transfer of electrons on electrode-solution interface hence can be used in fabrication of GCE for determination of SAL and other electro-active species.

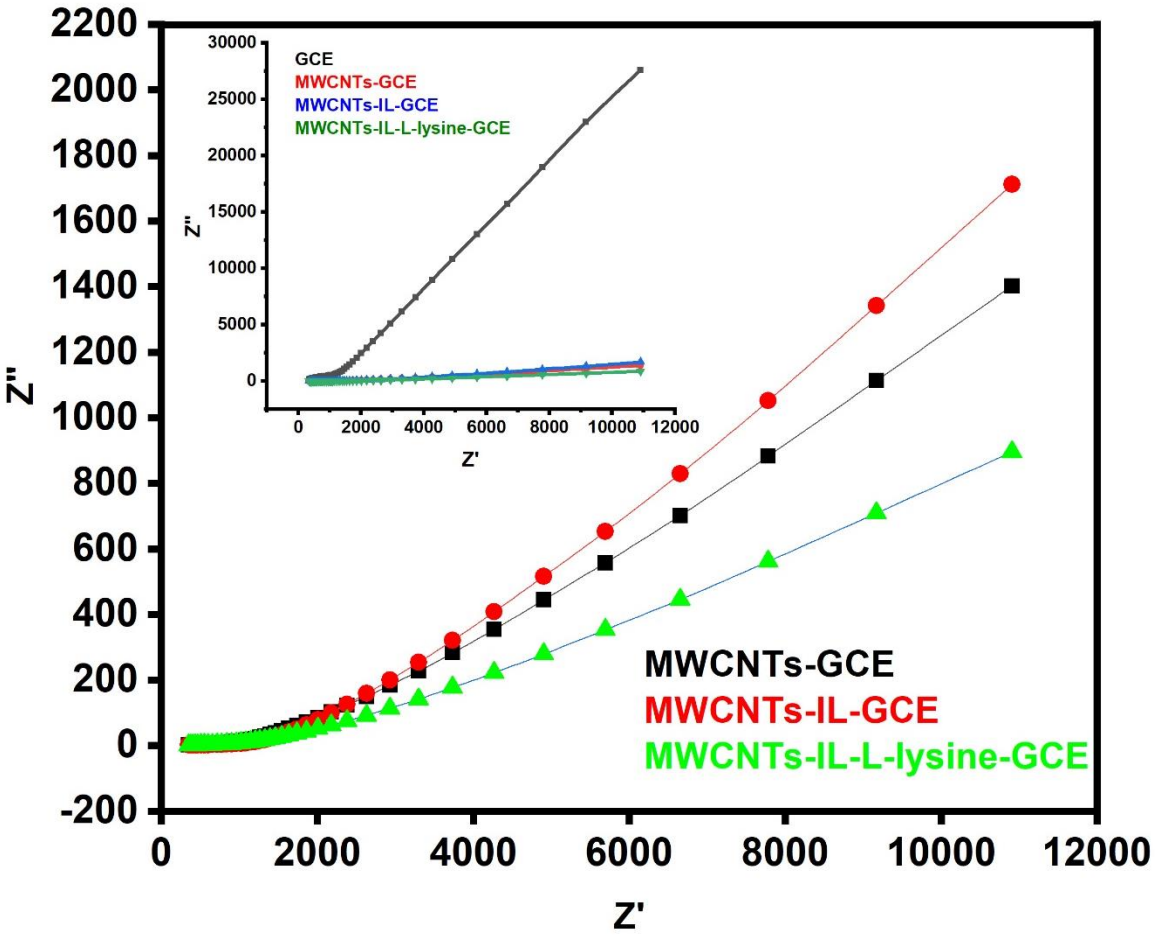

Figure 5.28: **Nyquist plots obtained at bare GCE, MWCNTs-GCE, MWCNTs-IL-GCE and MWCNTs-IL-L-lysine-GCE**

5.3.4 The electro-catalytic reduction of PDN

The electrochemical reduction behaviour of 0.1 M PDN in 0.2 M PBS of pH 6.8 was probed at the GCE as well as at the MWCNTs-IL-L-lysine nanocomposite modified GCE by CV. Figure 5. 29 displays the cyclic voltammograms of 0.1 M PDN on the bare and the different GCE modified electrodes. A cathodic peak was seen on addition of the 0.1 M PDN standard solution to the PBS during the potential scan in the range of -1.0 V to -1.8 V vs. Ag/AgCl. In the reverse scan within the investigated potential range, there was no anodic peak observed; thus suggesting that the reduction reaction was irreversible. The cathodic peak potentials appeared at -1.5 V, -1.38 V, -1.35 V and -1.34 V vs. Ag/AgCl for the bare GCE, MWCNTs/GCE, MWCNTs/IL-GCE and MWCNTs/IL/L-lysine /GCE, respectively, as shown in Figure 5. 29. The results show that the unmodified GCE gave a weak cathodic peak at very low cathodic peak-currents. In contrast, the nanocomposite modified GCE demonstrated excellent performance shown by significant increase in cathodic peak-currents and well-resolved peaks were recorded. The shift in reduction peak potential towards positive direction and the distinct increase of peak-current from the results obtained indicate that GCE modification with MWCNTs-IL-L-lysine nanocomposite enhances the electrochemical activity towards reduction of PDN. The outstanding electro-catalytic activity is because of the exceptional conductivity of MWCNTs-IL along with the unique of properties of L-lysine. MWCNTs-IL-L-lysine-GCE presented excellent performance comparing to GCE, MWCNTs-GCE and MWCNTs-IL-GCE, which suggests an enhanced electro-catalytic activity and sensing properties of the developed sensor due to additional synergetic effect between the nanocomposites materials used.

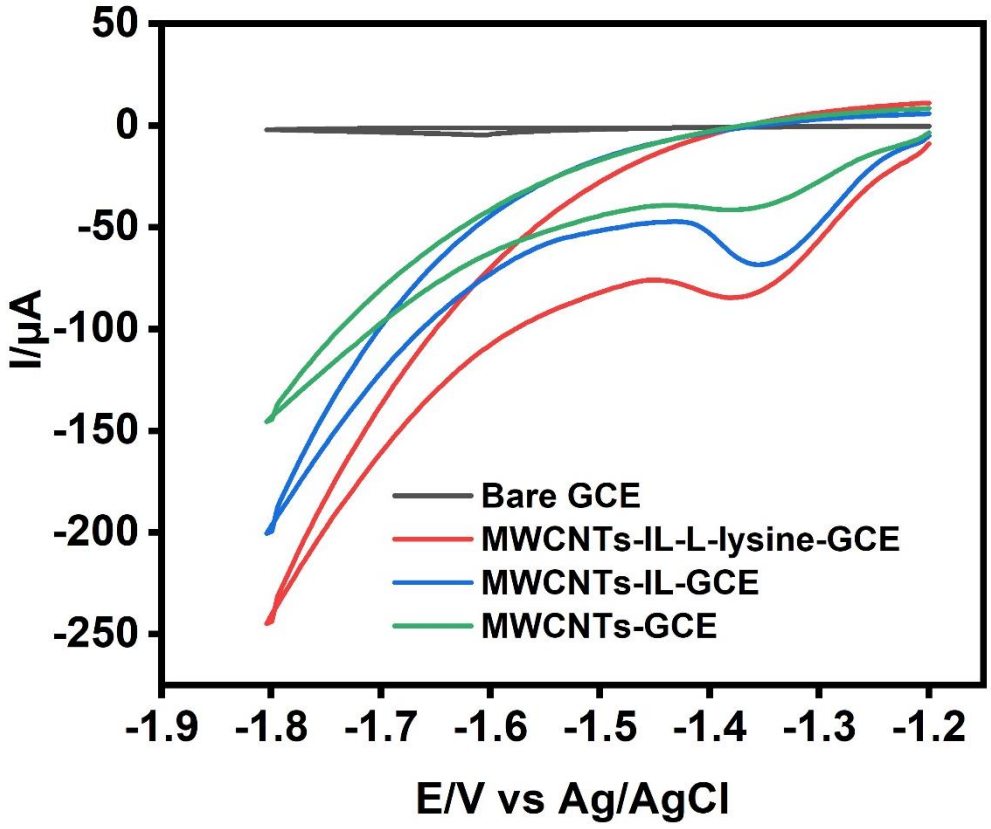

Figure 5.29: **Cyclic voltammograms of PDN at GCE (black curve), MWCNTs-GCE (green curve), MWCNTs-IL-GCE (blue curve) and MWCNTs-IL-L-lysine-GCE (red curve) electrodes**

5.3.5 Effect of pH

The effect of the pH of 0.2M PBS on the reduction peak potential and currents of 0.1 M PDN was examined via CV at the unmodified GCE. The cyclic voltammogram of 0.1 M PDN at the bare GCE (Figure 5. 30a) and plot of the cathodic peak-currents (I/µA) vs pH are shown in Figure 5. 30a (inset). The results show that when the pH of PBS was increased from 6.0 to 6.8 value, the reduction peak-currents of PDN also increased. Beyond this pH value, the cathodic currents of PDN started to decrease. For this reason, pH=6.8 was picked as the optimal pH. Furthermore, as the pH increased, the reduction peak shifted to the more negative potentials, which confirms the participation of protons in the reduction reaction of PDN.

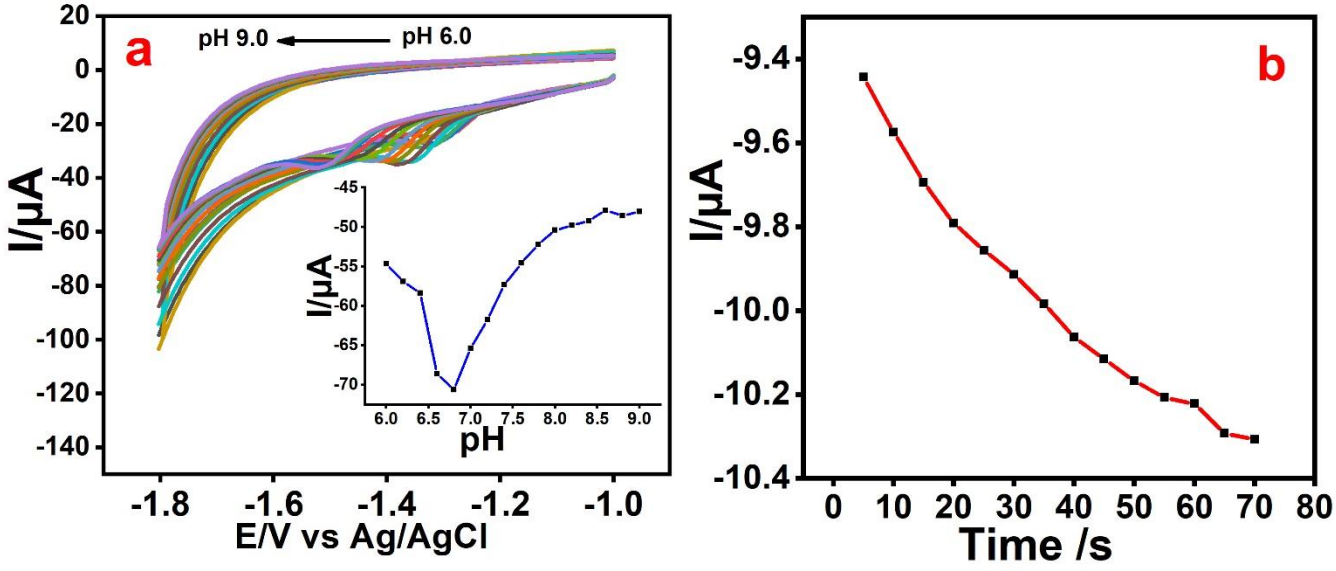

Figure 5.30: **Cyclic voltammograms of 0.1 M PDN obtained in the pH 6.0-pH 9.0 values of 0.2 M PBS (a); plot *of* $I/\mu A$ vs pH (inset) and plot of $I/\mu A$ vs deposition time (b)**

5.3.6 Influence of accumulation time

The movement of the PDN molecules towards the surface of GCE for electro-reduction reaction depends on time. The peak-currents of PDN increased significantly to approximately 50 s after which there was no significant increase in cathodic current observed (Figure 5. 30b). This may be due to saturation of the adsorbed PDN molecules on the GCE surface. Hence, further electro analysis of PDN were carried out at 50 s.

5.3.7 Impact of varying scan rate on both modified and unmodified GCE at constant concentration of PDN.

From previous work, the electrochemical redox reaction mechanism and the processes involved (either adsorption or diffusion controlled) can be acquired by studying the dependence of the peak potentials and the peak-currents on the sweep rates. Therefore, the electrochemical behaviour of PDN was investigated on the bare GCE surface (Figure 5. 31a) and on the modified GCE [MWCNTs-GCE (Figure 5. 31b), MWCNTs-IL-GCE Figure 5. 31c and MWCNTs-IL-L-lysine-GCE Figure 5. 31d)] at different scan rates under optimum pH, deposition time and at different scan rates. In all cases, it was noticed that the cathodic peak-currents of PDN gradually increased with the increase in sweep rates at each electrode (Figure 5. 31). In addition, the reduction peak of PDN shifted to potential values that are more negative on increasing the scan rate, which further indicates that reduction reaction of PDN is not

reversible. The plots of the I/μA vs. [V/s] (Figure 5. 31e) as well as that of I/μA vs. $[V/s]^{1/2}$ (Figure 5. 31f) at MWCNTs-IL-L-lysine-GCE sensor were constructed. The plots gave a good linear relationship and the equations obtained were as follows (equations 5.1 and 5.2):

$$I/\mu A = -993.3600\, x - 9.3813, R^2 = 0.9957 \qquad \textbf{(5.1)}$$

$$I/\mu A = -468.5900\, x + 44.0920, R^2 = 0.9798 \qquad \textbf{(5.2)}$$

Where *I* is current in microamperes (μA), *x* denotes the sweep rates and R^2 is the regression coefficient.

The excellent results obtained indicates that the electrochemical reaction of PDN at the developed MWCNTs-IL-L-lysine-GCE sensor was an adsorption-controlled process within the studied scan rate range. The PDN reduction at the MWCNTs-IL-L-lysine-GCE corresponds to a two-electron/two-proton transfer process (Smajdor et al., 2016)

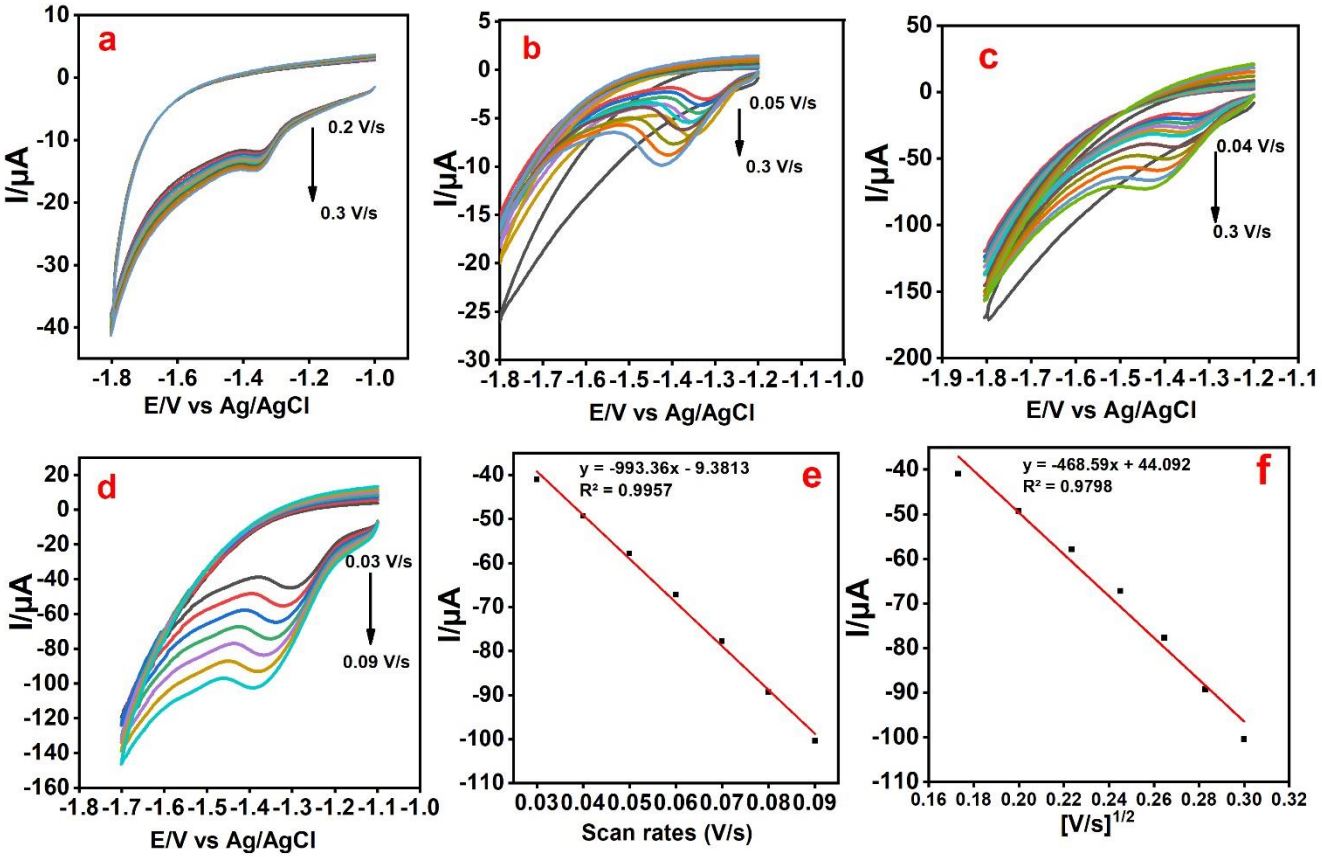

Figure 5.31: **Cyclic voltammogramms (a-d) of 0.1 M PDN (in 0.2 M PBS, at 50 s) on bare GCE, MWCNTs-GCE, MWCNTs-IL-GCE and MWCNTs-IL-L-lysine-GCE, respectively. The plots of the $I/\mu A$ vs. [V/s] (e) as well as $I/\mu A$ vs. $[V/s]^{1/2}$ (f)**

5.3.8 DPV analysis of PDN using MWCNTs-IL-L-lysine-GCE sensor

The important parameters that characterize performance of a developed sensor at trace concentration of electro-active analyte of interest are the LOD and LOQ. Therefore, DPV mode was employed for quantitative determination of different concentrations of PDN at the proposed MWCNTs-IL-L-lysine-GCE surface under optimum working parameters. The DP voltammogram (Figure 5. 32a) obtained shows a well-resolved reduction peak. The reduction peak-currents of PDN increased with increase in the concentration of PDN from 0.4 µM to1.4 µM. The calibration curve (plot of I/µA vs. concentration (µM)) was constructed to determine the linearity and the linear regression equation obtained was $I/\mu A = -0.7506c - 20.9750$, R^2 = 0.9937 (where c denotes PDN concentration in µM), as presented in Figure 5. 32b.

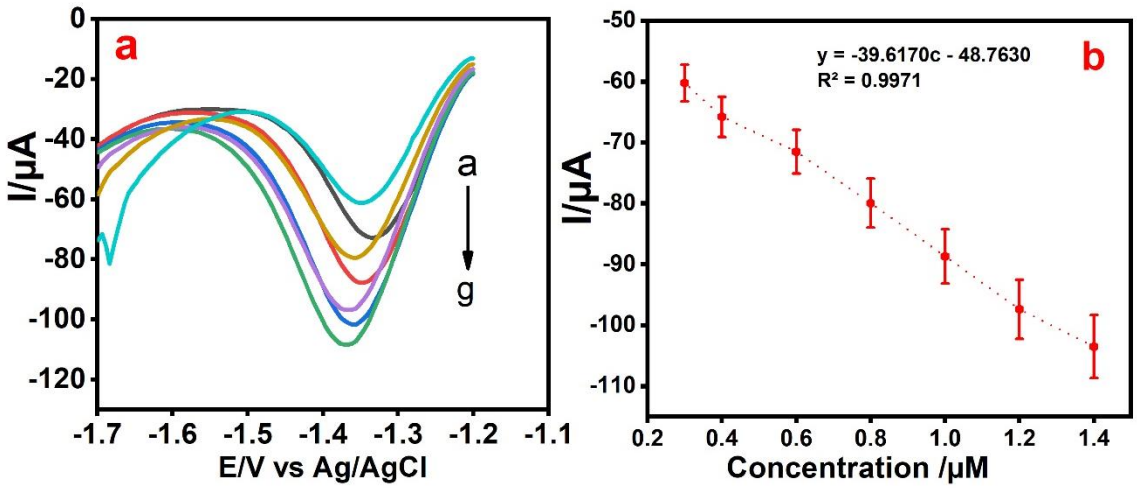

Figure 5.32: **DPV voltammogram of MWCNTs-IL-L-lysine-GCE in varying concentration of PDN (0.4 µM -1.4 µM) (a). Plot of $I/\mu A$ vs. [µM] (b)**

The detection limits (LOD =0.0214 µM and LOQ =0.3016 µM) values were calculated from the calibration curve based on the equations 5.3 and 5.4:

$$LOD = 3 \times Sd/x \qquad \textbf{(5.3)}$$

$$LOQ = 10 \times Sd/x \qquad \textbf{(5.4)}$$

where *Sd* represents the standard deviation of the blank and *x* represents the gradient obtained from the calibration curve.

The LOD obtained were compared with those of previously reported work on electrochemical detection of PDN (Table 5.6). It is evident that the LOD =0.0214 µM value was significantly lower than the recently reported modified electrodes for PDN detection (Table 5.6). The good linear range obtained and the lower LOD proves that the developed MWCNTs-IL-L-lysine-GCE sensor can be used for quantification of PDN at trace level.

Table 5.6: **Comparison of MWCNTs-IL-L-lysine-GCE with previous electrodes reported for PDN detection**

Electrode	LOD	Reference
Ordered Mesoporous Carbon Modified Glassy Carbon Electrode (OMC/GCE)	0.057 μM	(Munyentwali et al., 2015)
Single wall carbon nanotube modified edge plane pyrolytic graphite electrode (SWNT/EPPGE)	0.90×10^{-8} M	(Goyal et al., 2009a)
Fullerene C60 modified gold electrode/nanogold modified indium tin oxide electrode	26 Nm/90 nM	(Goyal et al., 2009b)
screen-printed carbon electrode (SPCE)	11.98 μg/ mL,	(Primpray et al., 2019)
MWCNTs-IL-L-lysine-GCE	0.0214 μM	This work

5.3.9 Effect of interferences and stability of MWCNTs-IL-L-lysine-GCE

The effect of various potentially interfering compounds on the height 0.1 M PDN peak-currents were investigated at the MWCNTs-IL-L-lysine-GCE surface. A reduction peak at −1.35 V vs. Ag/AgCl corresponding to the electrochemical reduction of PDN was recorded in the presence of possible interferences and there were no additional peaks (Figure 5. 33). Results depicts that in the presence of excess of biologically important compounds such as ascorbic acid, sucrose, starch, glucose, citric acid and some common salts ions such as Na^{+},Cl^{-1}, $Ca^{2+}$and K^{+} have no significant interference on the DPV response of PDN. The results show that the MWCNTs-IL L-lysine-GCE is effective for selective determination of PDN in existence of possible interfering compounds that may be present in drug formulations or biological fluids such as urine samples.

The stability of the MWCNTs-IL-L-lysine-GCE was tested by performing the DPV analysis of PDN under same experimental conditions and using the same electrode for four weeks. The

DPV measurements were recorded once a week and the electrode was kept in a dry place at room temperature. Only a very slight reduction of the cathodic current height of the proposed sensor was recorded during this period, where the electrode retained 89 % of its first peak-current response with an estimated standard deviation of 1.72 %. The outcome indicates good stability of the prepared electrodes for the electrochemical sensing of PDN.

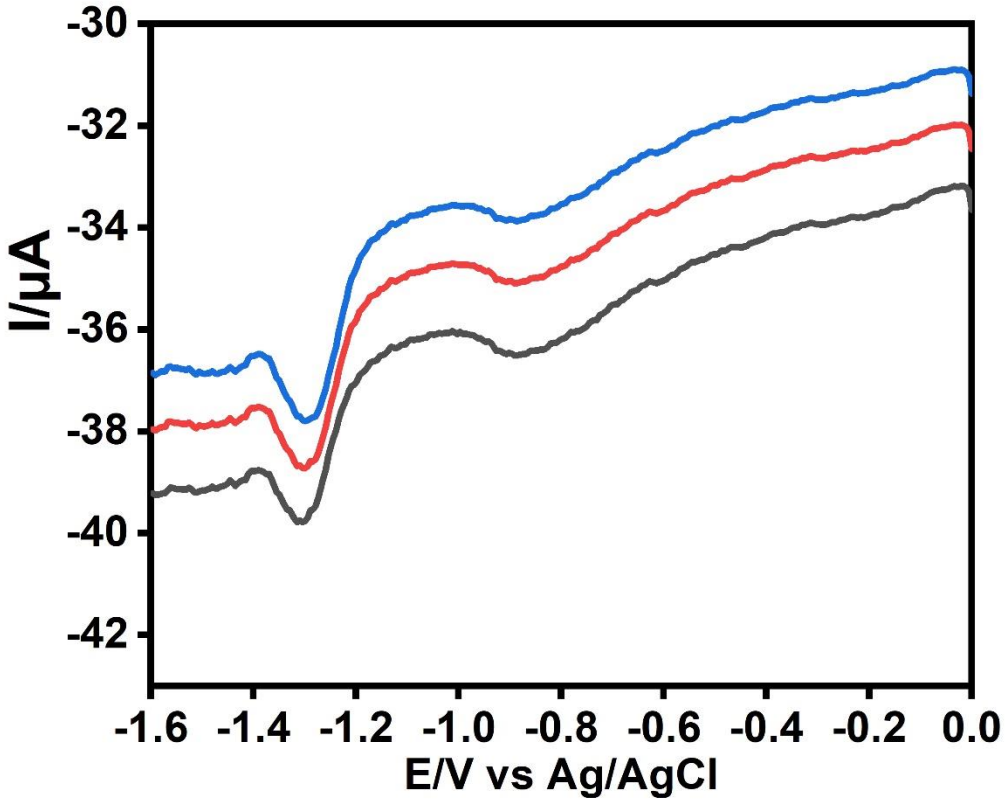

Figure 5.33: **DPV voltammogram of PDN in the presence of potential interferences**

5.3.10 Detection of PDN in pharmaceutical dosage sample

The developed MWCNTs-IL-L-lysine-GCE sensor was used to probe PDN in its pharmaceutical formulation sample (aspelone syrup-with a specified content of prednisolone as 15 mg/5mL) without any sample preparation procedures prior to DPV measurements. A known quantity of the PDN standard solution was added to an aliquot of the sample and then 10 mL of 0.2 M PBS was used to dilute the dosage sample. The DPV measurements of the real sample was carried out by the standard addition method. A reduction peak at same peak position was observed and the peak-currents gradually increased after successive addition of PDN standard solution. The outcome showed good recovery in the range of 94.5 % to 99.6 %,

indicating that the fabricated sensor can be used for determination of PDN in real sample analysis (Table 5.7).

Table 5.7: **Determination of PDN in pharmaceutical Aspelone syrup sample**

Sample	**Added (μM)**	**Found (μM)**	**Recovery (%)**	**RSD (%)**
Aspelone syrup (15mg/5mL)	2.00	1.89	94.50	1.72
	2.50	2.42	96.80	2.52
	5.00	4.98	99.60	2.89
	8.00	7.89	98.60	2.41

5.4 Electrochemical detection of terbutaline

In this work, TiO_2NPS were synthesized and a novel nanocomposite of TiO_2-MWCNTs-IL was successfully prepared. The TiO_2-MWCNTs-IL was used to modify the surface of GCE as shown in Figure 5. 34, for electrochemical quantification of TBS in its pharmaceutical dosage.

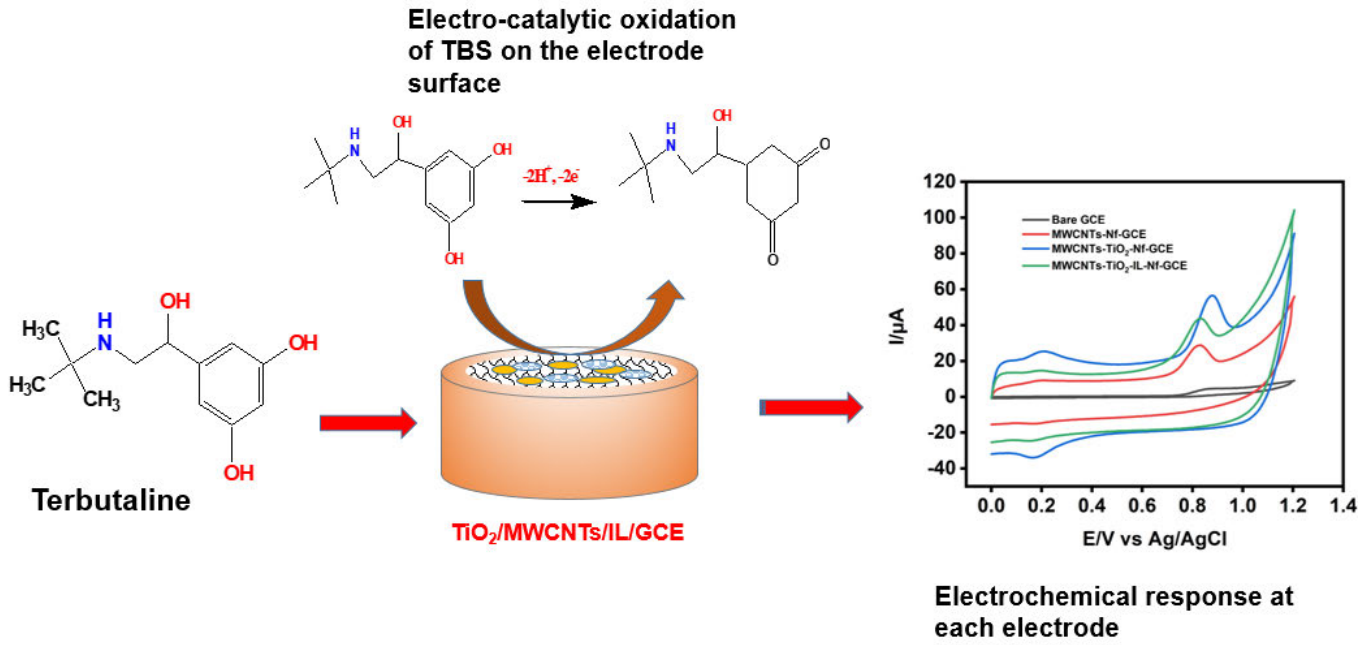

Figure 5.34: **Schematic illustration of the electrochemical detection of the of TBS at the TiO_2-MWCNTs-IL-GCE surface**

5.4.1 Thermal properties, functional groups and morphological properties of the nanocomposite

The TGA curves of the synthesized TiO_2NPs, MWCNTs and TiO_2-MWCNTs-IL nanocomposite samples are shown in Figure 5. 35a. For MWCNTs, the minor weight loss observed in the region 25 °C - 100 °C is because of the vaporization of absorbed water on the surface of MWCNTs. In addition, MWCNTs exhibited weight losses of less than 3 % from 25 °C to about 200 °C confirming its good thermal stability. A substantial weight loss (19.18%) was observed from 450 °C - 650°C due to the combustion of the MWCNTs (Figure 5. 35a). Beyond 650 °C there was no weight loss recorded (Figure 5. 35a). A weight loss of 17.11 % (80–110 °C) was recorded in the TiO_2NPs sample due to the loss of adsorbed water. The TiO_2NPs curve shown in Figure 5. 35a reveals that the TiO_2NPs were stable at temperatures over 450 °C owing to the insignificant weight loss. The TiO_2-MWCNTs-IL nanocomposites exhibited an initial weight loss before 400 °C corresponding to the loss of adsorbed solvents (blue curve, Figure 5. 35a). The second mass loss between 350 °C and 650 °C is attributed to

the combustion of MWCNTs content. Beyond 650 °C, the weight remains constant suggesting that the prepared nanocomposite is thermally stable.

Figure 5. 35b presents the FTIR spectra of the synthesized TiO_2NPs and its respective TiO_2-MWCNTs-IL nanocomposite. The broad peaks between 3000 cm^{-1} and 3435 cm^{-1} in both spectra are because of the stretching vibration of the hydroxyl (-OH) group due to the H_2O absorbed on the surface (Askari et al., 2017). The unique peaks at 717 cm^{-1} and 767 cm^{-1} in TiO_2-MWCNTs-IL and TiO_2NPs spectrum, respectively, are perhaps because of the stretching vibration modes of the (Ti-O) bond (Singh et al., 2018). Besides, the single peak at 1447 cm^{-1} on the TiO_2NPs spectrum corresponds to the stretching vibrations of Ti–O–Ti bond. The distinct peaks around 2164 cm^{-1} and 1988 cm^{-1} of the TiO_2-MWCNTs-IL nanocomposite were due to the C-H and C-O functional groups of the MWCNTs, respectively (Askari et al., 2018).

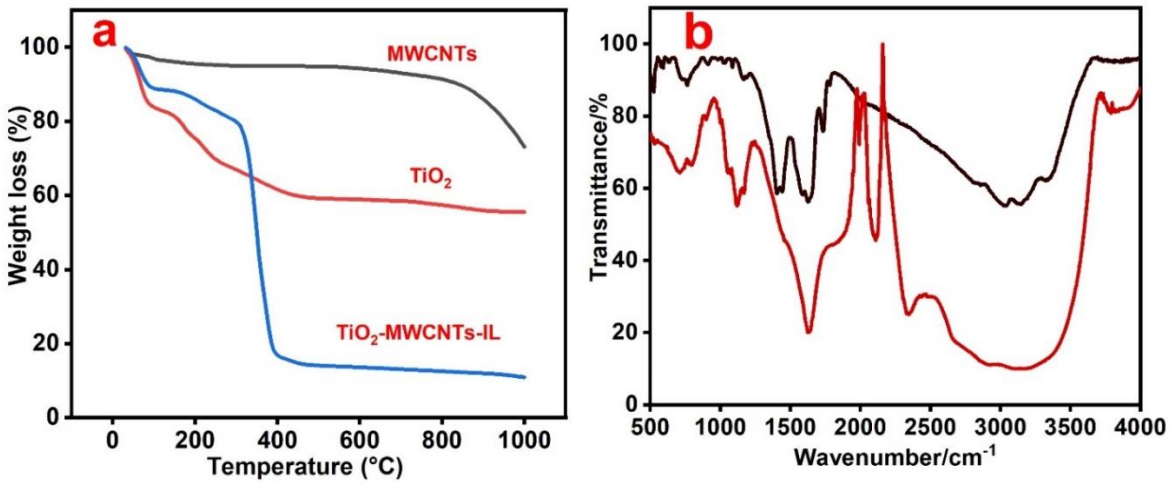

Figure 5.35: **TGA curves of MWCNTs, TiO_2NPs and TiO_2-MWCNTs-IL nanocomposite samples (a). FTIR spectra of TiO_2NPs (Black curve) and TiO_2-MWCNTs-IL nanocomposites (red curve) samples (b)**

Figure 5. 36 represents the SEM micrographs of the pure TiO_2NPs, MWCNTs-TiO_2 and MWCNTs-TiO_2-IL nanocomposite. Figure 5. 36a clearly reveals that the TiO_2NPs aggregate in clusters and it is difficult to separate one particle from the other. Upon modification of TiO_2NPs surface by mixing with MWCNTs, the nanocomposite reveals uniform dispersion as shown in Figure 5. 36b. Besides, the SEM micrograph of TiO_2-MWCNTs-IL (Figure 5. 36c) exhibit greatly improved dispersion as compared to the TiO_2NPs and MWCNTs-TiO_2 samples suggesting that MWCNTs-IL nanocomposite is exceptional for the stabilization of TiO_2NPs.

The TEM micrographs of MWCNTs sample clearly reveals the typical tubular structure of MWCNTs (Figure 5. 37a). Figure 5. 37b display the TEM images of the synthesized TiO_2NPs and the presence of TiO_2NPs attached to the MWCNTs surface is shown in Figure 5. 37c. Moreover, the TEM image in Figure 5. 37d show the morphology of the TiO_2-MWCNTs-IL nanocomposite, where the IL was incorporated to the TiO_2-MWCNTs nanocomposite and the basic shape of the MWCNTs did not change. Many small TiO_2NPs can be clearly seen on the surface of MWCNTs uniformly distributed with slight agglomeration.

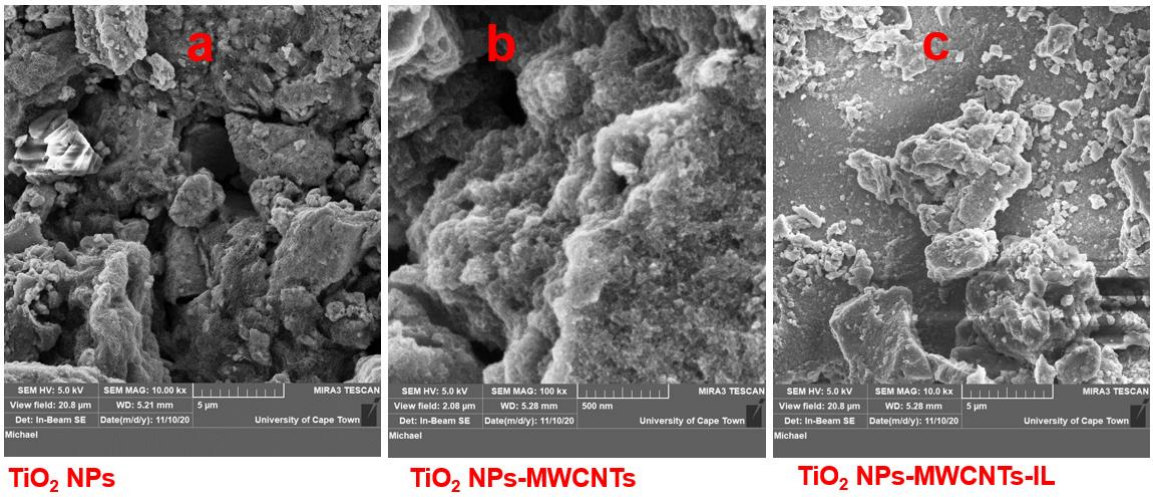

Figure 5.36: **SEM images of (a) TiO_2NPs, (b) TiO_2NPs supported on MWCNTs and (c) IL functionalised TiO_2-MWCNTs nanocomposite**

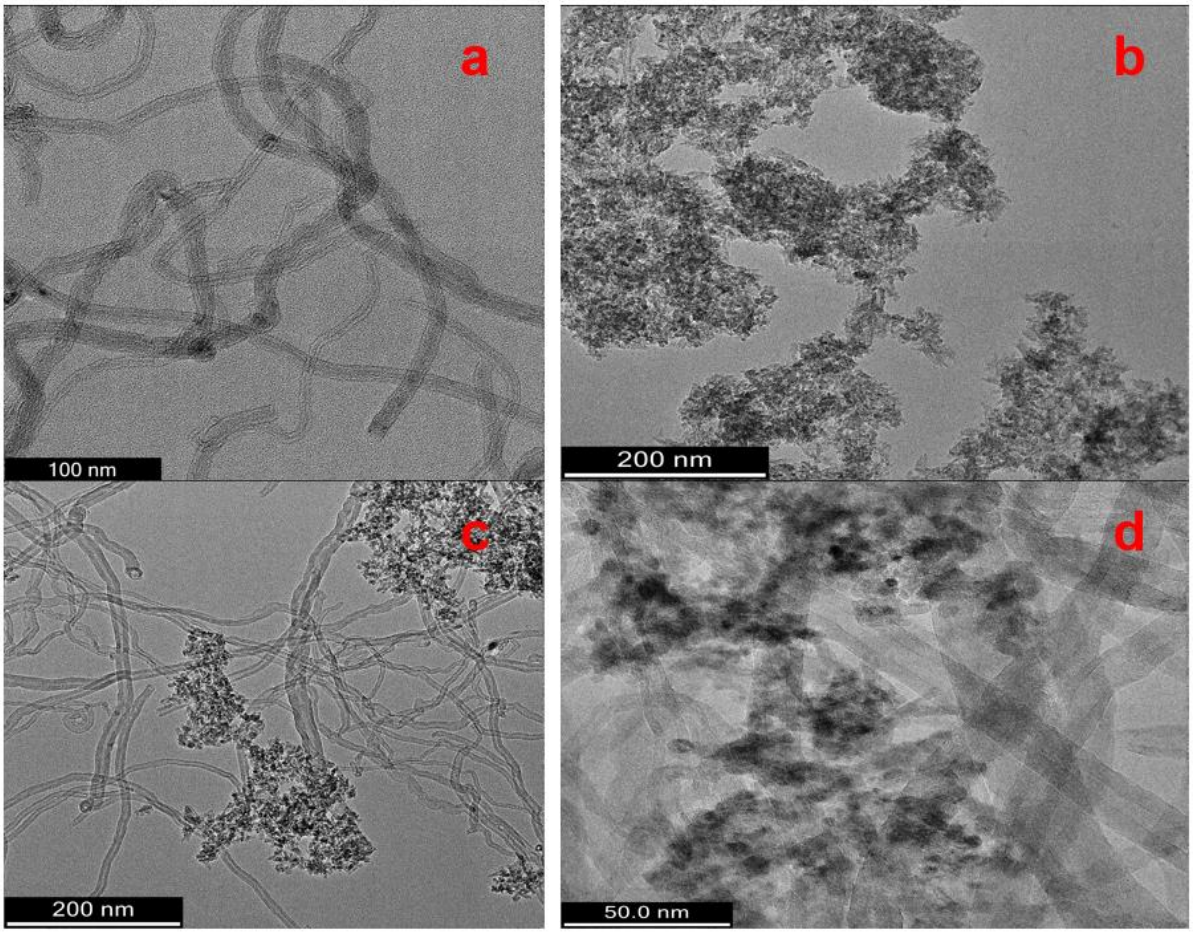

Figure 5.37: **TEM images of MWCNTs (a), TiO_2NPs (b), TiO_2-MWCNTs (c) and TiO_2-MWCNTs-IL nanocomposite (d)**

5.4.2 Electrochemical characterization of the modified GCE surface

Figure 5. 38 shows the Nyquist plots of the different TiO_2-MWCNTs-IL modified GCEs. The Rct of the electrodes were calculated by fitting the impedance data Randles circuit. The most important elements including the Rct, solution resistance (Rs), Warburg (W) and the double-layer capacitance (Cdl) are presented on the circuit (Figure 5. 38 inset) (Mustafov et al., 2019). The Rct values of the MWCNTs/GCE (curve b), MWCNTs/TiO_2/GCE (curve c) and MWCNTs/TiO_2/IL/GCE (curve a) were estimated to be 413.38 Ω, 716.83 Ω and 517.17 Ω, respectively. Generally, the charge transfer resistance of MWCNTs/TiO_2/IL/GCE (517.17 Ω) is less than that of unmodified GCE (7160.40 Ω) indicating that the synergistic effect of ionic liquid functionalised MWCNTs-TiO_2 nanocomposite improved the electro-catalytic activity of the resulting electrode thus enhanced rapid transfer of the electrons-transfer rate. These results evidently confirm the successful formation of MWCNTs-TiO_2-IL hybrid nanomaterial on the GCE surface.

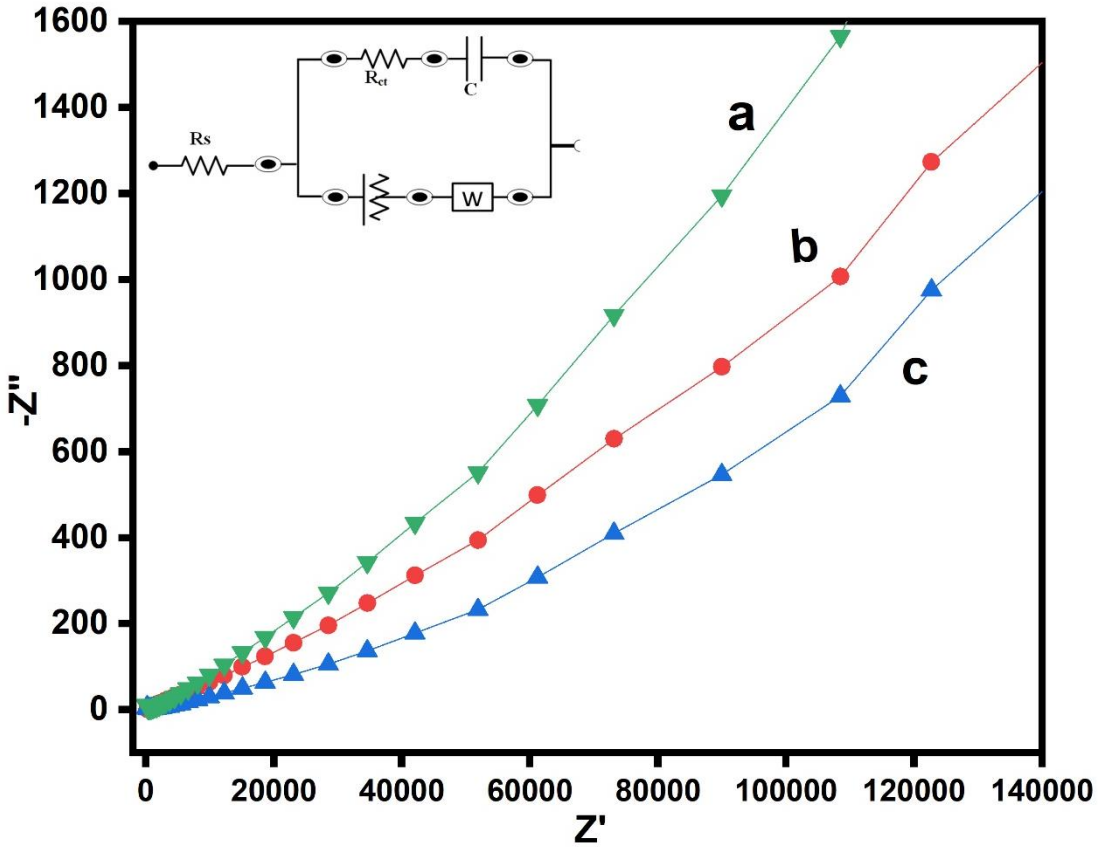

Figure 5.38: **Nyquist plots of EIS obtained at MWCNTs-TiO_2-IL-GCE (a), MWCNTs-GCE (b) and MWCNTs-TiO_2-GCE (c) performed in 0.5 mM $[Fe(CN)_6]^{3-/4-}$ containing 0.1 M KCl (Conditions; frequency range of 0.1 Hz to 10000 Hz, voltage amplitude of 0.01 V_{RMS} and scan rate of 0.05 V_{RMS})**

5.4.3 Electro-catalytic oxidation of terbutaline on TiO_2-MWCNTs-IL-GCE

In order to evaluate the electro-catalytic performance TiO_2-MWCNTs-IL-GCE on detection of TBS, the electrochemical behaviour of the modified and the unmodified GCE was studied by CV in 10 mL 0.1 M KPBS (pH 7.0) containing 0.1 M TBS standard solution. The bare GCE (Figure 5. 39a), exhibited a broad oxidation peaks with very low oxidation peak-currents (Figure 5. 39b) because of the sluggish transfer of electrons. In contrast, MWCNTs/GCE, MWCNTs/TiO_2/GCE and TiO_2/MWCNTs/IL/GCE presented well-defined oxidation peaks with high peak-currents illustrating that MWCNTs, MWCNTs-TiO_2 and TiO_2-MWCNTs-IL nanocomposites could effectively promote electron transfer. TiO_2-MWCNTs-IL-GCE recorded the highest peak-currents as compared to the other electrodes (Figure 5. 39b) indicating that the synergistic contribution between TiO_2-MWCNTs-IL hybrid nanocomposite plays a key role in enhancement of the electrochemical performance of the developed sensor.

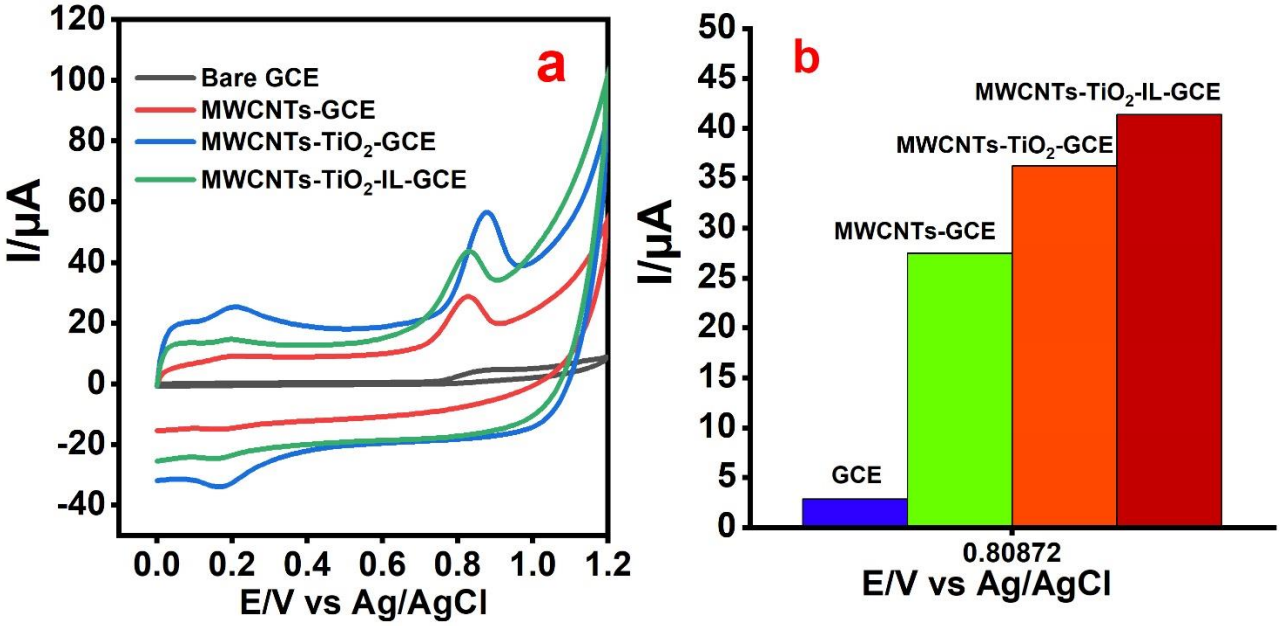

Figure 5.39: **(a) CVs of TBS at bare GCE (black curve), MWCNTs-GCE (red curve), MWCNTs-TiO_2-GCE (blue curve) and MWCNTs-TiO_2-IL-GCE (green curve) electrodes under optimal experimental conditions; (b) Comparison of the anodic peak-currents obtained at each electrode**

5.4.4 Optimization of working parameters

5.4.4.1 Effect of pH

The electrochemical response of GCE in solution containing 0.1 M TBS at various pH values (from 4.0 to 9.0) of 0.1 M KPBS was studied via CV. The peak-current of TBS gradually increased with increase in pH of KPBS from 4.0 to 7.0 beyond which the current started to decrease as shown in Figure 5. 40b. Therefore, pH 7.0 of 0.1 M KPBS was preferred as the optimal pH for further analysis of TBS. Figure 5. 40 reveals the dependence of anodic peak potential and peak-currents of TBS on the pH of the supporting electrolyte at the GCE surface. The oxidation peak potential of TBS shifted to negative direction as shown in Figure 5. 40a with increasing pH values of KPBS, proving that the protons takes part in the electro oxidation reaction of TBS. Moreover, the linear dependence between the oxidation potentials and pH was also determined (Figure 5. 40c) and the linear equation is as follows:

$$E/V = 0.1744\, pH - 0.5333, R^2 = 0.9883 \qquad \textbf{(5.5)}$$

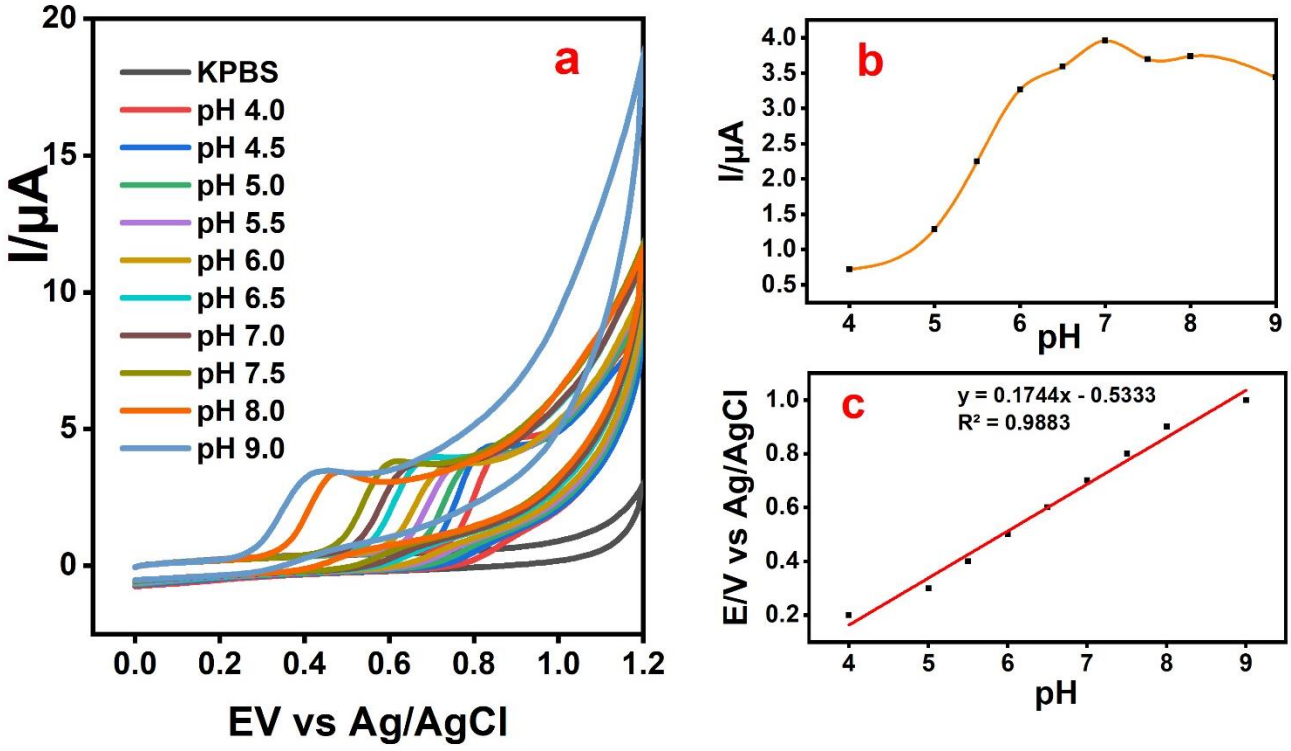

Figure 5.40: **Influence of pH of 0.1M KPBS on the anodic peak-current of TBS at bare GCE (a), plot of anodic peak-currents against pH (b) and plot of peak potentials against pH (c)**

5.4.4.2 Deposition time

Figure 5. 41a displays the influence of varying deposition time on the electrochemical peak-current response of 0.1 M TBS in 0.1 M KPBS (pH = 7) at unmodified GCE. It can be seen that by increasing deposition time over the range 20 s – 70 s, the peak-currents of TBS slightly increase up to around 55 s. The oxidation peak-currents decreased sharply thereafter as shown in Figure 5. 41b because of the saturation of the GC electrode surface. Thus, 55 s was selected as the maximum accumulation time for determination of TBS.

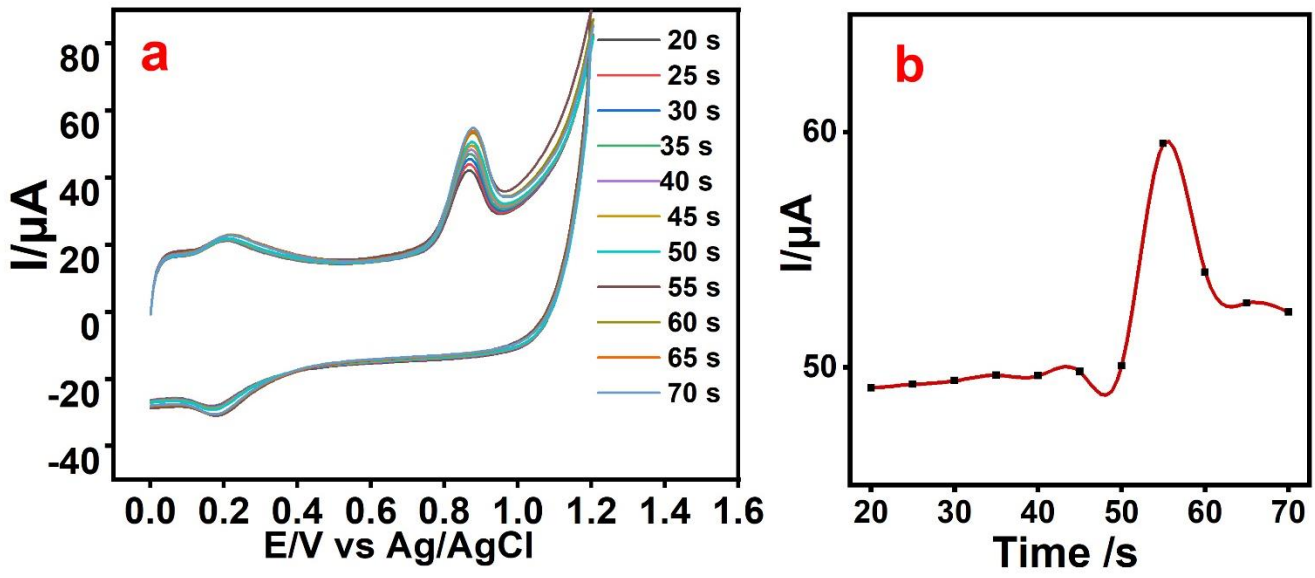

Figure 5.41: **Effect of accumulation time on the peak-current response of TBS at bare GCE surface (a). Plot of anodic peak-current vs. time (b)**

5.4.4.3 Scan rates

Figure 5. 42 and Figure 5. 43 shows the cyclic voltammograms of 0.1 M TBS at bare GCE and the TiO_2-MWCNTs-IL nanocomposite modified GCE, at various sweep rates in the range of 0.03 V/s-0.14 V/s. The bare GCE (Figure 5. 42a) displayed broad peaks with increase in the sweep rates while the modified GCE (Figure 5. 43 (a-c)) exhibited well-defined anodic peaks. As can be observed, anodic peak potentials shifted towards positive direction in all the electrodes, which confirms that the oxidation reaction of TBS is irreversible. In addition, a linear increase of anodic peak-currents with the sweep rates was perceived in all the electrodes, with the developed TiO_2-MWCNTs-IL-GCE sensor recording the highest peak-currents. This proves that the electro-oxidation reaction of TBS is predominantly diffusion controlled. The regression equations and correlation coefficient of the respective plots of I/µA vs. V/s are shown in Table 5.8. Furthermore, a linear correlation was established between logarithm of anodic currents and logarithm of sweep rates at the TiO_2-MWCNTs-IL-GCE as shown in Figure 5. 43d. The regression equation of log (I/µA) and log (V/s) can be expressed as follows;

$$I/\mu A = 1.2562x + 2.9146,\ R^2 = 0.9948 \qquad \textbf{(5.6)}$$

where I denotes current in micro Amperes, x is the sweep rate in volts per second and R^2 is regression coefficient.

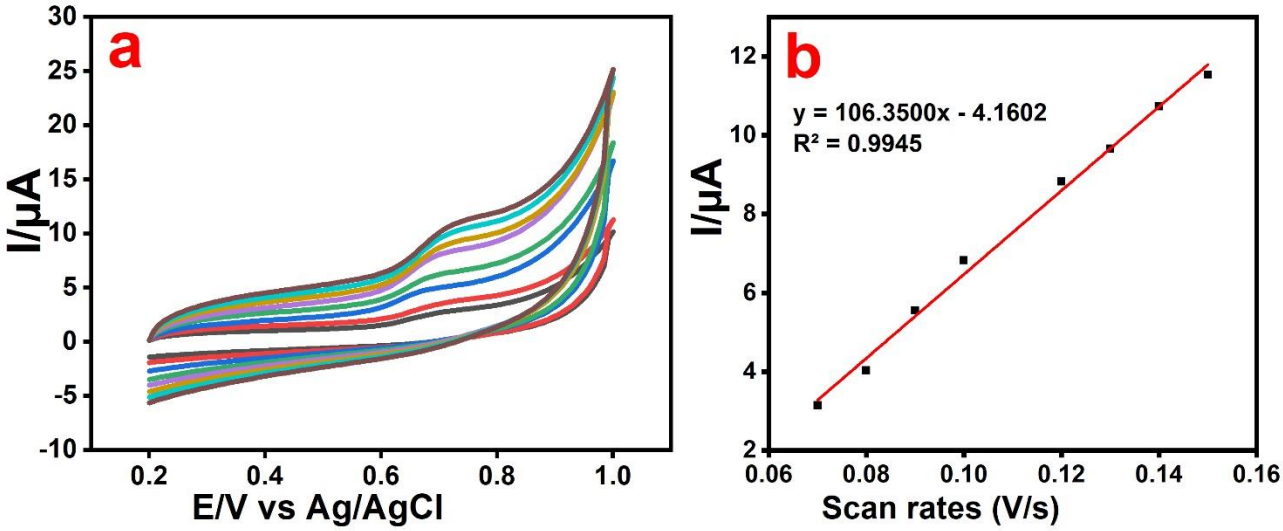

Figure 5.42: **Cyclic voltammograms of 0.1 M TBS in 0.1 M KBPS (pH 7) at different sweep rates (0.07 V/s-0.15 V/s) (a); Plot of peak-currents vs scan rates (b)**

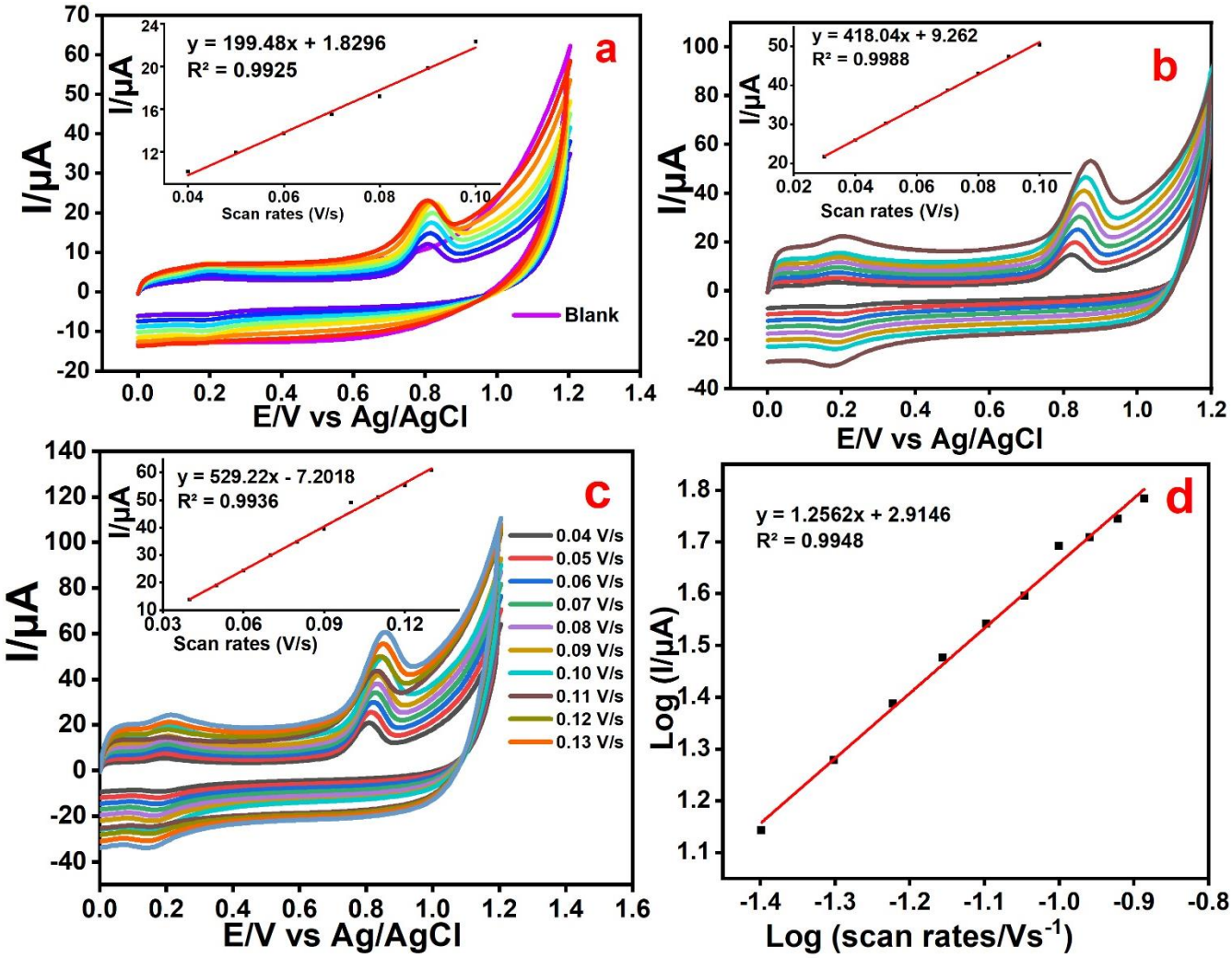

Figure 5.43: **Cyclic voltammograms of 0.1 M TBS at MWCNTs/GCE, MWCNTs/TiO_2/GCE and TiO_2/MWCNTs/IL/GCE, respectively (a-c), with their respective plots of I/µA vs. V/s(inset) and plot of log (I/µA) vs log (V/s) obtained at the TiO_2-MWCNTs-IL-GCE sensor (d)**

Table 5.8: **The regression equations and correlation coefficient of the respective plots of I/µA vs. V/s**

	Electrode	Linear regression equation	Correlation coefficient(R^2)
1	GCE	$y = 106.3500x - 4.1602$	0.9945
2	MWCNTs-GCE	$y = 199.4800x + 1.8296$	0.9925
3	MWCNTs-TiO_2-GCE	$y = 418.0400x + +9.2620$	0.9988
4	MWCNTs-TiO_2-IL-GCE	$y = 529.2200\,x - 7.2018$	0.9936

5.4.5 Quantitative determination of terbutaline using DPV

Quantification of TBS was done by scanning the potential in the range 0.6 V -1.0 V vs. Ag/AgCl under optimized DPV experimental conditions. Various concentrations of TBS standard solution were added into 10 mL 0.1 M KPBS and the currents generated because of electro-catalytic oxidation of TBS was recorded after deposition time of 30 s. Figure 5. 44a shows the DPV results obtained and it displays a distinct anodic peak at approximately 0.8 V vs. Ag/AgCl. The plot of oxidation peak-currents against concentration of TBS, Figure 5. 44b, presents a linear correlation in the range of 0.5 µM to 3.0 µM. The calibration equation obtained was $I/\mu A = 0.6549\,x + 13.2580$, with correlation coefficient (R^2) of 0.9983 (where x is the concentration of TBS). From the calibration curve, the ($3 \times SD/m$) and LOQ ($10 \times \mathrm{SD/m}$) were estimated to be 0.0162 µM and 0.2140 µM, respectively. Furthermore, the LOD of TiO_2-MWCNTs-IL-GCE sensor was compared to previous different electrochemical sensors used in detection of TBS and the results are presented in Table 5.9. The comparative data clearly signify that the proposed TiO_2-MWCNTs-IL-GCE sensor offered lower LOD as well as a good linear range. The outstanding results can be associated to the immobilization of the highly conductive IL-based TiO_2-MWCNTs nanocomposite at the GCE surface. This confirms that TiO_2-MWCNTs-IL-GCE can suitably be used as an electrochemical sensing platform of TBS.

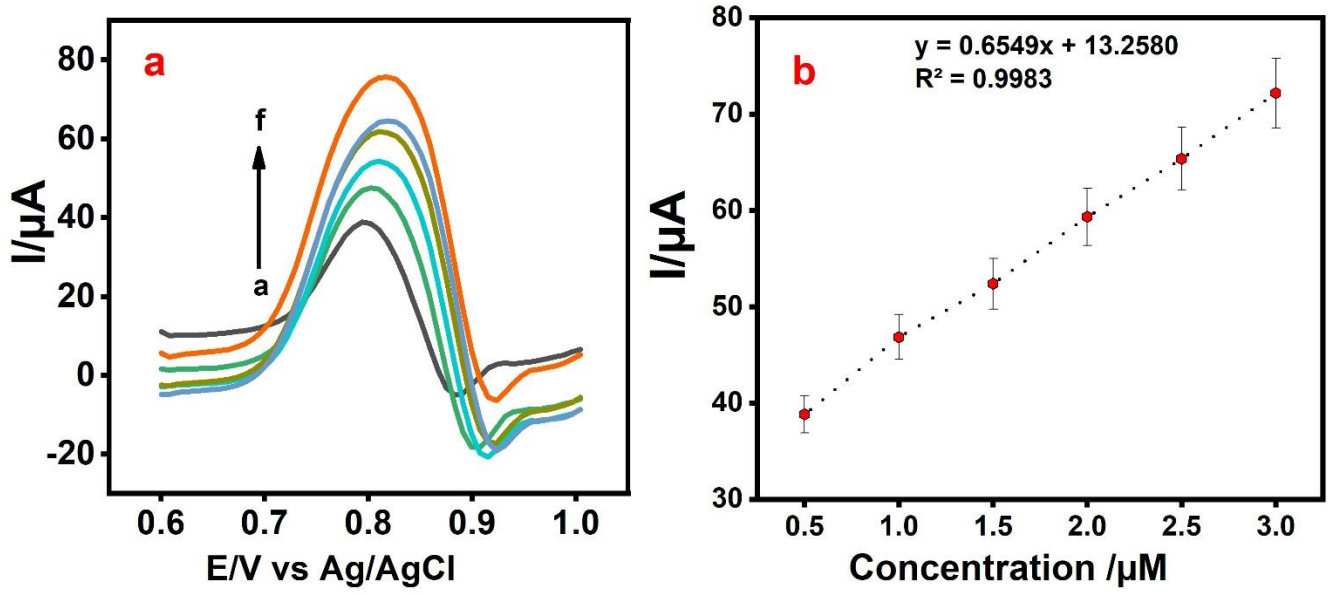

Figure 5.44: **DPV curve of TiO_2-MWCNTs-IL-GCE at different concentrations of TBS (a). Plot of anodic peak-current vs. concentration of TBS (b)**

Table 5.9: **Comparison of the LOD of TiO_2-MWCNTs-IL-GCE with previous reported electrodes for TBS detection**

	Electrode	LOD	References
1	MWCNT/graphene/GCE	6.527×10^{-7} M	(Gopal et al., 2018a)
2	f-MWCNTs/CD-R/ gold electrodes	5.8×10^{-7} M	(Felix et al., 2016)
3	ZrO_2NPs/MWCNTs/GCE	2.25 nM	(Baytak et al., 2016)
4	GNS–MWCNT–PANI composite-CPE	5.83×10^{-9} M	(Kalambate et al., 2017)
5	TiO_2-MWCNTs-IL-GCE	0.0162 µM	This work

5.4.6 Method validation studies using the developed sensor

The repeatability of TiO_2-MWCNTs-IL-GCE sensor was explored by studying the DPV current response for five successive determinations of 0.1 M TBS in 0.1M KPBS (pH 7.0) under the same optimum experimental working parameters. The estimated RSD (relative standard deviation) was 1.87 % suggesting that the developed sensor has good repeatability. In addition, five TiO_2-MWCNTs-IL-GC electrodes were prepared separately using the same procedure and the reproducibility of the electrodes was determined under same experimental conditions. Furthermore, the stability of the developed TiO_2-MWCNTs-IL-GCE sensor was probed for 4 weeks. TiO_2-MWCNTs-IL-GCE maintained 90 % of its original anodic current height after the end of the 4 weeks. Consequently, the proposed TiO_2-MWCNTs-IL-GC electrode proves to be stable enough for routine use. The selectivity of the developed TiO_2-MWCNTs-IL-GCE sensor towards detection of TBS was also studied by investigating the influence of interferences. Excess amount of drugs and biological chemicals such as glucose, ascorbic acid, acetaminophen, acetic acid, salbutamol and salts were added, but there was no appreciable change in electrochemical current responses, with no new peaks being recorded.

5.4.7 Determination of TBS in real drug sample using TiO_2-MWCNTs-IL-GCE

To investigate the viability of the TiO_2/MWCNTs/IL/GCE sensor, the developed method was utilized towards determination of TBS in real pharmaceutical sample (bricanyl) under

optimized DPV experimental conditions. The sample was diluted with 0.1 M KPBS (pH 7.0), spiked with known concentrations of TBS and was analysed by standard addition method. The added concentration values and the obtained recoveries results were presented in Table 5.10. Furthermore, satisfactory recovery results were obtained suggesting that the proposed TiO_2-MWCNTs-IL nanocomposite modified GCE is effective for the quantitative quantification of TBS in the real samples.

Table 5.10: **Determination of TBS in real pharmaceutical sample**

Sample	**Added (μM)**	**Found (μM)**	**Recovery (%)**	**RSD (%)**
Bricanyl syrup	3.00	2.79	93.00	1.56
(1.5mg/5mL)	3.50	3.51	100.20	2.21
	6.00	5.99	99.80	2.53
	8.50	8.46	99.50	1.98

CHAPTER 6

6 SUMMARY AND CONCLUSION

In the current research, a simple and relatively cheap voltammetric method for detection of four anti-asthma drugs in commercial pharmaceutical formulations was developed. In this regard, four different electrochemical sensors with excellent electro-catalytic activity were fabricated using novel nanocomposites for electrochemical sensing of TPN, SAL, PDN and TBS. Briefly, $CoFe_2O_4$NPs, ZnONPs and TiO_2NPs were synthesized and their respective $CoFe_2O_4$-MWCNTs-Lipase, ZnONPs-MWCNTs-Cyt c and TiO_2-MWCNTs-IL nanocomposites were prepared for GCE modification. In addition, MWCNTs-IL-L-lysine nanocomposite was also prepared. The NPs and the obtained nanocomposites were characterized through TEM, SEM, FTIR, TGA, XRD, BET and EIS.

The electrochemical behavior of TPN, SAL, PDN and TBS at the GCE and at the different $CoFe_2O_4$-MWCNTs-Lipase, ZnONPs-MWCNTs-Cyt c, TiO_2-MWCNTs-IL and MWCNTs-IL-L-lysine nanocomposite modified GCEs were studied using CV. In addition, the effects of pH of the supporting electrolytes, sweep rates and deposition time on the redox peak-currents and the peak potentials of each drug at the un-modified and modified GCE were explored using CV. Furthermore, the working parameters for each developed method were optimized. Broad redox peaks with low redox peak-currents were observed at the GCE surface, which may be attributed to the slow transfer of electrons. Interestingly, the peaks current increased dramatically with well-resolved peaks after modification of the GCE surface. Under optimum parameters, the fabricated ZnONPs-MWCNTs-Cyt c-GCE, $CoFe_2O_4$-MWCNTs-Lipase-GCE, MWCNTs-IL-L-lysine-GCE and TiO_2-MWCNTs-IL-GCE sensors exhibited outstanding electrochemical performance as compared to the unmodified GCE. This is probably because of the enhanced conductivity and the extensive large surface area of the nanocomposite that accelerated electron transfer between the drug molecules and the surface of the modified electrode. Therefore, the enhanced redox peak-currents response is due to the synergistic effect of the nanocomposite material.

The stability, selectivity, repeatability and detection limits for each of the proposed sensors were evaluated via the DPV method. The as-developed ZnONPs-MWCNTs-Cyt c-GCE biosensor showed great reproducibility, better stability as well as excellent selectivity with

lower LOD of 0.0012 µM. These analytical characteristics such as excellent electrochemical response brought about by the fabricated sensor was attributed to the additional advantageous properties of the ZnONPs-MWCNTs hybrid nanocomposite such as superior electro-catalytic activity. Furthermore, the composite offered a biocompatible platform for the immobilization of Cyt c, to investigate its electro-catalysis towards the oxidation of TPN. Similarly, the use of MWCNTs-IL-L-lysine nanocomposite modified GC electrode resulted to rapid transfer of electrons as well as the best electrochemical response towards PDN detection. This enhancement is also associated with synergistic effect. MWCNTs-IL-L-lysine-GCE exhibited outstanding sensitivity and selectivity. The estimated LOQ (0.0214 µM) and LOD (0.3016 µM) values were significantly lower than the corresponding values of previously reported electrodes for PDN detection.

The magnetic nanocomposite-based biosensor ($CoFe_2O_4$-MWCNTs-Lipase-GCE) exhibited enhanced electrochemical response towards SAL detection. The incorporation of $CoFe_2O_4$ NPS on MWCNTS and the immobilization of lipase enzyme on the $CoFe_2O_4$-MWCNTs nanocomposite enhanced the sensitivity towards electro-catalytic oxidation of SAL on the modified GCE surface. The anodic peak-currents and the concentration of SAL showed a good linear relationship in the concentration range of 0.05 µM - 3.90 µM with LOD and LOQ of 0.0240 µM and 0.0120 µM, respectively. Furthermore, the TiO_2-MWCNTs-IL-GCE sensor displayed excellent electro-catalytic activity towards determination of TBS compared to previous reported sensors for TBS detection. A distinct oxidation peak with greater peak-currents was recorded illustrating that the conductive TiO_2-MWCNTs-IL nanocomposite promoted rapid transfer of electrons. Therefore, the developed nanocomposite based sensors showed acceptable selectivity, reproducibility and stability.

The practical possibility of each fabricated sensor was also examined by quantifying each of the four drugs in their respective commercial pharmaceutical formulations, using DPV via standard addition method. The percentage recoveries of PDN, SAL, TPN and TBS in their pharmaceutical samples were in the range of 94.5 %–99.6 %, 96 %-100.6 %, 99.4 %-102.9 %, 93.0 %- 100.2 %, respectively. The successful electrochemical sensing of TPN, SAL, PDN and TBS in their pharmaceutical formulations using the fabricated sensors indicates that; these sensors offer promising applications in the quantitative analysis of drugs and other electro-active analytes in diverse sample matrices. Low-level detection of these anti-asthma drugs with shorter analysis time is of high priority. Overall, the proposed method is simple, affordable, fast, has a high sensitivity and superior selectivity.

REFERENCES

ABURUZ, S., MILLERSHIP, J., HEANEY, L. & MCELNAY, J. 2003. Simple liquid chromatography method for the rapid simultaneous determination of prednisolone and cortisol in plasma and urine using hydrophilic lipophilic balanced solid phase extraction cartridges. *Journal of Chromatography B,* 798**,** 193-201.

ACHARYA, J., RAJ, B. G. S., KO, T. H., KHIL, M.-S., KIM, H.-Y. & KIM, B.-S. 2020. Facile one pot sonochemical synthesis of CoFe2O4/MWCNTs hybrids with well-dispersed MWCNTs for asymmetric hybrid supercapacitor applications. *International Journal of Hydrogen Energy,* 45**,** 3073-3085.

ADAM, R. E., POZINA, G., WILLANDER, M. & NUR, O. 2018. Synthesis of ZnO nanoparticles by co-precipitation method for solar driven photodegradation of Congo red dye at different pH. *Photonics and Nanostructures - Fundamentals and Applications,* 32**,** 11-18.

ADELOYE, D., CHAN, K. Y., RUDAN, I. & CAMPBELL, H. 2013. An estimate of asthma prevalence in Africa: a systematic analysis. *Croatian medical journal,* 54**,** 519-531.

AFZALI, M., MOSTAFAVI, A., NEKOOIE, R. & JAHROMI, Z. 2019. A novel voltammetric sensor based on palladium nanoparticles/carbon nanofibers/ionic liquid modified carbon paste electrode for sensitive determination of anti-cancer drug pemetrexed. *Journal of Molecular Liquids,* 282**,** 456-465.

AGHAMIRI, Z. S., MOHSENNIA, M. & RAFIEE-POUR, H.-A. 2018. Immobilization of cytochrome c and its application as electrochemical biosensors. *Talanta,* 176**,** 195-207.

AL MAJIDI, M. I. H., EL-SHAHENY, R., EL-SHABRAWY, Y. & EL-MAGHRABEY, M. 2019. Screening and greenness profiling of oxidative-coupling and electrophilic aromatic substitution reactions for determination of three phenolic drugs. *Microchemical Journal,* 149**,** 104051.

ALAVI-TABARI, S. A. R., KHALILZADEH, M. A. & KARIMI-MALEH, H. 2018. Simultaneous determination of doxorubicin and dasatinib as two breast anticancer drugs uses an amplified sensor with ionic liquid and ZnO nanoparticle. *Journal of Electroanalytical Chemistry,* 811**,** 84-88.

ALGETHAMI, F. K., EID, S. M., KELANI, K. M., ELGHOBASHY, M. R. & ABD EL-RAHMAN, M. K. 2020. Chemical fingerprinting and quantitative monitoring of the doping drugs bambuterol and terbutaline in human urine samples using ATR-FTIR coupled with a PLSR chemometric tool. *RSC Advances,* 10**,** 7146-7154.

ALHARTHI, S. & EL RASSI, Z. 2019. CE with multi-walled carbon nanotubes (MWCNTs). Part I. Functionalized and SDS coated MWCNTs as pseudo-stationary phases in nanoparticle EKC–Studies on retention energetics. *Talanta,* 192**,** 534-544.

ALKAIM, A. F., KANDIEL, T. A., HUSSEIN, F. H., DILLERT, R. & BAHNEMANN, D. W. 2013. Solvent-free hydrothermal synthesis of anatase TiO2 nanoparticles with enhanced photocatalytic hydrogen production activity. *Applied Catalysis A: General,* 466**,** 32-37.

ALLEN, H., BACKHOUSE, S. H., HULL, J. H. & PRICE, O. J. 2019. Anti-doping Policy, Therapeutic Use Exemption and Medication Use in Athletes with Asthma: A Narrative Review and Critical Appraisal of Current Regulations. *Sports Medicine,* 49**,** 659-668.

ALRASHDI, A., FARGHALY, O. & HOSNY, A. 2019. *Voltammetric Determination of Pharmaceutical Compounds at Bare and Modified Solid Electrodes: A Review*.

AMARE, M. & MENKIR, G. 2017. Differential pulse voltammetric determination of salbutamol sulfate in syrup pharmaceutical formulation using poly (4-amino-3-hydroxynaphthalene sulfonic acid) modified glassy carbon electrode. *Heliyon,* 3**,** e00417.

ARABI, M., GHAEDI, M., OSTOVAN, A. & WANG, S. 2016. Synthesis of lab-in-a-pipette-tip extraction using hydrophilic nano-sized dummy molecularly imprinted polymer for purification and analysis of prednisolone. *Journal of Colloid and Interface Science,* 480**,** 232-239.

ARESTA, A., PALMISANO, F. & ZAMBONIN, C. G. 2005. Simultaneous determination of caffeine, theobromine, theophylline, paraxanthine and nicotine in human milk by liquid chromatography with diode array UV detection. *Food Chemistry,* 93**,** 177-181.

ASADIAN, E., GHALKHANI, M. & SHAHROKHIAN, S. 2019. Electrochemical sensing based on carbon nanoparticles: A review. *Sensors and Actuators B: Chemical,* 293**,** 183-209.

ASKARI, M. B., BANIZI, Z. T., SOLTANI, S. & SEIFI, M. 2018. Comparison of optical properties and photocatalytic behavior of TiO2/MWCNT, CdS/MWCNT and TiO2/CdS/MWCNT nanocomposites. *Optik,* 157**,** 230-239.

ASKARI, M. B., TAVAKOLI BANIZI, Z., SEIFI, M., BAGHERI DEHAGHI, S. & VEISI, P. 2017. Synthesis of TiO2 nanoparticles and decorated multi-wall carbon nanotube (MWCNT) with anatase TiO2 nanoparticles and study of optical properties and structural characterization of TiO2/MWCNT nanocomposite. *Optik,* 149**,** 447-454.

ASWINI, K., MOHAN, A. V. & BIJU, V. 2016. Molecularly imprinted poly (4-amino-5-hydroxy-2, 7-naphthalenedisulfonic acid) modified glassy carbon electrode as an electrochemical theophylline sensor. *Materials Science and Engineering: C,* 65**,** 116-125.

ATTA, N. F., ABDEL GAWAD, S. A., EL-ADS, E. H., EL-GOHARY, A. R. M. & GALAL, A. 2017. A new strategy for NADH sensing using ionic liquid crystals-carbon nanotubes/nano-magnetite composite platform. *Sensors and Actuators B: Chemical,* 251**,** 65-73.

AYDIN, E. B., AYDIN, M. & SEZGINTURK, M. K. 2019. Chapter 2 - Immobilization Techniques of Nanomaterials. *In:* OZKAN, S. A. & SHAH, A. (eds.) *New Developments in Nanosensors for Pharmaceutical Analysis.* Academic Press.

AYYAPPAN, S., PANNEERSELVAM, G., ANTONY, M. P. & PHILIP, J. 2011. High temperature stability of surfactant capped CoFe2O4 nanoparticles. *Materials Chemistry and Physics,* 130**,** 1300-1306.

BADEA, D. N. & LEVAI, C. 2017. Separation and Detection of Caffeine, Theophylline and Theobromine from Coffee Varieties, Carbonated Soft Drinks and Alcoholic Beverages. *REVISTA DE CHIMIE,* 68**,** 2704-2707.

BALDACCI, S., SIMONI, M., MAIO, S., ANGINO, A., MARTINI, F., SARNO, G., CERRAI, S., SILVI, P., PALA, A. P. & BRESCIANI, M. 2019. Prescriptive adherence to GINA guidelines and asthma control: An Italian cross sectional study in general practice. *Respiratory medicine,* 146**,** 10-17.

BANDI, A. B., SHETTI, N. P., MALODE, S. J., BUKKITGAR, S. D. & KULKARNI, R. M. 2019. Electroanalysis of 1, 3–dimethylexanthine at zinc oxide nanoparticles modified electrode. *Materials Today: Proceedings,* 18**,** 590-595.

BANSOD, B., KUMAR, T., THAKUR, R., RANA, S. & SINGH, I. 2017. A review on various electrochemical techniques for heavy metal ions detection with different sensing platforms. *Biosensors and Bioelectronics,* 94**,** 443-455.

BARBOSA, P. F. P., VIEIRA, E. G., CUMBA, L. R., PAIM, L. L., NAKAMURA, A. P. R., ANDRADE, R. D. A. & RIBEIRO, D. 2019. Voltammetric Techniques for Pesticides and Herbicides Detection-an Overview. *Int. J. Electrochem. Sci,* 14**,** 3418-3433.

BARNES, P. J. 2006. Drugs for asthma. *British journal of pharmacology,* 147**,** S297-S303.

BARTELLA, L., DI DONNA, L., NAPOLI, A., SICILIANO, C., SINDONA, G. & MAZZOTTI, F. 2019. A rapid method for the assay of methylxanthines alkaloids: Theobromine, theophylline and caffeine, in cocoa products and drugs by paper spray tandem mass spectrometry. *Food Chemistry,* 278**,** 261-266.

BATEMAN, E., HURD, S., BARNES, P., BOUSQUET, J., DRAZEN, J., FITZGERALD, M., GIBSON, P., OHTA, K., O'BYRNE, P. & PEDERSEN, S. 2008. Global strategy for asthma management and prevention: GINA executive summary. *European Respiratory Journal,* 31**,** 143-178.

BAYTAK, A. K., TEKER, T., DUZMEN, S. & ASLANOGLU, M. 2016. A sensitive determination of terbutaline in pharmaceuticals and urine samples using a composite electrode based on zirconium oxide nanoparticles. *Materials Science and Engineering: C,* 67**,** 125-131.

BAZLI, L., SIAVASHI, M. & SHIRAVI, A. 2019. A Review of Carbon Nanotube/TiO2 Composite Prepared via Sol-Gel Method. *Composites and Compounds,* 1.

BEOTRA, A., AHI, S., DUBEY, S., UPADHYAY, A. & JAIN, S. 2009. Application of liquid chromatography tandem mass spectrometry for the detection often long-term metabolites of Prednisolone. *Recent Advances in Doping Analysis, Sport und Buch Strauß,* 17**,** 309.

BIBI, M., ABBAS, S. M., AHMAD, N., MUHAMMAD, B., IQBAL, Z., RANA, U. A. & KHAN, S. U.-D. 2017. Microwaves absorbing characteristics of metal ferrite/multiwall carbon nanotubes nanocomposites in X-band. *Composites Part B: Engineering,* 114**,** 139-148.

BIJAD, M., KARIMI-MALEH, H. & KHALILZADEH, M. A. 2013. Application of ZnO/CNTs Nanocomposite Ionic Liquid Paste Electrode as a Sensitive Voltammetric Sensor for Determination of Ascorbic Acid in Food Samples. *Food Analytical Methods,* 6**,** 1639-1647.

BISSELL, K., ELLWOOD, P., ELLWOOD, E., CHIANG, C.-Y., MARKS, G. B., EL SONY, A., ASHER, I., BILLO, N., PERRIN, C. & GROUP, G. A. N. S. 2019. Essential medicines at the national level: The Global Asthma Network's essential asthma medicines survey 2014. *International journal of environmental research and public health,* 16**,** 605.

BONINI, M. & USMANI, O. S. 2020. Drugs for airway disease. *Medicine,* 48**,** 314-322.

BOOBPHAHOM, S., RUECHA, N., RODTHONGKUM, N., CHAILAPAKUL, O. & REMCHO, V. T. 2019. A copper oxide-ionic liquid/reduced graphene oxide composite sensor enabled by digital dispensing: Non-enzymatic paper-based microfluidic determination of creatinine in human blood serum. *Analytica Chimica Acta,* 1083**,** 110-118.

BUKKITGAR, S. D. & SHETTI, N. P. 2018. Electrochemical behavior of theophylline at methylene blue dye modified electrode and its analytical application. *Materials Today: Proceedings,* 5**,** 21474-21481.

BUKKITGAR, S. D., SHETTI, N. P., KULKARNI, R. M., REDDY, K. R., SHUKLA, S. S., SAJI, V. S. & AMINABHAVI, T. M. 2019. Electro-catalytic behavior of Mg-doped ZnO nano-flakes for oxidation of anti-inflammatory drug. *Journal of The Electrochemical Society,* 166**,** B3072-B3078.

BUKKITGAR, S. D., SHETTI, N. P., MALLADI, R. S., REDDY, K. R., KALANUR, S. S. & AMINABHAVI, T. M. 2020. Novel ruthenium doped TiO2/reduced graphene oxide hybrid as highly selective sensor for the determination of ambroxol. *Journal of Molecular Liquids,* 300**,** 112368.

CABAN, M., STEPNOWSKI, P., KWIATKOWSKI, M., MIGOWSKA, N. & KUMIRSKA, J. 2011. Determination of β-blockers and β-agonists using gas chromatography and gas chromatography-mass spectrometry - A comparative study of the derivatization step. *Journal of Chromatography A,* 1218**,** 8110-8122.

CALZETTA, L., HANANIA, N. A., DINI, F. L., GOLDSTEIN, M. F., FAIRWEATHER, W. R., HOWARD, W. W. & CAZZOLA, M. 2018. Impact of doxofylline compared to theophylline in asthma: a pooled analysis of functional and clinical outcomes from two multicentre, double-blind, randomized studies (DOROTHEO 1 and DOROTHEO 2). *Pulmonary pharmacology & therapeutics,* 53**,** 20-26.

CAO, Z., ZHAO, Y.-T., DAI, Y.-M., LONG, S., GUO, X.-C. & YANG, R.-H. 2011. Determination of salbutamol sulfate based on chitosan multi-wall carbon nanotubes film modified glassy carbon electrode. *Sensor Letters,* 9**,** 1985-1989.

CAZZOLA, M. & MATERA, M. G. 2020. The effect of doxofylline in asthma and COPD. *Respiratory Medicine,* 164**,** 105904.

CAZZOLA, M., PAGE, C. P., CALZETTA, L. & MATERA, M. G. 2012. Pharmacology and therapeutics of bronchodilators. *Pharmacological reviews,* 64**,** 450-504.

CHANG, K.-C., CHANG, Y.-T. & TSAI, C.-E. 2018. Determination of ractopamine and salbutamol in pig hair by liquid chromatography tandem mass spectrometry. *Journal of food and drug analysis,* 26**,** 725-730.

CHEN, D., YANG, M., ZHENG, N., XIE, N., LIU, D., XIE, C. & YAO, D. 2016. A novel aptasensor for electrochemical detection of ractopamine, clenbuterol, salbutamol, phenylethanolamine and procaterol. *Biosensors and Bioelectronics,* 80**,** 525-531.

CHEN, P., SHEN, J., WANG, C. & WEI, Y. 2018. Selective extraction of theophylline from plasma by copper-doped magnetic microspheres prior to its quantification by HPLC. *Microchimica Acta,* 185**,** 113.

CHEN, T.-W., CHINNAPAIYAN, S., CHEN, S.-M., HOSSAM MAHMOUD, A., ELSHIKH, M. S., EBAID, H. & TAHA YASSIN, M. 2020. Facile sonochemical synthesis of rutile-type titanium dioxide microspheres decorated graphene oxide composite for efficient electrochemical sensor. *Ultrasonics Sonochemistry,* 62**,** 104872.

CHEN, Y., HUANG, Y., GUO, D., CHEN, C., WANG, Q. & FU, Y. 2014. A chiral sensor for recognition of DOPA enantiomers based on immobilization of β-cyclodextrin onto the carbon nanotube-ionic liquid nanocomposite. *Journal of Solid State Electrochemistry,* 18**,** 3463-3469.

CHENG, J., SU, X.-O., HAN, C., WANG, S., WANG, P., ZHANG, S. & XIE, J. 2018. Ultrasensitive detection of salbutamol in animal urine by immunomagnetic bead treatment coupling with surface-enhanced Raman spectroscopy. *Sensors and Actuators B: Chemical,* 255**,** 2329-2338.

CHENG, J., WANG, X., NIE, T., YIN, L., WANG, S., ZHAO, Y., WU, H. & MEI, H. 2020. A novel electrochemical sensing platform for detection of dopamine based on gold nanobipyramid/multi-walled carbon nanotube hybrids. *Analytical and Bioanalytical Chemistry***,** 1-9.

CHIESA, L. M., NOBILE, M., BIOLATTI, B., PAVLOVIC, R., PANSERI, S., CANNIZZO, F. T. & ARIOLI, F. 2016. Detection of selected corticosteroids and anabolic steroids in calf milk replacers by liquid chromatography–electrospray ionisation – Tandem mass spectrometry. *Food Control,* 61**,** 196-203.

CHITLANGE, S. S., CHATURVEDI, K. K. & WANKHEDE, S. B. 2011. Development and validation of spectrophotometric and HPLC method for the simultaneous estimation of salbutamol sulphate and prednisolone in tablet dosage form. *J Anal Bioanal Techniques,* 2**,** 2.

CHOKKAREDDY, R., BHAJANTHRI, N., REDHI, G. G. & REDHI, D. G. 2018. Ultra-sensitive electrochemical sensor for the determination of pyrazinamide. *Current Analytical Chemistry,* 14**,** 391-398.

CHOKKAREDDY, R., BHAJANTHRI, N. K. & REDHI, G. G. 2017. An enzyme-induced novel biosensor for the sensitive electrochemical determination of isoniazid. *Biosensors,* 7**,** 21.

CHOKKAREDDY, R., NIRANJAN, T. & REDHI, G. G. 2020a. Ionic liquid based electrochemical sensors and their applications. *Green Sustainable Process for Chemical and Environmental Engineering and Science.* Elsevier.

CHOKKAREDDY, R., REDHI, G. G. & KARTHICK, T. 2019a. A lignin polymer nanocomposite based electrochemical sensor for the sensitive detection of chlorogenic acid in coffee samples. *Heliyon,* 5**,** e01457.

CHOKKAREDDY, R., THONDAVADA, N., BHAJANTHRI, N. K. & REDHI, G. G. 2019b. An amino functionalized magnetite nanoparticle and ionic liquid based electrochemical sensor for the detection of acetaminophen. *Analytical Methods,* 11**,** 6204-6212.

CHOKKAREDDY, R., THONDAVADA, N., KABANE, B. & REDHI, G. G. 2020b. A novel ionic liquid based electrochemical sensor for detection of pyrazinamide. *Journal of the Iranian Chemical Society***,** 1-9.

CLARK, M. D., SUBRAMANIAN, S. & KRISHNAMOORTI, R. 2011. Understanding surfactant aided aqueous dispersion of multi-walled carbon nanotubes. *Journal of colloid and interface science,* 354**,** 144-151.

CORDELL, R. L., VALKENBURG, T. S. E., PANDYA, H. C., HAWCUTT, D. B., SEMPLE, M. G. & MONKS, P. S. 2018. Quantitation of salbutamol using micro-volume blood sampling – applications to exacerbations of pediatric asthma. *Journal of Asthma,* 55**,** 1205-1213.

COSTA, P. V. F. D., SILVA, R. M. P. D., SUFFREDINI, H. B. & ALVES, W. A. 2018. Poly-L-Arginine-Modified Boron-Doped Diamond and Glassy Carbon Electrodes for Terbutaline Sulfate Detection. *Journal of nanoscience and nanotechnology,* 18**,** 4551-4558.

DAFFÉ, N., CHOUEIKANI, F., NEVEU, S., ARRIO, M.-A., JUHIN, A. L., OHRESSER, P., DUPUIS, V. & SAINCTAVIT, P. 2018. Magnetic anisotropies and cationic distribution in CoFe2O4 nanoparticles prepared by co-precipitation route: Influence of particle size and stoichiometry. *Journal of Magnetism and Magnetic Materials,* 460**,** 243-252.

DAKSHAYINI, B., REDDY, K. R., MISHRA, A., SHETTI, N. P., MALODE, S. J., BASU, S., NAVEEN, S. & RAGHU, A. V. 2019a. Role of conducting polymer and metal oxide-based hybrids for applications in ampereometric sensors and biosensors. *Microchemical Journal*.

DAKSHAYINI, B. S., REDDY, K. R., MISHRA, A., SHETTI, N. P., MALODE, S. J., BASU, S., NAVEEN, S. & RAGHU, A. V. 2019b. Role of conducting polymer and metal oxide-based hybrids for applications in ampereometric sensors and biosensors. *Microchemical Journal,* 147**,** 7-24.

DE LIMA, L. F., MACIEL, C. C., FERREIRA, A. L., DE ALMEIDA, J. C. & FERREIRA, M. 2020. Nickel (II) phthalocyanine-tetrasulfonic-Au nanoparticles nanocomposite film for tartrazine electrochemical sensing. *Materials Letters,* 262**,** 127186.

DE ROOS, E. W., LAHOUSSE, L., VERHAMME, K. M., BRAUNSTAHL, G.-J., IKRAM, M. A., STRICKER, B. H. C. & BRUSSELLE, G. G. 2018. Asthma and its comorbidities in middle-aged and older adults; the Rotterdam Study. *Respiratory medicine,* 139**,** 6-12.

DÉSI, E., KOVÁCS, Á., PALOTAI, Z. & KENDE, A. 2008. Analysis of dexamethasone and prednisolone residues in bovine milk using matrix solid phase dispersion-liquid chromatography with ultraviolet detection. *Microchemical Journal,* 89**,** 77-81.

DHARMAGE, S. C., PERRET, J. & CUSTOVIC, A. 2019. Epidemiology of asthma in children and adults. *Frontiers in pediatrics,* 7**,** 246.

DÍEZ, A. M., RIBEIRO, A. S., SANROMÁN, M. A. & PAZOS, M. 2018. Optimization of photo-Fenton process for the treatment of prednisolone. *Environmental Science and Pollution Research***,** 1-15.

DOMÍNGUEZ-ROMERO, J. C., GARCÍA-REYES, J. F., MARTÍNEZ-ROMERO, R., MARTÍNEZ-LARA, E., DEL MORAL-LEAL, M. L. & MOLINA-DÍAZ, A. 2013. Detection of main urinary metabolites of β2-agonists clenbuterol, salbutamol and terbutaline by liquid chromatography high resolution mass spectrometry. *Journal of Chromatography B,* 923-924**,** 128-135.

DONG, Y., YANG, L. & ZHANG, L. 2017. Simultaneous Electrochemical Detection of Benzimidazole Fungicides Carbendazim and Thiabendazole Using a Novel Nanohybrid Material-Modified Electrode. *Journal of Agricultural and Food Chemistry,* 65**,** 727-736.

DU, J., CHEN, W., ZHANG, C., LIU, Y., ZHAO, C. & DAI, Y. 2011. Hydrothermal synthesis of porous TiO2 microspheres and their photocatalytic degradation of gaseous benzene. *Chemical Engineering Journal,* 170**,** 53-58.

ELZAYAT, E. M., SHAKEEL, F., ALSHEHRI, S., IBRAHIM, M. A., ALTAMIMI, M. A., KAZI, M., ALANAZI, F. K. & HAQ, N. 2019. UHPLC assisted simultaneous separation of apigenin and prednisolone and its application in the pharmacokinetics of apigenin. *Journal of Chromatography B,* 1117**,** 58-65.

ENSAFI, A. A., ZANDI-ATASHBAR, N., GORGABI-KHORZOUGHI, M. & REZAEI, B. 2019. Nickel-Ferrite Oxide Decorated on Reduced Graphene Oxide, an Efficient and Selective Electrochemical Sensor for Detection of Furazolidone. *IEEE Sensors Journal,* 19**,** 5396-5403.

ERKMEN, C., KURBANOGLU, S. & USLU, B. 2020. Fabrication of poly (3, 4-ethylenedioxythiophene)-iridium oxide nanocomposite based tyrosinase biosensor for the dual detection of catechol and azinphos methyl. *Sensors and Actuators B: Chemical,* 316**,** 128121.

FAN, Y., HUANG, K.-J., NIU, D.-J., YANG, C.-P. & JING, Q.-S. 2011. TiO2-graphene nanocomposite for electrochemical sensing of adenine and guanine. *Electrochimica Acta,* 56**,** 4685-4690.

FANG, S., ZHANG, Y., LIU, X., QIU, J., LIU, Z. & KONG, F. 2019. Development of a highly sensitive time-resolved fluoroimmunoassay for the determination of trace salbutamol in environmental samples. *Science of The Total Environment,* 679**,** 359-364.

FARGHALI, R., AHMED, R. A. & ALHARTHI, A. A. 2018. Synthesis and Characterization of Electrochemical Sensor Based on Polymeric/TiO2Nanocomposite Modified with Imidizolium Ionic Liquid for Determination of Diclofenac. *Int. J. Electrochem. Sci,* 13**,** 10390-10414.

FARIDBOD, F., RASHEDI, H., GANJALI, M. R., NOROUZI, P. & RIAHI, S. 2011. *Application of room temperature ionic liquids in electrochemical sensors and biosensors*, INTECH Open Access Publisher.

FELIX, F. S., DANIEL, D., MATOS, J. R., LUCIO DO LAGO, C. & ANGNES, L. 2016. Fast analysis of terbutaline in pharmaceuticals using multi-walled nanotubes modified electrodes from recordable compact disc. *Analytica Chimica Acta,* 928**,** 32-38.

FENG, S., CHEN, C., WANG, W. & QUE, L. 2018. An aptamer nanopore-enabled microsensor for detection of theophylline. *Biosensors and Bioelectronics,* 105**,** 36-41.

FERNANDES, T. A. P., AGUIAR, J. P., FERNANDES, A. I. & PINTO, J. F. 2017. Quantification of theophylline or paracetamol in milk matrices by high-performance liquid chromatography. *Journal of Pharmaceutical Analysis,* 7**,** 401-405.

FIDANI, M., GAMBERINI, M. C., POMPA, G., MUNGIGUERRA, F., CASATI, A. & ARIOLI, F. 2013. Presence of endogenous prednisolone in human urine. *Steroids,* 78**,** 121-126.

FIEL, W., BORGES, P., LINS, V. & FARIA, R. 2019. Recent advances on the electrochemical transduction techniques for the biosensing of pharmaceuticals in aquatic environments. *Int J Biosen Bioelectron,* 5**,** 119-123.

FUKUSHIMA, T., KOSAKA, A., ISHIMURA, Y., YAMAMOTO, T., TAKIGAWA, T., ISHII, N. & AIDA, T. 2003. Molecular ordering of organic molten salts triggered by single-walled carbon nanotubes. *Science,* 300**,** 2072-2074.

GAN, T., LI, J., ZHAO, A., XU, J., ZHENG, D., WANG, H. & LIU, Y. 2018. Detection of theophylline using molecularly imprinted mesoporous silica spheres. *Food Chemistry,* 268**,** 1-8.

GAN, T., ZHAO, A., WANG, Z., LIU, P., SUN, J. & LIU, Y. 2017. An electrochemical sensor based on SiO 2@ TiO 2-embedded molecularly imprinted polymers for selective and sensitive determination of theophylline. *Journal of Solid State Electrochemistry,* 21**,** 3683-3691.

GANJALI, M. R., DOURANDISH, Z., BEITOLLAHI, H., TAJIK, S., HAJIAGHABABAEI, L. & LARIJANI, B. 2018. Highly sensitive determination of theophylline based on graphene quantum dots modified electrode. *Int. J. Electrochem. Sci,* 13**,** 2448-2461.

GEORGE, J. M., ANTONY, A. & MATHEW, B. 2018. Metal oxide nanoparticles in electrochemical sensing and biosensing: a review. *Microchimica Acta,* 185**,** 358.

GHANBARI, M. H., KHOSHROO, A., SOBATI, H., GANJALI, M. R., RAHIMI-NASRABADI, M. & AHMADI, F. 2019. An electrochemical sensor based on poly (L-Cysteine)@ AuNPs@ reduced graphene oxide nanocomposite for determination of levofloxacin. *Microchemical Journal,* 147**,** 198-206.

GHOLIVAND, M. B., AHMADI, E. & MAVAEI, M. 2019a. A novel voltammetric sensor based on graphene quantum dots-thionine/nano-porous glassy carbon electrode for detection of cisplatin as an anti-cancer drug. *Sensors and Actuators B: Chemical,* 299**,** 126975.

GHOLIVAND, M. B., SHAMSIPUR, M. & EHZARI, H. 2019b. Cetirizine dihydrochloride sensor based on nano composite chitosan, MWCNTs and ionic liquid. *Microchemical Journal,* 146**,** 692-700.

GOGOLASHVILI, A., TATUNASHVILI, E., CHANKVETADZE, L., SOHAJDA, T., SZEMAN, J., GUMUSTAS, M., OZKAN, S. A., SALGADO, A. & CHANKVETADZE, B. 2018. Separation of terbutaline enantiomers in capillary electrophoresis with cyclodextrin-type chiral selectors and investigation of structure of selector-selectand complexes. *Journal of Chromatography A,* 1571**,** 231-239.

GOLMOHAMMADI, M., HONARMAND, M. & GHANBARI, S. 2020. A green approach to synthesis of ZnO nanoparticles using jujube fruit extract and their application in photocatalytic degradation of organic dyes. *Spectrochimica Acta Part A: Molecular and Biomolecular Spectroscopy,* 229**,** 117961.

GONÇALVES-FILHO, D., SILVA, C. C. G. & DE SOUZA, D. 2020. Pesticides determination in foods and natural waters using solid amalgam-based electrodes: Challenges and trends. *Talanta,* 212**,** 120756.

GOPAL, P. & REDDY, T. M. 2018a. Fabrication of carbon-based nanomaterial composite electrochemical sensor for the monitoring of terbutaline in pharmaceutical formulations. *Colloids and Surfaces A: Physicochemical and Engineering Aspects,* 538**,** 600-609.

GOPAL, T. V., REDDY, T. M., VENKATAPRASAD, G., SHAIKSHAVALLI, P. & GOPAL, P. 2018b. Rapid and sensitive electrochemical monitoring of paracetamol and its simultaneous resolution in presence of epinephrine and tyrosine at GO/poly (Val) composite modified carbon paste electrode. *Colloids and Surfaces A: Physicochemical and Engineering Aspects,* 545**,** 117-126.

GOUD, K. Y., SATYANARAYANA, M., HAYAT, A., GOBI, K. V. & MARTY, J. L. 2019a. Chapter 7 - Nanomaterial-based electrochemical sensors in pharmaceutical applications. *In:* GRUMEZESCU, A. M. (ed.) *Nanoparticles in Pharmacotherapy.* William Andrew Publishing.

GOUD, K. Y., SATYANARAYANA, M., HAYAT, A., GOBI, K. V. & MARTY, J. L. 2019b. Nanomaterial-based electrochemical sensors in pharmaceutical applications. *Nanoparticles in Pharmacotherapy.* Elsevier.

GOYAL, R. N. & BISHNOI, S. 2009a. Simultaneous voltammetric determination of prednisone and prednisolone in human body fluids. *Talanta,* 79**,** 768-774.

GOYAL, R. N., OYAMA, M., BACHHETI, N. & SINGH, S. P. 2009b. Fullerene C60 modified gold electrode and nanogold modified indium tin oxide electrode for prednisolone determination. *Bioelectrochemistry,* 74**,** 272-277.

GUO, X.-C., WANG, H.-H., CHEN, X.-J., XIA, Z.-Y., KANG, W.-Y. & ZHOU, W.-H. 2017. One step electrodeposition of graphene-au nanocomposites for highly sensitive electrochemical detection of salbutamol. *Int J Electrochem Sci,* 12**,** 861-75.

HAN, L., ZHANG, Y., KANG, J., TANG, J. & ZHANG, Y. 2012a. Chemiluminescence determination of terbutaline sulfate in bovine urine and pharmaceutical preparations based on enhancement of the 2-phenyl-4, 5-di (2-furyl) imidazole-potassium ferricyanide system. *Journal of Pharmaceutical and Biomedical Analysis,* 58**,** 141-145.

HAN, L., ZHANG, Y., KANG, J., TANG, J. & ZHANG, Y. 2012b. Chemiluminescence determination of terbutaline sulfate in bovine urine and pharmaceutical preparations based on enhancement of the 2-phenyl-4, 5-di (2-furyl) imidazole–potassium ferricyanide system. *Journal of Pharmaceutical and Biomedical Analysis,* 58**,** 141-145.

HASSANEIN, A., SALAHUDDIN, N., MATSUDA, A., KAWAMURA, G. & ELFIKY, M. 2017. Fabrication of biosensor based on Chitosan-ZnO/Polypyrrole nanocomposite modified carbon paste electrode for electroanalytical application. *Materials Science and Engineering: C,* 80**,** 494-501.

HATAMLUYI, B., ES'HAGHI, Z., MODARRES ZAHED, F. & DARROUDI, M. 2019. A novel electrochemical sensor based on GQDs-PANI/ZnO-NCs modified glassy carbon electrode for simultaneous determination of Irinotecan and 5-Fluorouracil in biological samples. *Sensors and Actuators B: Chemical,* 286**,** 540-549.

HE, H., SUN, T., LIU, W., XU, Z., HAN, Z., ZHAO, L., WU, X., NING, B. & BAI, J. 2020. Highly sensitive detection of salbutamol by ALP-mediated plasmonic ELISA based on controlled growth of AgNPs. *Microchemical Journal,* 156**,** 104804.

HERRING, V. L. & JOHNSON, J. A. 2000. Simple method for determination of terbutaline plasma concentration by high-performance liquid chromatography. *Journal of Chromatography B: Biomedical Sciences and Applications,* 741**,** 307-312.

HOU, J., DU, W., MENG, F., ZHAO, C. & DU, X. 2018. Effective dispersion of multi-walled carbon nanotubes in aqueous solution using an ionic-gemini dispersant. *Journal of colloid and interface science,* 512**,** 750-757.

HU, J., STEIN, A. & BÜHLMANN, P. 2016. Rational design of all-solid-state ion-selective electrodes and reference electrodes. *TrAC Trends in Analytical Chemistry,* 76**,** 102-114.

HU, S., WANG, A., LI, X. & LÖWE, H. 2010. Hydrothermal synthesis of well-dispersed ultrafine N-doped TiO2 nanoparticles with enhanced photocatalytic activity under visible light. *Journal of Physics and Chemistry of Solids,* 71**,** 156-162.

HUANG, W.-S., LIN, S.-J., WU, H. L. & CHEN, S.-H. 2003. Simultaneous determination of theophylline and dyphylline by micellar electrokinetic chromatography and application in drug formulations. *Journal of Chromatography B,* 795**,** 329-335.

HUCK, C., GUGGENBICHLER, W. & BONN, G. 2005a. Analysis of caffeine, theobromine and theophylline in coffee by near infrared spectroscopy (NIRS) compared to high-performance liquid chromatography (HPLC) coupled to mass spectrometry. *Analytica chimica acta,* 538**,** 195-203.

HUCK, C. W., GUGGENBICHLER, W. & BONN, G. K. 2005b. Analysis of caffeine, theobromine and theophylline in coffee by near infrared spectroscopy (NIRS) compared to high-performance liquid chromatography (HPLC) coupled to mass spectrometry. *Analytica Chimica Acta,* 538**,** 195-203.

ITAGIMATHA, N. & MANJUNATHA, D. H. 2019. RP-HPLC-UV method development and validation for simultaneous determination of terbutaline sulphate, ambroxol HCl and guaifenesin in pure and dosage forms. *Annales Pharmaceutiques Françaises,* 77**,** 295-301.

JACOBSON, G. A., CHONG, F. V. & DAVIES, N. W. 2003. LC–MS method for the determination of albuterol enantiomers in human plasma using manual solid-phase extraction and a non-deuterated internal standard. *Journal of Pharmaceutical and Biomedical Analysis,* 31**,** 1237-1243.

JADON, N., JAIN, R., SHARMA, S. & SINGH, K. 2016. Recent trends in electrochemical sensors for multianalyte detection – A review. *Talanta,* 161**,** 894-916.

JAFARI, M. T., REZAEI, B. & JAVAHERI, M. 2011. A new method based on electrospray ionisation ion mobility spectrometry (ESI-IMS) for simultaneous determination of caffeine and theophylline. *Food Chemistry,* 126**,** 1964-1970.

JANAJ, A. A., SHETTI, N. P., MALODE, S. J., BUKKITGAR, S. D. & KULKARNI, R. M. 2019. TiO2 nanoparticles modified sensor for theophylline drug. *Materials Today: Proceedings,* 18**,** 606-612.

JAYAPRAKASH, G. K., SWAMY, B. K., RAMÍREZ, H. N. G., EKANTHAPPA, M. T. & FLORES-MORENO, R. 2018. Quantum chemical and electrochemical studies of lysine modified carbon paste electrode surfaces for sensing dopamine. *New Journal of Chemistry,* 42**,** 4501-4506.

KALAMBATE, P. K., RAWOOL, C. R. & SRIVASTAVA, A. K. 2016. Voltammetric determination of pyrazinamide at graphene-zinc oxide nanocomposite modified carbon paste electrode employing differential pulse voltammetry. *Sensors and Actuators B: Chemical,* 237**,** 196-205.

KALAMBATE, P. K., RAWOOL, C. R. & SRIVASTAVA, A. K. 2017. Fabrication of graphene nanosheet–multiwalled carbon nanotube–polyaniline modified carbon paste electrode for the simultaneous electrochemical determination of terbutaline sulphate and guaifenesin. *New Journal of Chemistry,* 41**,** 7061-7072.

KALYANI, L. & RAO, C. V. 2018. Simultaneous spectrophotometric estimation of Salbutamol, Theophylline and Ambroxol three component tablet formulation using simultaneous equation methods. *Karbala International Journal of Modern Science,* 4**,** 171-179.

KANAN, S., MOYET, M. A., ARTHUR, R. B. & PATTERSON, H. H. 2020. Recent advances on TiO2-based photocatalysts toward the degradation of pesticides and major organic pollutants from water bodies. *Catalysis Reviews,* 62**,** 1-65.

KANAZAWA, H., ATSUMI, R., MATSUSHIMA, Y. & KIZU, J. 2000. Determination of theophylline and its metabolites in biological samples by liquid chromatography–mass spectrometry. *Journal of Chromatography A,* 870**,** 87-96.

KAPLAN, R., ERJAVEC, B. & PINTAR, A. 2015. Enhanced photocatalytic activity of single-phase, nanocomposite and physically mixed TiO2 polymorphs. *Applied Catalysis A: General,* 489**,** 51-60.

KARAAGAC, O., YILDIZ, B. B. & KÖÇKAR, H. 2019. The influence of synthesis parameters on one-step synthesized superparamagnetic cobalt ferrite nanoparticles with high saturation magnetization. *Journal of Magnetism and Magnetic Materials,* 473**,** 262-267.

KARAMI, F., RANJBAR, S., GHASEMI, Y. & NEGAHDARIPOUR, M. 2019. Analytical methodologies for determination of methotrexate and its metabolites in pharmaceutical, biological and environmental samples. *Journal of Pharmaceutical Analysis,* 9**,** 373-391.

KARTHIKA, A., KARUPPASAMY, P., SELVARAJAN, S., SUGANTHI, A. & RAJARAJAN, M. 2019. Electrochemical sensing of nicotine using CuWO4 decorated reduced graphene oxide immobilized glassy carbon electrode. *Ultrasonics Sonochemistry,* 55**,** 196-206.

KEERTHIKA DEVI, R., MUTHUSANKAR, G., GOPU, G. & BERCHMANS, L. J. 2020. A simple self-assembly fabrication of tin oxide nanoplates on multiwall carbon nanotubes for selective and sensitive electrochemical determination of antipyretic drug. *Colloids and Surfaces A: Physicochemical and Engineering Aspects,* 598**,** 124825.

KESAVAN, S., GOWTHAMAN, N., ALWARAPPAN, S. & JOHN, S. A. 2019. Real time detection of adenosine and theophylline in urine and blood samples using graphene modified electrode. *Sensors and Actuators B: Chemical,* 278**,** 46-54.

KHAKBAN, A., FITZGERALD, J. M., TAVAKOLI, H., LYND, L., EHTESHAMI-AFSHAR, S. & SADATSAFAVI, M. 2019. Extent, trends, and determinants of controller/reliever balance in mild asthma: a 14-year population-based study. *Respiratory research,* 20**,** 44.

KHEZRIAN, S., SALIMI, A., TEYMOURIAN, H. & HALLAJ, R. 2013. Label-free electrochemical IgE aptasensor based on covalent attachment of aptamer onto multiwalled carbon nanotubes/ionic liquid/chitosan nanocomposite modified electrode. *Biosensors and Bioelectronics,* 43**,** 218-225.

KHOSHROO, A., HOSSEINZADEH, L., SOBHANI-NASAB, A., RAHIMI-NASRABADI, M. & AHMADI, F. 2019. Silver nanofibers/ionic liquid nanocomposite based electrochemical sensor for detection of clonazepam via electrochemically amplified detection. *Microchemical Journal,* 145**,** 1185-1190.

KIM, K. H., KIM, H. J., KIM, J.-H. & SHIN, S. D. 2001. Determination of terbutaline enantiomers in human urine by coupled achiral–chiral high-performance liquid chromatography with fluorescence detection. *Journal of Chromatography B: Biomedical Sciences and Applications,* 751**,** 69-77.

KLINSUNTHORN, N., PETSOM, A. & NHUJAK, T. 2011. Determination of steroids adulterated in liquid herbal medicines using QuEChERS sample preparation and high-performance liquid chromatography. *Journal of Pharmaceutical and Biomedical Analysis,* 55**,** 1175-1178.

KUBÁŇ, P., DVOŘÁK, M. & KUBÁŇ, P. 2019. Capillary electrophoresis of small ions and molecules in less conventional human body fluid samples: A review. *Analytica Chimica Acta,* 1075**,** 1-26.

KULKARNI, D. R., MALODE, S. J., KEERTHI PRABHU, K., AYACHIT, N. H., KULKARNI, R. M. & SHETTI, N. P. 2020. Development of a novel nanosensor using Ca-doped ZnO for antihistamine drug. *Materials Chemistry and Physics,* 246**,** 122791.

KUMAR, S., BUKKITGAR, S. D., SINGH, S., SINGH, V., REDDY, K. R., SHETTI, N. P., VENKATA REDDY, C., SADHU, V. & NAVEEN, S. 2019a. Electrochemical sensors and biosensors based on graphene functionalized with metal oxide nanostructures for healthcare applications. *ChemistrySelect,* 4**,** 5322-5337.

KUMAR, Y., PRAMANIK, P. & DAS, D. K. 2019b. Electrochemical detection of paracetamol and dopamine molecules using nano-particles of cobalt ferrite and manganese ferrite modified with graphite. *Heliyon,* 5**,** e02031.

KURBANOGLU, S., BAKIRHAN, N. K., GUMUSTAS, M. & OZKAN, S. A. 2019. Modern assay techniques for cancer drugs: electroanalytical and liquid chromatography methods. *Critical reviews in analytical chemistry,* 49**,** 306-323.

KURBANOGLU, S., ERKMEN, C. & USLU, B. 2020. Frontiers in electrochemical enzyme based biosensors for food and drug analysis. *TrAC Trends in Analytical Chemistry,* 124**,** 115809.

LAURINAVIČIUS, L., RADZEVIČ, A., IGNATJEV, I., NIAURA, G., VITKUTĖ, K., ŠIRŠINAITIS, T., TRUSOVAS, R. & PAULIUKAITE, R. 2019. Investigation of electrochemical polymerisation of L-lysine and application for immobilisation of functionalised graphene as platform for electrochemical sensing. *Electrochimica Acta,* 299**,** 936-945.

LEE, W., LEOW, C. Y., TAN, S. C. & LEOW, C. H. 2018. Isolation and characterization of a novel anti-salbutamol chicken scFv for human doping urinalysis. *Analytical biochemistry,* 555**,** 81-93.

LI, J., FENG, H., LI, J., JIANG, J., FENG, Y., HE, L. & QIAN, D. 2015. Bimetallic Ag-Pd nanoparticles-decorated graphene oxide: a fascinating three-dimensional nanohybrid as an efficient electrochemical sensing platform for vanillin determination. *Electrochimica Acta,* 176**,** 827-835.

LI, J., XU, Z., LIU, M., DENG, P., TANG, S., JIANG, J., FENG, H., QIAN, D. & HE, L. 2017a. Ag/N-doped reduced graphene oxide incorporated with molecularly imprinted polymer: An advanced electrochemical sensing platform for salbutamol determination. *Biosensors and Bioelectronics,* 90**,** 210-216.

LI, L., LI, L., JIN, Y., SHUANG, Y. & WANG, H. 2020. Preparation of a teicoplanin-bonded chiral stationary phase for simultaneous determination of clenbuterol and salbutamol enantiomers in meat by LC-MS/MS. *Microchemical Journal***,** 104925.

LI, M., ZHOU, J., GU, X., WANG, Y., HUANG, X. & YAN, C. 2009a. Quantitative capillary electrophoresis and its application in analysis of alkaloids in tea, coffee, coca cola, and theophylline tablets. *Journal of separation science,* 32**,** 267-274.

LI, S., WANG, J. & ZHAO, S. 2009b. Determination of terbutaline sulfate by capillary electrophoresis with chemiluminescence detection. *Journal of Chromatography B,* 877**,** 155-158.

LI, Y., WANG, H., YAN, B. & ZHANG, H. 2017b. An electrochemical sensor for the determination of bisphenol A using glassy carbon electrode modified with reduced graphene oxide-silver/poly-l-lysine nanocomposites. *Journal of Electroanalytical Chemistry,* 805**,** 39-46.

LI, Y., YE, Z., ZHOU, J., LIU, J., SONG, G., ZHANG, K. & YE, B. 2012. A new voltammetric sensor based on poly(L-arginine)/graphene–Nafion composite film modified electrode for sensitive determination of Terbutaline sulfate. *Journal of Electroanalytical Chemistry,* 687**,** 51-57.

LIMMATVAPIRAT, C., BURANA-OSOT, J., LAOPOONPAT, P., PHATTANWASIN, P., ROJANARATA, T., CHAIDEDGUMJORN, A., SUKONPAN, C., POCHANAKOM, K., SRIPHONG, L. & TOYAMA, O. 2012. Determination of dexamethasone and prednisolone adulterated in herbal medicines using thin-layer chromatography. *Res. J. Pharmaceut. Biol. Chem. Sci.,* 3**,** 1353-1358.

LIN, C.-H., WU, C.-C. & KUO, Y.-F. 2016. A high sensitive impedimetric salbutamol immunosensor based on the gold nanostructure-deposited screen-printed carbon electrode. *Journal of Electroanalytical Chemistry,* 768**,** 27-33.

LIN, K.-C., HONG, C.-P. & CHEN, S.-M. 2013. Simultaneous determination for toxic ractopamine and salbutamol in pork sample using hybrid carbon nanotubes. *Sensors and Actuators B: Chemical,* 177**,** 428-436.

LION-CACHET, H. C., MUSONDA, J. M. M. & OMOLE, O. B. 2021. Severe asthma in South Africa: A literature review and management approach for primary care. *South African family practice : official journal of the South African Academy of Family Practice/Primary Care,* 63**,** e1-e10.

LIU, D.-M. & DONG, C. 2020. Recent advances in nano-carrier immobilized enzymes and their applications. *Process Biochemistry,* 92**,** 464-475.

LIU, J.-M., HUANG, Q., CAI, P.-Y., LIN, C.-Q., ZHANG, L.-H. & ZHENG, Z.-Y. 2014. Design of a highly sensitive fluorescent sensor and its application based on inhibiting NaIO 4 oxidizing rhodamine 6G. *Analytical Methods,* 6**,** 5957-5961.

LIU, R., WANG, Y., LI, D., DONG, L., LI, B., LIU, B., MA, H., LI, F., YIN, X. & CHEN, X. 2019a. A Simple, Low-Cost and Efficient β-CD/MWCNTs/CP-based Electrochemical Sensor for the Rapid and Sensitive Detection of Methyl Parathion. *Int. J. Electrochem. Sci,* 14**,** 9785-9795.

LIU, X., CHEN, W., LIAN, M., CHEN, X., LU, Y. & YANG, W. 2019b. Enzyme immobilization on ZIF-67/MWCNT composite engenders high sensitivity electrochemical sensing. *Journal of Electroanalytical Chemistry,* 833**,** 505-511.

LIU, Y., ZHU, K., WANG, J., HUANG, X., WANG, G., LI, C., CAO, J. & DING, S. 2016. Simultaneous detection and comparative pharmacokinetics of amoxicillin, clavulanic acid and prednisolone in cows' milk by UPLC–MS/MS. *Journal of Chromatography B,* 1008**,** 74-80.

LIU, Z., ZHANG, B., SUN, J., YI, Y., LI, M., DU, D., ZHU, F. & LUAN, J. 2018. Highly efficient detection of salbutamol in environmental water samples by an enzyme immunoassay. *Science of The Total Environment,* 613-614**,** 861-865.

LOMAE, A., NANTAPHOL, S., KONDO, T., CHAILAPAKUL, O., SIANGPROH, W. & PANCHOMPOO, J. 2019. Simultaneous determination of β-agonists by UHPLC coupled with electrochemical detection based on palladium nanoparticles modified BDD electrode. *Journal of Electroanalytical Chemistry,* 840**,** 439-448.

LOPES, J. H., COLSON, F.-X., BARRALET, J. E. & MERLE, G. 2017. Electrically wired enzyme/TiO2 composite for glucose detection. *Materials Science and Engineering: C,* 76**,** 991-996.

LU, Y., LIANG, X., NIYUNGEKO, C., ZHOU, J., XU, J. & TIAN, G. 2018. A review of the identification and detection of heavy metal ions in the environment by voltammetry. *Talanta,* 178**,** 324-338.

LUO, W., ZHU, L., DENG, J., LIU, A., GUO, B., TAN, W. & DAI, R. 2010. Simultaneous analysis of bambuterol and its active metabolite terbutaline enantiomers in rat plasma by chiral liquid chromatography–tandem mass spectrometry. *Journal of Pharmaceutical and Biomedical Analysis,* 52**,** 227-231.

MA, B., CHEONG, L.-Z., WENG, X., TAN, C.-P. & SHEN, C. 2018. Lipase@ZIF-8 nanoparticles-based biosensor for direct and sensitive detection of methyl parathion. *Electrochimica Acta,* 283**,** 509-516.

MA, K., WANG, H., ZHAO, M. & XING, J. 2009. Purity determination and uncertainty evaluation of theophylline by mass balance method, high performance liquid chromatography and differential scanning calorimetry. *Analytica chimica acta,* 650**,** 227-233.

MAAZ, K., MUMTAZ, A., HASANAIN, S. K. & CEYLAN, A. 2007. Synthesis and magnetic properties of cobalt ferrite (CoFe2O4) nanoparticles prepared by wet chemical route. *Journal of Magnetism and Magnetic Materials,* 308**,** 289-295.

MADHAN KUMAR, A. & GASEM, Z. M. 2015. In situ electrochemical synthesis of polyaniline/f-MWCNT nanocomposite coatings on mild steel for corrosion protection in 3.5% NaCl solution. *Progress in Organic Coatings,* 78**,** 387-394.

MAHDI GHAZANFARI N, A. 2015. Influence ofMWCNTsontheformation,structureandmagnetic propertiesofmagnetite. *MaterialsScienceinSemiconductorProcessing,* 40**,** 152–157.

MAHEMUTI, G., ZHANG, H., LI, J., TIELIWAERDI, N. & REN, L. 2018. Efficacy and side effects of intravenous theophylline in acute asthma: a systematic review and meta-analysis. *Drug design, development and therapy,* 12**,** 99.

MAKINO, S., FUEKI, M. & FUEKI, N. 2004. Efficacy and safety of methylxanthines in the treatment of asthma. *Allergology International,* 53**,** 13-22.

MALLAKPOUR, S. & KHADEM, E. 2016. Carbon nanotube–metal oxide nanocomposites: Fabrication, properties and applications. *Chemical Engineering Journal,* 302**,** 344-367.

MALODE, S. J., SHETTI, N. P. & NANDIBEWOOR, S. T. 2012. Voltammetric behavior of theophylline and its determination at multi-wall carbon nanotube paste electrode. *Colloids and Surfaces B: Biointerfaces,* 97**,** 1-6.

MANICKAM, P., KAUSHIK, A., KARUNAKARAN, C. & BHANSALI, S. 2017. Recent advances in cytochrome c biosensing technologies. *Biosensors and Bioelectronics,* 87**,** 654-668.

MANSUR, A. H., HASSAN, M., DUFFY, J. & WEBSTER, C. 2020. Development and clinical application of a prednisolone/cortisol assay to determine adherence to maintenance oral prednisolone in severe asthma. *Chest*.

MASEKELA, R., GRAY, C., GREEN, J., MANJRA, A., KRITZINGER, F., LEVIN, M. & ZAR, H. 2018. The increasing burden of asthma in South African children: A call to action. *South African Medical Journal,* 108.

MATANDABUZO, M. & AJIBADE, P. A. 2018. Synthesis and surface functionalization of multi-walled carbon nanotubes with imidazolium and pyridinium-based ionic liquids: Thermal stability, dispersibility and hydrophobicity characteristics. *Journal of Molecular Liquids,* 268**,** 284-293.

MEKASSA, B., TESSEMA, M. & CHANDRAVANSHI, B. S. 2017. Simultaneous determination of caffeine and theophylline using square wave voltammetry at poly (l-aspartic acid)/functionalized multi-walled carbon nanotubes composite modified electrode. *Sensing and bio-sensing research,* 16**,** 46-54.

MERT, S., BANKOĞLU, B., ÖZKAN, A., ATAR, N. & YOLA, M. L. 2018. Electrochemical sensing of ractopamine by carbon nitride nanotubes/ionic liquid nanohybrid in presence of other β-agonists. *Journal of Molecular Liquids,* 254**,** 8-11.

MEYER, A., NGIRUWONSANGA, T. & HENZE, G. 1996. Determination of adenine, caffeine, theophylline and theobromine by HPLC with amperometric detection. *Fresenius' Journal of Analytical Chemistry,* 356**,** 284-287.

MIRAKI, M., KARIMI-MALEH, H., TAHER, M. A., CHERAGHI, S., KARIMI, F., AGARWAL, S. & GUPTA, V. K. 2019. Voltammetric amplified platform based on ionic liquid/NiO nanocomposite for determination of benserazide and levodopa. *Journal of Molecular Liquids,* 278**,** 672-676.

MOHAMED, A., ANAS, A. K., BAKAR, S. A., ARDYANI, T., ZIN, W. M. W., IBRAHIM, S., SAGISAKA, M., BROWN, P. & EASTOE, J. 2015. Enhanced dispersion of multiwall carbon nanotubes in natural rubber latex nanocomposites by surfactants bearing phenyl groups. *Journal of colloid and interface science,* 455**,** 179-187.

MOHAMED, M. A., FAYED, A. S., HEGAZY, M. A., SALAMA, N. N. & ABBAS, E. E. 2019. Fully optimized new sensitive electrochemical sensing platform for the selective determination of antiepileptic drug ezogabine. *Microchemical Journal,* 144**,** 130-138.

MONTASERI, H. & FORBES, P. B. C. 2018. Analytical techniques for the determination of acetaminophen: A review. *TrAC Trends in Analytical Chemistry,* 108**,** 122-134.

MOORE, L. E., KAPOOR, K., BYERS, B. W., BROTTO, A. R., GHODS-ESFAHANI, D., HENRY, S. L., ST JAMES, R. B. & STICKLAND, M. K. 2019. Acute effects of salbutamol on systemic vascular function in people with asthma. *Respiratory Medicine,* 155**,** 133-140.

MORALES, E. 2018. *The Global Asthma Report 2018*.

MOSTAFA, I. M., OMAR, M. A., NAGY, D. M. & DERAYEA, S. M. 2018. Analysis of quetiapine in human plasma using fluorescence spectroscopy. *Spectrochimica Acta Part A: Molecular and Biomolecular Spectroscopy,* 196**,** 196-201.

MUKDASAI, S., LANGSI, V., PRAVDA, M., SRIJARANAI, S. & GLENNON, J. D. 2016. A highly sensitive electrochemical determination of norepinephrine using l-cysteine self-assembled monolayers over gold nanoparticles/multi-walled carbon nanotubes electrode in the presence of sodium dodecyl sulfate. *Sensors and Actuators B: Chemical,* 236**,** 126-135.

MUNIR, A., BOZAL-PALABIYIK, B., KHAN, A., SHAH, A. & USLU, B. 2019. A novel electrochemical method for the detection of oxymetazoline drug based on MWCNTs and TiO2 nanoparticles. *Journal of Electroanalytical Chemistry,* 844**,** 58-65.

MUNYENTWALI, A. & ZHU, L. 2015. Electrochemical determination of prednisolone at ordered mesoporous carbon modified electrode: application to doping monitoring. *Journal of The Electrochemical Society,* 162**,** H278-H282.

MUSTAFOV, S. D., MOHANTY, A. K., MISRA, M. & SEYDIBEYOĞLU, M. Ö. 2019. Fabrication of conductive Lignin/PAN carbon nanofibers with enhanced graphene for the modified electrodes. *Carbon,* 147**,** 262-275.

MWAFY, E. A. & MOSTAFA, A. M. 2019. Multi walled carbon nanotube decorated cadmium oxide nanoparticles via pulsed laser ablation in liquid media. *Optics & Laser Technology,* 111**,** 249-254.

NAPPORN, T. W., HOLADE, Y., KOKOH, B., MITSUSHIMA, S., MAYER, K., EICHBERGER, B. & HACKER, V. 2018. Chapter 9 - Electrochemical Measurement Methods and Characterization on the Cell Level. *In:* HACKER, V. & MITSUSHIMA, S. (eds.) *Fuel Cells and Hydrogen.* Elsevier.

NAVEEN, M. H., GURUDATT, N. G. & SHIM, Y.-B. 2017. Applications of conducting polymer composites to electrochemical sensors: A review. *Applied Materials Today,* 9**,** 419-433.

NI, B.-J., JOSS, A. & YUAN, Z. 2014. Modeling nitrogen removal with partial nitritation and anammox in one floc-based sequencing batch reactor. *Water Research,* 67**,** 321-329.

OELLIG, C., SCHUNCK, J. & SCHWACK, W. 2018. Determination of caffeine, theobromine and theophylline in Mate beer and Mate soft drinks by high-performance thin-layer chromatography. *Journal of Chromatography A,* 1533**,** 208-212.

OJHA, V. H. & KANT, K. M. 2019. Temperature dependent magnetic properties of superparamagnetic CoFe2O4 nanoparticles. *Physica B: Condensed Matter,* 567**,** 87-94.

OZKAN, S. A. & USLU, B. 2016. From mercury to nanosensors: Past, present and the future perspective of electrochemistry in pharmaceutical and biomedical analysis. *Journal of pharmaceutical and biomedical analysis,* 130**,** 126-140.

ÖZKAN, S. A., USLU, B. & ABOUL-ENEIN, H. Y. 2003. Analysis of pharmaceuticals and biological fluids using modern electroanalytical techniques. *Critical reviews in analytical chemistry,* 33**,** 155-181.

PAL, N. 2020. Nanoporous metal oxide composite materials: A journey from the past, present to future. *Advances in Colloid and Interface Science,* 280**,** 102156.

PARK, K. S., OH, S. S., SOH, H. T. & PARK, H. G. 2014. Target-controlled formation of silver nanoclusters in abasic site-incorporated duplex DNA for label-free fluorescence detection of theophylline. *Nanoscale,* 6**,** 9977-9982.

PENG, A., YAN, H., LUO, C., WANG, G., WANG, Y., YE, X. & DING, H. 2017a. Electrochemical determination of theophylline pharmacokinetic under the effect of roxithromycin in rats by the MWNTs/Au/poly-L-lysine modified sensor. *Int J Electrochem Sci,* 12**,** 330-346.

PENG, A., YAN, H., LUO, C., WANG, G., YE, X. & DING, H. 2017b. Electrochemical determination of theophylline pharmacokinetic under the effect of roxithromycin in rats by the MWNTs/Au/poly-L-lysine modified sensor. *Int. J. Electrochem. Sci,* 12**,** 330-346.

PERILLO, P. M. & RODRÍGUEZ, D. F. 2012. The gas sensing properties at room temperature of TiO2 nanotubes by anodization. *Sensors and Actuators B: Chemical,* 171-172**,** 639-643.

PRABHAKARAN, T. & HEMALATHA, J. 2016. Combustion synthesis and characterization of cobalt ferrite nanoparticles. *Ceramics International,* 42**,** 14113-14120.

PRIMPRAY, V., CHAILAPAKUL, O., TOKESHI, M., ROJANARATA, T. & LAIWATTANAPAISAL, W. 2019. A paper-based analytical device coupled with electrochemical detection for the determination of dexamethasone and prednisolone in adulterated traditional medicines. *Analytica Chimica Acta,* 1078**,** 16-23.

PUTZBACH, W. & RONKAINEN, N. J. 2013. Immobilization techniques in the fabrication of nanomaterial-based electrochemical biosensors: A review. *Sensors,* 13**,** 4811-4840.

QU, C. H., LI, X. L., ZHANG, L., XI, C. X., WANG, G. M., LI, N. B. & LUO, H. Q. 2011. Simultaneous determination of cimaterol, salbutamol, terbutaline and ractopamine in feed by SPE coupled to UPLC. *Chromatographia,* 73**,** 243-249.

QUINTANILLA, G., USARRALDE, A., PEREZ, I., GARGIULO, M. L., YAKUPOGLU, G., MARTIN, A. & BARBA, F. 2016. Anodic Oxidation of Caffeine and Theophylline in Glacial Acetic Acid. *ChemistrySelect,* 1**,** 414-416.

RAHI, A., KARIMIAN, K. & HELI, H. 2016. Nanostructured materials in electroanalysis of pharmaceuticals. *Analytical Biochemistry,* 497**,** 39-47.

RAJKUMAR, M., LI, Y.-S. & CHEN, S.-M. 2013. Electrochemical detection of toxic ractopamine and salbutamol in pig meat and human urine samples by using poly taurine/zirconia nanoparticles modified electrodes. *Colloids and Surfaces B: Biointerfaces,* 110**,** 242-247.

RAO, U. S., SRINIVAS, G. & RAO, T. P. 2015. Influence of precursors on morphology and spectroscopic properties of ZnO Nanoparticles. *Procedia Materials Science,* 10**,** 90-96.

RAVISHANKAR, T., SURESH KUMAR, K., TEIXEIRA, S., FERNANDEZ, C. & RAMAKRISHNAPPA, T. 2016. Ag Doped Titanium Dioxide Nanocomposite-modified Glassy Carbon Electrode as Electrochemical Interface for Catechol Sensing. *Electroanalysis,* 28**,** 452-461.

REICH, G. 2005. Near-infrared spectroscopy and imaging: Basic principles and pharmaceutical applications. *Advanced Drug Delivery Reviews,* 57**,** 1109-1143.

REVATHI, J., ABEL, M. J., ARCHANA, V., SUMITHRA, T., THIRUNEELAKANDAN, R. & JOSEPH PRINCE, J. 2020. Synthesis and characterization of CoFe2O4 and Ni-doped CoFe2O4 nanoparticles by chemical Co-precipitation technique for photo-degradation of organic dyestuffs under direct sunlight. *Physica B: Condensed Matter,* 587**,** 412136.

REZAEI, B. & MIRAHMADI-ZARE, S. 2011. Nanoscale Manipulation of prednisolone as electroactive configuration using molecularly imprinted-multiwalled carbon nanotube paste electrode. *Electroanalysis,* 23**,** 2724-2734.

REZVANI, S. A. & SOLEYMANPOUR, A. 2019. Application of a sensitive electrochemical sensor modified with WO3 nanoparticles for the trace determination of theophylline. *Microchemical Journal,* 149**,** 104005.

SAAR-REISMAA, P., TRETJAKOVA, A., MAZINA-ŠINKAR, J., VAHER, M., KALJURAND, M. & KULP, M. 2019. Rapid and sensitive capillary electrophoresis method for the analysis of Ecstasy in an oral fluid. *Talanta,* 197**,** 390-396.

SALAJEGHEH, M., ANSARI, M., FOROGHI, M. M. & KAZEMIPOUR, M. 2019. Computational design as a green approach for facile preparation of molecularly imprinted polyarginine-sodium alginate-multiwalled carbon nanotubes composite film on glassy carbon electrode for theophylline sensing. *Journal of pharmaceutical and biomedical analysis,* 162**,** 215-224.

SALEEM, A., MUHAMMAD, N., ULLAH, Z., KHAN, A. S. & RAHIM, A. 2019. Applications of Ionic Liquids in Sensors and Biosensors. *Industrial Applications of Green Solvents: Volume II,* 54**,** 29-50.

SANATI, A. L., FARIDBOD, F. & GANJALI, M. R. 2017. Synergic effect of graphene quantum dots and room temperature ionic liquid for the fabrication of highly sensitive voltammetric sensor for levodopa determination in the presence of serotonin. *Journal of Molecular Liquids,* 241**,** 316-320.

SANDHYARANI, N. 2019. Chapter 3 - Surface modification methods for electrochemical biosensors. *In:* ENSAFI, A. A. (ed.) *Electrochemical Biosensors.* Elsevier.

SANGHAVI, B. J., WOLFBEIS, O. S., HIRSCH, T. & SWAMI, N. S. 2015. Nanomaterial-based electrochemical sensing of neurological drugs and neurotransmitters. *Microchimica Acta,* 182**,** 1-41.

SANKAR, J., LODHA, R. & KABRA, S. 2008. Doxofylline: The next generation methylxanthine. *The Indian Journal of Pediatrics,* 75**,** 251-254.

SANTOS, A. M., WONG, A. & FATIBELLO-FILHO, O. 2018. Simultaneous determination of salbutamol and propranolol in biological fluid samples using an electrochemical sensor based on functionalized-graphene, ionic liquid and silver nanoparticles. *Journal of Electroanalytical Chemistry,* 824**,** 1-8.

SAYED, S., IBRAHIM, H. K., MOHAMED, M. I. & EL-MILLIGI, M. F. 2013. Fast-dissolving sublingual films of terbutaline sulfate: formulation and in vitro/in vivo evaluation. *Molecular pharmaceutics,* 10**,** 2942-2947.

SCHREIBER-DETURMENY, E. & BRUGUEROLLE, B. 1996. Simultaneous high-performance liquid chromatographic determination of caffeine and theophylline for routine drug monitoring in human plasma. *Journal of Chromatography B: Biomedical Sciences and Applications,* 677**,** 305-312.

SEARS, M. R. & LÖTVALL, J. 2005. Past, present and future—β2-adrenoceptor agonists in asthma management. *Respiratory Medicine,* 99**,** 152-170.

SEBASTIAN, N., YU, W.-C., HU, Y.-C., BALRAM, D. & YU, Y.-H. 2019. Sonochemical synthesis of iron-graphene oxide/honeycomb-like ZnO ternary nanohybrids for sensitive electrochemical detection of antipsychotic drug chlorpromazine. *Ultrasonics Sonochemistry,* 59**,** 104696.

SEPTIANI, N. L. W., KANETI, Y. V., YULIARTO, B., DIPOJONO, H. K., TAKEI, T., YOU, J. & YAMAUCHI, Y. 2018. Hybrid nanoarchitecturing of hierarchical zinc oxide wool-ball-like nanostructures with multi-walled carbon nanotubes for achieving sensitive and selective detection of sulfur dioxide. *Sensors and Actuators B: Chemical,* 261**,** 241-251.

SHABANI-NOOSHABADI, M. & ROOSTAEE, M. 2016. Modification of carbon paste electrode with NiO/graphene oxide nanocomposite and ionic liquids for fabrication of high sensitive voltammetric sensor on sulfamethoxazole analysis. *Journal of Molecular Liquids,* 220**,** 329-333.

SHAIKSHAVALI, P., MADHUSUDANA REDDY, T., VENU GOPAL, T., VENKATAPRASAD, G., KOTAKADI, V. S., PALAKOLLU, V. N. & KARPOORMATH, R. 2020a. A simple sonochemical assisted synthesis of nanocomposite (ZnO/MWCNTs) for electrochemical sensing of Epinephrine in human serum and pharmaceutical formulation. *Colloids and Surfaces A: Physicochemical and Engineering Aspects,* 584**,** 124038.

SHAIKSHAVALI, P., REDDY, T. M., GOPAL, T. V., VENKATAPRASAD, G., KOTAKADI, V. S., PALAKOLLU, V. & KARPOORMATH, R. 2020b. A simple sonochemical assisted synthesis of nanocomposite (ZnO/MWCNTs) for electrochemical sensing of Epinephrine in human serum and pharmaceutical formulation. *Colloids and Surfaces A: Physicochemical and Engineering Aspects,* 584**,** 124038.

SHAIKSHAVALI, P., REDDY, T. M., PALAKOLLU, V., KARPOORMATH, R., RAO, Y. S., VENKATAPRASAD, G., GOPAL, T. V. & GOPAL, P. 2019. Multi walled carbon nanotubes supported CuO-Au hybrid nanocomposite for the effective application towards the electrochemical determination of acetaminophen and 4-aminophenol. *Synthetic Metals,* 252**,** 29-39.

SHALAUDDIN, M., AKHTER, S., BASIRUN, W. J., BAGHERI, S., ANUAR, N. S. & JOHAN, M. R. 2019. Hybrid nanocellulose/f-MWCNTs nanocomposite for the electrochemical sensing of diclofenac sodium in pharmaceutical drugs and biological fluids. *Electrochimica Acta,* 304**,** 323-333.

SHAMS, A. & YARI, A. 2019. A new sensor consisting of Ag-MWCNT nanocomposite as the sensing element for electrochemical determination of Epirubicin. *Sensors and Actuators B: Chemical,* 286**,** 131-138.

SHANMUGAM, S. & SUBRAMANIAN, B. 2020. Evolution of phase pure magnetic cobalt ferrite nanoparticles by varying the synthesis conditions of polyol method. *Materials Science and Engineering: B,* 252**,** 114451.

SHASHIKUMARA, J. & SWAMY, B. K. 2020. Electrochemical Investigation of Dopamine in Presence of Uric acid and Ascorbic acid at Poly (Reactive Blue) Modified Carbon Paste Electrode: A Voltammetric Study. *Sensors International***,** 100008.

SHATERIAN, M., AGHAEI, A., KOOHI, M., TEYMOURI, M. & MOHAMMADI-GANJGAH, A. 2020. Synthesis, characterization and electrochemical sensing application of CoFe2O4/graphene magnetic nanocomposite for analysis of atenolol. *Polyhedron,* 182**,** 114479.

SHETTI, N. P., BUKKITGAR, S. D., KAKARLA, R. R., REDDY, C. & AMINABHAVI, T. M. 2019a. ZnO-based nanostructured electrodes for electrochemical sensors and biosensors in biomedical applications. *Biosensors and Bioelectronics***,** 111417.

SHETTI, N. P., BUKKITGAR, S. D., REDDY, K. R., REDDY, C. V. & AMINABHAVI, T. M. 2019b. ZnO-based nanostructured electrodes for electrochemical sensors and biosensors in biomedical applications. *Biosensors and Bioelectronics,* 141**,** 111417.

SHETTI, N. P., MALODE, S. J., NAYAK, D. S., BUKKITGAR, S. D., BAGIHALLI, G. B., KULKARNI, R. M. & REDDY, K. R. 2020. Novel nanoclay-based electrochemical sensor for highly efficient electrochemical sensing nimesulide. *Journal of Physics and Chemistry of Solids,* 137**,** 109210.

SHETTI, N. P., MALODE, S. J., NAYAK, D. S. & REDDY, K. R. 2019c. Novel heterostructured Ru-doped TiO2/CNTs hybrids with enhanced electrochemical sensing performance for Cetirizine. *Materials Research Express,* 6**,** 115085.

SHETTI, N. P., NAYAK, D. S., MALODE, S. J., KAKARLA, R. R., SHUKLA, S. S. & AMINABHAVI, T. M. 2019d. Sensors based on ruthenium-doped TiO2 nanoparticles loaded into multi-walled carbon nanotubes for the detection of flufenamic acid and mefenamic acid. *Analytica Chimica Acta,* 1051**,** 58-72.

SHUMYANTSEVA, V. V., BULKO, T. V., KUZIKOV, A. V., MASAMREKH, R. A., KONYAKHINA, A. Y., ROMANENKO, I., MAX, J. B., KÖHLER, M., GILEP, A. A., USANOV, S. A., PERGUSHOV, D. V., SCHACHER, F. H. & SIGOLAEVA, L. V. 2020. All-electrochemical nanocomposite two-electrode setup for quantification of drugs and study of their electrocatalytical conversion by cytochromes P450. *Electrochimica Acta,* 336**,** 135579.

SIDDIQUI, M. R., ALOTHMAN, Z. A. & RAHMAN, N. 2017. Analytical techniques in pharmaceutical analysis: A review. *Arabian Journal of Chemistry,* 10**,** S1409-S1421.

SINGH, A., SINSINBAR, G., CHOUDHARY, M., KUMAR, V., PASRICHA, R., VERMA, H. N., SINGH, S. P. & ARORA, K. 2013. Graphene oxide-chitosan nanocomposite based electrochemical DNA biosensor for detection of typhoid. *Sensors and Actuators B: Chemical,* 185**,** 675-684.

SINGH, R. & DUTTA, S. 2018. Synthesis and characterization of solar photoactive TiO2 nanoparticles with enhanced structural and optical properties. *Advanced Powder Technology,* 29**,** 211-219.

SMAJDOR, J., PIECH, R. & PACZOSA-BATOR, B. 2016. A novel method of high sensitive determination of prednisolone on renewable mercury film silver based electrode. *Electroanalysis,* 28**,** 394-400.

SOBCZAK-KUPIEC, A., VENKATESAN, J., ALHATHAL ALANEZI, A., WALCZYK, D., FAROOQI, A., MALINA, D., HOSSEINI, S. H. & TYLISZCZAK, B. 2016. Magnetic nanomaterials and sensors for biological detection. *Nanomedicine: Nanotechnology, Biology and Medicine,* 12**,** 2459-2473.

SOLANKI, T. D., PATEL, S. K. & PATEL, B. K. 2016. Development and validation of stability indicating method for simultaneous estimation of ofloxacin and prednisolone in pharmaceutical dosage form. *Pharm. Biol. Eval,* 3**,** 256-263.

SOLEYMANI, J., HASANZADEH, M., ESKANDANI, M., KHOUBNASABJAFARI, M., SHADJOU, N. & JOUYBAN, A. 2017. Electrochemical sensing of doxorubicin in unprocessed whole blood, cell lysate, and human plasma samples using thin film of poly-arginine modified glassy carbon electrode. *Materials Science and Engineering: C,* 77**,** 790-802.

SOUSA, C. P., RIBEIRO, F. W., OLIVEIRA, T. M., SALAZAR-BANDA, G. R., DE LIMA-NETO, P., MORAIS, S. & CORREIA, A. N. 2019. Electroanalysis of Pharmaceuticals on Boron-Doped Diamond Electrodes: A Review. *ChemElectroChem,* 6**,** 2350-2378.

SOYLAK, M. & ERBAS, Z. 2017. Magnetic solid phase extraction of trace lead and copper on chromotrope FB impregnated magnetic multiwalled carbon nanotubes from cigarette and hair samples for measurement by flame AAS. *Atomic Spectroscopy,* 38**,** 57-61.

SOYLAK, M. & SAHINBAS, D. H. 2013. Copper, iron, and lead levels in fertilizer and water samples: separation and preconcentration on multiwaled carbon nanotubes. *Desalination and Water Treatment,* 51**,** 7296-7303.

SUN, H.-W., QIAO, F.-X. & LIU, G.-Y. 2006. Characteristic of theophylline imprinted monolithic column and its application for determination of xanthine derivatives caffeine and theophylline in green tea. *Journal of Chromatography A,* 1134**,** 194-200.

TAEI, M., HASANPOUR, F., SALAVATI, H. & MOHAMMADIAN, S. 2016. Fast and sensitive determination of doxorubicin using multi-walled carbon nanotubes as a sensor and CoFe2O4 magnetic nanoparticles as a mediator. *Microchimica Acta,* 183**,** 49-56.

TALAY PINAR, P., ALI, H. S., ABDULLAH, A. A., YARDIMI, Y. & ŞENTÜRK, Z. 2018. Electroanalytical determination of salbutamol in pharmaceutical formulations using cathodically pretreated boron-doped diamond electrode. *Marmara Pharmaceutical Journal,* 22.

TEKER, T. & ASLANOGLU, M. 2019. Sensitive Determination of Terbutaline Using a Platform Based on Nanoparticles of Europium Oxide and Carbon Nanotubes. *Electroanalysis,* 31**,** 146-152.
THAPLIYAL, N., CHIWUNZE, T. E., KARPOORMATH, R., GOYAL, R. N., PATEL, H. & CHERUKUPALLI, S. 2016. Research progress in electroanalytical techniques for determination of antimalarial drugs in pharmaceutical and biological samples. *RSC advances,* 6**,** 57580-57602.
THU, P. T. K., TRINH, N. D., HOAN, N. T. V., DU, D. X., MAU, T. X., TRUNG, V. H., PHONG, N. H., TOAN, T. T. T. & KHIEU, D. Q. 2019. Synthesis of cobalt ferrite and simultaneous determination of ascorbic acid, acetaminophen and caffeine by voltammetric method using cobalt ferrite modified electrode. *Journal of Materials Science: Materials in Electronics,* 30**,** 17245-17261.
TOUBER, M. E., VAN ENGELEN, M. C., GEORGAKOPOULUS, C., VAN RHIJN, J. A. & NIELEN, M. W. F. 2007. Multi-detection of corticosteroids in sports doping and veterinary control using high-resolution liquid chromatography/time-of-flight mass spectrometry. *Analytica Chimica Acta,* 586**,** 137-146.
TRAPIELLA-ALFONSO, L., RAMÍREZ-GARCÍA, G., D'ORLYÉ, F. & VARENNE, A. 2016. Electromigration separation methodologies for the characterization of nanoparticles and the evaluation of their behaviour in biological systems. *TrAC Trends in Analytical Chemistry,* 84**,** 121-130.
USLU, B. & OZKAN, S. A. 2011. Electroanalytical methods for the determination of pharmaceuticals: a review of recent trends and developments. *Analytical letters,* 44**,** 2644-2702.
VADIVEL, M., BABU, R. R., RAMAMURTHI, K. & ARIVANANDHAN, M. 2016. CTAB cationic surfactant assisted synthesis of CoFe2O4 magnetic nanoparticles. *Ceramics International,* 42**,** 19320-19328.
VAJEDI, F. S. & DEHGHANI, H. 2020. A high-sensitive electrochemical DNA biosensor based on a novel ZnAl/layered double hydroxide modified cobalt ferrite-graphene oxide nanocomposite electrophoretically deposited onto FTO substrate for electroanalytical studies of etoposide. *Talanta,* 208**,** 120444.
VALIZADEH, M., SOHRABI, M. R. & MOTIEE, F. 2021. Simple spectrophotometric method for simultaneous determination of salmeterol and fluticasone as anti-asthma drugs in inhalation spray based on artificial neural network and support vector regression. *Optik,* 240**,** 166879.
VARGHESE, B., VV, L. & NAIR, A. 2017. ANALYTICAL TECHNIQUES USED IN QUALITY CONTROL OF DRUGS.
WANG, J., CHENG, W., MENG, F., YANG, M., PAN, Y. & MIAO, P. 2018a. Hand-in-hand RNA nanowire-based aptasensor for the detection of theophylline. *Biosensors and Bioelectronics,* 101**,** 153-158.
WANG, W., ZHANG, Y., WANG, J., SHI, X. & YE, J. 2010. Determination of β-agonists in pig feed, pig urine and pig liver using capillary electrophoresis with electrochemical detection. *Meat science,* 85**,** 302-305.
WANG, X., CHENG, C., DONG, R. & HAO, J. 2012. Sensitive voltammetric determination of rutin at a carbon nanotubes-ionic liquid composite electrode. *Journal of Solid State Electrochemistry,* 16**,** 2815-2821.
WANG, X. & HAO, J. 2016. Recent advances in ionic liquid-based electrochemical biosensors. *Science Bulletin,* 61**,** 1281-1295.
WANG, Y., DING, Y., LI, L. & HU, P. 2018b. Nitrogen-doped carbon nanotubes decorated poly (L-Cysteine) as a novel, ultrasensitive electrochemical sensor for simultaneous determination of theophylline and caffeine. *Talanta,* 178**,** 449-457.
WANG, Z., MA, B., SHEN, C. & CHEONG, L.-Z. 2019. Direct, selective and ultrasensitive electrochemical biosensing of methyl parathion in vegetables using Burkholderia cepacia lipase@MOF nanofibers-based biosensor. *Talanta,* 197**,** 356-362.
WANG, Z., ZHANG, Z., FU, Z., CHEN, D. & ZHANG, X. 2003. Flow-injection chemiluminescence detection for studying protein binding of terbutaline sulfate with on-line microdialysis sampling. *Journal of Pharmaceutical and Biomedical Analysis,* 33**,** 765-773.

WOOD, T. P., DU PREEZ, C., STEENKAMP, A., DUVENAGE, C. & ROHWER, E. R. 2017. Database-driven screening of South African surface water and the targeted detection of pharmaceuticals using liquid chromatography - High resolution mass spectrometry. *Environmental Pollution,* 230**,** 453-462.

WU, H., LIU, G., WANG, X., ZHANG, J., CHEN, Y., SHI, J., YANG, H., HU, H. & YANG, S. 2011a. Solvothermal synthesis of cobalt ferrite nanoparticles loaded on multiwalled carbon nanotubes for magnetic resonance imaging and drug delivery. *Acta Biomaterialia,* 7**,** 3496-3504.

WU, J., DING, C., GE, Q., LI, Z., ZHOU, Z. & ZHI, X. 2011b. Simultaneous determination of ipratropium and salbutamol in rat plasma by LC–MS/MS and its application to a pharmacokinetic study. *Journal of Chromatography B,* 879**,** 3475-3483.

XU, F., YU, J., TESSO, T., DOWELL, F. & WANG, D. 2013. Qualitative and quantitative analysis of lignocellulosic biomass using infrared techniques: A mini-review. *Applied Energy,* 104**,** 801-809.

XU, M., QIAN, X., ZHAO, K., DENG, A. & LI, J. 2015. Flow injection chemiluminescent competitive immunoassay for the β-adrenergic agonist salbutamol using carboxylic resin beads and enzymatic amplification. *Sensors and Actuators B: Chemical,* 215**,** 323-329.

YAN, H., WANG, R., HAN, Y. & LIU, S. 2012. Screening, recognition and quantitation of salbutamol residues in ham sausages by molecularly imprinted solid phase extraction coupled with high-performance liquid chromatography–ultraviolet detection. *Journal of Chromatography B,* 900**,** 18-23.

YÁÑEZ-SEDEÑO, P., CAMPUZANO, S. & PINGARRÓN, J. 2019. Electrochemical (Bio) Sensors: Promising Tools For Green Analytical Chemistry. *Current Opinion in Green and Sustainable Chemistry*.

YANG, Y. J., GUO, L. & ZHANG, W. 2016. The electropolymerization of CTAB on glassy carbon electrode for simultaneous determination of dopamine, uric acid, tryptophan and theophylline. *Journal of Electroanalytical Chemistry,* 768**,** 102-109.

YILMAZ, S., SKRZYPEK, S., DILGIN, Y., YAGMUR, S. & COSKUN, M. 2007. Electrochemical oxidation of prednisolone at glassy carbon electrode and its quantitative determination in human serum and tablets by Osteryoung square wave voltammetry. *Current Analytical Chemistry,* 3**,** 41-46.

YOGAMALAR, R., SRINIVASAN, R., VINU, A., ARIGA, K. & BOSE, A. C. 2009. X-ray peak broadening analysis in ZnO nanoparticles. *Solid State Communications,* 149**,** 1919-1923.

YUAN, S., BO, X. & GUO, L. 2019. In-situ insertion of multi-walled carbon nanotubes in the Fe3O4/N/C composite derived from iron-based metal-organic frameworks as a catalyst for effective sensing acetaminophen and metronidazole. *Talanta,* 193**,** 100-109.

YUSOF, N. A. A., ZAIN, N. M. & PAUZI, N. 2019. Synthesis of ZnO nanoparticles with chitosan as stabilizing agent and their antibacterial properties against Gram-positive and Gram-negative bacteria. *International Journal of Biological Macromolecules,* 124**,** 1132-1136.

ZDARTA, J., MEYER, A. S., JESIONOWSKI, T. & PINELO, M. 2018. A general overview of support materials for enzyme immobilization: characteristics, properties, practical utility. *Catalysts,* 8**,** 92.

ZHAI, C., LI, Y., PENG, Y., YANG, Y. & LI, Y. 2017. Rapid detection of salbutamol in fresh muscle tissues based on surface enhanced Raman spectroscopy. *Transactions of the Chinese Society of Agricultural Engineering,* 33**,** 275-280.

ZHANG, B., WANG, P., XU, J., HAN, Y., JIN, H., JIN, D., PENG, X., HONG, B., LI, J. & GONG, J. 2015. Microwave absorption and magnetic properties of cobalt ferrites/carbon nanotubes nanocomposites. *Nano,* 10**,** 1550070.

ZHANG, D., LI, L., MA, W., CHEN, X. & ZHANG, Y. 2017. Electrodeposited reduced graphene oxide incorporating polymerization of l-lysine on electrode surface and its application in simultaneous electrochemical determination of ascorbic acid, dopamine and uric acid. *Materials Science and Engineering: C,* 70**,** 241-249.

ZHANG, X., CHU, Y., YANG, H., ZHAO, K., LI, J., DU, H., SHE, P. & DENG, A. 2016. Ultrasensitive and Specific Detection of Salbutamol in Swine Feed, Meat, and Urine Samples by a Competitive Immunochromatographic Test Integrated with Surface-Enhanced Raman Scattering. *Food Analytical Methods,* 9**,** 3396-3406.

ZHOU, L., SLEIMAN, M., FERRONATO, C., CHOVELON, J.-M., DE SAINTE-CLAIRE, P. & RICHARD, C. 2017a. Sulfate radical induced degradation of β2-adrenoceptor agonists salbutamol and terbutaline: Phenoxyl radical dependent mechanisms. *Water Research,* 123**,** 715-723.

ZHOU, N., QIAN, Q., QI, P., ZHAO, J., WANG, C. & WANG, Q. 2017b. Identification of Degradation Products and Process Impurities from Terbutaline Sulfate by UHPLC-Q-TOF-MS/MS and In Silico Toxicity Prediction. *Chromatographia,* 80**,** 793-804.

ZHU, Y.-H., ZHANG, Z.-L. & PANG, D.-W. 2005. Electrochemical oxidation of theophylline at multi-wall carbon nanotube modified glassy carbon electrodes. *Journal of Electroanalytical Chemistry,* 581**,** 303-309.

ZHUANG, X., CHEN, D., WANG, S., LIU, H. & CHEN, L. 2017. Manganese dioxide nanosheet-decorated ionic liquid-functionalized graphene for electrochemical theophylline biosensing. *Sensors and Actuators B: Chemical,* 251**,** 185-191.

ZOU, Y., QI, Z., MA, Z., JIANG, W., HU, R. & DUAN, J. 2017. MOF-derived porous ZnO/MWCNTs nanocomposite as anode materials for lithium-ion batteries. *Journal of Electroanalytical Chemistry,* 788**,** 184-191.

ZVEREVA, E., ZHERDEV, A., XU, C. & DZANTIEV, B. 2018a. Highly sensitive immunochromatographic assay for qualitative and quantitative control of beta-agonist salbutamol and its structural analogs in foods. *Food control,* 86**,** 50-58.

ZVEREVA, E. A., ZHERDEV, A. V., XU, C. & DZANTIEV, B. B. 2018b. Highly sensitive immunochromatographic assay for qualitative and quantitative control of beta-agonist salbutamol and its structural analogs in foods. *Food Control,* 86**,** 50-58.

APPENDIX

Journal of the Taiwan Institute of Chemical Engineers 111 (2020) 228–238

Contents lists available at ScienceDirect

Journal of the Taiwan Institute of Chemical Engineers

journal homepage: www.elsevier.com/locate/jtice

A novel electrochemical sensor for selective determination of theophylline in pharmaceutical formulations

Joan Chepkoech Kilele[a], Rajasekhar Chokkareddy[a,*], Nicholas Rono[b], Gan G. Redhi[a]

[a] Department of Chemistry, Durban University of Technology, Durban 4001, South Africa
[b] School of Chemistry and Physics, University of KwaZulu-Natal, Durban 4000, South Africa

ARTICLE INFO

Article History:
Received 17 March 2020
Revised 30 April 2020
Accepted 4 May 2020
Available online 13 June 2020

Keywords:
Theophylline
Electrochemical impedance spectroscopy
Cytochrome c
Zinc oxide nanoparticles

ABSTRACT

Theophylline (TPN) is a medication commonly used in treatment of chronic asthma disorder. However, it is associated with a number of known troublesome side effects, hence, the need to monitor its concentration levels in pharmaceutical formulations. In this work, a nanocomposite based on ZnONPs – MWCNTs – Cyt c (zinc oxide nanoparticles – multiwalled carbon nanotubes – Cytochrome c) were used in the modification of a highly sensitive electrochemical sensor for quantification of TPN in pharmaceutical formulations. The synthesized ZnONPs, ZnONPs-MWCNTs and ZnONPs-MWCNTs-Cyt c were characterized using Thermogravimetric analysis (TGA), Fourier-transform infrared spectroscopy (FT-IR), X-ray diffraction (XRD), Transmission electron microscopy (TEM), surface area analysis by Brunauer–Emmett–Teller (BET) and electrochemical impedance spectroscopy (EIS). Cyclic voltammetry was employed to study electro-catalytic properties of ZnONPs-MWCNTs-Cyt c-GCE towards oxidation of TPN. The dependence of peak currents and potentials on scan rates and pH were also investigated and the working parameters were optimized. Remarkably, ZnONPs-MWCNTs-Cyt c-GCE exhibited improved anodic peak currents as compared to ZnONPs-MWCNTs-GCE, MWCNTs-GCE and bare GCE for 0.1 M TPN at 1.0 V vs. Ag/AgCl. The linear range of the established electrochemical biosensor was from 0.4 to 15 μM (R^2 = 0.9903) with detection limit of 0.0012 μM, thus making it a better candidate for the detection of TPN in pharmaceutical formulation.

1. Introduction

Theophylline (TPN) is an alkaloid that is naturally found in beverages such as coffee, tea and cocoa beans [1]. This alkaloid has been used extensively as a bronchodilator for many years to cure ailments like asthma, emphysema and infant apnea [2, 3]. The acceptable therapeutic concentration of TPN is in the range of 5–20 μg/mL. Dosage concentrations greater than 20 μg/mL are reportedly toxic, and can lead to adverse side effects such as vomiting, seizures and cardiac arrest [4–6]. Therefore, determination of TPN concentration in pharmaceutical dosages and other samples via a rapid, simple, cheap, highly selective and sensitive method is paramount.

In the recent past, several conventional methods such as capillary electrophoresis, chromatographic methods (gas chromatography coupled to mass spectrometry, liquid chromatography and high performance liquid chromatography coupled to ultraviolet detector), spectrometry and electrochemical techniques, have been used to detect and quantify TPN in pharmaceutical formulations as well as in food products [1, 7–14]. However, although chromatographic and spectrometric techniques are well established for quantitative analyses of TPN, a number of limitations such as costly and complicated instrumentation, tedious sample preparations and the consumption of large amounts of expensive and toxic solvents still affect them [15]. Furthermore, in some cases, low selectivity and sensitivity makes them unsuitable for regular analyses [16]. Therefore, it is vital to develop a relatively cheap analytical method, which is reliable, sensitive, selective and environmentally friendly for the determination of TPN in pharmaceutical formulations.

Electrochemical methods are extremely promising in determination of drugs in body fluids, pharmaceutical formulations and other sample matrices owing to their high sensitivities, portability, low-cost and requirement of small amounts of samples [17]. In addition, the excipients do not interfere or the interfering substances do not cause an obvious influence on the current response recorded. Consequently, the sample preparation procedures such as separation and extraction steps are not necessary [18]. A number of electrochemical sensors fabricated using hybrid nanocomposite materials have been applied for electrochemical sensing of electroactive compounds of interest such as drugs due to their novel and multi-functional properties [19, 20]. For instance, Ca-ZnO/GCE, TiO_2/ErGO/CPE and Nano clay/CPE were reportedly used to detect antihistamine, ambroxol and nimesulide drugs respectively in pharmaceutical dosage forms as well as in human urine samples [21–25] also reported on the use of

* Corresponding author.
E-mail address: chokkareddys@gmail.com (R. Chokkareddy).

https://doi.org/10.1016/j.jtice.2020.05.007
1876-1070/

Ru-TiO_2/MWCNTs/CPE and Mg-ZnO/CPE for the detection of mefanic acid and flufenamic acid in human urine samples only. The as-fabricated sensors reported lower limits of detection, promising sensitivity and good potential application in quantification of these drugs in their formulations samples and body fluids.

From previous reports, semi-conductor metal oxide nanoparticles-MWCNTs based nanocomposites are well known electro-catalysts for the redox reactions of electro active species [26]. Furthermore, the addition of a biological molecule such as proteins and enzymes to the proposed organic nanocomposite has much attracted attention. This is because of their high specificity, hence they are principally used as the recognition agents [27–29]. These nanocomposites have proven to play a crucial role in amplifying the performance in electrochemical sensing of drugs due to the synergistic effect between the nanocomposites material [30]. With regard to recent electrochemical detection of TPN, its electro-oxidation reaction is poor at bare glassy carbon electrode (GCE) [31, 32]. As a result, there is need to modify the surface of the bare GCE electrode using novel nanomaterials based on carbon nanotubes, enzymes and metal oxides having excellent electro-catalytic properties using simple approaches. Among these nanocomposites, composites of ZnONPs and MWCNTs are of great interest. ZnO, a semiconductor, having large excitation binding energy of 60 meV and a wide band gap (3.37 eV), has been used widely for fabrication of cheap electrodes for sensing owing to its superior electro catalytic properties. It has good electrical conductivity, low toxicity, readily available, high chemical and thermal stability, easy to synthesis at low-cost and is biocompatible [24, 33]. MWCNTs nanomaterials are suitable for electrochemical sensing among its applications due to its unique properties such as high adsorption ability, its large surface area to volume ratio as well as its excellent conductivity [34, 35]. MWCNTs based sensors generally exhibit rapid electron transfer, high sensitivity with reduced limits of detection compared to unmodified conventional electrodes [36].

The aim and novelty of this study therefore, is to develop a ZnONPs-MWCNTs-Cyt c nanocomposite modified GCE electrochemical sensor for the determination of TPN using cyclic voltammetry (CV) and Differential pulse voltammetry (DPV). To the best of our knowledge, there have been no reports concerning detection of TPN using ZnONPs-MWCNTs-Cyt c-GCE. In this case, MWCNTs was used as support material for ZnONPs [37–39] and the ZnONPs-MWCNTs nanocomposite was prepared via mechanomixing. Further, Cytochrome c (Cyt c) enzyme was immobilized on ZnONPs-MWCNTs nanocomposite in order to improve specificity towards TPN detection. The resulting ZnONPs-MWCNTs-Cyt c nanocomposite modified GCE was tested for the electrochemical determination of TPN using CV. Appreciable, ZnONPs-MWCNTs-Cyt c-GCE presented excellent performance as compared to the ZnONPs-MWCNTs-GCE, MWCNTs-GCE and the unmodified GCE. DPV was employed to investigate ZnONPs-MWCNTs-Cyt c modified GCE for TPN detection in terms of stability, sensitivity, reproducibility, selectivity, the linear range and the detection limits. The limit of detection (LOD) obtained was much lower than most of the given literature studies (Table 1) hence it is evident that it is highly sensitive and the proposed sensor was successfully used for the determination of TPN in pharmaceutical formulation.

Table 1
Comparison of the performance of ZnONPs-MWCNTs-Cyt c-GCE sensor with various electrochemical sensors for detection of theophylline.

Electrochemical electrodes	Limit of detection (μM)	References
Graphene quantum dots–screen printed electrode	0.2	[6]
Multiwalled carbon nanotubes -Au-Poly-L-Lysine–screen printed electrode	2.0	[18]
Multiwalled carbon nanotubes–-glassy carbon electrode	0.05	[47]
Poly(L-aspartic acid/f- Multiwalled carbon nanotubes–glassy carbon electrode	0.02	[48]
Poly(CTAB)–glassy carbon electrode	0.11	[49]
Molecularly imprinted polyargine-sodium alginate–multiwalled carbon nanotubes	0.0032	[50]
MIP by (MIP) of 4-amino-5-hydroxy-2,7-naphthalenedisulfonic acid-–glassy carbon electrode	0.32	[51]
Nitrogen-doped carbon nanotubes decorated poly (L-Cysteine)–glassy carbon electrode	0.033	[52]
Zinc oxide nanoparticles – multi-walled carbon nanotubes – cytochrome c–Glassy carbon electrode	0.0012	This work

2. Experimental section

2.1. Chemicals

Sodium dihydrogen orthophosphate (NaH_2PO_4), anhydrous disodium hydrogen orthophosphate (Na_2HPO_4), potassium chloride(KCl), potassium hexacyanoferrate(III) ($K_3[Fe(CN)_6]$), potassium hexacyanoferrate(II) trihydrate ($K_4[Fe(CN)_6].3H_2O$), zinc chloride ($ZnCl_2$), potassium hydroxide (KOH), N, N dimethyl formamide (DMF), sulphuric acid (H_2SO_4), methanol (CH_3OH), sodium hydroxide (NaOH), and ethanol (C_2H_6O) from Associated Chemical Enterprises (Pty) Ltd (Johannesburg, South Africa) were used. Theophylline, chlorogenic acid, glucose, sucrose, ascorbic acid, streptomycin, acetaminophen, nafion® perfluorinated resin solution (5 wt%) and MWCNTs (95% carbon, 6–9 nm diameter and 5 μm long) were procured from Sigma-Aldrich (Durban, South Africa). All the other solvents and chemicals used were of analytical grade and they were used as received.

2.2. Synthesis of ZnO nanoparticles

Pure ZnONPs were synthesized via wet chemical methods [40]. Typically, 0.4 M $ZnCl_2$ was dissolved in 200 mL deionized water with vigorous magnetic stirring. A 100 mL ethanolic solution containing 0.8M KOH was added drop by drop into the solution until a white precipitate was formed. The mixture was then stirred for 2 h at 25 °C for complete reaction. The obtained suspension was allowed to settle for 12 h and a precipitate was collected by decantation. The precipitate was washed several times using deionized water by way of centrifuging and thereafter dried in an oven at a temperature of 70 ° C, under a stream of air in order to remove water and to decompose $Zn(OH)_2$ to ZnONPs. The dried product (ZnO) was ground to powder.

2.3. Characterization

Thermal stabilities of nanocomposites was investigated using a thermal gravimetric analysis (TGA)-differential scanning calorimetry (DSC) 1SF model 1346 (Columbus, USA) with a STARe software version (Mettler Toledo) instrument. XRD patterns of the ZnONPs was obtained by a Bruker AXS D8 diffractometer with CuKα radiation (λ=1.5418 E) operating at 40 kV at a scan rate of 0.5 min^{-1}. The surface morphology of ZnONPs, MWCNTs and ZnONPs-MWCNTs were determined using TEM, (JEM 2100 Max Oxford Instrument, JEOL Inc., Peobody, MA, USA). The functional groups were identified by a Cary 630 (Santa Clara, USA) Fourier transform infrared (FTIR) Spectrometer in the range of 400–4000 cm^{-1}. The Brunauer-Emmett Teller (BET) surface areas and the total pore sizes distribution of pure MWCNTs and ZnONPs-MWCNTs composites were determined from N_2 adsorption–desorption isotherms at 77 K with a Micromeritics TriStar II surface area and porosity analyzer (Tristar II 3020, USA)

2.4. Modification of glassy carbon electrode

Prior to each modification, the bare GCE surface was thoroughly cleaned by polishing it using alumina slurry on a polishing cloth and repeatedly rinsed with de-ionized water. The cleaned GCE was then dried at room temperature. 0.2 g of ZnONPs and 0.1 g of MWCNTs (commercial) was ultra-sonicated in 10 mL DMF solution for about one hour to obtain well-dispersed ZnONPs-MWCNTs black paste. 2 μL nafion solution (used as a binder) was added to the resulting suspension and stirred for further 10 min. A given quantity of ZnONPs-MWCNTs dispersion was drop-casted onto the surface of thoroughly cleaned bare GCE and dried at 40 °C in the oven to evaporate the solvent used [41]. For comparison, MWCNTs-GCE electrodes was prepared the same way but using both MWCNTs and nafion solutions only. To prepare ZnONPs-MWCNTs-Cyt c-GCE; a solution of Cyt c enzyme was prepared by dissolving approximately 2 mg in deionized water and was sonicated for few minutes to obtain a homogeneous. Cyt c was immobilized on the ZnO-MWCNTs-GCE surface by dropping approximately 2 μL of the enzyme solution on it and was allowed to dry at 4 °C for about 20 min.

2.5. Preparation of TPN standard solution and phosphate buffer solution (PBS)

TPN standard solution (0.1 M) was prepared by accurately weighing the calculated amount into a conical flask and diluting it up to the calibration mark with de-ionized water. 0.1 M PBS (supporting electrolyte) was prepared from Na_2HPO_4 and NaH_2PO_4 salts by accurately weighing appropriate quantity of Na_2HPO_4 and NaH_2PO_4 into 500 mL volumetric flask and dissolving to the calibration mark with deionized water. The pH (1.0–8.0) of 0.1 M PBS was adjusted as necessary using 1 M NaOH and 1 M H_2SO_4. All the prepared solutions were stored in the fridge at 4 °C during the course of study.

2.6. Electrochemical measurements

All the electrochemical experiments were performed using 797 VA computrace system (Metrohm, Herisau, Switzerland) which uses a three-electrode system, namely; working, counter and reference electrodes. In this study, the following electrodes were used; ZnONPs-MWCNTS-Cyt c-GCE, MWCNTs-GCE and bare GCE as the working electrode, Ag/AgCl/KCl (standard calomel electrode) as the reference electrode and platinum wire as auxiliary electrode. Before each voltammetry measurements, the electrolyte was purged using nitrogen gas for 20 min to remove dissolved oxygen. In addition, the electrochemical impedance measurements were performed with CHI 660 E (Beijing, China) electrochemical working station.

2.7. Real sample preparation

Theophylline oral solution with the commercial name of Adco-Alcophyllin (labeled to contain 26.667 mg/5 mL of TPN) was purchased from a local pharmacy. Before the measurement, approximately 1 mL aliquot of the sample solution was transferred to 10 mL

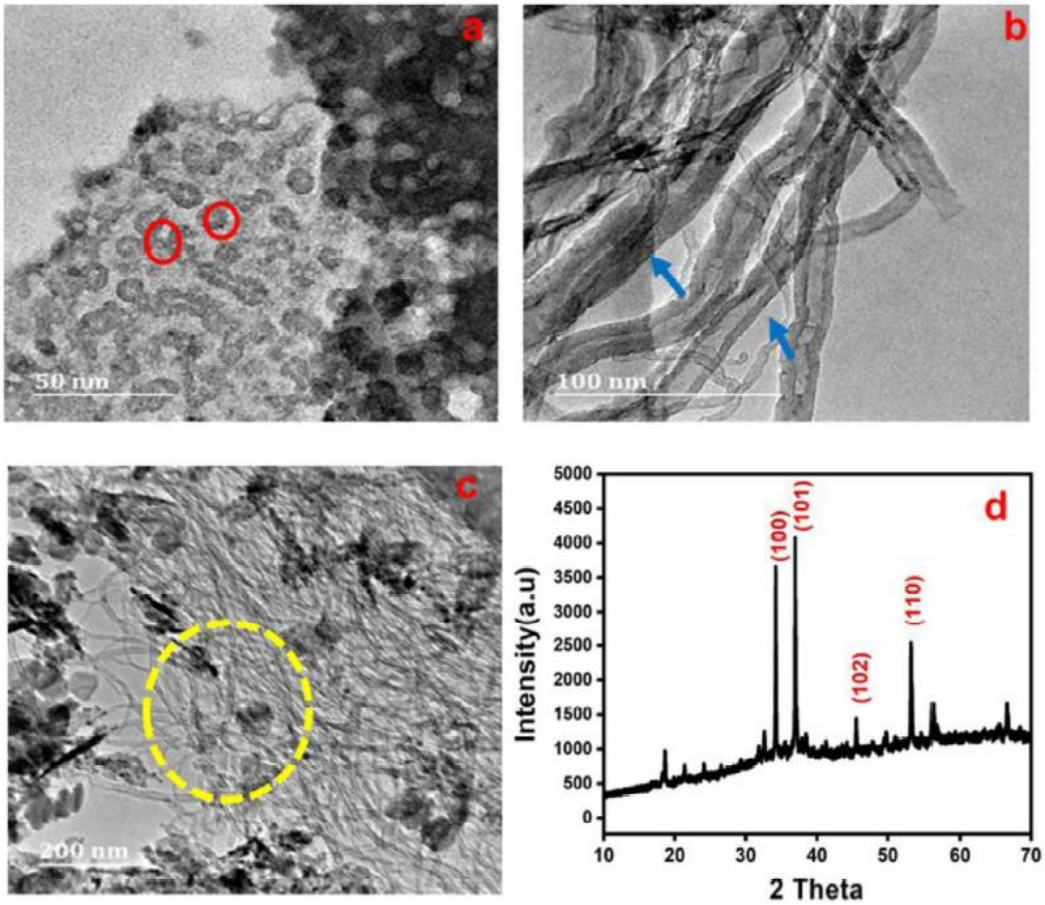

Fig. 1. TEM images of (a) ZnONPs, (b) MWCNTs, (c) ZnONPs-MWCNTs composite and (d). XRD pattern of ZnONPs. (For interpretation of the references to color in this figure, the reader is referred to the web version of this article.)

measuring cylinder and top up with 0.1 M PBS (pH 3.5) without any pre-treatment step. DPV was used in quantification analysis of TPN in real samples by standard addition method.

3. Results and discussion

3.1. Surface morphology, crystal structure and chemical structure of nanocomposites

The surface and morphological characteristics of the prepared samples were explored using TEM and the images of ZnONPs, MWCNTs and ZnONPs-MWCNTs obtained are presented in Fig. 1(a), (b) and (c) respectively. As clearly shown, ZnONPs exhibited spherical (circled red in Fig. 1(a)) with no agglomeration and the average size of particle was found to be about 18 nm, while MWCNTs were tubular in shape (shown by the blue arrow in Fig. 1(b)). As observed in Fig. 1(c) (circled yellow), there was a formation or attachment of ZnO spherical nanoparticles on tube-like MWCNTs surface, which confirms the interaction between metal oxide and carbon nanotubes forming hybrid nanocomposite. The corresponding XRD patterns obtained from the synthesized ZnONPs samples are displayed in Fig. 1(d). The sharp and strong diffraction peaks at $2\theta = 34.23°$, 36.95°, 45.53° and 53.27° correspond to reflections planes (100), (101), (102) and (110) respectively, these peaks correspond to the wurtzite type structure of ZnO nanoparticles [42]. The chemical structure of the as-synthesized materials was measured using FTIR spectrometer. The spectra of pure synthesized ZnONPs and ZnONPs-MWCNTs-Cyt c nanocomposite identifying the surface functional groups are shown in Fig. 2. The typical broad peaks at approximately 3390 cm^{-1} and 3450 cm^{-1} are due to the stretching of OH (hydroxyl) groups. The sharp and strong bands appearing at 711 cm^{-1}, 657 cm^{-1} and 898 cm^{-1} are assigned to the stretching vibration of Zn–O bonds which confirms that the composite consist of synthesized ZnO nanoparticles. After immobilization of cytochrome c enzyme on to the ZnONPs-MWCNTs nanocomposite, new peaks emerged as shown in Fig. 2 (red curve). The presence of the immobilized enzyme is revealed by the peak at about 1646 cm^{-1} corresponding to the amide vibrational band of Cyt c. The additional peaks at about 2931 cm^{-1} and 1099 cm^{-1} are due to the stretching and bending of C–H respectively. Thermal gravimetric analysis curves of ZnONPs, MWCNTs and that of ZnONPs-MWCNTs are presented in Fig. 3. It can be observed that ZnONPs exhibited two decomposition steps. The initial mass loss in the temperature range of 25 °C–150 °C is due to the evaporation of water absorbed on the surface of the synthesized product. The second step that occurred at 350 °C–440 °C temperature range is due to the decomposition of $Zn(OH)_2$ to obtain ZnONPs. Beyond the temperature of 440 °C, there is no further mass loss, which confirms that pure ZnONPs were successfully synthesized. ZnONPs-MWCNTs composite exhibits two decomposition steps; the first mass loss (25 °C–130 °C) is due to the loss of adsorbed water and the solvent used to prepare the composite and the second one at around (300 °C–400 °C) is likely to be due to thermal decomposition of MWCNTs. Thermal curve of MWCNTs shows one decomposition step only below 100°C due to removal of adsorbed water on its surface.

3.2. Surface area and porosity

The porosity and surface area of the samples measurement were carried out using BET instrument and the results are presented in Figs. 4 and 5. As shown, the isotherms were type IV and exhibited H3 hysteresis loops implying that the sample was powder in crystalline form [43]. The calculated surface areas were 31.38 m^2/g and 119.99 m^2/g for MWCNTs and ZnONPs-MWCNTs samples respectively. The results show that addition of MWCNTs to ZnONPs can enhance the surface area of the nanocomposite owing to the high surface area characteristic of the MWCNTs. In addition, the total pore volume for MWCNTs and ZnONPs-MWCNTs were 1.36 cm^3/g and 0.32 cm^3/g respectively.

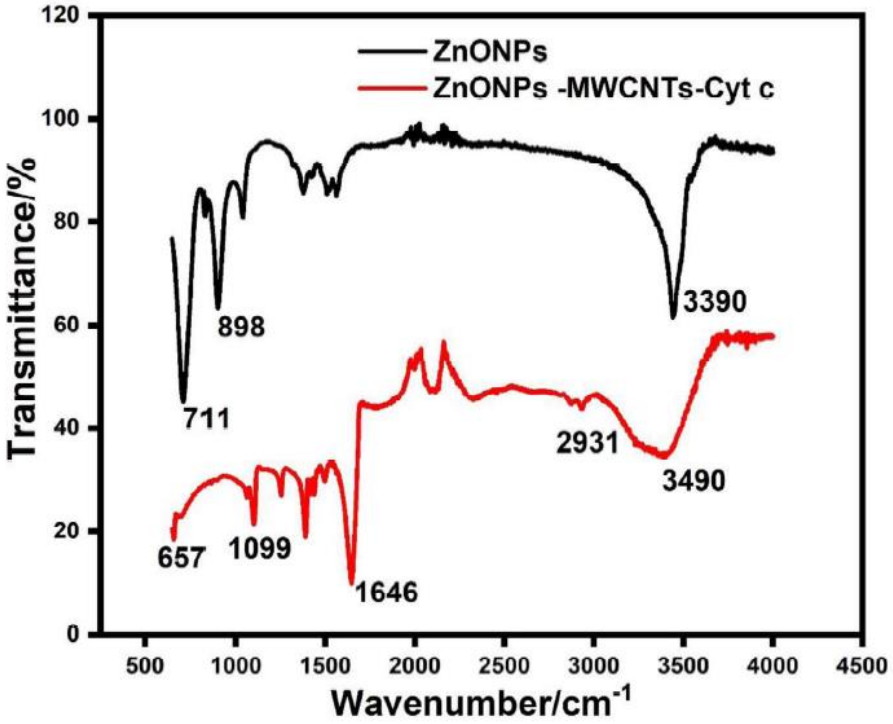

Fig. 2. FTIR spectrum of ZnONPs and ZnONPs-MWCNTs-Cyt c nanocomposite. (For interpretation of the references to color in this figure, the reader is referred to the web version of this article.)

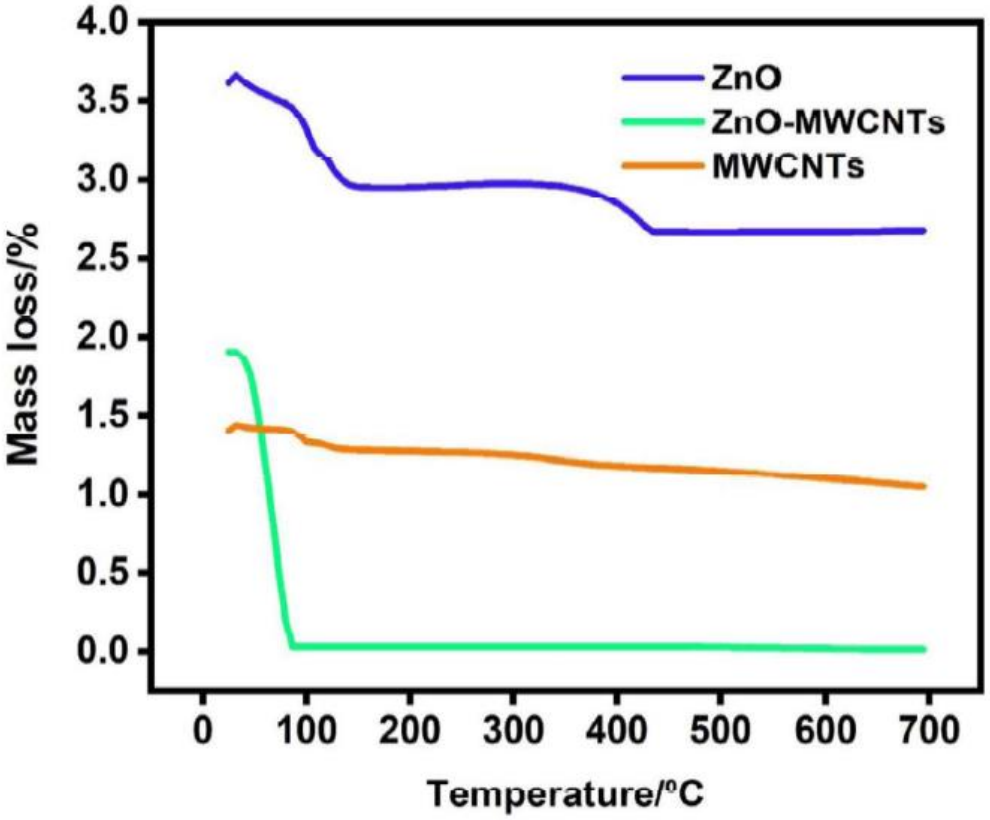

Fig. 3. TGA thermal curves of ZnONPs, MWCNTs and ZnONPs-MWCNTs composite.

3.3. Electrochemical impedance spectroscopy (EIS)

EIS characterization of the developed sensor ZnONPs-MWCNTs-Cyt c-GCE (black curve) and the control electrodes ZnONPs-MWCNTs-GCE and MWCNTs-GCE were investigated in 0.1 M KCl electrolyte solution containing 0.1 mM $[Fe(CN)_6]^{-3/-4}$. Only the linear part corresponding to the diffusion process was exhibited for all the electrode probe layers as shown in Fig. 6. This shows greater conductivity of the prepared nanocomposite modified electrodes with insignificant transfer resistance (Rct) values [26]. Owing to the

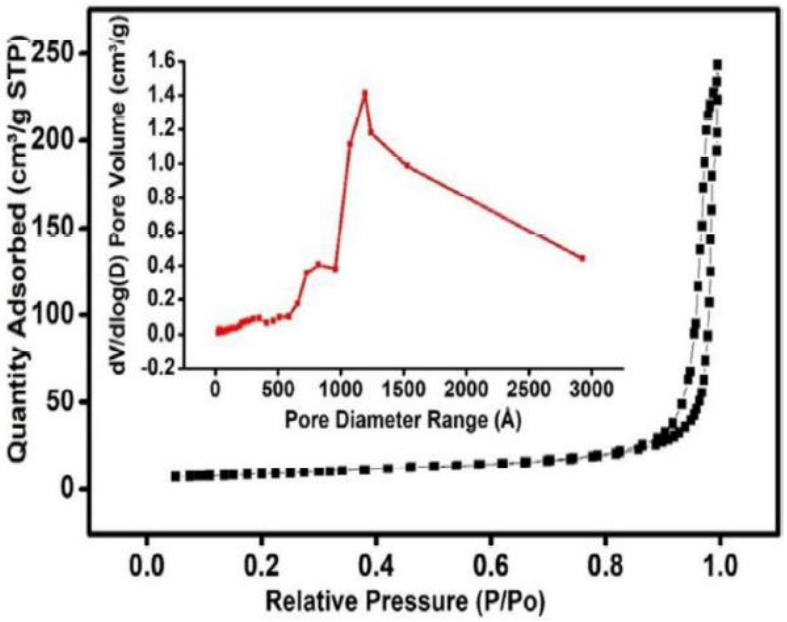

Fig. 4. Nitrogen adsorption–desorption and pore size distribution curve of ZnONPs-MWCNTs samples (inset).

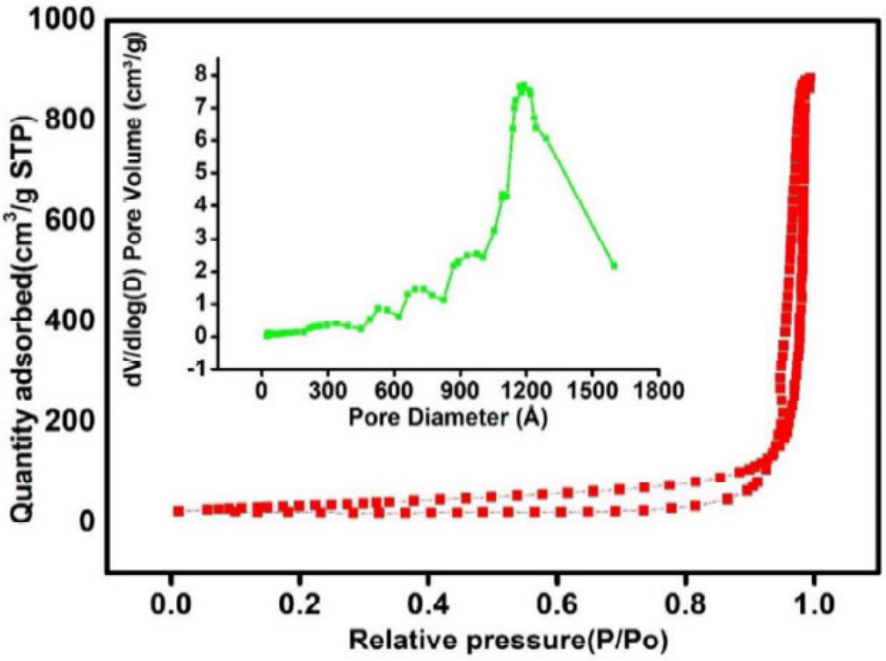

Fig. 5. Nitrogen adsorption desorption isotherm and pore size distribution curve (Inset) of MWCNTs samples.

excellent conductive nature of MWCNTs, MWCNTs-GCE showed very low Rct value. Furthermore, ZnONPs-MWCNTs-Cyt c-GCE showed Rct value almost to zero. The results suggest that the proposed sensor has less charge transfer resistance in compare to other fabricated electrodes. This may be because of the existence of Cyt c enzyme immobilized on ZnONPs-MWCNTs nanocomposite, which facilitates transfer of electrons rapidly. This demonstrates that the ZnONPs-MWCNTs-Cyt c composite might provide good conductive material, that is, with higher electron conduction networks due to the synergistic effects brought by its components.

3.4. Electro-oxidation of theophylline on the GCE and nanocomposite modified GCE

The electro-catalytic ability of the developed sensor towards oxidation of theophylline was studied using cyclic voltammetry (CV). Cyclic voltammograms at unmodified GCE, MWCNTs-GCE, ZnONPs-MWCNTs-GCE and ZnONPs-MWCNTs-Cyt c-GCE were recorded in 0.1 M PBS containing 40 μL TPN in the applied potential window of 0.7 to 1.6 V vs. Ag/AgCl. The pH of the supporting electrolyte, deposition time and scan rate parameters were optimized at bare GCE. The

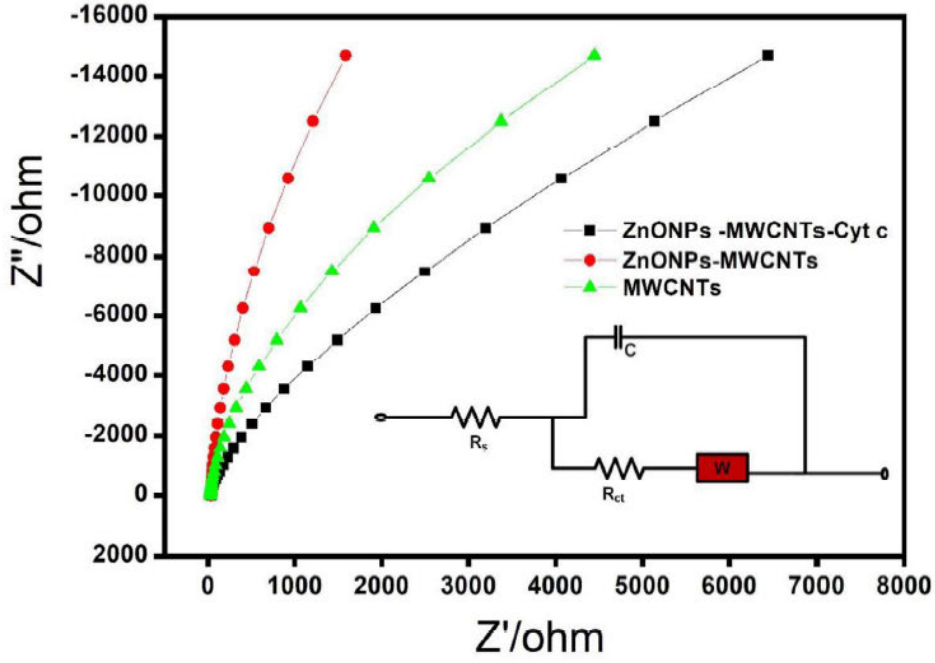

Fig. 6. Nyquist plots of different modified electrodes; MWCNTs-GCE, ZnONPs -MWCNTs-GCE and ZnONPs -MWCNTs-Cytochrome C-GCE in 0.1 M KCl electrolyte solution containing 0.1 mM [Fe(CN)6] −3/−4.

optimal values to be used for further analysis were selected mainly based on good peak separation, high peak current response and the anodic peak shape of the TPN recorded.

3. 5 pH of the supporting electrolyte

From previous works, peak current response and redox potentials are dependent on the pH of the supporting electrolyte. Therefore, in this work, the effect of pH on the oxidation of TPN were studied by monitoring the peak currents and potentials of TPN in 0.1 M PBS over the pH range of 1.0–8.0 by CV at a sweep rate of 0.1 V/s and accumulation time of 60 s. In absence of TPN standard, the GCE did not show any peak under the scanned potential window (Fig. 7(b), blank). In addition of 40 μL of 0.1 M TPN, an irreversible oxidation peak was recorded in the pH range of 1–5 as shown in Fig. 7(b). However, from pH 6.0–8.0 (Fig. 7(b) inset), the electrochemical response was very poor suggesting that in basic medium the oxidation of TPN required more number of protons. Protonation of TPN is more favorable at lower pH values as revealed by broad and stable peaks. However, based on the best response in terms of the peak shape, maximum peak separation and peak currents, pH value of 3.5 was selected for further investigations. Moreover, the anodic peak potential shifted toward negative potential with increase in the pH value (Fig. 7(b)). This may be due to two proton and electrons transfer during the electro oxidation reaction of TPN.

3.6. Effect of accumulation time

Investigation of deposition time to obtain information regarding the amount of TPN on the GCE surface to achieve higher oxidation current response was carried out from 5 s to 60 s at pH 3.5, 0.1 M PBS (Fig. 7(a)). The oxidation peak current response of TPN at bare GCE gradually increased with increasing accumulation time from 5 s to 60 s and reached maximum current response at 60 s. On further increasing accumulation time, there was almost no change in current response. This could be attributed to the saturated adsorption of TPN on the surface of GCE at 60 s. Accordingly, 60 s was chosen for subsequent investigations since the peak current response at accumulation time at 60 s was significant.

3.7. Effect of sweep rate

The change of the anodic peak current and peak potential with change in the scan rates on the oxidation reaction of 0.1 M TPN was investigated under the potential window of 0.7 to 1.4 V vs. Ag/AgCl, at scan rates (0.1–1.0 V/s) under optimal pH (3.5) and time (60 s). Voltammogram (Fig. 7(c)) at the bare GCE obtained exhibited an oxidation peak at 1.0 V and the anodic peak currents vary linearly in the selected scan rate range with a slope of 24.7050 and a correlation coefficient of 0.9924 (as shown in Fig. 7(c) inset). In addition, the linear regression equation related to the plot of ($I/\mu A$) versus $\sqrt{V/s}$ was found to be $I/\mu A = 33.4080x - 6.2790$ with $R^2 = 0.9949$ (Fig. 7(d)). The TPN anodic peak potential shifted to more positive values as the sweep rate increased suggesting that the electrochemical reaction was adsorption-controlled process. Owing to the well-separated oxidation peak obtained with higher oxidation currents, 1.0 V/s scan rate was selected as optimal sweep rate for further analysis of TPN.

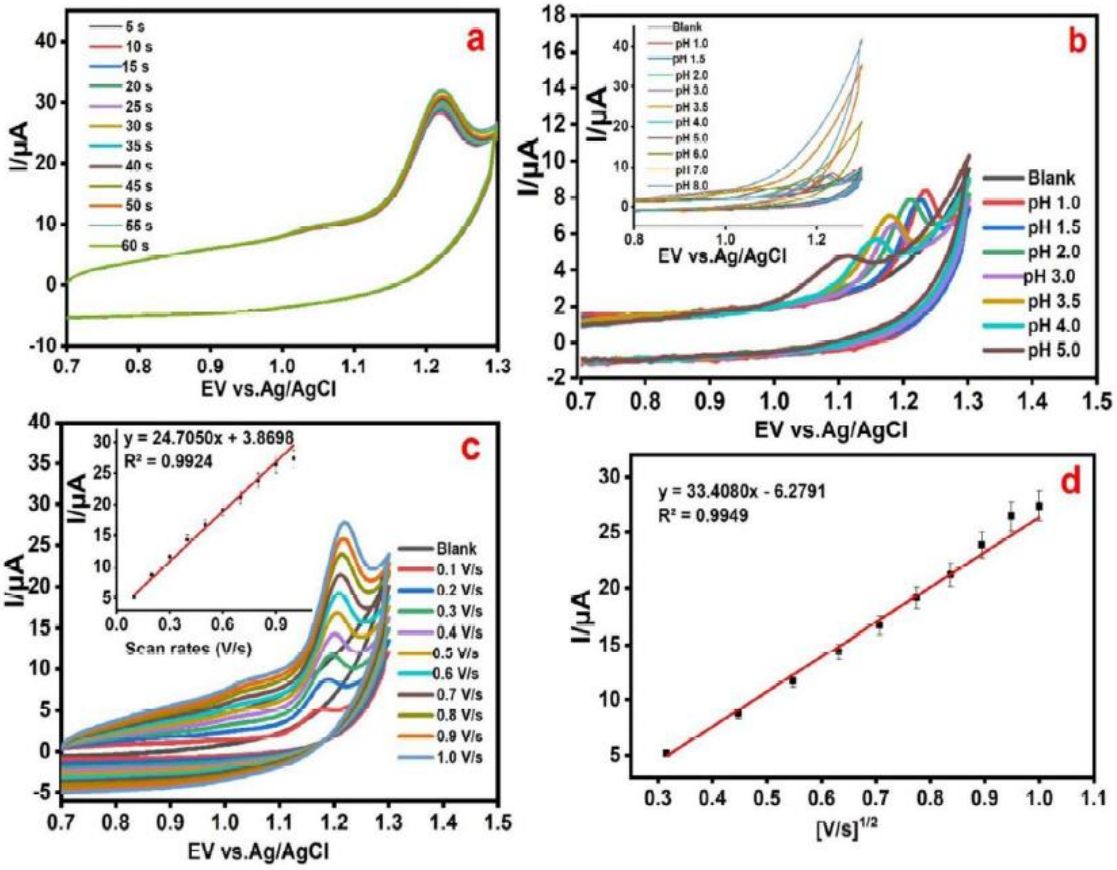

Fig. 7. Cyclic voltammograms of TPN recorded at bare GCE; (a) deposition time 5 s–60 s at optimum pH 3.5, at a scan rate of 0.1 V/s, (b) influence of pH of PBS, at a scan rate of 0.1 V/s and time 60 s, (c) effect of scan rates (0.1–1.0 V/s) at optimal time (60 s) and optimum pH (3.5) and (d) Plot of peak current ($I/\mu A$) Vs $[V/s]^{1/2}$.

3.8. Electrochemical response of TPN on modified GCE

The electrochemical behavior of the developed ZnONPs-MWCNTs-Cyt c-GCE sensor on the catalytic oxidation of 40 μL TPN using CV at scan rates in the range of 0.1–1.0 V/s was studied. A well-defined anodic peak was recorded on the modified GCE surface in comparison to that of bare GCE. The anodic peak currents of TPN at the MWCNTs-GCE were higher as compared to that of the bare GCE. This may be attributed to the high conductivity nature of the MWCNTs. On the other hand, ZnONPs-MWCNTs-GCE showed a greater peak current response due to the excellent electro-catalytic activity and electrical conductivity property of the nanocomposite, which accelerates transfer of electrons. The obtained anodic peak currents produced by the oxidation reaction of TPN on bare GCE were much lower as compared to that of the final sensor ZnONPs-MWCNTs-Cyt c-GCE (Fig. 7(c) and Fig. 8). The increase in the peak current response of TPN clearly indicates a synergy between the MWCNTs, ZnONPs and Cyt c, which enhances the electrical conductivity of hybrid nanocomposite and amplifies the current response. In addition, ZnONPs-MWCNTs composite coated on the GCE surface acts as the supporting material to immobilize cytochrome c. This could further effectively facilitate rapid transfer of electrons between the electrode surface and Cyt c provides abundant active sites for adsorption of TPN and, hence the greater peak current response results obtained compared to the bare electrode surface. These results confirm the successful fabrication of the working electrode for sensitive detection of TPN. There was also distinct increase in the peak current for each step of electrode fabrication which can be justified via Randles – Sevick equation.

$$i_{pa} = 2.69 \times 10^5 A C_0 n^{3/2} {D_R}^{1/2} v^{1/2} \quad (1)$$

Where A is the surface area of the electrode, i_{pa} is the anodic peak current, n is the number of electrons transferred, C_0 is the concentration of TPN, v is the scan rate and D_R is the diffusion coefficient. The surface area of ZnONPs-MWCNTs-Cyt c-GCE was found to be 18.29 mm^2 in comparison to bare GCE of 3.14 mm. Therefore, the modified electrode provides a very large enhancement of the anodic currents as observed. There was essential enhancement in current response as showed in Fig. 8. The proposed mechanism of TPN is based on two-electron two-proton transfer oxidation reaction and as a result, TPN is converted to 1, 3-dimethyluric acid [44, 45].

3.9. Method validation studies using DPV

DPV is characterized by excellent sensitivity; hence, it is often used for the detection of electro active analytes at lower concentrations. Thus, DPV was used in this part for the quantitative assay of TPN concentration at the proposed ZnONPs –MWCNTs-Cyt c-GCE sensor. Fig. 9(a) shows the differential pulse voltammogram of at different concentrations of TPN at ZnONPs-MWCNTs-Cyt c-GCE. In absence of TPN standard, there was no clear response in the scanned potential range. This shows that the ZnONPs-MWCNTs-Cyt c-GCE working electrode is not electrochemically active at this potential range in 0.1 M PBS (pH =3.5). A well resolved anodic peak at about 1.0 V vs. Ag/AgCl was observed and the obtained results showed that under optimum conditions, the anodic peak current increases with increase in TPN concentration (as shown in Fig. 9). The plotted calibration curve; peaks current (I/μA) against TPN concentration (μM) shown in Fig. 9(b) presents a linear correlation between peak current and TPN concentration over the range of 0.4–15 μM with a regression value of 0.9903. The limit of detection (LOD =0.0012 μM) was calculated from the calibration curve using the equation (3 × SD/Slope) where SD is the standard deviation. The obtained results were comparable to previous literature values (Table 1) estimated by different developed sensors for detection of TPN in pharmaceutical formulations and other matrices.

3.10. Selectivity, reproducibility and stability studies of the fabricated sensor

To study the selectivity of the ZnONPs-MWCNTs-Cyt c-GCE sensor, DPV response of 0.1 M TPN was examined in presence of various salts, carbohydrates and other drugs as interfering substances. Addition of Na^+, K^+, glucose, sucrose, ascorbic acid, acetaminophen, chlorogenic acid and streptomycin exhibit negligible influence at the anodic peak current of TPN. ZnONPs-MWCNTs-Cyt c-GCE sensor displayed a phenomenal selectivity for TPN over other co-existing interfering species, with only two additional anodic peaks at 0.29 V vs. Ag/

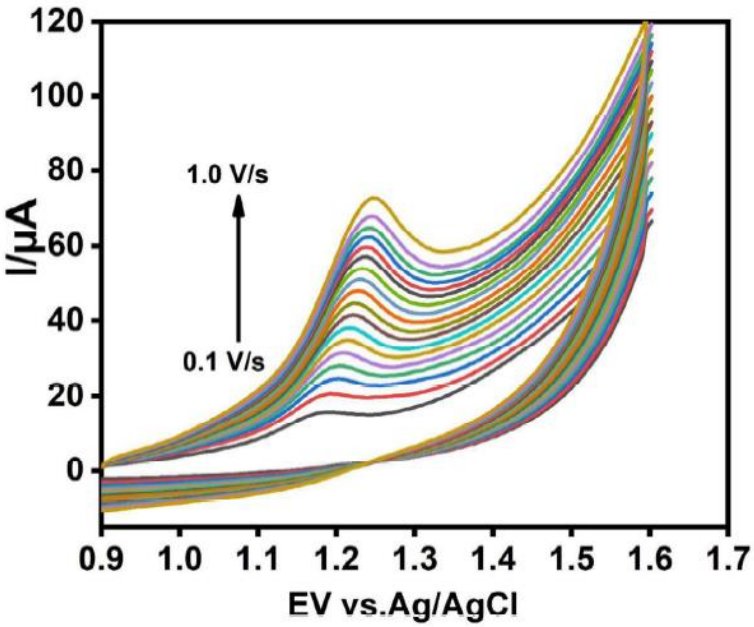

Fig. 8. Cyclic voltammogram of TPN recorded at ZnONPs-MWCNTs-Cyt c-GCE sensor with different scan rates (0.1–1.0 V/s) in 0.1 M PBS pH 3.5 within 60 s.

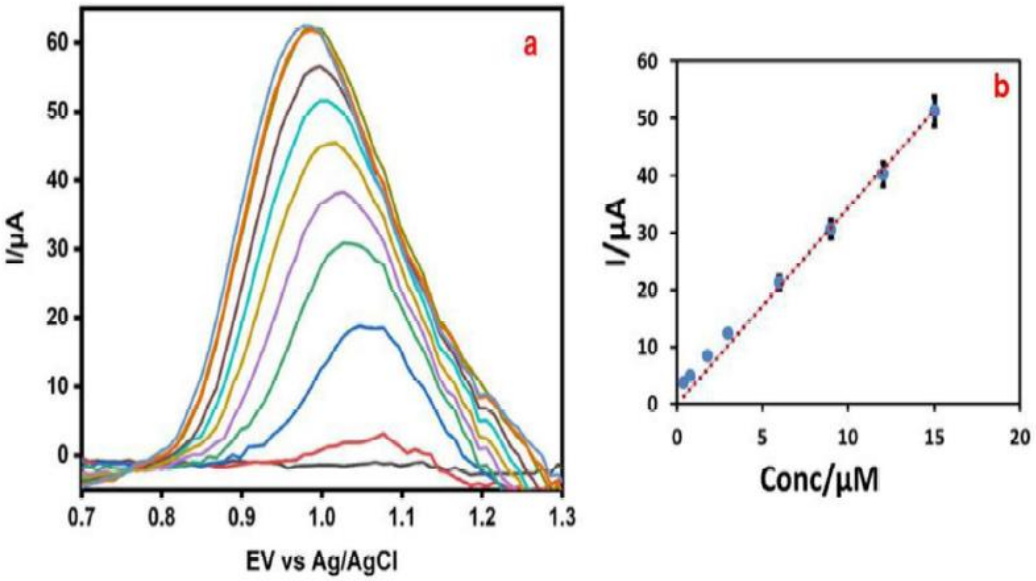

Fig. 9. (a) Differential pulse voltammogram of the ZnONPs-MWCNTS-Cyt c-GCE in 0.1 M PBS (pH 3.5) over 0.4–15 μM concentration range of TPN (Conditions: sweep rate 0.1 V/s, pulse amplitude 0.09 V, Pulse time 0.05 s, deposition time 60 s, deposition potential −0.1009 V; voltage step 0.005951 V). (b) Plot of peak current (μA) versus TPN concentration (μM).

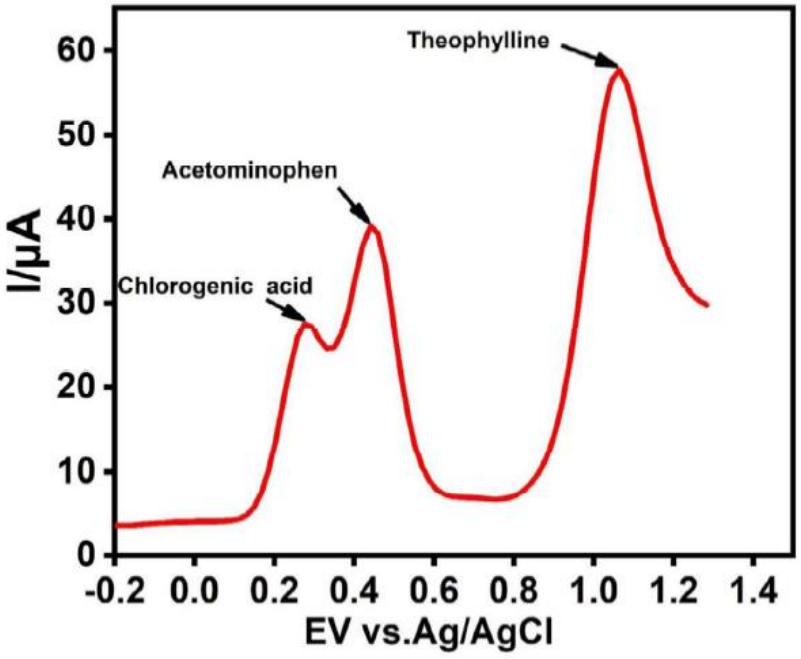

Fig. 10. Differential pulse voltammogram with the current response of ZnONPs-MWCNTs-Cyt c-GCE sensor upon addition of various interfering species in presence of 0.1 M TPN.

Table 2
Determination of theophylline in pharmaceutical formulation sample.

Sample	Spiked (mg/mL syrup)	Found (mg/mL syrup)	Recovery (%)	RSD (%)
Adco-Alcophyllin syrup (26.667 mg/5 mL)	10	10.29	102.9	1.62
	20	19.88	99.4	1.38
	30	32.05	106.8	1.86
	40	41.02	102.5	1.52

AgCl and 0.45 V vs. Ag/AgCl for chlorogenic acid and acetaminophen respectively as shown in (Fig. 10) suggesting good selectivity of the developed method. The anti-interference ability achieved is due to the immobilization of Cyt c on ZnONPs-MWCNTs composite. Cytochrome c act as recognition agent since it is highly selective and specific in nature [46]. To investigate the reproducibility of the developed method, six different ZnONPs-MWCNTs-Cyt c-GCE sensors were studied in 0.1 M TPN under the same optimal conditions. All the working electrodes displayed approximately similar anodic peak currents at the same peak position. The obtained current responses exhibited a relative standard deviation (RSD) of 1.38–1.62 which suggests that this method had acceptable reproducibility. The as-prepared ZnONPs-MWCNTs-Cyt c-GCE sensor was further investigated for its stability by measuring DPV current each day for five days. The sensor was stored at 4 °C each day after use. There was no distinct change in peak current variation after the five days.

3.11. Analytical application of the proposed sensor in real samples

The proposed biosensor was used to quantify TPN in Adco-Alcophyll; a pharmaceutical dosage sample, containing TPN anhydrous syrup (26.667 mg/5 mL), to evaluate its applicability. The prepared real sample solution was analyzed by using standard addition method. Known concentration of TPN standard solution was spiked into the real sample and the recoveries were calculated (as shown in Table 2). Acceptable recovery and relative standard deviation percentage results were obtained.

4. Conclusion

In the present study, a novel electrochemical biosensor-based on ZnONPs-MWCNTs-Cyt c modified GCE was successfully used to detect TPN in pharmaceutical syrup dosage with no significant interference in presence of possible interfering substances was developed. The as-developed biosensor exhibited good reproducibility, stability, selectivity, sensitivity and lower limit of detection (0.0012 μM) compared to previous reported sensors as in Table 1. The remarkable analytical characteristics observed may be ascribed to the synergy effect of the ZnONPs-MWCNTs-Cyt-c hybrid nanocomposite, which resulted in amplification of the electrochemical response. The proposed method is simple, affordable and rapid compared to other analytical techniques used to quantify TPN. Based on the performance of the as fabricated electrode, it may be employed in qualitative and quantitative analysis of pharmaceuticals and other electroactive target compounds in various sample matrices.

Declaration of Competing Interest

The authors declare that they have no known competing financial interests or personal relationships that could have appeared to influence the work reported in this paper.

Acknowledgments

The authors would like to acknowledge the National Research Foundation (NRF grant no. 122312) and the Durban University of Technology.

References

[1] Bartella L, Di Donna L, Napoli A, Siciliano C, Sindona G, Mazzotti F. A rapid method for the assay of methylxanthines alkaloids: theobromine, theophylline and caffeine, in cocoa products and drugs by paper spray tandem mass spectrometry. Food Chem 2019;278:261–6.
[2] Cazzola M, Page CP, Calzetta L, Matera MG. Pharmacology and therapeutics of bronchodilators. Pharmacol Rev 2012;64(3):450–504.
[3] Wang J, Cheng W, Meng F, Yang M, Pan Y, Miao P. Hand-in-hand RNA nanowire-based aptasensor for the detection of theophylline. Biosens Bioelectron 2018;101:153–8.
[4] Mahemuti G, Zhang H, Li J, Tieliwaerdi N, Ren L. Efficacy and side effects of intravenous theophylline in acute asthma: a systematic review and meta-analysis. Drug Des Dev Therapy 2018;12:99.
[5] Calzetta L, Hanania NA, Dini FL, Goldstein MF, Fairweather WR, Howard WW, et al. Impact of doxofylline compared to theophylline in asthma: a pooled analysis of functional and clinical outcomes from two multicentre, double-blind, randomized studies (DOROTHEO 1 and DOROTHEO 2). Pulm Pharmacol Therapeutics 2018;53:20–6.
[6] Ganjali MR, Dourandish Z, Beitollahi H, Tajik S, Hajiaghababaei L, Larijani B. Highly sensitive determination of theophylline based on graphene quantum dots modified electrode. Int J Electrochem Sci 2018;13:2448–61.
[7] Badea DN, Levai C. Separation and detection of caffeine, theophylline and theobromine from coffee varieties, carbonated soft drinks and alcoholic beverages. Rev Chim 2017;68(11):2704–7.
[8] Oellig C, Schunck J, Schwack W. Determination of caffeine, theobromine and theophylline in Mate beer and Mate soft drinks by high-performance thin-layer chromatography. J Chromatogr A 2018;1533:208–12.
[9] Li M, Zhou J, Gu X, Wang Y, Huang X, Yan C. Quantitative capillary electrophoresis and its application in analysis of alkaloids in tea, coffee, coca cola, and theophylline tablets. J Sep Sci 2009;32(2):267–74.
[10] Ma K, Wang H, Zhao M, Xing J. Purity determination and uncertainty evaluation of theophylline by mass balance method, high performance liquid chromatography and differential scanning calorimetry. Anal Chim Acta 2009;650(2):227–33.
[11] Zhuang X, Chen D, Wang S, Liu H, Chen L. Manganese dioxide nanosheet-decorated ionic liquid-functionalized graphene for electrochemical theophylline biosensing. Sens Actuat B: Chem 2017;251:185–91.
[12] Park KS, Oh SS, Soh HT, Park HG. Target-controlled formation of silver nanoclusters in abasic site-incorporated duplex DNA for label-free fluorescence detection of theophylline. Nanoscale 2014;6(17):9977–82.
[13] Kesavan S, Gowthaman N, Alwarappan S, John SA. Real time detection of adenosine and theophylline in urine and blood samples using graphene modified electrode. Sens Actuat B: Chem 2019;278:46–54.
[14] Chen P, Shen J, Wang C, Wei Y. Selective extraction of theophylline from plasma by copper-doped magnetic microspheres prior to its quantification by HPLC. Microchim Acta 2018;185(2):113.
[15] Chen T-W, Chinnapaiyan S, Chen S-M, Hossam Mahmoud A, Elshikh MS, Ebaid H, et al. Facile sonochemical synthesis of rutile-type titanium dioxide microspheres decorated graphene oxide composite for efficient electrochemical sensor. Ultrason Sonochem 2020;62:104872.
[16] Gan T, Zhao A, Wang Z, Liu P, Sun J, Liu Y. An electrochemical sensor based on SiO_2@ TiO_2-embedded molecularly imprinted polymers for selective and sensitive determination of theophylline. J Solid State Electrochemy 2017;21(12):3683–91.
[17] Shashikumara J, Swamy BK. Electrochemical investigation of dopamine in presence of uric acid and ascorbic acid at poly (reactive blue) modified carbon paste electrode: a voltammetric study. Sens Int 2020:100008.
[18] Peng A, Yan H, Luo C, Wang G, Ye X, Ding H. Electrochemical determination of theophylline pharmacokinetic under the effect of roxithromycin in rats by the MWNTs/Au/poly-L-lysine modified sensor. Int J Electrochem Sci 2017;12:330–46.
[19] Goud KY, Satyanarayana M, Hayat A, Gobi KV, Marty JL. Chapter 7 - Nanomaterial-based electrochemical sensors in pharmaceutical applications editor. In: Grumezescu AM, editor. Nanoparticles in pharmacotherapy. William Andrew Publishing; 2019. p. 195–216.
[20] Kumar S, Bukkitgar SD, Singh S, Singh V, Reddy KR, Shetti NP, et al. Electrochemical sensors and biosensors based on graphene functionalized with metal oxide nanostructures for healthcare applications. ChemistrySelect 2019;4(18):5322–37.
[21] Bukkitgar SD, Shetti NP, Malladi RS, Reddy KR, Kalanur SS, Aminabhavi TM. Novel ruthenium doped TiO_2/reduced graphene oxide hybrid as highly selective sensor for the determination of ambroxol. J Mol Liquids 2020;300:112368.
[22] Kulkarni DR, Malode SJ, Prabhu KK, Ayachit NH, Kulkarni RM, Shetti NP. Development of a novel nanosensor using Ca-doped ZnO for antihistamine drug. Mater Chem Phys 2020;246:122791.
[23] Shetti NP, Malode SJ, Nayak DS, Bukkitgar SD, Bagihalli GB, Kulkarni RM, et al. Novel nanoclay-based electrochemical sensor for highly efficient electrochemical sensing nimesulide. J Phys Chem Solids 2020;137:109210.
[24] Bukkitgar SD, Shetti NP, Kulkarni RM, Reddy KR, Shukla SS, Saji VS, et al. Electrocatalytic behavior of Mg-doped ZnO nano-flakes for oxidation of anti-inflammatory drug. J Electrochem Soc 2019;166(9):B3072–B8.
[25] Shetti NP, Nayak DS, Malode SJ, Kakarla RR, Shukla SS, Aminabhavi TM. Sensors based on ruthenium-doped TiO_2 nanoparticles loaded into multi-walled carbon nanotubes for the detection of flufenamic acid and mefenamic acid. Anal Chim Acta 2019;1051:58–72.
[26] Shaikshavali P, Reddy TM, Gopal TV, Venkataprasad G, Kotakadi VS, Palakollu V, et al. A simple sonochemical assisted synthesis of nanocomposite (ZnO/MWCNTs) for electrochemical sensing of Epinephrine in human serum and pharmaceutical formulation. Colloids Surf A: Physicochem Eng Asp 2020;584:124038.
[27] Ghanbari MH, Khoshroo A, Sobati H, Ganjali MR, Rahimi-Nasrabadi M, Ahmadi F. An electrochemical sensor based on poly (L-Cysteine)@ AuNPs@ reduced graphene oxide nanocomposite for determination of levofloxacin. Microchem J 2019;147:198–206.
[28] Chokkareddy R, Bhajanthri NK, Redhi GG. An enzyme-induced novel biosensor for the sensitive electrochemical determination of isoniazid. Biosensors 2017;7(2):21.

[29] Chokkareddy R, Bhajanthri N, Redhi GG, Redhi DG. Ultra-sensitive electrochemical sensor for the determination of pyrazinamide. Curr Anal Chem 2018;14 (4):391–8.
[30] Dakshayini B, Reddy KR, Mishra A, Shetti NP, Malode SJ, Basu S, et al. Role of conducting polymer and metal oxide-based hybrids for applications in ampereometric sensors and biosensors. Microchem J 2019;147:7–24.
[31] Bandi AB, Shetti NP, Malode SJ, Bukkitgar SD, Kulkarni RM. Electroanalysis of 1, 3–dimethylexanthine at zinc oxide nanoparticles modified electrode. Mater Today: Proc 2019;18:590–5.
[32] Janaj AA, Shetti NP, Malode SJ, Bukkitgar SD, Kulkarni RM. TiO2 nanoparticles modified sensor for theophylline drug. Mater Today: Proc 2019;18:606–12.
[33] Shetti NP, Bukkitgar SD, Kakarla RR, Reddy C, Aminabhavi TM. ZnO-based nanostructured electrodes for electrochemical sensors and biosensors in biomedical applications. Biosens Bioelectron 2019:111417.
[34] Soylak M, Erbas Z. Magnetic solid phase extraction of trace lead and copper on chromotrope FB impregnated magnetic multiwalled carbon nanotubes from cigarette and hair samples for measurement by flame AAS. Atom Spectrosc 2017;38 (3):57–61.
[35] Soylak M, Sahinbas DH. Copper, iron, and lead levels in fertilizer and water samples: separation and preconcentration on multiwaled carbon nanotubes. Desalin Water Treat 2013;51(37–39):7296–303.
[36] Keerthika Devi R, Muthusankar G, Gopu G, Berchmans LJ. A simple self-assembly fabrication of tin oxide nanoplates on multiwall carbon nanotubes for selective and sensitive electrochemical determination of antipyretic drug. Colloids Surf A: Physicochem Eng Asp 2020;598:124825.
[37] Mwafy EA, Mostafa AM. Multi walled carbon nanotube decorated cadmium oxide nanoparticles via pulsed laser ablation in liquid media. Opt Laser Technol 2019;111:249–54.
[38] Mukdasai S, Langsi V, Pravda M, Srijaranai S, Glennon JD. A highly sensitive electrochemical determination of norepinephrine using l-cysteine self-assembled monolayers over gold nanoparticles/multi-walled carbon nanotubes electrode in the presence of sodium dodecyl sulfate. Sens Actuat B: Chem 2016;236:126–35.
[39] Chokkareddy R, Redhi GG, Karthick T. A lignin polymer nanocomposite based electrochemical sensor for the sensitive detection of chlorogenic acid in coffee samples. Heliyon 2019;5(3):e01457.
[40] Rao US, Srinivas G, Rao TP. Influence of precursors on morphology and spectroscopic properties of ZnO Nanoparticles. Proc Mater Sci 2015;10:90–6.
[41] Chokkareddy R, Thondavada N, Bhajanthri NK, Redhi GG. An amino functionalized magnetite nanoparticle and ionic liquid based electrochemical sensor for the detection of acetaminophen. Anal Methods 2019;11(48):6204–12.
[42] Yogamalar R, Srinivasan R, Vinu A, Ariga K, Bose AC. X-ray peak broadening analysis in ZnO nanoparticles. Solid State Commun 2009;149(43):1919–23.
[43] Septiani NLW, Kaneti YV, Yuliarto B, Dipojono HK, Takei T, You J, et al. Hybrid nanoarchitecturing of hierarchical zinc oxide wool-ball-like nanostructures with multi-walled carbon nanotubes for achieving sensitive and selective detection of sulfur dioxide. Sens Actuat B: Chem 2018;261:241–51.
[44] Bukkitgar SD, Shetti NP. Electrochemical behavior of theophylline at methylene blue dye modified electrode and its analytical application. Mater Today: Proc 2018;5(10):21474–81.
[45] Quintanilla G, Usarralde A, Perez I, Gargiulo ML, Yakupoglu G, Martin A, et al. Anodic oxidation of caffeine and theophylline in glacial acetic acid. ChemistrySelect 2016;1(3):414–6.
[46] Aghamiri ZS, Mohsennia M, Rafiee-Pour H-A. Immobilization of cytochrome c and its application as electrochemical biosensors. Talanta 2018;176:195–207.
[47] Zhu YH, Zhang ZL, Pang DW. Electrochemical oxidation of theophylline at multiwall carbon nanotube modified glassy carbon electrodes. J Electroanal Chem 2005;581:303–9.
[48] Mekassa B, Tessema M, Chandravanshi BS. Simultaneous determination of caffeine and theophylline using square wave voltammetry at poly (l-aspartic acid)/functionalized multi-walled carbon nanotubes composite modified electrode. Sens Bio-Sens Res 2017;16:46–54.
[49] Yang YJ, Guo L, Zhang W. The electropolymerization of CTAB on glassy carbon electrode for simultaneous determination of dopamine, uric acid, tryptophan and theophylline. J Electroanal Chem 2016;768:102–9.
[50] Salajegheh M, Ansari M, Foroghi MM, Kazemipour M. Computational design as a green approach for facile preparation of molecularly imprinted polyarginine-sodium alginate-multiwalled carbon nanotubes composite film on glassy carbon electrode for theophylline sensing. J Pharmaceut Biomed Anal 2019;162:215–24.
[51] Aswini K, Mohan AV, Biju V. Molecularly imprinted poly (4-amino-5-hydroxy-2, 7-naphthalenedisulfonic acid) modified glassy carbon electrode as an electrochemical theophylline sensor. Mater Sci Eng: C 2016;65:116–25.
[52] Wang Y, Ding Y, Li L, Hu P. Nitrogen-doped carbon nanotubes decorated poly (L-Cysteine) as a novel, ultrasensitive electrochemical sensor for simultaneous determination of theophylline and caffeine. Talanta 2018;178:449–57.